



Escola de Camins
Escola Tècnica Superior d'Enginyeria de Camins, Canals i Ports
UPC BARCELONATECH

Study of UHPC reinforced by graphene oxide & carbon nanotubes composites and steel fibers

Treball realitzat per:

Albert López Deulofeu

Dirigit per:

Antonio Ricardo Marí Bernat

Màster en:

Enginyeria de Camins, Canals i Ports

Barcelona, 31/05/19

Departament d'Enginyeria Civil i Ambiental

TREBALL FINAL DE MÀSTER

Abstract

The demands for taller and bigger structures, but also lighter and less expensive, shows that developing new construction materials and techniques is more important than ever. The most used material on construction is concrete and it is upgrading continually through its composite's advancements. The latest researches on concrete came up with Ultra High Performance Concrete (UHPC) that outstands the properties of regular concrete. Technology is improving in nanomaterials and methods to apply it to concrete are investigated. These methods include using separately steel fibers with carbon nanotubes (CNT) and/or graphene oxide (GO) added as admixtures. This research aims to study the effect of using steel fibers, CNT and GO materials altogether. Included in the method is from the initial mixing step to formulating a numerical model for the new concrete. The modelling involves an analysis of an experimentally obtained compressive stress-strain curve. The results show that steel fibers are needed to have post-peak resistance. A crucial factor in concrete admixtures with nanomaterials is the process of mixing and dosage. A goodness analysis of the data has been conducted that shows that the numerical model represents correctly the tests, even though testing instrumentation should be upgraded. The results of the modelling and analysis are presented such that they can be used as an aid to the future experimental campaigns with such materials, while performing tensile strength test to progress on the numerical model and obtain a different approach on the nanomaterials usage in concrete.

Key words: ultra high performance concrete, UHPC, compressive strength test, carbon nano tubes, CNT, graphene oxide, GO, characterization.

Resumen

La demanda de estructuras más altas y más grandes, pero también más livianas y más baratas, muestra que desarrollar nuevos materiales y técnicas de construcción es ahora más importante que nunca. El hormigón es el material más utilizado en la construcción y está en constante desarrollo a través de los avances en su composición. Las investigaciones más recientes sobre hormigón se centran en un hormigón de ultra altas prestaciones (UHPC) que mejora significativamente las propiedades del hormigón convencional. La tecnología está mejorando en el tratamiento de los nanomateriales y se investigan los métodos para aplicarla al hormigón. Estos métodos incluyen usar separadamente fibras de acero con nanotubos de carbono (CNT) y/o óxido de grafeno (GO) como aditivos. Esta investigación tiene como objetivo estudiar el efecto del uso de fibras de acero, CNT y materiales GO en conjunto. En el método están incluidos desde la mezcla inicial hasta la formulación de un modelo numérico para el nuevo hormigón. La modelación implica un análisis de una curva de tensión - deformación en compresión obtenida experimentalmente. Los resultados muestran que las fibras de acero son necesarias para tener resistencia post-pico. Un factor crucial en las mezclas de hormigón con nanomateriales es el proceso de mezcla y dosificación. Se realizó un análisis de bondad de los datos que muestra que el modelo numérico representa fielmente los ensayos, aunque se debería mejorar el equipamiento usado. Los resultados de la modelación y análisis se presentan de manera tal que se pueden usar como ayuda para las futuras campañas experimentales con dichos materiales, mientras se realiza la prueba de resistencia a la tracción para avanzar en el modelo numérico y obtener un enfoque diferente sobre el uso de nanomateriales en hormigón.

Palabras clave: hormigón de ultra altas prestaciones, UHPC, ensayo a compresión, nanotubos de carbono, CNT, óxido de grafeno, GO, caracterización del hormigón.

Acknowledgements

First and foremost, I would like to express my most honest thankfulness to my academic advisor, Dr. Antonio Mari Bernat, for his wise advice, critical spirit and patience towards the composition of this Master Thesis. He has contributed to rewarding Master Degree experience by giving me intellectual freedom in my work, demanding a high quality of work in all my endeavors, engaging me in new ideas and supporting me both personally and institutionally.

Secondly, I would like to express my sincere gratitude to the company Graphenea for providing graphene oxide and to XuzhouNano, Nanocyl and Cheaptubes for providing Carbon Nanotubes, as without their help and good materials it would have been impossible to start this research. Also to my advisor in China Dr. Zhu Peng that helped me through my stay in China.

Furthermore, my gratitude is deposited to whom have emotionally supported this enriching and priceless process. This would have not been possible without Gerard Espinet, Magí Domingo, Alex Olivera, Irene Josa, Isaac Moya, Martí Carrera, Rous Palau, Sergi Conesa and Isaac Sayol.

I am indebted to Kim-Lou Monnier, who has stood unconditionally next to me during these years. I cannot measure with words how grateful I am for the care you have given to me.

Finally, I would like to acknowledge my family for always supporting my decisions and want the best for me, specially my father for being supportive and helping in whatever he was able to do.

THANKS

Table of contents

ABSTRACT	I
RESUMEN	II
CHAPTER 1 - INTRODUCTION	2
CHAPTER 2 - LITERATURE REVIEW	6
2.1.- ULTRA-HIGH PERFORMANCE CONCRETE (UHPC)	7
2.1.1.- UHPC Tests standards	10
2.2.- NANO-REINFORCEMENT	13
2.2.1.- Nanoparticles	13
2.2.2.- Carbon nanofibers and Carbon nanotubes	15
2.2.2.1.- Mixing and Dispersion of CNT	16
2.2.3.- Dosage and performance of MWCNTs	16
2.2.3.1.- High range concentration composites	18
2.2.3.2.- Low range concentration composites	18
2.2.4.- Graphene Oxide (GO)	20
2.2.4.1.- Dosage and performance of GO	21
2.2.5.- CNT&GO composites, the co-effect	22
2.2.6.- Cost of carbon nanotubes and graphene oxide	23
2.3.- NUMERICAL MODELING	26
2.3.1.- Discretization method	26
2.3.1.1.- Finite Element Method	26
2.3.1.2.- Discrete Element Method	27
2.3.1.3.- Choosing the software	27
2.3.2.- Constitutive Equation	29
2.3.2.1.- Examples of constitutive equations in compression	29
2.3.2.2.- Examples of constitutive equations in tension	33
2.3.2.3.- Proposed formulation of the constitutive equation	35
CHAPTER 3 - LAB METHODS	43
3.1.- TEST PLAN	47
3.1.1.- Specimens	47
3.1.1.1.- Number of specimens to be created	47
3.1.1.2.- Calculated costs	49
3.1.2.- Specimens preparation procedures.	52
3.1.2.1.- Preparing the CNT and GO mixture	52
3.1.2.2.- Making the UHPC specimens	54
3.1.3.- Compression test procedure	59
3.1.4.- Planning of tests calendar	60
3.2.- IMPLEMENTATION OF THE TEST PLAN	61
3.2.1.- Obtaining the materials	61
3.2.2.- Molds	62
3.2.3.- Mixing, casting and curing	62
3.2.4.- Compression test	64
CHAPTER 4 - LAB RESULTS	70
4.1.- RAW DATA	71
4.2.- PRETREATING OF THE DATA	74
4.2.1.- Filtering extensometers	74
4.2.2.- Adjusting the initial slope	76
4.3.- PARAMETERS RESULTING FROM THE EXPERIMENTAL DATA	79

4.4.- PARAMETRIC ANALYSIS OF SF AND CNT	82
CHAPTER 5 - FINITE ELEMENT MODEL FOR A BIAXIAL STRESS ON UHPC	84
5.1.- MATHEMATICAL FORMULATION FOR BIAXIAL UHPC CONSTITUTIVE EQUATIONS	86
5.1.1.- Uniaxial Constitutive Relationships	86
5.1.2.- Biaxial Constitutive Relationships	87
5.2.- PROPOSED UMAT (ABAQUS) SUBROUTINE	90
5.2.1.- Pseudocode for UMAT Subroutine	90
5.2.1.1.- Inputs	90
5.2.1.2.- Outputs	90
5.2.1.3.- Local Variables	90
5.2.1.4.- External Process	90
5.2.1.5.- Process	90
5.2.2.- Pseudocode for SLOPE Subroutine	92
5.2.2.1.- Inputs	92
5.2.2.2.- Outputs	92
5.2.2.3.- Local Variables	92
5.2.2.4.- Process	92
5.3.- FORTRAN CODE FOR ORTHOTROPIC BIAXIAL NONLINEAR MODEL FOR UHPC	93
5.3.1.- UMAT4UHPC SUBROUTINE	93
5.3.2.- Subroutine SWAP(A,B)	95
5.3.3.- Subroutine SLOPE	96
5.4.- CHECKING THE GOODNESS OF THE PROPOSED MODEL	97
5.4.1.- Model geometry	97
5.4.2.- Material properties	99
5.4.3.- Load application and measurement of results	100
5.4.4.- Presentation of results of the FEM for UHPC	101
CHAPTER 6 - DISCUSSION OF RESULTS	104
6.1.- EFFECT OF THE INCIDENTS IN THE TESTS ON THE RAW RESULTS	105
6.2.- INFLUENCE OF CNT AND SF DOSAGE ON THE UHPC'S MECHANICAL CHARACTERISTICS	106
6.3.- INFLUENCE OF CURING TIME IN UHPC WITH CNT&GO ADDITIONS	112
6.4.- RELIABILITY OF THE PROPOSED FINITE ELEMENT MODEL	114
CHAPTER 7 - CONCLUSIONS	116
REFERENCES	119
ANNEX 1 RAW DATA AND TEST ANNOTATIONS	124
ANNEX 2 PRETREATED DATA	140
ANNEX 3 PARAMETERS RESULTING FROM THE EXPERIMENTAL DATA	156
ANNEX 4 PARAMETRIC ANALYSIS OF SF AND CNT	172
ANNEX 5 FEM RESULTS OUTPUT – MONITOR DATA FILE	179
ANNEX 6 FEM RESULTS OUTPUT – MONITOR MESSAGE FILE	188

Figures

Figure 2-1 Comparison of nanofillers with supplementary cementitious materials and aggregates in concrete [25]	14
Figure 2-2 Optimum amount of MWCNTs and superplasticizer according to the aspect ratio of CNTs. [52].....	20
Figure 2-3 Compression stress-strain curve corresponding to Smith and Young's formula [102].....	30
Figure 2-4 Stress-strain relationship of concrete based on Collins et al. model. [105] .	32
Figure 2-5 Stress-strain relationship of concrete based on 1990's Spanish Model Code [100].....	33
Figure 2-6 Different diagrams $\sigma - \epsilon$ of discrete type for tension behaviour [107-110]..	34
Figure 3-1 Sonicated sample	53
Figure 3-2 Materials weighted and ready to mix	56
Figure 3-3 Activating the mixing machine	57
Figure 3-4 Demoulding of a specimen.....	58
Figure 3-5 Standard mold for our specimens.....	62
Figure 3-6 Storing a molded specimen in a moist cabinet	62
Figure 3-7 Mixing of powder (left); adding steel fibers (center); specimen after vibrating (right)	63
Figure 3-8 EpsilonTech extensometer	64
Figure 3-9 Test setup with the adapter cylinders.....	65
Figure 3-10 Compression test result examples [123,125].....	65
Figure 3-11 Example of LVDT placement [124]	66
Figure 3-12 Failure modes [125].....	66
Figure 3-13 Behavior of concrete vs steel [126].....	67
Figure 3-14 First test design (left); Final test design for practical purposes (right)	68
Figure 4-1 Example of one extensometer not recording correctly	71
Figure 4-2 Example of disruptive post-peak data of a specimen without steel fibers...	72
Figure 4-3 Specimen results obtained with the LVDT of the hydraulic press	72
Figure 4-4 Force-displacement graph for UHPC28D2SF050-01 specimen.....	73
Figure 4-5 Example of a sudden loss of strength	73
Figure 4-6 UHPC28D0SF000-02 Raw Data and resulting data after filtering wrong extensometer	74
Figure 4-7 UHPC28D4SF008-01 Raw Data and resulting data after filtering wrong extensometer	74
Figure 4-8 UHPC28D2SF000-02 Raw Data and averaged data of both extensometers. 75	
Figure 4-9 Averaged extensometers data of UHPC28D4SF050-01	76
Figure 4-10 In red, the initial slope obtained with the Matlab code	77
Figure 4-11 Simulation of the iteration performed by the code.....	78
Figure 4-12 Final curve with the initial slope modified	78
Figure 5-1 Proposed constitutive relationships.....	86
Figure 5-2 Failure envelope to the biaxial state of stresses of concrete [127]	87
Figure 5-3 Section of the model. 3D (left); Axisymmetric (right)	97
Figure 5-4 Interaction between specimen and steel cylinders (left); Displacements conditions between steel cylinders and loading plates and centre of specimen (right) 98	

Figure 5-5 Test used to compare the finite element model with the experimental results	99
Figure 5-6 Simulation of the consecutive steps of the vertical strain of the compressive test	101
Figure 5-7 Vertical Stress 3D simulation of the compressive tests	102
Figure 5-8 Stress-Strain curve obtained with the FEM.....	102
Figure 5-9 Force-Displacement curve obtained with the FEM.....	103
Figure 6-1 Adjusting the loss of effective resistant area.....	106
Figure 6-2 f_c parametric curves and experimental values by CNT dosage	107
Figure 6-3 f_c parametric curves and experimental values by SF dosage	107
Figure 6-4 ε_c parametric curves and experimental values by CNT dosage	108
Figure 6-5 ε_c parametric curves and experimental values by SF dosage	108
Figure 6-6 E parametric curves and experimental values by CNT dosage	109
Figure 6-7 E parametric curves and experimental values by SF dosage	109
Figure 6-8 σ_2/f_c parametric curves and experimental values by SF dosage.....	110
Figure 6-9 σ_2/f_c parametric curves and experimental values by CNT dosage.....	110
Figure 6-10 $\varepsilon_2/\varepsilon_c$ parametric curves and experimental values by SF dosage	111
Figure 6-11 $\varepsilon_2/\varepsilon_c$ parametric curves and experimental values by CNT dosage	111
Figure 6-12 $\varepsilon_3/\varepsilon_c$ parametric curves and experimental values by SF dosage	112
Figure 6-13 $\varepsilon_3/\varepsilon_c$ parametric curves and experimental values by SF dosage	112
Figure 6-14 Variation of f_c on UHPC specimens with 0.08% CNT dosage	113
Figure 6-15 Variation of e_c on UHPC specimens with 0.08% CNT dosage	113
Figure 6-16 Stress-Strain curves of both FEM and Experimental results.....	114
Figure 6-17 Force - displacement comparison curve	115

Tables

Table 2-1 Constitution list of typical Ductal® UHPFRC [13].....	8
Table 2-2 Material properties of typical fillers [25].	9
Table 2-3 Summary of CNT, GO and CNT&GO researches.....	17
Table 2-4 Materials Costs	25
Table 3-1 Name coding and quantities for the different specimens	48
Table 3-2 Quantities for each UHPC dosage	49
Table 3-3 Costs of each material in each 3 specimens dosages.....	51
Table 3-4 Costs of each material in 1 m3 of each UHPC dosage.....	51
Table 3-5 Materials and Instrumentation	52
Table 3-6 CNT&GO dosages to be created through sonication	53
Table 3-7 Materials and Instrumentation to create the UHPC specimens	54
Table 3-8 Quantities for each UHPC dosage	55
Table 3-9 Materials and Instrumentation needed to perform the tests	59
Table 3-10 Name coding of the specimens created and tested.....	69
Table 4-1 Summary table.....	79
Table 5-1 Average mechanical properties constants values.....	99
Table 5-2 Values from FEM results.....	103

Chapter 1 - Introduction

In this chapter we introduce the topic of the dissertation, the formulation of the problem statement and an overview of the whole research.

Chapter 1 - Introduction

Concrete is the most used material on construction and it is continually improving to satisfy the demands of taller and bigger structures, but also lighter and less expensive. The only thing that humans consume more than water, by volume, is cement and sand, concrete's keys ingredients.

Concrete can be manufactured to desired strength with economy, ingredients of concrete are easily available in most of the places, and it can be cast to any desired shape in working site which makes it economical. Concrete is resistant to wind, water, fire and icing. The durability of concrete is very high, not deterioration is appreciable with age and its maintenance cost is almost negligible.

However, compared to other binding materials, the tensile strength of concrete is relatively low, it's less ductile compared to steel and the weight is high compared to its strength. Their inherent cracks due to lesser tensile strength and strain capacity constitute a main drawback. Cement composites have a noticeable feature of relatively high compressive strength and low tensile and flexural strength, which belong to brittle materials. The cracking of the concrete weakens its structural strength and reduces its durability. Therefore, in the construction is usually used together with steel reinforcing bars that reduce cracks resulting in structures of reinforced and / or pre-stressed concrete.

Improving the control and reduction of cracks and enhancing the mechanical properties of concrete, while maintaining its ductility in tension and its reduced cost, has always been essential. For this purpose, various additives (siliceous fumes, fine-graded aggregates, ...) have been used in the cement to improve their tensile strength and different types of fibers (steel, plastic, natural, ...) added to the concrete mixture to reduce and distribute cracking. These resulting concretes are commonly called UHPC (Ultra-High Performance Concretes).

Until recently, with the different analyzed fiber reinforcement concrete, it was possible to strengthen the concrete, control cracks behavior and improve the flexural strength. The fibers used as a reinforcement were capable of acting as a bond once a crack was created, so it was not propagating any further. Nonetheless, to prevent this initial crack, we need to add a reinforcement admixture to the cement capable of leading to a significant increase on the mechanical properties by acting at a finer scale, lowering the possibility of the cracks to start, since after the crack occurs all tensile strength of the concrete is lost, which must then be entrusted to the fibers, and if any, to the reinforcing bars.

The latest researches show that nanomaterials are consistently reported as improving fracture toughness, compressive, flexural and tensile strengths due to their addition in cement. The main reason is these materials are able to modify the concrete in a nano-scale, allowing an improved control of cracks and nanostructure modification.

These new nano-materials are arising as candidates to be the perfect reinforcement for cement to be used in UHPC, combining quality strengths performance improvement and aiming to be the best cost-efficient solution. However, the relatively high cost of the materials, even with recent drop in prices due to improved fabrication technology, and the difficulties of dispersion due to van der Waals attraction forces, makes investigation necessary to obtain an accurate dosage and optimal dispersion.

Some studies have been made using carbon nanotubes (CNTs) and/or graphene oxide (GO) as reinforcing materials for the cement, proving that the increase on strength is possible when the material is properly proportioned and dispersed in it. There are not so many researches about it but the few already done seem promising. The newest studies focused on analyzing the characteristics and improvements of the CNTs&GO cement composite, showing great results reciprocally, as it seems that GO can ease the difficulties on CNT dispersion. However, analyzing the effects and viability on a UHPC with this nano-reinforcements has not been done yet. Even though some research has been made on the cement CNT&GO composite, few are the studies on the real performance of the final resulting UHPC using the cement analyzed, which is, in short, the ultimate objective of the research: to produce a UHPC of better characteristics that is economically applicable in future construction works, and compare it with other cheaper options to evaluate the applicability of the method.

As to advance on this subject, this thesis will focus on analyzing the possibility of increasing the mechanical properties of UHPC with CNT&GO cement composite and aggregating (or not) steel fibers in the mix. The final result of this work will be a better knowledge of their dosing, mixing and commissioning conditions as well as to identify the strength characteristics of the UHPC obtained from CNT & GO cement composites with aggregated (or not) steel fibers.

The properties of these new UHPCs will be identified and reproduced in a finite element model. The results of this finite element study will provide more information to help establish a prediction material model for the behavior of the concrete which will facilitate its study.

In order to achieve the proposed objective, a laboratory test campaign will be necessary to obtain experimental results of the characteristics of a concrete made from different dosages of CNT & GO cement composite with the addition or not of steel fibers. The analysis and reporting of these trials and their results already constitute in themselves a very interesting partial result of this thesis since no other equivalent known tests have been reported.

The research to be completed in this thesis will be the opening to better knowledge about UHPC reinforced with new forms of nano-reinforcements and its results will be able to analyze its convenience on a commercial use.

Without question, as concrete demands on strength and performance are increasing constantly, the results obtained will be of great significance for further

studies on the future to accomplish the properties desired and create better concretes for the infrastructures that are to come.

UHPCs obtained from CNT & GO cement composites promise exceptional characteristics of strength and ductility that can open new perspectives in the design of concrete structures, lighter, more resistant and more daring. Identifying the properties of these new materials will allow us to reconsider the design criteria and mechanical quantities of reinforced and prestressed reinforcing steel, since the higher tensile and ductility resistance they present will allow lower reinforcing steel needs and better performance under extreme stress.

In addition, an interesting perspective is opened for the use of these materials in structures specially requested to dynamic loads since its greater elastic tensile strength limit should improve remarkably its behavior to fatigue, although this extreme will require of an experimental analysis beyond the purpose of this thesis. It is possible that, despite the excellent characteristics of these UHPCs, their application still does not spread massively because, given the high price of nanomaterials additions and the specialized handling required, the final cost of putting them in civil works will be initially disproportionate. However, the increasing demand for more and more performant materials, the constant decrease of the costs of manufacturing the nanomaterials and a better knowledge of their use and their properties, could allow that in a short time the use of this type of solutions to be cost-effective.

This thesis will be a great advance in the characterization and the study of the UHPC with CNT & GO cement composites collaborating with its knowledge and to have specific design tools and analysis for these advanced materials, which we still do not know enough today.

Chapter 2 - Literature review

- 2.1.- ULTRA-HIGH PERFORMANCE CONCRETE (UHPC)
 - 2.1.1.- UHPC Tests standards
- 2.2.- NANO-REINFORCEMENT
 - 2.2.1.- Nanoparticles
 - 2.2.2.- Carbon nanofibers and Carbon nanotubes
 - 2.2.2.1.- Mixing and Dispersion of CNT
 - 2.2.3.- Dosage and performance of MWCNTs
 - 2.2.3.1.- High range concentration composites
 - 2.2.3.2.- Low range concentration composites
 - 2.2.4.- Graphene Oxide (GO)
 - 2.2.4.1.- Dosage and performance of GO
 - 2.2.5.- CNT&GO composites, the co-effect
 - 2.2.6.- Cost of carbon nanotubes and graphene oxide
- 2.3.- NUMERICAL MODELING
 - 2.3.1.- Discretization method
 - 2.3.1.1.- Finite Element Method
 - 2.3.1.2.- Discrete Element Method
 - 2.3.1.3.- Choosing the software
 - 2.3.2.- Constitutive Equation
 - 2.3.2.1.- Examples of constitutive equations in compression
 - 2.3.2.2.- Examples of constitutive equations in tension
 - 2.3.2.3.- Proposed formulation of the constitutive equation

In this chapter a review of all the available literature on our topic is presented, focusing in UHPC, nanomaterials and numerical modeling. It will be documenting the state of the art of the UHPC materials and procedures, as well as overviewing the possible solutions to different problems.

2.1.- Ultra-High Performance Concrete (UHPC)

With the development of the infrastructure, a concrete with improved performance is urgently needed in the key projects such as high-rise buildings, cross-sea bridges, subsea tunnel and hydraulic or marine works [3]. For this, a new kind of concrete was developed being referred as Ultra High-Performance Fibre Reinforced Concrete (UHPRFC) [4], sometimes characterized by being a steel fibre-reinforced cement composite material, even though it can include all kinds of fibres. Compared with the conventional concrete, UHPC implies a concrete with considerably improved performances such as high strength, high durability, high chloride ion migration resistivity, high freeze resistance, high sulphate resistance, low shrinkage, low abrasion and low carbon footprint etc. [5,6] with compressive strengths over 150 MPa, tensile strength over 7 MPa and ductile behaviour under mechanical load [7].

Many types of UHPRFC have already been developed worldwide with different mix compositions, types and amounts of fibers, flowability, compressive strength, tensile behavior, thermal curing, etc. However, according to the most recent standards in UHPRFC (AFGC, 2013) (NF P18-470, 2016) (SIA 2052: 2014-12), a general definition of UHPRFC has been proposed:

“Ultra-High Performance Fibre-Reinforced Concrete (UHPRFC) is defined as a hydraulic cement-based composite material, which combines three technologies in concrete: (i) high characteristic compressive strength of more than 130 MPa; (ii) ductile behaviour under tension due to the presence of fibres, which can provide or not a pseudo strain-hardening stress-strain response accompanied by multiple cracking depending on fibre volumetric fraction, fibre aspect ratio, and also fibre distribution inside the structural element; (iii) a special selection of fine and ultrafine aggregates that provides dense particle packing, high durability and certain degree of flowability.”[94]

Although before it was defined as a concrete exhibiting a compressive strength higher than 150 MPa, nowadays this is corrected and adjusted to the optimum solution to guarantee competitiveness for several applications falling within the 130 MPa range [95]. Anyway, this high compressive strength of the matrix is achieved by using only fine aggregates that ensure good homogeneity and compactness and the appropriate granular mixture also reduces the air entrapped and creates a rigid structural skeleton.

Even though, there are multiple mix designs for UHPC, essentially changing the additional fibers and aggregates, the typically used raw materials are Portland cement, quartz powder, silica fume, quartz sand (with a grain size no higher than 2 mm), superplasticizer and water, and with a water to cement ratio that is commonly lower than 0.25. Fibers provide increased toughness and tensile strength to the cement matrix by carrying part of the applied load and above all, permitting crack and pore-bridging capabilities [22].

The general used fibers are made of steel, and most of them are smooth-straight steel fibers with a length range of 6 mm to 20 mm, and with a slenderness ratio above

65 (to improve the matrix-fiber bond) and below 80 (to improve workability). Although their use is less frequent, twisted and hooked-end fibers can also be employed as well as a combination of different fiber types when specific requirements need to be fulfilled. The use of different types and amounts of fibers leads to distinct tensile behaviors and they play an important role in the pre- and post- cracking behavior. Commonly, the fraction of fibers used ranges from 2% to 6% by volume [94].

Constituents of a typical UHPFRC (Ductal®, the most used UHPC in North America and available off-the-shelf) can be found in Table 2-1:

*Table 2-1 Constitution list of typical Ductal® UHPFRC [13].
(HRWR=high-range water-reducing admixture, Portland Cement Type 1)*

Material	kg/m³	Percentage by Weight
Portland Cement	712	28.5
Fine Sand	1,020	40.8
Silica Fume	231	9.3
Ground Quartz	211	8.4
HRWR	30.7	1.2
Accelerator	30.0	1.2
Steel Fibers	156	6.2
Water	109	4.4

The Portland cement to be used should be Type 1 Portland cement, and if possible with moderate fineness and C3A content significantly lower than 8 percent. It was found that the best performance comes with C3A<4%, Na2Oe <0.4% and the specific surface should be about 3400 cm²/g.

Fine sand was researched and found that the optimal diameter size should be around 0-2 mm (QQ) and ground quartz sizes smaller than 1 mm and bigger than 10µm. Silica fume would be better with very low carbon content.

As reference, the HRWR used for Ductal composite is GLENIUM 3000 NS, a polycarboxylate superplasticizer, and the accelerator in use is RHEOCRETE CNI, which is an additive formulated with a calcium nitrite base to inhibit the corrosion of steel in reinforced concrete and also works as an accelerator.

Even though UHPC is an outstanding material, there is always a further step to be reached in science. Hence, some studies have been carried out on micro- and nano-reinforcing the UHPC composites through different sized aggregates. Micro-reinforced ultra-high-performance concrete is already a reality, thanks to early developing companies like Ducon® [15], which has been used in the construction of the New World Trade Center of NY.

In addition to high compressive strength, durability and abrasion resistance of UHPC, micro-reinforced UHPC is characterized by extreme ductility, energy absorption and resistance to chemicals, water and temperature. The continuous, multi-layered, three dimensional micro-steel mesh exceeds UHPC in durability, ductility and strength.

The performance of the discontinuous and scattered fibers in UHPC is relatively unpredictable. Micro-reinforced UHPC is used in blast, ballistic and earthquake resistant construction, structural and architectural overlays, and complex facades.

Although the inclusion of microfibers enhances the ductility and toughness [23], microfibers pose problems to the reinforced cement by entrapping air voids and degrading workability. Even though it has been demonstrated that, in the presence of large cracks, microfibers will form a dense system of micro-cracks allowing the concrete to reduce the crack size, they fail to stop the initiation of cracks. In this regard, nanomaterials present a better solution than traditional fibers because the former provides reinforcement or modification at the nanoscale being able to reinforce the matrix to prevent cracks [24].

Following the previous argument is why the most recent investigated UHPC is including nano-reinforcement, which means the reinforcement of concrete using nanometre-size particles, platelets, or filaments. These materials can be arranged depending on their shape: 0D nanoparticles like nano-silica (nS), 1D nanofibers such as carbon nanotubes (CNT) and carbon nanofibers (CNF) and 2D nano-sheets like graphene oxide (GO).

We can see the summarisation of different properties of material on the following Table 2-2:

Table 2-2 Material properties of typical fillers [25].

Material	Elastic modulus (GPa)	Tensile strength (GPa)	Elongation at break (%)	Density (kg/m ³)	Diameter/ thickness (nm)	Surface area (m ² /g)	Aspect ratio
Graphene	1000	~130	0.8	2200	~0.08	2600	6000-600,000
GO	23-42	~0.13	0.6	1800	~0.67	700-1500	1500-45,000
CNTs	950	11-63	12	1330	15-40	70-400	1000-10,000
Carbon fiber	7-400	0.4-5	1.7	1770	6000-20,000	0.134	100-1000
Polymeric fiber (Polypropylene and Nylon)	3-5	0.3-0.9	18	900	18,000-30,000	0.225	160-1000
Glass fiber	72	3.45	4.8	2540	5000-10,000	0.3	600-1500
Steel fiber	200	1.50	3.2	7800	50,000-900,000	0.02	45-80

In a research by [9], they found that both straight and twisted steel fibers embedded in UHPC with CNT had the slip-dependent bond stress higher than that of UHPC without. Whereas half the fibers broke during pulling out of UHPC, all the fibers broke during pulling out of UHPC with CNT matrices and exhibited improved bond behavior before failure, suggesting the use of CNT for UHPC.

The emergence of carbon nanotubes and lower-cost nanomaterials (e.g., carbon nanofiber) offers new opportunities for balanced improvement of concrete materials properties. The close spacing of nanomaterials benefits their ability to hinder the formation and propagation of fine microcracks in concrete. The distinct geometric attributes and mechanical characteristics of carbon nanotubes (CNTs) and carbon nanofibers (CNFs) could be used to complement the reinforcing effects of conventional fibers towards significant improvement of diverse concrete material properties.

Explanatory studies undertaken in recent years have demonstrated the value of graphite nanomaterials (CNTs and CNFs) in cementitious pastes as far as uniform

dispersion and adequate interfacial bonding of nanomaterials are ensured. Graphite nanomaterials improve the crack resistance of cementitious paste at relatively low volume fractions, while preserving acceptable fresh mix workability.

In UHPC, which relies upon a high packing density to realize distinct material properties, nanomaterials could further improve the packing density by extending the size distribution of particulate/fibrillar matter well into the nanoscale region. [96]

As an example Sbia, L. A. et al., in their optimization of UHPC with nano- and micro-scale reinforcement [14], which comprised Polyvinyl Alcohol fiber and Carbon Nano Fiber with 0.37% and 0.047% respectively, by volume of UHPC, discovered an improvement of flexural strength and compressive strength of plain UHPC by 9.2 and 7.5%, respectively. This indicates that even at low concentrations of CNT, there is an improvement in the mechanical properties of the UHPC.

2.1.1.- UHPC Tests standards

As it was explained before, UHPC has compressive strength, flexural strength and tensile strength that are way bigger than those of regular concrete. Taking this into account, and thinking on a lab context, we will need smaller size specimens to be able to reach the maximum strength as if we were doing it in regular concrete. However, it is important to notice that in different researches, the smaller cylinders and cubes had a larger standard deviation compared to the bigger ones.

Compressive strength is an important property in the design of any concrete structure. It is also the property that is most frequently measured. Both cylinder and cube compression test methods can be used for conventional concrete and are appropriate for the determination of UHPC compressive strength. Minor modifications to the test code and analysis methods may be required.

Some researches [7,18] also investigated the effect of cylinder and cube size on the measured compressive strength and cubes had compressive strengths about 5 percent higher than the cylinders.

The Federal Highway Administration, USA [7], and Kay Wille and Kenneth J. Loh [9] and [18] reported that the compressive strength determined through the use of an ASTM C109 type of test on concrete cubes is very similar to the strength reported with ASTM C39 tests on cylinders. Thus, cubes, which do not require end preparation of the specimen, will be used as a surrogate for cylinders.

As UHPC is a hydraulic cement-based composite with small particle size, the testing codes for mortar can be used as they might represent the UHPC better than the codes for regular concrete with big aggregate size. In accordance with ASTM C109 and C109M procedures and previous presented researches, compression strength tests can be performed on cubic specimens with an edge length of 50 mm (2 in.). Three specimens should be made for each period of time. [19].

Also, according to ASTM C348 and C349 and suggested on the research by [97], it is possible to perform a compressive strength test using the halves specimens from a finished flexural 3-point bending strength test, therefore creating less specimens.

As for the flexural strength test, the ASTM C348 [20] procedures stated the use of three-point bending tests on 40×40×160 mm (1.6×1.6×6.3 in.) specimens fabricated from UHPC. Three or more specimens should be made for each period of time [20]. The experimental results obtained must be analysed to obtain their equivalent bending strength, σ , using the following equation: [7,9]

$$\sigma = \frac{3 * F * L}{2 * B * H^2} \quad (2.1)$$

where

F = maximum load applied,

L = span,

B and H = specimen depth and height, respectively.

Another available alternative [94] is using a 4-point bending test following the ASTM C1609 code, with the loading bearings located at thirds of the span.

To obtain the stress-strain curve of both the compressive and tensile behaviour, it is widely documented [7,13,94] the use of LVDTs to measure the strain of the specimen and a load/strain control machine.

The compressive stress-strain curve is easily obtained by the same C349 test code using the aforementioned instrumentation and applying an equation to obtain the stress, σ , from the load (F)/applied area (A) relation:

$$\sigma = \frac{F}{A} \quad (2.2)$$

The tensile stress-strain curve however, has more difficulties as performing accurate direct tensile test is not easy and it usually leads to mistakes, either by wrong specimen cracking or wrong test procedure. This is why other method to obtain an indirect tensile behaviour were analysed, named tensile splitting test and flexural test.

The tensile splitting and flexural tests are preformed using cylinder and prism specimens, respectively. These tests are widely used for normal concrete and easy to perform due to their simplicity and commercially available equipment.

The cylinder splitting test for normal concrete is defined by many standards [99,100]. This method is preferable for brittle material testing (such as normal concrete) where complete failure occurs with a single crack. However, such test should be avoided for UHPFRC, in which considerable compressive crushing occurs at the platens of the testing machine due to steel fibre content. In this test, the specimen is subjected to a complex combination of shear, tension, compression stresses with significant stress gradients which may result in an inaccurate tensile strength result [98,101]. The local

zones of high compressive stresses at the extremes results in higher values than the actual tensile strength [102].

On the other hand, flexural test methods, whose implementation is well established, present a test procedure capable of assessing this property. Nevertheless, these methods provide indirect information and need to be complemented by inverse analysis in order to quantify the intrinsic tensile behaviour of tested materials. Moreover, bias or scatter can be induced when simplified constitutive laws are assumed for the analysis. Flexural tests are also used to determine the tensile strength of normal concrete and UHPFRC.

In this test, notched and unnotched prism specimens are tested in three or four-point bending and detailed guidance is provided in several standards [e.g. 103]. This method of testing is based on simple beam-bending theory and linear elastic stress-strain behaviour up to failure. However, concrete is a non-linear material and the assumption of a linear stress distribution is not valid. Therefore, results obtained using this method is always greater than the direct tensile strength. [12]

On the extended research by López [94] about the characterisation of tensile behaviour of UHPFRC, the different test methods are explained, remarking the use of the 4-point bending test ASTM C1609, that with the help of finite element modelling, proves as the simplest and easiest test method to reproduce in a lab environment test.

2.2.- Nano-reinforcement

In the past 30 years, there have been many studies on newly produced nanomaterials such as nanosilica, nanofibers, carbon nanotubes (CNTs) and graphene oxide (GO) sheets.

These nanomaterials may be classified according to their shape or morphology: zero-dimensional (0D) particles (e.g. nanosilica), one-dimensional (1D) fibers (e.g. CNT) and two-dimensional (2D) sheets (e.g. GO). [26] Nanomaterials are appreciated for their large surface areas that can be exploited for reaction with cement paste but, although they are beneficial as attachment sites for hydration products, there is great chance of agglomeration of nanomaterials because of the strong van der Waal attractive forces that exist at the nanoscale. Also, extra free water is needed to wet the large surface area of nanomaterials, thereby compromising the cement workability. Nevertheless, the tiny particles are able to fill the pores to provide a compact microstructure as well as having air purification, antimicrobial surfaces, and self-cleaning properties to the current conventional concrete. Thus, it is important to rightly mix and disperse the nanomaterials. Better performance is anticipated by reinforcing cement matrix at the nanoscale since their sizes are closer to that of calcium silicate hydrate (C–S–H) gel [27].

Unlike 0D nanoparticles, 1D fibers and 2D sheets behave as reinforcing materials to bridge cracks. Hence, it is essential for 1D fibers and 2D sheets to have high aspect ratios and intrinsic strength. [25].

Sanchez and Sobolev and Raki et al., [28]. Chen et al. [16] and Siddique and Mehta [17] documented the state of the art in the nanotechnology in cement and concrete, especially in the advancement made in experimental instrumentation and computational simulations as well as nano-engineering and nano-modification of cement-based materials using a broad range of nanomaterials, specially nanofibers and nanosheets. However, until recently, because of the technology and cost-efficiency, the use of nanomaterials was confined to cement and mortar matrices, with the long term view for commercial application in concretes.

2.2.1.- Nanoparticles

Nanosized particles have a high surface area to volume ratio (Figure 2-1), providing the potential for tremendous chemical reactivity. Much of the work to date with nanoparticles has been with nano-silica (nano-SiO₂) [29,30] and nano-titanium oxide (nano-TiO₂) [31,32]. There are a few studies on incorporating nano-iron (nano-Fe₂O₃) [33], nano-alumina (nano-Al₂O₃) [34], and nano-clay particles [35].

Among all the nano-materials, nano-silica is the most widely used material in the cement and concrete to improve the performance because of its pozzolanic reactivity, besides the pore-filling effect.

When nano-silica is added into cement, it promotes the hydration increasing the amount of C–S–H gel, which is responsible for the increase on compressive and flexural

strengths [36]. Concrete containing 4 wt.% nano-silica was recorded with compressive, tensile and flexural strengths greater than control specimens by 70%, 120% and 60% respectively after 28 days [37]. Addition of 10% nano-SiO₂ with dispersing agents was observed to increase the compressive strength of cement mortars at 28 days by as much as 26%, compared to only a 10% increase with the addition of 15% silica fume [38]. Small amounts (0.25%) of nano-silica were observed to increase the 28-day compressive strength by 10% and flexural strength by 25% [39].

Li et al. [38] reported 3-day compressive strength increase by 81% and also at later stages, same trend was observed with 4% nano-silica in high volume fly ash concrete. Sobolev K. et al. [28] reported that 2% nano-silica addition led to an increase of strength by 15–20%. These results lead to observe that optimum quantity of nano-silica to be used is still contradictory and further studies should be made. However, it was confirmed that the finer nano-silica supplies more filler and fewer weak zones when compared to the use of agglomerated nano-silica [40]. Recently, a study proves that nano-silica at 3% replacement of cementitious weight is the optimum percentage for high performance concrete admixture [120].

Nano-TiO₂ has proven very effective for the self-cleaning of concrete and provides the additional benefit of helping to clean the environment (41). Few studies stated a low improvement on concrete compression and flexural strength [28].

Even though nanoparticles were demonstrated to improve at some degree the strength of cement and concrete composites, it was found of interest to investigate on carbon fibers and carbon sheets, as their higher specific surface area (SSA) and smaller particle size (Figure 2-1), added to the mechanical properties that characterize them (Table 2-2), make these nano-reinforcement more suitable for construction materials, as they can also provide preliminary prevention for crack propagation.

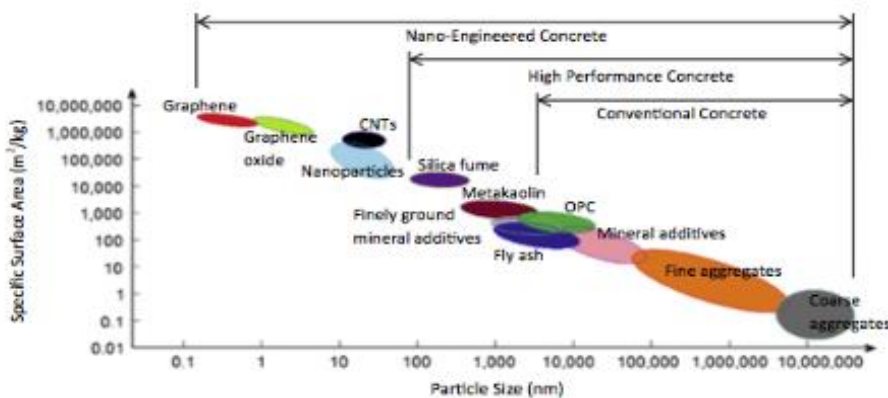


Figure 2-1 Comparison of nanofillers with supplementary cementitious materials and aggregates in concrete [25]

2.2.2.- Carbon nanofibers and Carbon nanotubes

Carbon nanofibers (CNFs), also known as Stacked-Cup Carbon Nanotubes (SCCNT), have a unique morphology in that graphene planes are canted from the fiber axis, resulting in exposed edge planes on the interior and exterior surfaces of the fiber, generally described as an ultra-high-strength material characterized by a high tensile modulus, tensile strength, electrical and thermal conductivity and corrosion resistance. Their properties can be seen on Table 2-2.

Carbon nanotubes (CNTs), are one-dimensional carbon nanofibers with hollow tubular structure, formed either by single wall (SWCNTs) or multi walls (MWCNTs) of rolled graphene sheets [21].

Unlike carbon nanotubes, CNFs are less affected by Van der Waals forces and tend to stay dispersed for longer periods of time. This difference enables the CNFs to be dispersed through purely mechanical processing techniques without the need for additional, and costly, processing steps, making CNFs easier and cheaper to process. In recent studies, there is proof of CNFs providing nano-bridges in fine cracks to compensate the autogenous shrinkage caused by silica flour [121]. Also, CNFs present numerous exposed edge planes along the surface that constitute potential sites for advantageous chemical or physical interaction. However, most research efforts have focused on CNTs compared to CNFs and have been performed on cement pastes, likely because of its own original mechanical properties (Table 2-2). [42,43]. Thus, and analyzing the information obtained from the studies and taking into account that is a newer material, it seems appropriate to focus this research on the use of CNT, as the possibilities are wider and the future looks more optimistic with decrease on costs.

As it can be seen in Table 2-2, even that SWCNTs have higher Young's modulus and strength when compared to MWCNTs, the use of the former in industrial applications is limited due to their high cost and difficulties associated with mass production. In [44] was experimented that although MWCNTs lack some of the desirable material properties of SWCNTs, they are still considered a useful material because of their relatively low cost, convenient mode of production, and easy dispersion. Therefore, it seems more practical to employ MWCNTs in cement composite applications, and many researchers have attempted to incorporate MWCNTs into cementitious materials.

Josef Foldyna et al. [45] also showed that MWCNTs are more widely used than SWCNTs because they are cheaper to manufacture and offer better reinforcement in cement composites, while proving its arising interest in scientific and industrial field due to their exceptional chemical and physical properties that make them suitable for numerous applications. The authors stated that because of the nanometer-range diameters and high aspect ratios of MWCNTs, one can potentially enhance the compressive strength of UHPCs and the bond behavior of embedded steel fibers. Morsy et al. [46] concluded that MWCNTs reinforce the voids inside cement through a bridging effect.

However, there are also disadvantages of using CNTs as reinforcement for cementitious composites and they have been widely reported. Firstly, as said before, the strong van der Waals force between CNTs makes it difficult to disperse them homogeneously, due to large surface-area-to-volume ratio (Table 2-2), making CNTs tend to attract agglomerate and sediment. Secondly, the hydrophobicity (repelling water) of CNTs leads to weak bonding of CNTs to the cement matrix [47].

2.2.2.1.- Mixing and Dispersion of CNT

Knowing the problems of agglomeration that can affect the CNT, good dispersion is essential for an efficient use of the products. As stated by many authors, good dispersion can be achieved by use of ultrasonic mixer with surfactants in aqueous solution, with specific time and amount of energy. [14,40] Zou et al. and Josef Foldyna et al. [45] obtained the best mechanical performance of CNTs/cement pastes with ultrasonication energy of 20 J/mL per unit CNTs to cement (C/c) with 84% of maximum dispersion [48], taking care that excessive force should not be applied as CNTs might tear into pieces. Compatibility of surfactant with cement is also very important, as the hydration, chemical reactions and hardening process could be delayed or even stopped [49]. Musso et al. [26] demonstrated that excessive water content could prevent adequate hydration and thus degrade the compressive strength of cementitious composites. As researched by Josef Foldyna et al. [45], the following methods are suitable to improve dispersion:

- Ultra-sonication of solution to facilitate dispersion
- Using a surfactant to improve affinity between carbon nanotubes and matrix
- Chemical modification of CNTs

Chemical activation places functional groups on the surfaces of CNTs and facilitating dispersion as well as improving the bonding between CNTs and the matrix. Methods include surface modification with exposure to ozone gas at high temperatures and the formation of carboxyl groups through acid treatment. The formation of carboxyl groups on the surface improves the bonding by inducing chemical reactions with hydraulic cementitious materials. Kang et al. used acid treatment to improve tensile and compressive strength by more than 30% without any surfactant [47].

2.2.3.- Dosage and performance of MWCNTs

Several research groups have investigated the use of MWCNTs in cementitious composites, with the main researches exposed below, and more available as a summary in the Table 2-3. Concentrations are always presented as wt%, by weight of cement.

Table 2-3 Summary of CNT, GO and CNT&GO researches.

Reference	Matrix	Material used; wt%	w/c	Results (increased %)	Methodology	
CNT	[78]	Concrete	MWCNT 0,003%	0,2	Compressive: 17,65%	Mixing
	[78]	Mortar	MWCNT 0,01%	0,2	Compressive: 21,2%	Mixing
	[9]	Paste	MWCNT 0,022%	0,22	Improved bond behavior	Mixing and superplasticizer
	[79]	Paste	CNT 0,048	0,5	Elastic Modulus: 75% Flexural: 50%	Debulking, sonication and surfactant
	[80]	Paste	FMWCNT 0.02–0.09%	0,4	Compressive: 97,2%	Sonication and purified from carboxylated carbonaceous fragments
	[55]	Paste	MWCNT 0,08%	0,4	Elastic Modulus: 35% Flexural: 40%	Sonication and surfactant
	[56]	Paste	MWCNT 0.08%	0,48	Elastic Modulus: 35% Flexural: 35%	Sonication, surfactant and swing centrifugation
	[57]	Paste	MWCNT 0.08%	0,3	Elastic Modulus: 45% Flexural: 25%	Sonication and surfactant
	[58]	Paste	MWCNT 0,08	0,35	Flexural toughness index: 57.5%	Sonication and Gum Arabic surfactant with tributyl phosphate defoamer
	[43]	Paste	FMWCNT 0.045–0.15%	0,25 ; 0,3	Compressive: 50% Flexural: 10%	Sonication with Polyacrylic acid
	[49]	Paste	MWCNT 0.04–0.2%	0,4	Flexural : 269% Ductility: 81%	Sonication and water reducing admixture ADVA cast 575
	[59]	Paste	N-doped CNTs 0.05, 0.25%	0,5	Compressive: 40%	Sonication and surfactant (Brij35 and foam reducing agent)
	[46]	Mortar	MWCNT 0.005, 0,11%	0,5	Compressive: 29%	Dry mixing
	[83]	Mortar	MWCNT 0,1%	0,45	Compressive: 7,5%	Sonication
	[84]	Paste	CNT&CNF 0,1/0,2%	0,4	CNF 0,1% 7d: Flexural 82%	Ultrasonication and surfactant
	[60]	Mortar	MWCNT 0,1%	0,5	Compressive: 7% Bending Strength: 6%	Mixing and Ultrasonication
	[81]	Mortar	0.15% MWCNT and 10% silica fume	0,25	Compressive: 32%	Mixing and 1.6% Polycarboxylic acid admixture
	[54]	Paste	MWCNT 0.25%	0,5	Load capacity: 47% Toughness: 25%	Sonication and polyvinylpyrrolidone organic solvent
	[50]	Mortar	Functionalized MWCNT 0.5%	0,45	Compressive: 19% Flexural: 25%	Sonication and carboxylation with sulfuric and nitric acid
	[26]	Mortar	Annealed MWCNT 0.5%	0,4	Compressive: 11% Flexural: 34%	Sonication with acetone and modified acrylic polymer and superplasticisers
	[82]	Mortar	FMWCNT 0.3–0.75%	0,4	Modulus: 14% Compressive: 12% Splitting tensile: 34%	Naphthalene-sulfonate plasticizer and modified polycarboxylate admixtures
	[51]	Paste	MWCNT 0.5–1%	0,4	Compressive: 15% Splitting tensile: 36%	Sonication
	[53]	Mortar	MWCNT 0.5, 1%	0,5	Compressive: 10%	Sonication for 10 min
	[16]	Paste	MWCNT 0,5%	0,22	Compressive: 12%	Sonication
	[52]	Mortar	MWCNT 0,5%	0,5	Flexural: 30%	Ultrasonifacion and acrylic polymer surfactant
	[85]	Mortar	MWCNT 0,25 to 1%	0,4	Compressive: 26%	Sonication
	[86]	Paste	0.75% MWCNT and 0.25% CF	0,4	Flexural: 88.42% Load carrying capacity: 366.67%	MWCNT: sonication in ethanol CF: sonication in hydroxyethyl cellulose (HEC)
	[87]	Paste	MWCNT/SWCNT 1%	0,36	Compressive: SWCNT : 6% MWCNT: 30%	Ultrasonication
[88]	Paste	MWCNT 0.5–2%	0,35-0,6	Compressive: 25%	Sonication and polycarboxylate admixture	
GO	[65]	Mortar	GO 0,08%	0,2	Compressive: 24,8%, Tensile: 37,7%, Flexural: 80,6%, Toughness: 105%	Mixing and superplasticizer
	[71]	Paste	GO 0,05%	0,37	28 d Compressive: 40,4%, Flexural: 90,5%	Mixing and Polycarboxylate superplasticiser
	[70]	Paste	GO 0,01-0,05%	0,33	0,03%-Compressive: 56,62%, 0,04%-Flexural: 25,28%	Ultrasonication
	[69]	Paste	GO 0,05%	0,3	Compressive: 15-33%, Flexural: 41-59%	Mixing and superplasticizer
	[68]	Mortar	GO 0,03%	0,37	Compressive: 38,9%, Flexural: 60,7%, Tensile: 78,6%	Mixing and polycarboxylate superplasticizer
CNT + GO	[62]	Water	0,05% SWCNT + 0,05% GO	N/A	Formation of a black stable suspension	Sonication
	[74]	Paste	0,5% SWCNT + 1,5% GO	0,3	Bending strength: 72,7%	Ultrasonication

2.2.3.1.- High range concentration composites

On one side, there's a group of researchers with tendency on using, mainly, 0.5wt% or over MWCNT concentrations.

Li et al. [50] examined the mechanical performance of cement composites by fixing the MWCNT concentration at 0.5 wt% (% weight of cement) and comparing the resulting compressive and flexural strengths to those of normal concrete, having the best pore refining effect on that proportion, with the total porosity decreased by 39%.

Cwirzen et al. [43] conducted a study whereby the compressive strength of cement mortar mixed with an aqueous solution of 0.5 wt% MWCNTs functionalized by carboxyl groups was compared to that of cement mortar mixed with a pure MWCNT solution. It was found that the carboxyl groups stabilized the MWCNTs within the composite mortar, thereby improving the compressive strength.

On the contrary, Musso et al. [26] found that 0.5% carboxyl-functionalized MWCNTs adversely influence the compressive and flexural strength of cementitious specimens. Consistent to that, it was claimed that commercially obtained functionalized CNTs are inferior to pristine and annealed CNTs, the latter obtaining compressive increase of 11% and flexural increase of 34%.

As for the mechanical properties of composites, Kumar et al. [51] and [52] conducted compressive strength tests determining that the highest value for all curing ages was when the MWCNT concentration was 0.5 wt%. However, it was lower when the MWCNT content was increased to 1.0 wt%. Moreover, Kowald [16] incorporated 0.5wt% MWCNTs in a UHPC (water/cement ratio = 0.22) and observed a 12% increase in compressive strength and an influence of MWNTs on the hydration products.

Contradictorily, Chaipanich et al. [53] compared the strength of MWCNT-cement mortars with MWCNT concentrations of 0.5 and 1.0 wt% to that of OPC mortar, concluding that the 0.5 and 1.0 wt% MWCNT cement mortars had compressive strengths that were 7% and 9% higher, respectively, than that of OPC mortar.

Chan et al. [54] employed industrial grade MWCNTs with a purity of 90 wt% and a concentration of 0.25 wt%. It was found that CNTs increased the load-carrying capacity by about 47% and toughness by 25% on average. Industrial grade MWCNTs are usually cheaper and could lead to the creation of a cost-efficient composite.

Furthermore, and as a reference for our MWCNT supplier (www.sunnano.com), Kowald T. [16] analyzed the addition of 0.0%/0.25%/0.5%/0.75% and 1% in UHPC, concluding that the highest increase in compressive strength was on 0.5% untreated MWCNT addition, by 12% after 14 days.

2.2.3.2.- Low range concentration composites

On the other side, there's some other studies based on low concentrations of MWCNTs and their performance, analyzing that only a small amount of effectively dispersed CNTs is needed to achieve an enhanced reinforcing effect of the cementitious

matrix and the production of a low-cost nanocomposite, and they have less negative effects for the workability.

Metaxa ZS et al. [55,56,57] found that small amounts of effectively dispersed MWCNTs (0.025–0.08 wt.% of cement) can significantly increase the strength and the stiffness of the cementitious matrix. In particular, lower amounts of long MWCNTs (0.025–0.048 wt.%) provide effective reinforcement, while higher amounts (close to 0.08 wt.%) of short MWCNTs are required to achieve the same level of reinforcement. On the same tendency was the study of Al-Rub et al. [49], showing that low concentration (0.04 wt.%) of long MWCNTs give comparable mechanical performance to the nanocomposites with higher concentration of short MWCNTs.

Consistent with the previous studies, Shah et al. [26] found that, after dispersion in water using surfactant and ultrasonic energy, small amounts of CNTs (0.048 wt.% and 0.08 wt.%) produced a significant (50 %) increase in the Young's modulus of cement paste, and Wang B et al. [58] experimented the flexural toughness index of composites increased by up to 57.5% for a 0.08 wt.% addition of MWCNTs, also having lower porosity and a more uniform pore size distribution.

Cwirzen A. et al. [43] observed the highest increase in the compressive strength was nearly 50% in cement paste incorporating only 0.045% of the the polyacrylic acid polymer-treated MWCNTs, and 10% for flexural strength, similar to the stated by Sobolkina A et al. [59], modification of the cement pastes with dispersions of CNTs 0.05% led to an increase, up to 40%, in compressive strength and, in some cases, to a moderate increase in tensile strength.

Regarding the use of low concentrations in UHPC, Kay Wille and Kenneth J. Loh [9] proved the bond behavior of steel fibers pulled out of UHPP and UHPC significantly increased with the addition of low concentrations of MWCNTs (1-mg/mL MWCNT solutions or 0.022% relative to cement weight) within the concrete mix.

The highest MWCNTs concentration permitted was experimented by Camacho et al. [60] and Sobolkina A et al. [59] and Morsy MS et al. [61] over 0.1~0.25 wt%, leading to a decrease in the compressive strength after that point.

In all cases of low concentration, the maximum concentration stated where further from it the mechanical properties start to decrease is about 0.08 wt%, and is selected for some authors as the optimal dosage. In the following Figure 2-2 it can be seen a relation between the amount of Superplasticizer and amount of CNTs for low concentrations according to aspect ratio of CNTs.

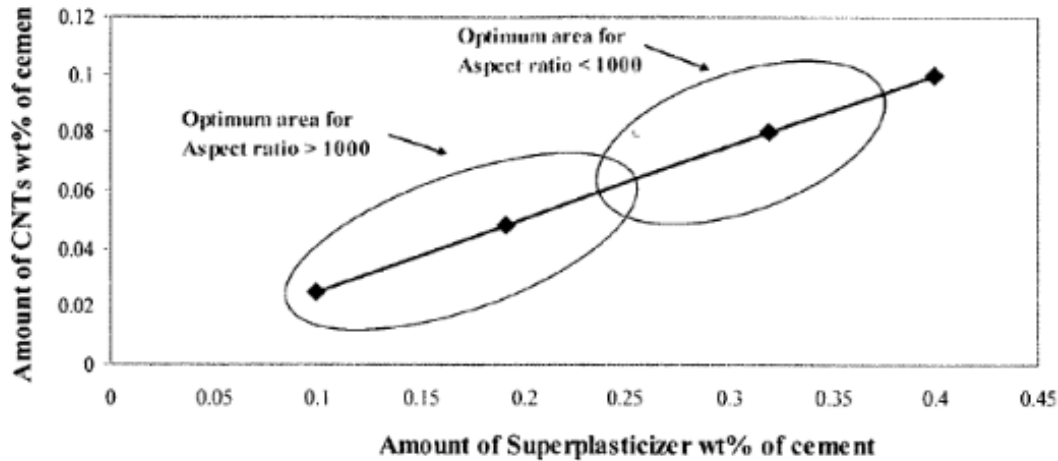


Figure 2-2 Optimum amount of MWCNTs and superplasticizer according to the aspect ratio of CNTs. [52]

It can be concluded that for being able to create a cost-efficient composite, it is necessarily to correctly perform the dispersion and mixing of the materials but also as important is to select the optimal concentration for the specific case. Thanks to the previous studies, we are able to select three concentrations to use on our tests and be able to select the optimal. It is not possible to choose only one dosage as the different studies differ on two main concentrations, and a third one should be taken as an intermediate dosage to find the optimal one. Thus, the concentrations taken will be 0.08%, 0.25% and 0.5%, which seemed to be rather persistent in the literature showing good improvements on composites.

2.2.4.- Graphene Oxide (GO)

A newly investigated cementitious composite reinforcement is graphene oxide (GO), an oxidation product of graphite. Few are the articles reporting mechanical properties investigations with this cementitious composite, presented here. A summary is presented in the previous Table 2-3.

Min Wang et al. researched on its chemical properties to found that GO not only possesses the perfect mechanical properties, but also contains many active groups in the GO sheet, such as hydroxyl groups ($-OH$), epoxy group ($-CH(O)CH-$) and carboxyl group ($-COOH$). These oxygen-containing functional groups render GO sheets hydrophilic and highly dispersible in water [62,63], altering the van der Waals interactions between the GO sheets. Therefore, two-dimensional GO offers a larger surface area for C-S-H nucleation than the much-researched CNTs.

It is also hypothesized, [27] that the carbon-based nano-material can enhance the pore structure of cement matrix in such a way that would enhance the concrete permeability to resist fluid ingress and subsequent chemical attacks. This is in addition to the chemical and electrical influence of GO on cement matrix, which could play an important role to impede steel reinforcement corrosion process.

However, it is also demonstrated in recent researches that GO is hydrophilic enough to absorb most of the water contained in the cement mortar, and it has been shown to hamper the proper hydration of the cement, making dispersion of the GO within the matrix difficult. Thus, Dimitar Dimitov et al. show that it is important to add the GO as water-stabilized graphene dispersions [122].

Several authors used the general approach to synthesize the GO by exfoliated graphite using the chemical method at which concentrated acids with help of a strong oxidizing agent yield graphite oxide [40] and according to the modified Hummers' method [64,65]. Other researchers [66] acquired the GO on the market on form of solution, to assure an investigation not dependable on errors made on the synthesis of GO.

Also, it was found that utilizing the aforementioned property of high water dispersion of GO, makes cement based-materials mixing practical (more applicable than mixing cement with GO as powder, and easier to mix than CNT) thus, it is practical to obtain them in form of a solution of aqueous oxidized graphene.

2.2.4.1.- Dosage and performance of GO

In the contrary of CNTs, there is more agreement on the concentration to be used, generally using more or less the same amount.

Mohammed A. et al. [66], incorporated GO in the cement mixture at three different percentages namely, 0.01%, 0.03% and, 0.06% (wt%), concluding that the effectiveness strongly depends on GO fraction and further test should be made with different proportions and, although small modifications on cement pore distribution were found, Gong et al. [67] reported that the introduction of 0.03 wt% GO into cement paste increased the compressive strength and tensile strength by more than 40%. Furthermore, Shenghua Lv. Et al., [68], indicated that tensile and flexural strength increased by 78.6% and 60.7% with increasing GO dosage up to 0.03%, but decreased on higher dosage.

M. Wang et al. [70] used GO addition of 0.03% and obtained the maximum flexural strength increase, by 56%, whereas using a concentration of 0.04% the compressive strength reached its maximum increasing by 25%. They concluded that the ideal GO content in that research was 0.03–0.04 wt%.

Shenghua Lv. Et al. [68] found the compressive strength increased, at its highest, by 47.9% until GO dosage was 0.05 wt%. In the same way, Z Pan et al. [69] reported an introduction of 0.05 wt% GO increasing the GO–cement composite compressive strength by 15-33% and also, an increase on the flexural strength by 41–59%. Qin Wang et al. [71] also experimented an increase when the dosage of GO was 0.05%, the flexural strength of hardened cement paste increased by 86.1, 68.5 and 90.5% and the compressive strength by 52.4%, 46.5% and 40.4% at 3, 7 and 28 days, respectively.

C. Lu et al. [65] added 0.08 wt% GO leading to 24.8% increase in compressive strength, 37.7% increase in tensile strength while ultimate strain remained unchanged, 80.6% increase in flexural strength and 105% increase in flexural toughness.

As aforementioned and reviewed, most of the studies use a GO concentration near or exactly 0.04 wt%, with similar results and performance. Thus, this will be the concentration use in this research.

The latest researches about nanomaterials focus on joining both the CNTs and the GO, as to take advantage of their positive properties co-effect. As some studies suggested [65,72,72], using GO to interact with CNTs should be possible.

2.2.5.- CNT&GO composites, the co-effect

The latest researches about nanomaterials focus on joining both the CNTs and the GO, as to take advantage of their positive properties co-effect. As some studies suggested [65,72,72], using GO to interact with CNTs should be possible. As they are both fairly new nanocomposites, the literature regarding the addition of a combination of CNT and GO in cement or concrete composites, is still short. A summary is presented in the previous Table 2-3.

Ling Qiu et al. [62], were the first to combine them and found that sonicating a mixture of GO dispersion and CNTs powder (0.05 wt %, respectively) resulted in the formation of a black suspension. The suspension was very stable and no visible sediment was observed over two years. When the content of GO and CNT was increased to 0.5 wt %, a GO/CNT hydrogel was formed. In contrast, no hydrogels were produced when only single components were used at the same concentrations. The formation of the GO/CNT hydrogel at such a low solid content indicated a strong interaction between GO and CNTs. However, no test on cement/concrete was done.

In the research of Xueguang Li et al. [74] it was the first time that both combined and separately samples of SWCNTs and GO, were used to research about the co-effect of these materials in a cement composites mechanical properties test. The paper concludes that the mixture of graphene oxide (GO) sheets and single-walled carbon nanotubes (SWCNTs) exhibited an excellent co-effect, leading to 72.7% increase in bending strength of cement, which is much larger than the strength enhancements contribution of both materials separately, being 51.2% by GO and 26.3% by SWCNTs in each case. The optimum amounts of GO and SWCNTs that they experimented were 1.5 wt% and 0.5 wt% respectively. Furthermore, it was demonstrated that the bending strength of cement composite materials with GO and SWCNTs is proportional to the sizes of crystal SiO₂ particles and so, the combination of SWCNT and GO makes the particle size of SiO₂ even larger.

The authors proved that the larger the crystal particle size is, the smaller the number of weaker connection between particles, as the connection between crystals is weaker than the chemical bond between particles [74].

Recent studies investigated the dispersion of GO/CNT suspensions and mechanical and microstructural properties in GO/CNT Portland Cement pastes in time- and power-controlled ultrasonication with a horn sonicator, coming to the conclusion that the increment of ultrasonication time and power may effectively enhance the dispersion of GO/CNTs powders in solutions until the dispersion plateau is reached, confirms that the ultrasonication time plateau occurs after 15 min and the ultrasonic power plateau occurs from 81 to 94 W [113].

2.2.6.- Cost of carbon nanotubes and graphene oxide

Commercialization of carbon nanotubes and other electrically conductive nano-particles have been hampered by high cost and minuscule supply, but both limitations are well on their way to being resolved. These wisps of carbon appear to be headed toward a much broader scope of commercial use than the other less expensive nanomaterials.

The global carbon nanotube market size is estimated to be valued at USD 1.571 million in 2018 and is expected to witness a high CAGR of 17.09% until 2023, owing to increase in the utilization of carbon nanotubes in the electronics industry. [115] Technological advancement has greatly shaped this industry wherein the prices has declined from USD 900 per gram to just USD 30-40 per g, and even lower when buying in bulk.

Since its discovery, the CNTs has shown immense potential that could revolutionize the manufacturing industry. Increased dependency on carbon nanotubes will cut down the operational cost and thus increase the competitiveness level. Developed economies including North America and Europe are at the forefront of the race, wherein, CNTs leverage could help the regional players to compete with global players at competitive prices.

Furthermore, much of the demand for CNTs is expected to generate from construction sector and automotive sectors. As per the estimates, construction and automotive sector is expected to account for over 72% of total carbon nanotubes market size by 2021.

Most of the commercial activity involves the use of hollow multi-wall carbon nanotubes (MWCNTs), which are a single tube with five to 15 layers; and the closely related carbon nanofibers (CNFs). Less advanced commercially are single-wall carbon nanotubes (SWCNTs), which are hollow tubes with one layer. MWCNTs are easier to produce in high volume quantities than SWCNTs. However, the structure of MWCNT is less well understood because of its greater complexity and variety. The challenge in producing SWCNT on a large scale as compared to MWNT is reflected in the prices of SWCNT, which currently remain higher than MWCNT.

Although high cost is a barrier to commercialization of all these carbon nano-particles, prices of all types of carbon nano-particles are gradually declining, as capacities are being scaled up by old and new players alike.

Suppliers concede that various price reductions have occurred over the last few years for these carbon nano-particles. Within the last year, Nanocyl's MWCNT prices have dropped by as much as 40%, below \$200/kg down from \$275/kg, for multi-ton purchases. With recent scale-ups, prices are lower by a factor of 2 or 3 than 6 years ago. Other sources' prices of MWCNTs have dropped by more than 50% (\$300/kg versus \$700/kg, just 18 months ago.

This generalized tendency is expected to last for the next years and lower prices of carbon nanotubes are expected, as the production is scalable and the demand will continue to grow, according to experts. [113]

On the other hand, the cost-effective and scalable production of graphene still holds the key to its commercialization. In terms of mass production of graphene, the main factors are the production cost, scalability, reproducibility, processability and the quality of the graphene products.

Considering the low cost and abundance of graphite flakes, the wet chemical approaches in exfoliation of graphite to graphene seem to fit all the requirements, except that there is question on the quality of graphene. However, we should take note that the definition on the quality of graphene or rather the efficacy of graphene is highly dependent on its application.

The price of graphene is linked to its quality, and not all applications require superb material quality. For example, graphene oxide powder (graphene functionalized with oxygen and hydrogen) is inexpensive and has been used to make a conductive graphene paper, for DNA analysis, and for other advanced composite and biotechnology applications. Graphene oxide in solution sells for 99€ euros per 250 mL from Graphenea. On the contrary, mechanically exfoliated graphene comes in small, high-quality flakes. The price of such graphene can be on the order of several thousands of dollars per flake.

However, the most promising is CVD graphene, available with high quality from Graphenea, which offers sufficient quality for almost any graphene application, with low cost for bulk orders. [114]

Below there is a summary table of the market prices for the typical nanomaterials used as filler for different cement/concrete applications.

Table 2-4 Materials Costs

Product	State	Price per 100g
NanoSilica	Powder form	USD \$170-200
NanoAlumina	Powder form	USD \$600-750
NanoIron	Powder form	USD \$824-1.200
NanoTitanium Oxide	Powder form	USD \$150-1.000
Carbon Nano Fibers	Powder form	USD \$400-550
Single-Walled Carbon Nano Tubes	Powder form	USD \$2500-40.000
Multi-Walled Carbon Nano Tubes	Powder form	USD \$800-12.000
Graphene nanoplatelets	Powder form / Water dispersion	USD \$60-2.000
Graphene Oxide	Water Dispersion	USD \$350-30.000

For reference, all prices are obtained from the SigmaAldrich database as they have a broad portfolio of materials for science and engineering usage. Packaging of 100g is primary selected. Local suppliers might have better prices but less range of products.

2.3.- Numerical modeling

The numerical modeling for the calculation of structures are widely used since it allows to predict and to know the behavior of structures in phase of project or design and to verify before being constructed their resistant capacities. Numerical models allow us to test different material options or structural typologies to analyze and compare different solutions without requiring costly and complicated laboratory tests. With the numerical test of different solutions, we can reproduce project alternatives and evaluate, for example, which one would result in a lower cost of construction.

All methods of computation of structures, analytical or numerical, require knowing the mechanical and resistant characteristics of the materials with which we are working; we will typically need the relations between tension and deformation. When these relationships are complex (e.g., nonlinear relations, fractures, discontinuities ...) the use of numerical methods is imperative. From the first part of the works of this thesis, it will be possible to characterize sufficiently, through laboratory tests, the constitutive properties (stress-strain relationships) of the UHPC with CNT & GO.

2.3.1.- Discretization method

2.3.1.1.- Finite Element Method

At present, several commercial and / or academic FEM software are available (Abaqus, ANSYS, Cosmos, CivilFEM, Catia, SolidWorks, OpenFEM ...). In general, the configuration of these is simple because they already include some preconfigured cases of typical finite elements for the most common materials and structures. The software to be used will be selected from the ones available at the Tongji University, being able to access any software manuals needed.

Numerical modeling is a field widely studied and there is an assortment of literature available. Within the numerical methods of calculation, the Finite Elements Method is the most widely used, best referenced, best considered and widely accepted by the scientific community for multiple applications, and especially for the calculation of complex concrete structures. The finite difference method (FDM) is also a well-known alternative to the finite element method (FEM). The most attractive feature of the FEM is its ability to handle complicated geometries (and boundaries) with relative ease. The quality of a FEM approximation is often higher than in the corresponding FDM approach, but this is extremely problem-dependent and several examples to the contrary can be provided. Generally, FEM is the method of choice in all types of analysis in structural mechanics (i.e. solving for deformation and stresses in solid bodies or dynamics of structures) [89-92].

On the research by Ali A. Abbas et al. [75], the authors assessed steel fiber reinforced concrete structural members with a simplified finite element model,

concluding that the model employed, despite its simplicity, was capable of providing realistic predictions of the key aspects of structural behavior.

Faezeh Faghih and Ashraf Ayoub [76] reported a finite element modeling of carbon nanofiber concrete structural members demonstrating the enhanced behavior of concrete composite when CNF are introduced, taking into account the tensile properties of concrete. Parameters that describe the behavior of CNF concrete were found and used to characterize the behavior of a column and a beam member.

A numerical modeling of flexural enhancement in Carbon Nanotube/Cement Composite was showed by Lai Yin Christina Chan and Bassem Andrawes, [77] where numerical models already developed were calibrated using the experimental results, and it was verified that the numerical method could successfully predict the behavior of CNT/cement composite.

An important consideration for the research is that a finite element model is generally considered capable of yielding realistic predictions concerning the nonlinear response of concrete structures when the deviation of the predicted values from their experimentally measured counterparts (of particular structural characteristics) does not exceed a value of the order of 20%. [75]

2.3.1.2.- Discrete Element Method

One other method that is being developed is the discrete element method (DEM), also called a distinct element method, which is any of a family of numerical methods for computing the motion and effect of a large number of small particles. Though DEM is very closely related to molecular dynamics, the method is generally distinguished by its inclusion of rotational degrees-of-freedom as well as stateful contact and often complicated geometries (including polyhedra).

Within the analysis of solids with the DEM the material is typically represented as a collection of rigid particles (spheres in three dimensions (3D) and discs in two dimensions (2D)) interacting among themselves at the contact interfaces in the normal and tangential directions. Material deformation is assumed to be concentrated at the contact points.

Appropriate contact laws are defined in order to obtain the desired macroscopic material properties. The contact law can be seen as the formulation of the material model of the underlying continuum at the microscopic level. For frictional cohesive material, the contact law takes into account the cohesive bonds between rigid particles. Cohesive bonds can be broken, thus allowing to simulate fracture of the material and its propagation [95].

2.3.1.3.- Choosing the software

The most difficult part on working with these kinds of methods is understanding how to write the codes with the different available platforms or software. That is why we researched the most university used software and found out that Abaqus software

is an extensively used software, specially having a lot of documentation and support. As it has an user-friendly interface, it is easier to start learning the way it works and apply simple problems, to later be able to code our material in it.

As a simple guide, to model fiber reinforced concrete in ABAQUS, you should provide: Density, Modulus of Elasticity, Poisson ratio and concrete damage plasticity parameters included: plasticity, compressive behavior and tensile behavior. You can have tension or compression damage as well. It all can be introduced as an input directly through the interface or from an input file [96]. Even though Abaqus already has several failure modes, we will try to input our material behavior on the program, from the analysis of the experimental tests.

2.3.2.- Constitutive Equation

In physics and engineering, a constitutive equation or constitutive relation is a relation between two physical quantities (especially kinetic quantities as related to kinematic quantities) that is specific to a material or substance, and approximates the response of that material to external stimuli, usually as applied fields or forces. In our case, we will work on a constitutive relation between strain and stress of our different dosages.

For rigorous analysis of concrete structure, a complete stress-strain equation is needed. Low and medium strength concrete is rather easier than high strength concrete to get a full stress-strain curve. Due to the brittleness of high strength concrete, it needs special technique to get a full curve. The axial deformation has been used for test control, but for high strength concrete, the large energy release during failure causes unstable descending section [97]. To overcome this problem, one might use the circumferential deformation [98] or the combination of axial deformation and axial load proposed by Okubo and Nishimatsu on 1985 [99].

Until now, different constitutive equations have been developed that characterize the behavior of UHPC. We need to keep in mind that most of the models made to date are models of discrete equations; only the multi exponential models present the behavior of the UHPC continuously. The most important instructions that take fiber-reinforced concrete into account, adopt a discrete-type calculation diagram, because the multi exponential models are harder to calculate and to adapt to every situation, as well as less intuitive and less related to the experimental results.

For the compression behavior, the existence of more than thirty different mathematical expressions that claim to represent the stress-strain evolution of a concrete cylinder specimen subjected to monotonic uniaxial compression (including those proposed in the official regulations of the different countries that have regulated by law the use of concrete as structural material), it seems to require additional effort when formulating a universally accepted expression.

The evolution of the stress-strain proposed equations include from the first proposals of Ritter and Bach (1897-1899) [101], going through the more or less complex polynomial truncations of the Smith and Young equation (1956) [102], to the contributions based on statistical distributions of the damage model, and more recent, the analysis of the treatment given by the different versions of the Model Code and the Spanish Structural Concrete Instruction (EHE-08) [100]. Some equations are reviewed below.

2.3.2.1.- Examples of constitutive equations in compression

Ritter, professor of graphic statics and bridge construction at the ETH, was one of the first to deepen in the scientific control of reinforced concrete, proposing in 1899, in the journal *Schweizerische Bauzeitung* [101] an exponential type law for the deformation curve of concrete. The equation proposed by Ritter and BAch was written:

$$\sigma = f'_c \cdot (1 - e^{-N\varepsilon}) \quad (2.3)$$

where f'_c represents the maximum stress reached in the compression fracture test of the concrete specimen and N assumed to be equal to 1000.

Smith and Young's proposal is the most cited among all the equations enunciated on the stress-strain behavior of concrete. In a first article of 1955, Smith and Young [102], they design a calculation in flexion based on the previously proposed Bach's equation but suggesting that the value N in the exponent must be proportional to the ultimate compressive strength of the concrete. Immediately after, they abandon the Bach equation in their article [102] of 1956 to propose an exponential function in the following stress-strain relationship:

$$\sigma = \varepsilon \cdot M \cdot e^{-N\varepsilon} \quad (2.4)$$

It fitted quite well to the results of the crash test of cylindrical test pieces that showed a decrease in stress beyond the maximum stress. The values of M and N would be constants evaluated in terms of the properties of the concrete, imposing the following boundary conditions:

$$\sigma = f'_c \Leftrightarrow \varepsilon = \varepsilon_0; \quad \left. \frac{d\sigma}{d\varepsilon} \right|_{\varepsilon = \varepsilon_0} = 0 \quad (2.5)$$

being ε_0 the deformation experienced by the concrete at the point of maximum stress.

After imposing these boundary conditions, the equation (2.4) becomes equation (2.6):

$$\sigma = \frac{f'_c}{\varepsilon_0} \cdot \varepsilon \cdot e^{\left(1 - \frac{\varepsilon}{\varepsilon_0}\right)} \quad (2.6)$$

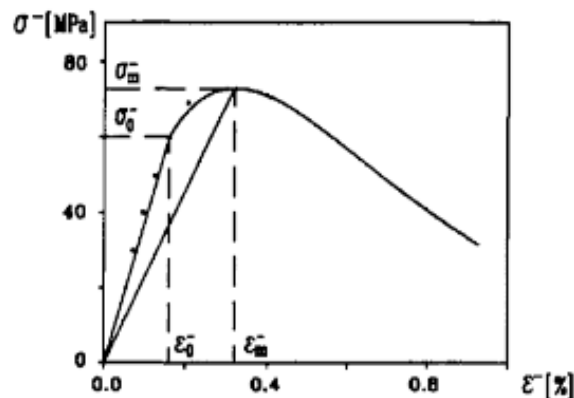


Figure 2-3 Compression stress-strain curve corresponding to Smith and Young's formula [102]

From the sixties of the last century, a large number of proposals based on rational functions of the following type, began to appear:

$$\sigma = \frac{P(\varepsilon)}{Q(\varepsilon)} \quad (2.7)$$

where $P(\varepsilon)$ and $Q(\varepsilon)$ are polynomials of varying degrees of the relative deformation ε .

Furthermore, the originally proposed by Kachanov [103] in 1956, subsequently modified by Rabotnov [104] and developed mainly from the eighties of the last century, the Continuous Damage Mechanics (CDM) has been widely accepted to simulate the complex behavior constitutive of many materials used in engineering. In particular, the models based on an internal variable of damage represented by a scalar function - isotropic damage - are characterized by their simplicity of implementation and versatility. This damage variable reflects the level of deterioration of the material as it is deformed and transforms the real stress into effective stress, so that a general equation relating stresses with deformations can be written in the form:

$$\sigma = \Psi(\varepsilon) \cdot [1 - \omega(\varepsilon)] \quad (2.8)$$

where $\Psi(\varepsilon)$ represents the response of the undamaged material and $\omega(\varepsilon)$ a scalar function of damage that varies between 0 (when the material has not yet been stressed) and 1 (when the material collapses).

Collins, Mitchell and MacGregor in 1993 [105], considered that two different expressions are necessary, one for the ascending part of the curve and another for the descending one, both coinciding in the stress peak f'_c , and on the other, because while Wang et al., [106] proposes that the constants of the equation must be changed according to the section considered, Collins et al. argue that what must be modified in said equation is the exponent, to adapt to the ascending or descending part, as the case may be, formulating the following multi-exponential equation:

$$\sigma = \frac{n \cdot f'_c \cdot \left(\frac{\varepsilon}{\varepsilon_0}\right)}{n - 1 + \left(\frac{\varepsilon}{\varepsilon_0}\right)^{nk}} \quad (2.9)$$

For the ascending part of the curve, the value of k would be equal to 1. For the exponent n , both in the ascending and the descending part, they propose the equation (2.10):

$$n = 0.8 + \left(\frac{f'_c}{17} \right) \quad (2.10)$$

It is in the descending part that the exponent is “adapted” to the new shape of the curve by means of equation (2.11):

$$k = 0.67 + \left(\frac{f'_c}{62} \right) \quad (2.11)$$

Although the article provides a formula for the calculation of ε_0 , the best result has been obtained by taking its experimental value, and for n and k the values $n = 2.922$ and $k = 1.281$. However, the results only improve very slightly from previous equations.

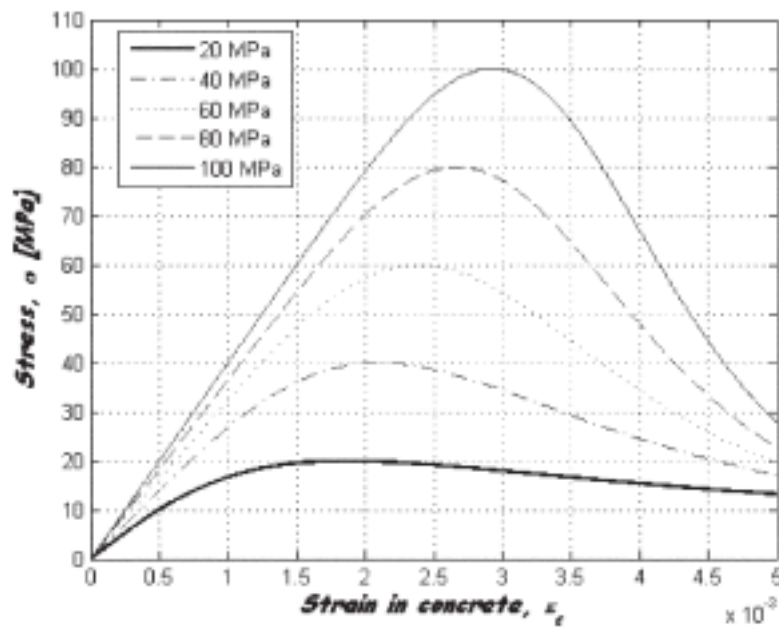


Figure 2-4 Stress-strain relationship of concrete based on Collins et al. model. [105]

Lastly, several countries or institutions have codes or instructions for the stress-strain curve mathematical modeling.

The Spanish Model Code for Concrete Structures [100] was an initiative from the time when there were no international codes. Because, in those initial moments, other organizations were designed to synthesize and compile international scientific research and experiments, it was considered as an important step forward to convert this knowledge and experience into practical documents of design and calculation, in such a way that the national normative committees could take advantage of them. In fact, the first codes (regarded in the form of “recommendations”) of 1964 and 1970 were used in this way. Finally, the first EU Model Code for Concrete Structures was published in 1978. The equation proposed by the Model Code of 1990, slightly changed afterwards for both the ascending section and a part of the descendant section, is written as:

$$\sigma = \frac{f'_c \cdot \left[\frac{E}{E_s} \cdot \left(\frac{\varepsilon}{\varepsilon_0} \right) - \left(\frac{\varepsilon}{\varepsilon_0} \right)^2 \right]}{1 + \left(\frac{\varepsilon}{\varepsilon_0} \right) \cdot \left(\frac{E}{E_s} - 2 \right)} \quad (2.12)$$

Where

$$E = \left. \frac{d\sigma}{d\varepsilon} \right|_{\varepsilon=0} \quad E_s = \frac{f'_c}{\varepsilon_0} \quad (2.13)$$

that is, the tangent of the angle formed by the line joining the origin with the stress peak (ε_0, f'_c) , called the secant module from the origin to the stress peak.

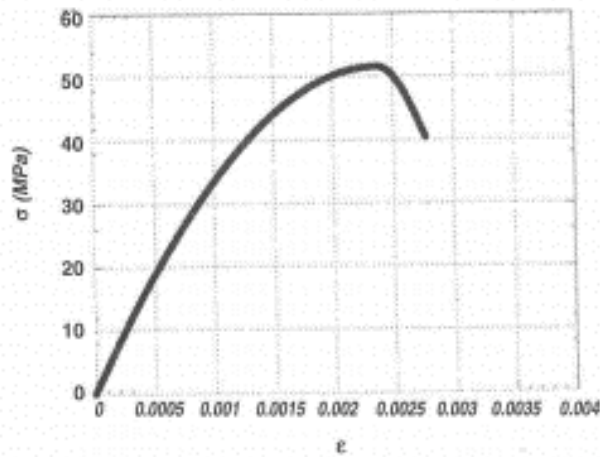


Figure 2-5 Stress-strain relationship of concrete based on 1990's Spanish Model Code [100]

2.3.2.2.- Examples of constitutive equations in tension

The following diagrams represent diagrams $\sigma - \varepsilon$ of discrete type for tension behavior, that is, the equation changes when the shape of the curve changes. These constitutive equations are the most important studies carried out to date.

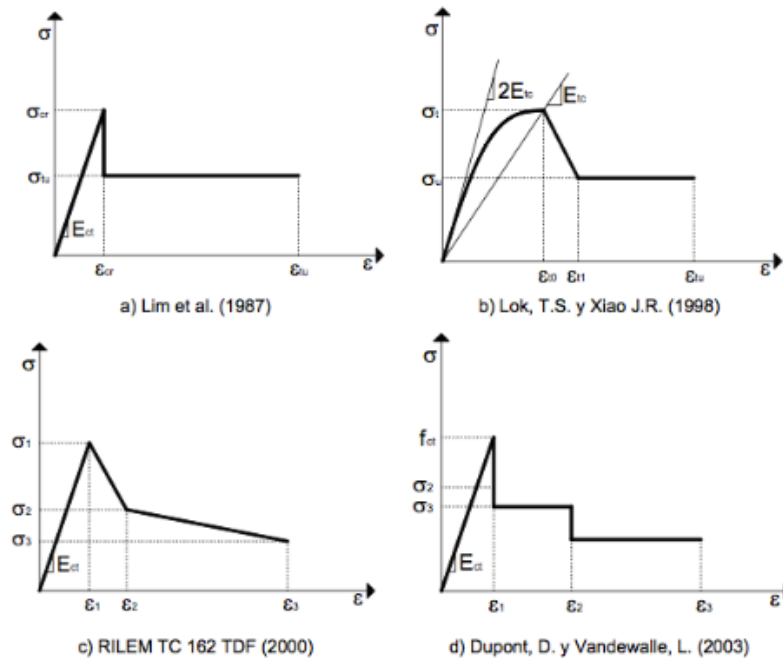


Figure 2-6 Different diagrams $\sigma - \varepsilon$ of discrete type for tension behaviour [107-110]

Diagram [a] (Lim et al., 1987) [107] was one of the first $\sigma - \varepsilon$ diagram studies for the HRFA, in this study the authors consider small amounts of fibers, and consider that in the pre-cracking zone of the concrete the effect of the fibers in this area of the curve is considered negligible.

Model [b] (Lok, T.S. and Xiao J.R., 1998) [108] proposes three stages, the first being of parabolic type, and the intermediate zone was included to better estimate post-peak resistance.

The diagram [c] (RILEM TC 1162 TDF, 2000) [109] proposes a diagram $\sigma - \varepsilon$ that uses the results of the test "3 points bending test" the RILEM regulation. The values of the stresses (σ_1 , σ_2 and σ_3) are obtained for some values of controlled deformations (ε_1 , ε_2 and ε_3). The value σ_1 is the peak value and the values σ_2 and σ_3 are values of the post-crack tension.

The model [d] (Dupont, D. and Vandewalle, L., 2003) [110] is a constitutive equation model that is posterior to that of the RILEM. The authors developed this stress-strain diagram to avoid a disadvantage of the RILEM model ([c]). The new model makes the post-cracking behavior totally independent of the tensile strength. The tensile strength f_{ct} will not influence the crack behavior, however, with the trilinear model of the RILEM, as can be seen in the previous figure, there is influence.

The authors consider that the tension jump after reaching the maximum peak (f_{ct}) is close to reality since at the time of cracking, the tension taken by the fibers is still small and most fibers need a bit of deformation before acting by welding the fissures.

The expressions of the deformations ε_1 , ε_2 and ε_3 and of the respective stresses σ_1 , σ_2 and σ_3 to obtain the model can be found in the research developed by Dupont and Vanderwalle.

2.3.2.3.- Proposed formulation of the constitutive equation

To the present, different constitutive equations have been developed that characterize the behavior of UHPC. We have to keep in mind that most of the models made to date are models of discrete equations; only the multi-exponential models present the behavior of the UHPC continuously. The most important regulations that take fiber-reinforced concrete into account adopt a discrete-type calculation diagram. In the literature review, the different constitutive equation models are explained.

On this section we will propose a mathematical formulation of a constitutive equation that meets the following requirements:

- It is built by using variables that are easily obtained from lab tests, and therefore, these variables have a physical meaning. They are not random parameters used to adjust the curve so it fits.
- Represents the phenomenon detected on the tests
- It becomes straightforward to compare the results
- It is as close as possible to past formulations from the literature, that can be seen below.
- It will be a continuous equation with its first derivative also continuous, except on the softening point.

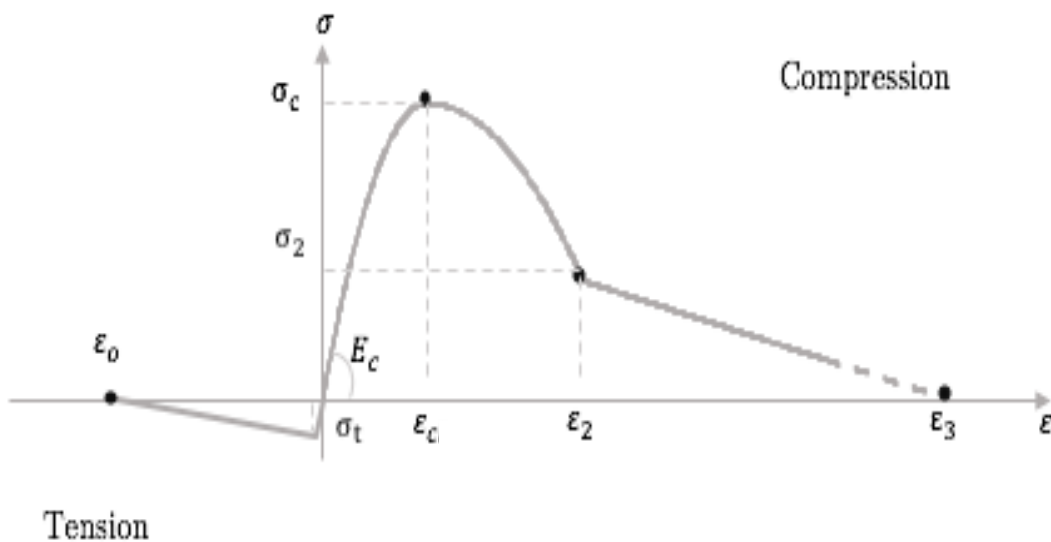
Our curve will be determined by a few values and assumptions, which all will be explained below.

1. Pre-Cracking: For the first part of the graph, until the peak value, as we have compression with slow cracking, we will impose the initial slope of our curve to be the elastic modulus, E . then the curve will reach the peak value either as a curved line or as a more straight line. We will also establish a horizontal slope at peak value $[f_c, \varepsilon_c]$. The factor used to decide whether is a more straight or more curved line is usually the division between the elastic modulus and the secant modulus, E/E_c , we will see later how well this factor approximates the curve. The general equation of the first section (I) is: $y = ax^n + bx$
2. Post-Cracking: On those cases where we have a post-cracking behavior, we need to formulate two more segments of the equation. The resistance left after the concrete is fully compressed is by the help of the steel fibers at tensile behavior. We impose the start point (peak point $[f_c, \varepsilon_c]$) and a second point ($[\sigma_2/f_c, \varepsilon_2/\varepsilon_c]$) called softening point, obtained from the tests, that adequates the shape to the experimental curve. It can either be shaped as a straight line or as a curved line, whichever adjusts better to experimental curve, and we will see later that we

can obtain a factor directly from the experimental results. The general equation of the second section (II) is: $y = c \cdot (x - 1)^m + 1$

3. Crushing: Finally, we just need to establish the end point of the diagram, by obtaining the point of the experimental diagram where the stress becomes to zero, or in case it stays parallel, selecting a parallel line, both cases starting from the second point ($[\sigma_2/f_c, \varepsilon_2/\varepsilon_c]$) used before. The general equation of the third section (III) is: $y = p \cdot (x - d)$
4. Tension: When the concrete is in tension, we assume a linear behavior, with elastic module E_c , until the tensile strength and then a loss of resistance to the point where tensile stress becomes zero.

As we can see, these expressions can simulate perfectly the other simplified expressions from the codes, and we are able to make any combination of them.



Next, we will present our constitutive equation in compression, proving that it could be explained using only parameters obtained from the experimental test, so that it can be reproduced in the future. We will describe a continuous equation, with its first derivative also continuous, except on the softening point.

We have divided our constitutive equations into 3 sections, has explained before and that can be seen in the following figure, where we will use normalized variables that allows to a non-dimensional formulation ($y=\sigma/f_c$, $x=\epsilon/\epsilon_c$)

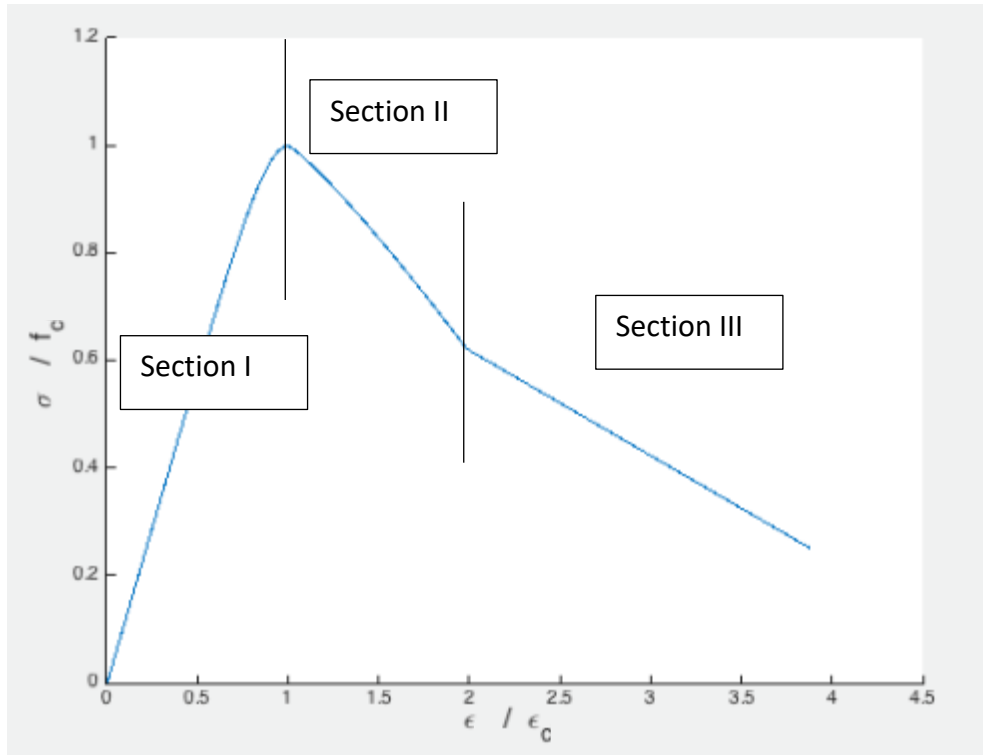


Figure 2-7 The three sections of our proposed equation

The equation of the first section (I) is: $y = ax^n + bx$

The equation of the second section (II) is: $y = c \cdot (x - 1)^m + 1$

The equation of the third section (III) is: $y = p \cdot (x - d)$

Being a piecewise-defined function, it can be written as:

$$f(x) = \begin{cases} ax^n + bx, & x \leq 1 \\ c \cdot (x - 1)^m + 1, & 1 < x \leq \epsilon_2/\epsilon_c \\ p \cdot (x - d), & \epsilon_2/\epsilon_c < x \end{cases} \quad (4.3)$$

The values (a, b, c, d, m, n, and p) will be defined from the characteristic values of any UHPCConcrete ($E_c, f_c, \epsilon_c, \sigma_2/f_c, \epsilon_2/\epsilon_c, \epsilon_3/\epsilon_c$) for each type of dosage of UHPC, steel fibers and carbon nanotubes. It is important that these values are defined using data obtained from experimental tests and not obtained from mathematical approximation, otherwise reproducing future tests with these same equations will not be as accurate. Furthermore, the usage of these equations for other proposed dosages will be possible only if using the experimental test data, because contrary to an approximated constant value, it will actually modify for every dosage test.

As noted previously, we define $\sigma_2/f_c, \epsilon_2/\epsilon_c$ as the stress and strain points where the normalized curve has a change of slope on the post-cracking section and ϵ_3 as the strain point where the curve has $\sigma_3=0$. These values are directly obtained from the experimental results, without any other calculations, just by graphical observation.

Section I – Pre-cracking

We will analyze how can we define the values, starting on the ones from the Section I equation, “a, b, n”.

Starting from our Section 1 equation, we will determine the values by setting our boundary conditions of the equation.

$$y = ax^n + bx \quad (4.4)$$

The coordinates at the origin must be, by definition, (0,0):

$$y(0) = a \cdot 0^n + b \cdot 0 = 0 \quad \text{OK} \quad (4.5)$$

The coordinates at normalized peak strength must be, by definition, (1,1):

$$\begin{aligned} y(1) &= a \cdot 1^n + b \cdot 1 = a + b = 1 \\ a &= 1 - b \end{aligned} \quad (4.6)$$

The first derivative at x=1, will be imposed as $y'(1)=0$, meaning that at (1,1), our equation reaches an horizontal asymptote, hypothesis that we came up with by analyzing our experimental results.

$$y'(1) = n \cdot a \cdot 1^{n-1} + b = n \cdot a + b = 0 \quad (4.7)$$

$$n = -\frac{b}{a} = \frac{b}{b-1} = \frac{a-1}{a} \quad (4.8)$$

Finally, we will calculate the derivative at the origin, that must be, by definition, equal to the elastic Young’s modulus of the material, E_c , as this value represents the slope on the stress-strain diagram for the elastic behavior. As we are working with normalized

stress-strain curves, our derivative at the origin must be equal to the ratio E_c/E_s , the ratio between the elastic Young's modulus and the elastic secant modulus at peak, i.e. ($E_s = f_c/\varepsilon_c$), becoming the slope on the elastic part of a normalized stress-strain curve.

$$y'(0) = n \cdot a \cdot 0^{n-1} + b = \frac{E_c}{E_s} \quad (4.9)$$

$$b = \frac{E_c}{E_s}$$

The value $b=E_c/E_s$ will always be greater than 1 and typically, smaller than 2.

It is important to verify that the tangent always decrease, so that the curve approaches the peak strength by a convex function and not by a concave function, otherwise our equation wouldn't be reflecting the behavior of concrete on the experimental tests, as it never has a convex function.

$$y''(x) = n \cdot (n - 1) \cdot a \cdot x^{n-2} \quad (4.10)$$

Because $b>1$, $a<0$ and $n>1$, $y''(x = 0:1) < 0$. OK, our curve is a convex function

Summarizing for Section I,

$$a = 1 - \frac{E_c}{E_s} \quad (4.11)$$

$$b = \frac{E_c}{E_s} \quad (4.12)$$

$$n = \frac{\frac{E_c}{E_s}}{1 - \frac{E_c}{E_s}} = \frac{E_c}{E_s - E_c} \quad (4.13)$$

Section II – Post-Cracking

Following, we need to define the variable “c, m” from the Section II equation.

$$y(x) = c \cdot (x - 1)^m + 1 \quad (4.14)$$

The coordinates at normalized peak strength must be, by definition, (1,1):

$$y(1) = c \cdot (1 - 1)^m + 1 = 1 \quad \text{OK} \quad (4.15)$$

The derivative at (1,1) must be null, as we imposed on our Section I, that the approximation to the coordinates (1,1) must be done by reaching an horizontal asymptote, which has a null derivative.

$$y'(1) = c \cdot m \cdot (1 - 1)^{m-1} = 0 \quad \text{OK} \quad (4.16)$$

The stress value, at strain value $\varepsilon_2/\varepsilon_c$, must be σ_2/f_c .

$$y(\varepsilon_2) = c \cdot (\varepsilon_2/\varepsilon_c - 1)^m + 1 = \sigma_2/f_c \quad (4.17)$$

$$c = \frac{(\sigma_2/f_c - 1)}{(\varepsilon_2/\varepsilon_c - 1)^m} \quad (4.18)$$

To define the variable “m”, we do not have any restriction on the boundary conditions of the Section II, so we will hypothesize that “m” is equal to the ratio between the elastic Young’s modulus and the elastic secant modulus, E_c/E_s . It is a ratio easy to obtain, either graphically from the experimental tests on any stress-strain graphical results or from a table-organized data by calculating a few numbers. This will be our first approach, to be verified later on as we check the goodness of our approximation. Defining the variable “m” by this ratio, we ensure that all the variables are described by simply obtained results from the experimental tests and are not subjective mathematically obtained values that are susceptible to changes. Summarizing for Section II,

$$m = \frac{E_c}{E_s} \quad (4.19)$$

$$c = \frac{(\sigma_2/f_c - 1)}{(\varepsilon_2/\varepsilon_c - 1)^{\frac{E_c}{E_s}}} \quad (4.20)$$

Section III - Crushing

To find the variable “p, d” of Section III, we will analyze its boundary conditions and determine them.

The stress value, at strain value ε_3 , must be by definition, null.

$$y(\varepsilon_3) = (p \cdot (\varepsilon_3/\varepsilon_c - d) = 0 \quad (4.21)$$

As the variable p is different than 0, we find that:

$$d = \varepsilon_3/\varepsilon_c \quad (4.22)$$

The stress value, at strain value $\varepsilon_2/\varepsilon_c$, must be σ_2/σ_c .

$$y(\varepsilon_2) = (p \cdot (\varepsilon_2/\varepsilon_c - \varepsilon_3/\varepsilon_c) = \sigma_2/f_c \quad (4.23)$$

$$p = \frac{\sigma_2/f_c}{(\varepsilon_2/\varepsilon_c - \varepsilon_3/\varepsilon_c)} \quad (4.24)$$

Summarizing for Section III,

$$d = \varepsilon_3/\varepsilon_c \quad (4.22)$$

$$p = \frac{\sigma_2/f_c}{(\varepsilon_2 - \varepsilon_3)/\varepsilon_c} \quad (4.24)$$

The final equations are presented below:

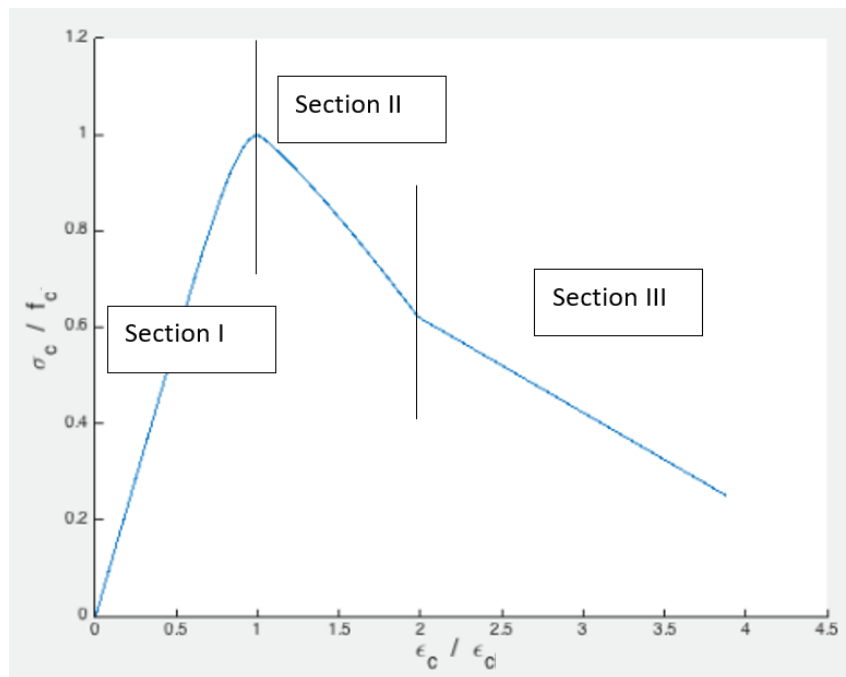
$$\sigma(x = \varepsilon/\varepsilon_c) = f_c \cdot \begin{cases} \left(1 - \frac{E_c}{E_s}\right) \cdot x^{\frac{E_c}{E_s - E_c}} + \frac{E_c}{E_s} \cdot x, & x \leq 1 \\ (\sigma_2/f_c - 1) \cdot \left[\frac{(x-1)}{(\varepsilon_2/\varepsilon_c - 1)}\right]^{\frac{E_c}{E_s}} + 1, & 1 < x \leq \varepsilon_2/\varepsilon_c \\ \sigma_2/f_c \cdot \frac{(\varepsilon_3/\varepsilon_c - x)}{(\varepsilon_3 - \varepsilon_2)/\varepsilon_c}, & \varepsilon_2/\varepsilon_c < x \end{cases} \quad (4.25)$$

σ_2/f_c , $\varepsilon_2/\varepsilon_c$ are the stress and strain points where the normalized curve has a change of slope on the post-cracking section. They are determined numerically from experimental data to optimize the adjustment of the proposed equation or estimated directly from the experimental curve.

$\varepsilon_3/\varepsilon_c$ is the strain point where the normalized curve would reach a stress value of $\sigma_3/f_c = 0$, or the theoretical point where this would happen if the graph never reaches $\sigma_3/f_c = 0$.

This equation $\sigma(\varepsilon)$ is obtained only with variables that are directly obtained from the experimental data, and having a physical meaning.

As we will see later, the equation represents truly the experimental behavior of our material and it has simple interpretation, where the first part is the compression load absorbed without breaking, second part includes the cracking behavior of the specimen and its failure, finishing with the third part where it has only residual strength.



Chapter 3 - Lab Methods

3.1.- TEST PLAN

3.1.1.- Specimens

3.1.1.1.- Number of specimens to be created

3.1.1.2.- Calculated costs

3.1.2.- Specimens preparation procedures.

3.1.2.1.- Preparing the CNT and GO mixture

3.1.2.2.- Making the UHPC specimens

3.1.3.- Compression test procedure

3.1.4.- Planning of tests calendar

3.2.- IMPLEMENTATION OF THE TEST PLAN

3.2.1.- Obtaining the materials

3.2.2.- Molds

3.2.3.- Mixing, casting and curing

3.2.4.- Compression test

As it is indicated in the title, this chapter includes the explanation of research methods of the dissertation. In more details, it outlines the research strategy, the research method, the research approach, the methods of data collection, the selection of the sample, the research process, the type of data analysis and the research limitations of the project.

Chapter 3 – Lab Methods

In order to achieve the proposed objective, a laboratory test campaign will be necessary to obtain experimental results of the characteristics of a concrete made from different dosages of CNT & GO cement composite with the addition or not of steel fibers. **The analysis and reporting of these trials and their results already constitute in themselves a very interesting partial result of this thesis since no other equivalent known tests have been reported.**

- Choose a serie of CNT&GO dosages, obtained from the literature reviewed and looking for the properties wanted.
- Design and create a “better as possible” concrete from the previous reviewed cement and reinforcements with aggregated (or not) steel fibers.
- Analysis of strength results of the CNTs&GO concrete, through tests on real pieces of concrete with applied compression load.
- Identification and Characterization of the strength properties of CNTs&GO concretes with added (or not) steel fibers by numerical modeling. Characteristics Stress-Strain curves.

In order to reproduce the behavior of these newly created concretes, a constitutive equation that incorporates the mechanical characteristics found in our own tests and those that have been reported in the existing documentation will be developed and implemented. The constitutive equation will be calibrated against the tests performed until a high reproducibility of the results is obtained, therefore assuring their validity.

As a collateral result of this work, **it will be obtained a formulation of characteristics stress-strain laws of this kind of UHPC that can be used for future research lines or to define technical design criteria.**

The test campaign was designed to obtain information about the following properties of these new kind of UHPC:

- Recommendations on how to mix the components constituting the fresh mass of the UHPC with the new materials, CNT, GO and SF. In the corresponding section we propose a procedure that, according to the literature review, is the one that has given better results, but it is required of the laboratory to report if the method of mixing has been effective, analyzing characteristics such as ease of dispersion, work speed, complexity, excessive sensibility of the dosage, manipulability, etc.

- The dosing of new nanomaterials is very controversial in the review literature. For the GO there seems to be some consensus about a dosage of 0.04 wt% (weight of cement %) but the results for the addition of CNT varies greatly between 0.08 and 0.5 wt%. We have proposed three different dosages to obtain new information about which would be an optimal dosage of CNT according to the characteristics of the UHPC that we wish to obtain. For this reason, an analysis based on the mechanical results obtained is required, to propose what would have been the optimum dosage and an estimate of the results that could be expected for this hypothetical optimal mixing in the case of Steel Fibers addition or not. Different dosages will be explained clearly further in the chapter.
- Tests are planned at different curing ages (7 and 28 days). Even though it was firstly planned to add two more curing ages (3 and 90 days), that would have allowed us to obtain the evolution of the strength characterization, knowing the evolution of the properties over time and if the characteristics of the different dosages and adding or not of steel fibers, have a different impact throughout the different initial stages of curing of the concrete. However, as economical and time resources are limited, we will not plan tests for other curing ages and we will stick to only the 7 days and 28 days curing times.
- Before each test, it is necessary to rigorously document all the dimensions of the piece, weight and other physical parameters that may affect the results (check of flatness, parallelism of faces, deformations, defects, holes, etc.). It should be kept in mind that when working with reduced size specimens any small error can cause a large dispersion of results.
- At each test, verify and record the configuration and geometry of the elements. Measure with extreme precision the final position of the part, the load, the instrumentation and environmental test conditions.
- During the tests, digitally record the stress and strain data obtained from the instrumentation, so as to obtain a report on the full stress-strain curves of this type, that is to say, with a register of the descending curve, in which, after cracking the piece, some of the specimens might continue to deform but with less effort.
- During the tests, manually record the incidents or anomalies that can be detected, reporting if possible an interpretation of what happened.
- During the tests, photographically document the test, referring to the load state, with at least: a photo of the test before starting, a photo at the time of

appearance of the first fissure, detail photo of the first fissure (measure initial angle), a photo upon reaching the maximum load, a photo at the end of the test, a detail photo of the cracking on the piece once the test finished. It is interesting to know if the "cracks map" in these UHPCs with additions is very different from that of conventional concretes.

In this chapter we show the expected test plan and the actual testing campaign that took place, to denote the differences and the solutions given to different unexpected problematics.

3.1.- Test plan

We will be performing a test on which we want to obtain the full compressive stress-strain curve, so it is important that the instrumentation is capable of recording it. The technical requirements of the tests will be those applied when performing a compressive test with the ASTM standard “ASTM C 469: Standard Test Method for Static Modulus of Elasticity and Poisson's Ratio of Concrete in Compression” [111].

This test method covers determination of a chord modulus of elasticity (Young's) and Poisson's ratio of molded concrete cylinders and diamond-drilled concrete cores when under longitudinal compressive stress, providing a stress to strain ratio value and a ratio of lateral to longitudinal strain for hardened concrete at whatever age and curing conditions may be designated. It is important to implement a displacement-controlled load test procedure to obtain the post-cracking behavior of the concrete, otherwise, with a simple loading test, it is not possible. After the maximum compression strength, some concretes can keep deforming, without completely failing, with less effort than the one needed to reach that maximum point, so it is necessary to reduce the strength applied to keep observing this deformation behavior.

At least three specimens of each dosage mixture will be tested and, later on, averaged to be able to obtain the standard dosage tested curve.

Henceforth, we will deepen on the specifics of the experimental campaign.

3.1.1.- Specimens

3.1.1.1.- Number of specimens to be created

In recent years, new carbon materials, such as carbon fibers, carbon nanotubes (CNT) and graphene oxide (GO), are being used to enhance cement composites in order to create concretes with the desired mechanical properties. The main reason is these materials are able to modify the concrete in nano-scale, allowing an improved control of cracks and nanostructure modification.

However, the relatively high cost of the materials, even with the recent drop in prices due to improved fabrication technology, and the difficulties of dispersion due to van der Waals attraction forces, makes investigation necessary to obtain an accurate dosage and optimal dispersion.

As research proceed, promising composites combining reinforcing materials arise, like steel fibers + CNTs or CNT + GO, demonstrating the probable positive results. As to advance in ultrahigh performance concrete (UHPC), a combination of CNT + GO + steel fibers will be used and tested whether it is an improvement to be able to present a new composite.

The literature reviewed shows that for CNT, is not possible to take an optimal dosage and be sure that it will be the correct one, so we will try with 3 different dosages to have a broader range of possibilities. Both the GO and Steel Fibers were found to be

usually around one specific dosage, which was found on the literature reviewed and will be the one used.

The used dosages and the number of specimens (n) will be presented on the table below, with their coding name to facilitate their future referencing.

Table 3-1 Name coding and quantities for the different specimens

GO(*) →	0%		0.04%	
	0%		0.08%	0.50%
CNT(*) →	0%		0.08%	0.50%
0% SF(**)	UHPC07D0SF000_xx (3) UHPC28D0SF000_xx (3)		UHPC07D0SF008_xx (3) UHPC28D0SF008_xx (3)	UHPC07D0SF050_xx (3) UHPC28D0SF050_xx (3)
2% SF(**)	UHPC07D2SF000_xx (3) UHPC28D2SF000_xx (3)		UHPC07D2SF008_xx (3) UHPC28D2SF008_xx (3)	UHPC07D2SF050_xx (3) UHPC28D2SF050_xx (3)

4% SF(**)(***)	UHPC07D4SF000_xx (3) UHPC28D4SF000_xx (3)		UHPC07D4SF008_xx (3) UHPC28D4SF008_xx (3)	UHPC07D4SF050_xx (3) UHPC28D4SF050_xx (3)
-----------------------	--	--	--	--

xx= [01, 02, 03, ... n]

(*) The proportion is expressed on % weight material/weight cement.

(**) The proportion is expressed on % by volume.

(***) The 4% Steel Fibers specimens were not originally planned on the tests but we made them as we had extra material for the 28 days test.

3.1.1.2.- Calculated costs

As we mentioned before, the cost-efficiency of construction materials is the key for their implementation. In this section we will analyze the generalized cost of the different specimens by counting the cost of the materials.

All the instrumentation and machinery used for the mixing, curing and testing is not calculated because we are considering the cost of the material itself in case to be reproduced in small or large scale.

Therefore, we will be analyzing and describing the different costs of all the raw materials used in the process, as well as giving an approximate cost of the different types of specimens

Before starting, we find important to note that geography might play an important role on pricing, since it is not the same to buy the materials in Europe, USA or China, where the analysis takes place.

The materials needed for the modified UHPC are: water, Portland cement, silica fume, ground quartz, fine sand, accelerator, high range water reducer (HRWR), steel fibers, carbon nanotubes and graphene oxide. The necessary amounts of each material for every set of specimens can be found in the following table, that will be explained in detail in section 3.1.2.2.

Table 3-2 Quantities for each UHPC dosage

	UHPC 0% CNT&GO	UHPC 0.08% CNT&GO	UHPC 0.50% CNT&GO
Portland cement (g)	461.343	461.343	461.343
Fine sand (g)	660.913	660.913	660.913
Silica fume (g)	149.677	149.677	149.677
Ground quartz (g)	136.718	136.718	136.718
HRWR (g)	19.892	15.279	10.665
Accelerator (g)	19.439	19.439	19.439
Steel fibers (g)	101.081	101.081	101.081
Water (g)	101.495	39.983	39.983
CNT&GO (aq) (mL)	0	66.126	70.739

As it can be seen, the amount of water needed is approximately 100 mL, so its price can be neglected because the water used is tap water, which price is in the order of cents for every cubic meter or thousand liters.

Continuing, the main ingredient for a concrete is cement, in this case Portland cement obtained from a trusted local supplier that has been working for long time with the research group. The price is CNY 20 (about USD 3 at change) for a bag of 50 kg without transport, which can be considered at CNY 70 (USD 10.5). With this, we will assume a cost of CNY 100 (USD 15) for every bag of 50kg. As we need about 0.5kg of

cement for every set of 3 specimens, we can consider a cost of CNY 1 (USD 0.15) for every set.

For the high range water reducer and the accelerator additives, we contacted the local BASF supplier as it was assuring the quality as well as the same materials used in the literature review. The price for 3 kg of each was CNY 500 each (USD 74.4).

Therefore, as we used about 20 grams of each additive for every set of specimens, the amount to be accounted from each of these materials is CNY 3.33 (USD 0.5). Note that the difference in HRWR in the dosages with nanomaterials is due the addition of HRWR in the sonication process.

Fine sand and ground quartz were bought directly from the mixing laboratory. Fine sand, which is used to save money compared to ground quartz, costs about CNY 15 (~USD 2) for every 50kg. Ground quartz cost is around CNY 7 (USD 1) for every 1kg.

We need about 700 grams of fine sand for every set, accounting for CNY 0.21 (USD 0.03), and 140 grams of ground quartz per set, accounting for CNY 0.98 (USD 0.15).

Steel fibers bought from local suppliers cost around CNY 7 (USD 1) per 1kg and as we need 100 gram per set of specimens, it accounts for CNY 0.7 (USD 0.1).

Silica fume bulk's price from a local supplier is equivalent to CNY 1200 (USD 180) per ton. As we need 150 grams for every 3 specimens, the amount accountable is CNY 0.18 (USD 0.03).

Finally, and leaving the most expensive materials for the end, we will calculate the costs of carbon nanotubes and graphene oxide.

We obtained the carbon nanotubes from different sources and, even though the different companies were so kind to provide us with some samples, we need to be rigorous and account for the theoretical price of its costs. The market price for the desired multi-wall carbon nanotubes has a wide range, from CNY 53 (USD 8) per gram for bulk orders up to CNY 100 (USD 15) for small orders. Since we would consider ordering in bulk, we will calculate the costs with bulk prices.

For the 0.08wt%, which includes 0.36 g of CNT per set of specimens, the accountable cost would be CNY 19 (USD 2.9). For the 0.5wt%, which includes 2.28 g of CNT per set of specimens, the accountable cost would be CNY 121 (USD 18.26).

The graphene oxide was obtained from one company that was interested in the research and provided us with the samples required, but like with the CNT, we need to calculate the theoretical cost. The graphene oxide water dispersion (0.4 wt% Concentration) was supplied in a bottle of 1 litre costs CNY 907 (USD 137). The cost for the sets of specimens that include GO, both dosages having 46 ml of graphene oxide water dispersion, accounts for CNY 42 (USD 6.3).

As we can see from the calculations, and as it was seen in the literature reviewed, the cost of these nanomaterials exceeds by large the cost of the rest of the materials. Moreover, the cost of graphene oxide is important, as it costs more than double the carbon nanotubes.

As a summary of all the costs, we elaborate the table below to have an easy idea of the theoretical costs of the materials included in these specimens. Note that the quantities are referred to a production of 3 specimens of each type.

Table 3-3 Costs of each material in each 3 specimens dosages

Costs	UHPC 0% CNT&GO	UHPC 0.08% CNT&GO	UHPC 0.50% CNT&GO
Portland cement		CNY 1.00 (USD 0.15)	
Fine sand		CNY 0.21 (USD 0.03)	
Silica fume		CNY 0.18 (USD 0.03)	
Ground quartz		CNY 0.98 (USD 0.15)	
HRWR		CNY 3.33 (USD 0.50)	
Accelerator		CNY 3.33 (USD 0.50)	
Steel fibers		CNY 0.70 (USD 0.10)	
Water		-	
CNT	-	CNY 19.00 (USD 2.90)	CNY 121.00 (USD 18.26)
GO	-	CNY 42.00 (USD 6.30)	CNY 42.00 (USD 6.30)
Total w/ steel fibers	CNY 9.73 (USD 1.46)	CNY 70.73 (USD 10.66)	CNY 172.73 (USD 26.02)
Total w/out steel fibers	CNY 9.03 (USD 1.36)	CNY 70.03 (USD 10.56)	CNY 172.03 (USD 25.92)

Additionally, we calculate the cost for 1 m3 of each UHPC dosage disaggregated by material. There are extra amount of materials in the calculation in order to simulate real conditions, where the complete totality of a mix is not usable and we will waste some materials.

Table 3-4 Costs of each material in 1 m3 of each UHPC dosage

Costs	UHPC 0% CNT&GO	UHPC 0.08% CNT&GO	UHPC 0.50% CNT&GO
Portland cement		CNY 1,698 (USD 255)	
Fine sand		CNY 357 (USD 51)	
Silica fume		CNY 357 (USD 51)	
Ground quartz		CNY 1,664 (USD 255)	
HRWR		CNY 5,653 (USD 849)	
Accelerator		CNY 5,653 (USD 849)	
Steel fibers		CNY 1,188 (USD 170)	
Water		-	
CNT	-	CNY 32,255 (USD 4,923)	CNY 205,416 (USD 30,999)
GO	-	CNY 71,301 (USD 10,695)	CNY 71,301.4 (USD 10,695)
Total w/ steel fibers	CNY 16,158 (USD 2,479)	CNY 120,075 (USD 18,097)	CNY 293,231 (USD 44,173)
Total w/out steel fibers	CNY 15,330 (USD 2,309)	CNY 118,887 (USD 17,927)	CNY 292,047 (USD 44,003)

3.1.2.- Specimens' preparation procedures.

3.1.2.1.- Preparing the CNT and GO mixture

Working with MWCNT and GO makes the procedure of creating the specimens technically more complicated than using other common materials of concrete. Nanomaterials are appreciated for their large surface areas that can be exploited for reaction with cement paste but, although they are beneficial as attachment sites for hydration products, there is great chance of agglomeration of nanomaterials because of the strong van der Waal attractive forces that exist at the nanoscale. Also, extra free water is needed to wet the large surface area of nanomaterials, thereby compromising the cement workability. It is important to rightly mix and disperse the nanomaterials. In the literature is explained how to perform the mixing of the MWCNT and GO, to achieve a proper dispersion of both materials, using sonication systems.

Table 3-5 Materials and Instrumentation

Tools needed	Materials needed
Sonicator (probe or bath) Container High precision scale Beaker Test tube Lab spoon	Carbon Nanotubes (CNT) Graphene Oxide (GO) Distilled Water High-Range Water Reducer

It is also experimented that, as GO is a hydrophilic material and very dispersible in water, is better to obtain it as an aqueous solution. Furthermore, using an aqueous solution of GO makes it possible to dissolve the MWCNT in it by using HRWR and make the dispersion in the UHPC less problematic.

To proceed on the mixing of the MWCNT and the GO, we will sonicate the dispersed GO solution with the MWCNT powder form.

The specimens will be prepared with the dosages explained in the previous chapter, which includes two dosages of CNT and GO solutions, being them 0.04wt% GO + 0.08wt% CNT and 0.04wt% GO + 0.50wt% CNT.

To begin with the mixing of these materials, we will have to weigh and mix them before sonicating. We will prepare a certain quantity of CNT + GO solution that will allow us to have a few extra specimens than the minimum necessary, in case we have any problems later and we need to redo some of them.

As the GO is in aqueous solution with a density of 4mg GO/1 mL of solution, we will use the volume calculation for GO solution and weight calculation for CNT. The HRWR and water that will be added to help with the sonicating process will also be measured accordingly and taken into account later on the UHPC mixing.

The two different dosages will be created as follows:

Table 3-6 CNT&GO dosages to be created through sonication

0.04wt% GO + 0.08wt% CNT	0.04wt% GO + 0.50wt% CNT
1.2 g CNT 150 mL GO solution (0.6g GO) 15 mL HRWR 50 mL extra water Total: 215 mL solution	7.5 g CNT 150 mL GO solution (0.6g GO) 30 mL HRWR 50 mL extra water Total: 230 mL solution

This quantities are for each of the curing times. Ideally, we should do all the sonication mixings at the same time, without distinguishing between curing times. In practice, as time constraints won't allow us to mix all the 7 days and 28 days specimens at once, it is better to split the sonication processes for each curing times.

When we have all the materials measured and ready to be mixed, we place them inside a beaker and we start the sonication process, one for each dosage. We will subject each CNT&GO mixture to pulsed sonication for 10 min (5 s on and 5 s off), ideally in an ice bath to prevent overheating sonicating, or until a visually homogeneous dispersion is formed. Ideally we should have a sonication probe as it has more efficiency on the process, being directly in contact with the material. Otherwise, if we don't have a sonication probe available, it might be done with a sonication bath but it is hypothesized that it will take a longer time.

When the sonication process is finished, these two solutions will be placed in a container until they are used for the UHPC mixing, trying to do the sonication process as close on time to the UHPC mixing as possible, so there are no sedimentation effects whatsoever.



Figure 3-1 Sonicated sample

3.1.2.2.- Making the UHPC specimens

Table 3-7 Materials and Instrumentation to create the UHPC specimens

Tools needed	Materials needed
Laboratory Electric Cement Mortar Mixer Precision Scale Test tube Laboratory utensils 50x100 mm Molds	CNT&GO solutions Portland cement Fine sand Silica fume Ground quartz HRWR Accelerator Steel fibers Water

Before going into the preparation of the UHPC specimens, we have to note that there is a critical point on the test planning, which is the number of available molds or the number of tests that might be possible to do in a day. Ideally, all concrete specimens' mixing and casting should be done at the same day, to have better knowledge of the mixings proportions and ensure greater homogeneity of the mix. However, considering that is more important the correct timing of curing rather than the homogeneity of the mix, we will divide our casting into different days to adjust to the testing capacity. Knowing how many molds can we have and when do we have them available is as important as knowing the availability of the lab to do the testing, and should be planned beforehand to be coordinated with the test timing.

The properties of the materials are a really important factor as they will determine the results of the test.

As we are using newly experimented materials for concrete, we will acquire more material than the exactly calculated to prevent future problems that may occur, and in case everything goes according to the plan, it could be use in the future to create extra specimens and use them as a backup or to perform different tests, such as fatigue test with loading/unloading cycles.

As for where to obtain the materials, the different providers for each material will be compared and contacted, finding the most suitable solutions in terms of quality and taking into account the cost.

The object of this report is to study UHPC, so we need to obtain the usual materials to prepare it. The following chart shows the dosage of each material and the quantity needed for each set of 3 specimens of UHPC that will be produced. For the mixing quantity, we calculated a total quantity of 3 specimens + 10% as a backup.

Table 3-8 Quantities for each UHPC dosage

	UHPC 0% CNT&GO	UHPC 0.08% CNT&GO	UHPC 0.50% CNT&GO
Portland cement (g)	461.343	461.343	461.343
Fine sand (g)	660.913	660.913	660.913
Silica fume (g)	149.677	149.677	149.677
Ground quartz (g)	136.718	136.718	136.718
HRWR (g)	19.892	15.279	10.665
Accelerator (g)	19.439	19.439	19.439
Steel fibers (g)	101.081	101.081	101.081
Water (g)	101.495	39.983	39.983
CNT&GO (aq) (mL)	0	66.126	70.739

The Portland cement to be used should be Type 1 Portland cement, and if possible with moderate fineness and C3A content significantly lower than 8 percent. It was found that the best performance comes with C3A<4%, Na2Oe <0.4% and the specific surface should be about 3400 cm²/g.

Fine sand was researched and found that the optimal diameter size should be around 0-2 mm [11], intended to save costs against ground quartz.

Ground quartz sizes smaller than 1 mm and bigger than 10µm, being the strength greater than ordinary fine sand, however more expensive, so its use is reduced.

Silica fume would be better with very low carbon content.

As reference, the HRWR used for Ductal® composite is GLENIUM 3000 NS, a polycarboxylate superplasticizer to increase the workability, and the accelerator in use is RHEOCRETE CNI, which is an additive formulated with a calcium nitrite base to inhibit the corrosion of steel in reinforced concrete and also works as an accelerator.

It is important to acquire polycarboxylate superplasticizer, also referred as HRWR, as it is an indispensably admixture for cement composites to reduce the water consumption without losing fluidity of the cement pastes.

The general used fibers are made of steel, and most of them are smooth-straight steel fibers with a length range of 6 mm to 20 mm, and with a slenderness ratio above 65 (to improve the matrix-fiber bond) and below 80 (to improve workability). Although their use is less frequent, twisted and hooked-end fibers can also be employed as well as a combination of different fiber types when specific requirements need to be fulfilled. The use of different types and amounts of fibers leads to distinct tensile behaviors and they play an important role in the pre- and post- cracking behavior. Commonly, the fraction of fibers used ranges from 2% to 6% by volume.



Figure 3-2 Materials weighted and ready to mix

For the MWCNT, it was considered in different researches the outer diameter between 10-20nm, lengths between 10-30 μm and purity higher of 90%. With that requirements, we will be looking for the optimal cost-efficiency through several providers, as CNT are very costly.

For the GO, it was considered in most of the researches that the best option would be having a GO aqueous solution, to be able to disperse the MWCNT in it before mixing with the concrete.

The UHPC materials used in this study can be divided into three parts: premix (cement, fine sand, ground quartz, silica fume), fibers, and liquids. For the purpose of this study, all of the premixes are assumed to be identical; however, it is realized that manufacturing processes can vary with time, and the final premix product could show slight variations.

The liquids that were mixed with the UHPC included water, accelerator, a high-range water-reducing admixture (HRWR) and CNT&GO solution, which are all considered identical.

The CNT&GO solution explained on the chapter before, will be considered as a liquid and the quantity of total liquid included should match the original mix value, therefore we need to take into account that at each mix of mortar with GO&CNT, a part of normal mix water and HRWR will be substituted with graphene oxide and CNT aqueous solution to keep the amount of mixing water and HRWR constant at all mixes.

The mixing procedure for UHPC includes the following steps, which will be followed with strict timing:

- Weigh all constituent materials. Add half of HRWR and the CNT&GO solution to water.
- Place premix in mixer pan and mix for 2 minutes.
- Add water (with half of HRWR and CNT&GO) to premix slowly over the course of 2 minutes.
- Wait 1 minute, then add remaining HRWR to premix over the course of 30 seconds.

- Wait 1 minute, then add accelerator over the span of 1 minute.
- Continue mixing as the UHPC changes from a dry powder to a thick paste. The time for this process will vary.
- Add fibers to the mix slowly over the course of 2 minutes.
- After the fibers have been added, continue running mixer for 1 minute to ensure that the fibers are well dispersed.



Figure 3-3 Activating the mixing machine

It is important that no CNT&GO residue stays in the test tube. It is recommended to keep some of the mixing water to “clean” the residues and add them to the mixing.

The casting of all UHPC specimens should be completed right after or, at most, within 20 minutes after the completion of mixing. All specimens will be thoroughly put into previously oiled molds, flush the top, cast on a vibrating table and allowed to remain on the table for approximately 30 seconds after filling. It is important to secure the molds on the vibrating table to attain efficiency, otherwise longer vibrating times might be needed. It is also important not to vibrate for too long or the steel fibers might get orientated.



Figure 3-4 Demoulding of a specimen

The molds will be then tagged with the specimens code name and put into the moist room or cabinet, ideally at 25°C and 98% humidity. After 24 hours, the molds should be removed and the specimens should remain in the moist cabinet or room until the testing day. It is important to be careful at this early stage with any movement of the specimens, as they might get damaged on the process.

If the specimens are removed from the molds before 24 h, keep them on the shelves of the moist closet or moist room until they are 24h old, and then immerse the specimens in saturated lime water in storage tanks constructed of no-corroding materials. Keep the storage water clean by changing as required.

After removing the specimens from the molds, the molds should be cleaned and stored dry to prevent corrosion.

There will be samples to be tested at 7 and 28 curing days to investigate the evolution of the specimens with the curing time, and they should be marked accordingly. In case any of the specimens got broken or damaged during casting or curing, it is important to inform immediately.

3.1.3.- Compression test procedure

Table 3-9 Materials and Instrumentation needed to perform the tests

Instrumentation needed	Materials needed
Hydraulic press Extensometers/LVDT Computer General lab tools	Specimens

Uniaxial compression tests will be performed on cylinder specimens of 50 mm diameter and 100 mm height (smaller than standard specimens to reduce costs of materials) using a modified method because, in the literature reviewed, it was seen that the standard methods cannot measure precisely the post-cracking behavior for UHPFRC specimens, which is one of the results we want to obtain from the test.

One test method that can be performed is using the guidance from the BS 1881-121:1983. The specimens would be loaded at a rate of 0.5 MPa/s and measurements taken using electrical strain gauges. As this method is designed only for the determination of the static modulus of elasticity, it is unable to capture the post-cracking behavior for the UHPFRC specimens. The strain gauges detach from the surface of the specimen and come off at peak strength due to concrete spalling, therefore not obtaining post-crack behavior.

Another method is in compliance with ASTM C469 using two rigid circular rings, to be secured at approximately two thirds the height of the specimen using clamping screws. Two LVDT's are introduced between the rings and positioned on opposite sides of the specimen. Tests are conducted using a displacement control testing machine at a rate of 0.04 mm/min and measurements are recorded.

This method is able to capture the stress-strain values up to the first crack strength for the UHPFRC specimens (or ultimate strength for the UHPC samples). However, it is observed that the method is unsuitable for capturing the post-cracking behavior of the UHPFRC specimens because the clamping screws start to rotate with the occurrence of shear line failure.

To overcome the difficulties encountered with the other test methods, a third method of testing is proposed. In this method, the circular rings with the LVDT's are used only to measure the elastic stage of the test. In addition, two more LVDT's are placed parallel to the specimen and to the loading machine, to measure the cross-head movement of the test machine, hence, the post-cracking stage is recorded. The full compressive stress-strain response is then obtained by combining the two sets of results. All the cylinder specimens are grinded to minimize uneven surfaces at each end.

Prior to deciding the final method of testing, we need to make sure of the instrumentation available at the lab and, if they don't have it, which modifications can be made to be able to do the test.

3.1.4.- Planning of tests calendar

Detail of steps for lab tests. In case of some problems with the molds, materials or lab capacity, availability and instrumentation, it should be rearranged.

- **Acquirement of materials and lab – 21 Days before Day 0**
Process of acquiring the materials from the manufacturers and booking lab dates, making any annotations on unexpected problems. The dates will depend on the manufacturers and authorizations from university.
- **Mixing and Curing – Day 0, 1**
 - Day 0: Mixing the components following the guidelines of previous chapter. and cast into molds.
 - Day 1: Take Day 0 specimens out of the molds and follow curing as on previous chapter
- **7 day tests – Day 7**
Day 7: Test 7 day curing time specimens
- **Early Report to check procedures and preliminary results – Day 10**
Report on the first time period test to control that everything is working as expected.
- **28 day tests – Day 28**
Day 28: Test 28 day curing time specimens
- **Report of Main Tests Results – Day 35**
Main Report with the 7 and 28 days' results, which should allow us to extract some conclusions.

3.2.- Implementation of the Test Plan

Once the test plan was proposed, we were able to start implementing it. However, due to lack of resources, logistics problematics and lack of lab's instrumentation and lab availability, there were significant changes on the original test plan. Here, the steps taken during the whole testing procedure will be explained with all the solutions proposed.

3.2.1.- Obtaining the materials

The most important part of the testing campaign was obtaining the materials, some of them being slightly rare to find, especially if we were demanding special properties. However, most of the materials were found in China, mainly in Shanghai or around, and only some of them were needed to be bought from foreign manufacturers.

- Concrete was obtained from a local factory at the outskirts of Shanghai, ensuring the quality as it was coming directly from the manufacturer. It was a trusted product as it was used before by some researchers from our department with great results.
- Fine sand, Ground Quartz, Silica fume and Steel Fibers were all provided by a research team from our department, ensuring good quality and easing the logistics problems.
- HRWR and accelerator were looked for on manufacturers that had good reputation with the department researchers but neither of them were able to produce them anymore, so we chose the already known BASF products to ensure the quality, even though they had higher costs. We acquired MasterGlenium Sky 8860CN and Rheocrete CNI, as they were available in China.
- CNT were one of the most important part of the materials and, with the graphene oxide, the most expensive ones. Thus, we contacted several manufactures local and abroad to do a collaboration in exchange of some samples for the tests, always ensuring that the quality of the manufacturer was on our standards. There were three kind manufacturers that offered us samples: HongWu Nanometer (China) MWCNT, NANOCYL (Belgium) providing the MWCNT-NC7000 and CheapTubes (USA) providing MWCNT.
- GO production is very limited and expensive if certain quality parameters are required, even more if we ask for it in aqueous solution. We contacted the few companies able to provide it and Graphenea (Spain) provided us with the Graphene Oxide in 4mg/mL aqueous solution.

3.2.2.- Molds

While we were obtaining all the materials, we needed to check whether we had molds available or not, as the size we were using was not the standard test size of 100x200mm that all research teams used previously. We need to remember that we discarded the 100x200mm size because of costs.

Unluckily, there were none available 50x100mm molds, nor the mixing labs had any available. We had to buy and order them, made of steel to ensure the quality. They can be seen below.



Figure 3-5 Standard mold for our specimens

3.2.3.- Mixing, casting and curing

The next step was to obtain available spots on the mixing lab and on the testing lab. The mixing lab allowed us, after a bit of wrangling and letting us know that we would make the mixing by ourselves without help, to mix our specimens and cure them there in the cabinet room until they were all demolded. We also managed to acquire a time window in the testing lab, however, only to be able to perform the 28 days test, so we would only mix the 28 days specimens on the first batch and try to mix the other 7 days specimens later on.



Figure 3-6 Storing a molded specimen in a moist cabinet

The maximum number of specimens to be tested on a day was, approximately, 6 per day, as per lab's technician suggestion. Consequently, we were able to mix only 6 specimens per day to keep constant the 28 days curing time, also needing less amount of molds than if we were doing all of them the same day. We were not able to mix both the 7 days specimens and the 28 days specimens because we didn't have an available time of 7 days until after the testing of 28 days, meaning we had to wait to mix them until 7 days before the available testing time. Therefore, we ended up mixing every day two dosages and the calendar planned had to be changed.

The specimens were mixed following the described process from section 4.1.2, however, we were not allowed to store for long the specimens in the mixing lab's moist cabinet and they had to be demolded and moved, after 24h, to a moist room next to the testing lab.



Figure 3-7 Mixing of powder (left); adding steel fibers (center); specimen after vibrating (right)

A complication on the mixing occurred when casting the molds. The vibrating table present in the mixing lab, that can be seen above, was designed for 40x40x160 sets of molds and it didn't allow us to secure our molds on it. Therefore, we had to manage to vibrate the specimens without any correct support, probably affecting the compaction rate, adding more time to the procedure timing, up to 8 minutes on the vibrating table, checking every 2' the compaction. It was noticed that high CNT&GO dosages took longer times than lower or zero concentrations.

3.2.4.- Compression test

After mixing the specimens and knowing which day were the tests going to be performed, we encountered a major problem that was not revealed before and needed immediate solving: the extensometer available at the lab was set at 100mm height, not allowing us to use it on our specimens, which were 100mm height or lower, after smoothing the surfaces.

To solve this situation, we contacted the manufacturer of the extensometer, EpsilonTech to ask them whether it would be possible to modify the extensometer to reduce its length, to for example 50mm, allowing us to place it on our specimen. On the figure below, a representation of the hypothetical plan is represented.



Figure 3-8 EpsilonTech extensometer

The picture shows how removing the piece crossed in red, and changing the right side frame piece, the extensometer could be modified. However, the company informed us about the cost of all the procedure and it was not something we could've afford, especially because it would've meant having to redo it, and repay, to change it back to 100mm length. Solving the problem through this way was discarded.

The final solution we applied, that was used before by some researchers and suggested by the head professor of the testing lab, was to use an adaptor for the extensometer.

So, we created two steel cylinders, with 52 mm diameter width and 50 mm height, creating a hole of 50mm diameter width and 1.5 mm depth on one face, to be able to insert the specimen on it without any force and attach the extensometers on the outside of the hole, being able to record the total displacement of the specimen. However, a remark should be about the effects on the results by having used the cylindrical adaptors.



Figure 3-9 Test setup with the adapter cylinders

When a cylindrical concrete specimen is tested in simple compression, the regulations require the use of specimens of slenderness greater than $H / d = 2/1$. Smaller slender relations give rise to apparently greater resistances due to the effect of the confinement exerted by the plates of the press. The high rigidity of the press plates, facing the flat face of the specimen, produces at its ends a biaxial stress state without transverse deformation due to Poisson effect and thanks to the friction in the steel-concrete contact. However, in the central section of the specimen, the stress state is purely uniaxial, with significant transverse deformation since this is not impeded. The state of tensions described leads to failure of the specimen by a typical fracture in the form of opposed cones as can be seen in the following figures.

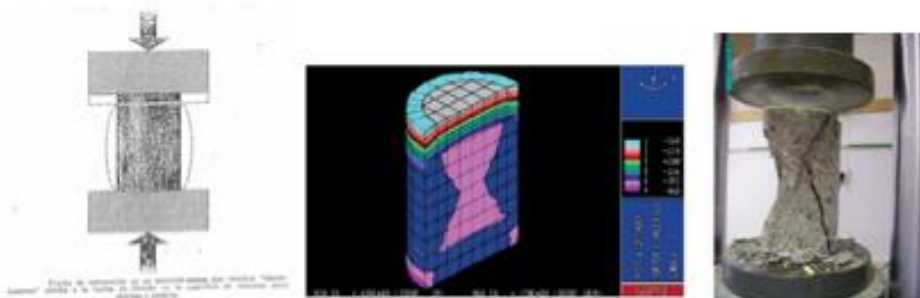


Figure 3-10 Compression test result examples [123,125]

If the only purpose of the test is to measure the compressive strength of the concrete, this arrangement is more than sufficient, with no need to take additional precautions. If in addition it is required to measure the deformations of the concrete in compression then it is convenient to take the measurements only in the central third of the height of

the specimen, where the state of tensions is practically uniaxial, giving rise to LVDT dispositions like the one of the figure below.



Figure 3-11 Example of LVDT placement [124]

In case the plates of the press are not rigid or the friction with the specimen does not exist, the state of tensions in the specimen can be considered uniaxial in all its height and will result in a typical fracture mode in parallel vertical fractures.

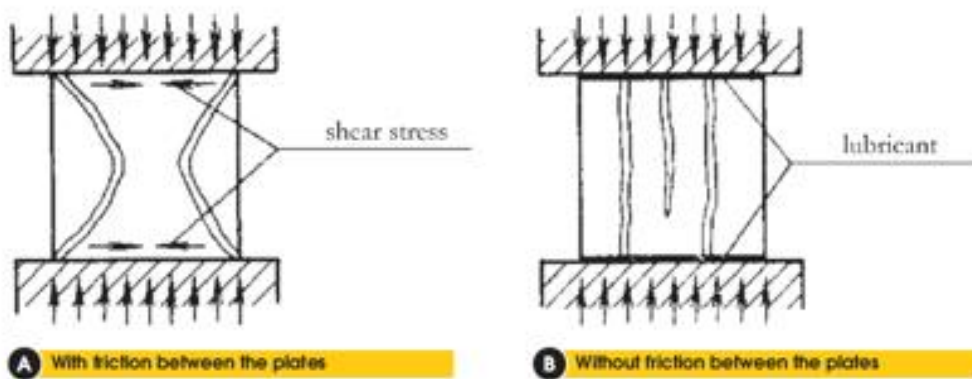


Figure 3-12 Failure modes [125]

In our case, the interposition of the metallic rings adapters to be able to reuse the extensometers of the laboratory can cause some distortion in the results, namely:

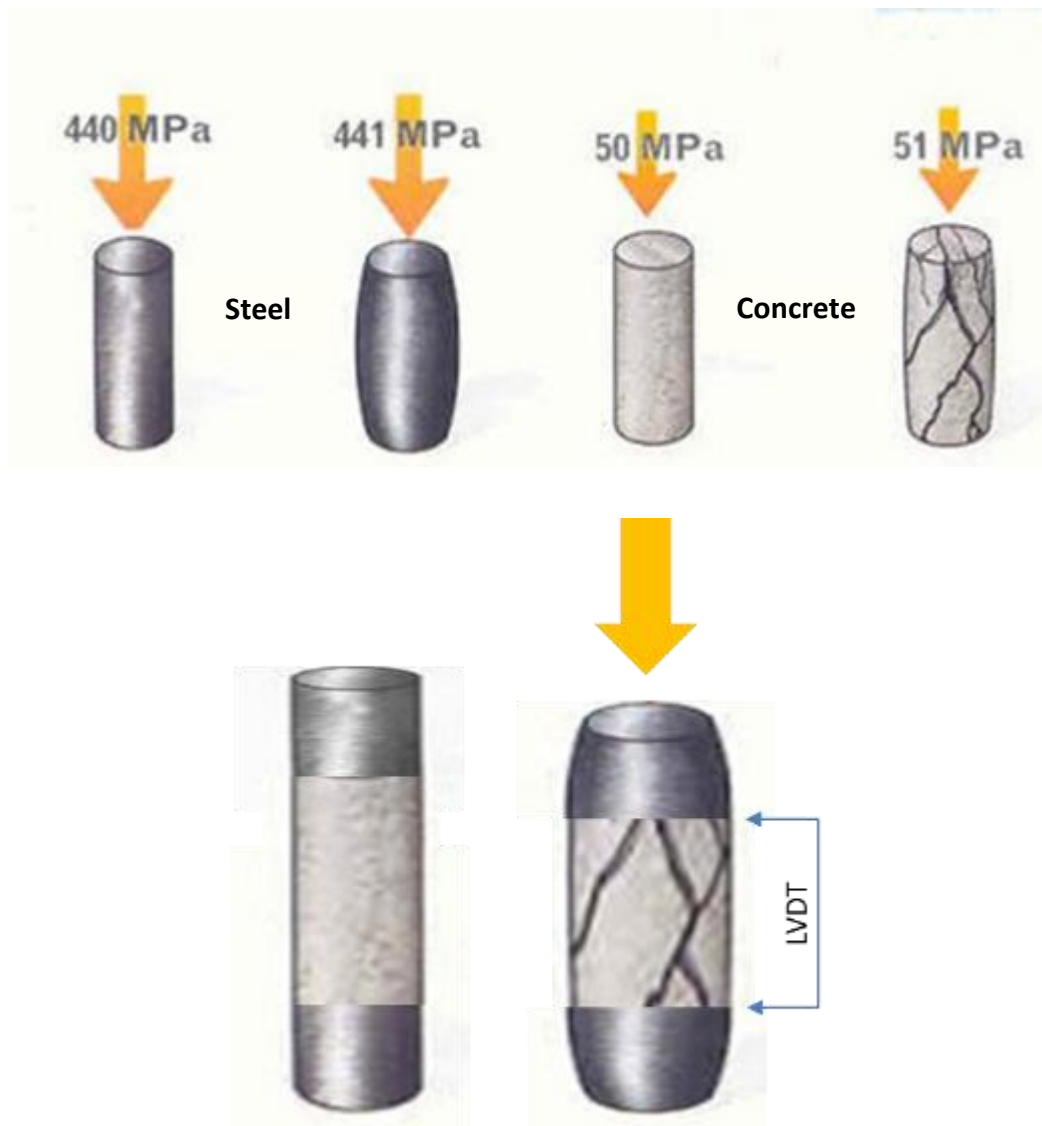


Figure 3-13 Behavior of concrete vs steel [126]

- The extensometers are supported on the metal rings taking advantage of a couple of lateral slits prepared to achieve a firm contact, however, throughout the test some of the supports of the extensometer can slide giving erroneous records.
- The extensometers will measure the total deformation of the specimen plus the deformation that appears in the adaptation and accommodation of the metal-specimen interface; This will give us greater initial deformations and an initial modulus of elasticity apparently low but increasing when the load increases.
- The Poisson modulus of the steel is approximately 0.3, while the Poisson modulus of the un-cracked concrete is 0.2, although this will increase rapidly from the first cracks. Thus, the degree of confinement in the flat faces of the specimen will change throughout the test, going from an initial state of tensions as in case B of FIG. 5 to a situation similar to that of case A of the same figure.

- When the tensile strength is small (UHPC without SF) the Poisson module will increase excessively, with the state of dominant stresses similar to type B, producing the detachment of vertical slabs that suddenly reduce the effective section of the specimen and leading to the ruin the trial quickly.
- When the tensile strength is improved by the addition of steel fibers, the Poisson modulus will increase more slowly, the breaking mode being more in accordance with type A, giving prolonged elongation records.
- Due to lack of adequate instrumentation, the transverse deformation (swelling) of the specimen could not be monitored, which could have confirmed these hypotheses.

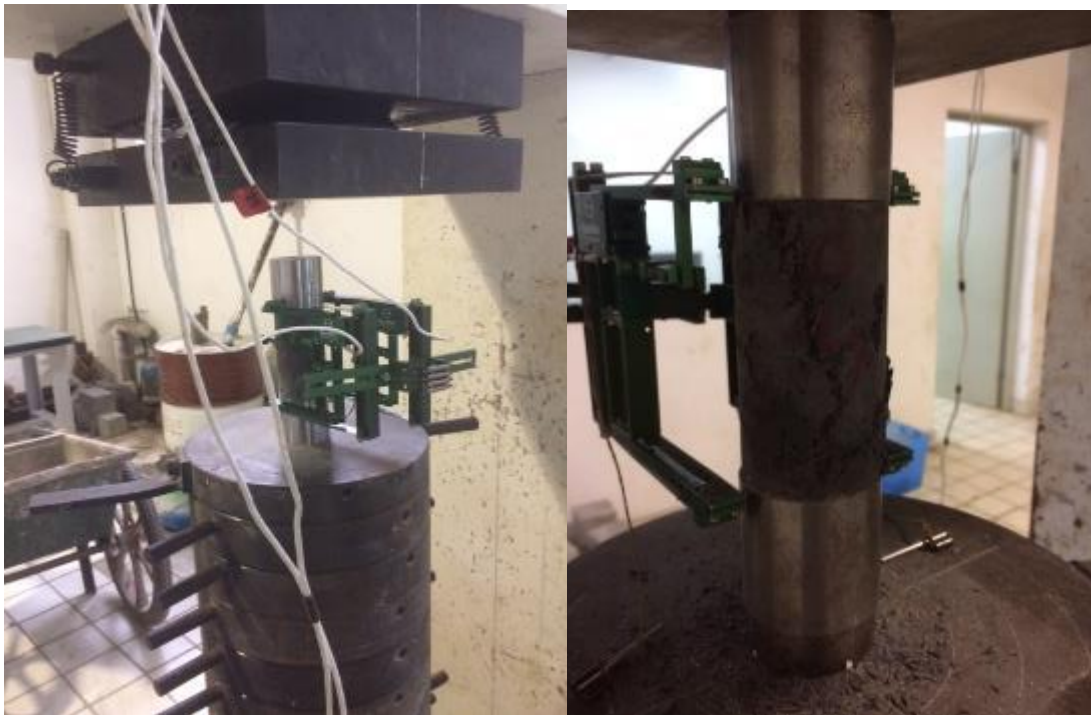


Figure 3-14 First test design (left); Final test design for practical purposes (right)

Even though the intention was to use the adaptor as the left picture, we ended up using it like the right picture, because the hole made on the steel cylinder was difficult to clean after the tests, and the technicians thought it was faster, and same results, the other way, adding a 50 mm diameter steel plate to cover the hole, as it can be seen on the right picture. There was sand added on the faces of contact between steel cylinders and specimen to flatten any imperfection that the specimen might had.

Following the described process in section 4.1.3 we performed the tests of the specimens. Pictures were taken at different steps of the process for graphical documentation.

For every test, the extensometers needed to be calibrated and, in the beginning, it took up to 2 hours for only one test, as the technicians didn't have much practice with it. Later on, the efficiency increased as the technicians got the specimens better prepared.

At some point of the test, being those the moments where a loss of force was occurring, and as suggested by the test technician, we were decreasing the displacement rate to 0.01 mm/min. Once the speed was reduced, it kept unchanged to not damage the specimen.

A very few specimens were tested without extensometers to increase the efficiency on the testing procedure and analyze whether it would make a difference, which we will comment on the discussion of the results.

The specimens that were too damaged or that were not meeting the curing requirements, were discarded from the tests.

All the results from the tests were obtained in worksheet files and transferred to be analyzed.

The specimens that we were able to test and obtain results from, are the following:

Table 3-10 Name coding of the specimens created and tested

GO →	0%	0.04%	
CNT →	0%	0.08%	0.50%
0% SF	UHPC07D0SF000_xx (3) UHPC28D0SF000_xx (3)	UHPC07D0SF008_xx (3) UHPC28D0SF008_xx (3)	UHPC07D0SF050_xx (2) UHPC28D0SF050_xx (0)
2% SF	UHPC07D2SF000_xx (3) UHPC28D2SF000_xx (3)	UHPC07D2SF008_xx (3) UHPC28D2SF008_xx (3)	UHPC07D2SF050_xx (0) UHPC28D2SF050_xx (3)
4% SF	UHPC07D4SF000_xx (0) UHPC28D4SF000_xx (3)	UHPC07D4SF008_xx (0) UHPC28D4SF008_xx (3)	UHPC07D4SF050_xx (0) UHPC28D4SF050_xx (2)

xx= [01, 02, 03, ... n]

Chapter 4 - Lab Results

4.1.- RAW DATA

4.2.- PRETREATING OF THE DATA

4.2.1.- Filtering extensometers

4.2.2.- Adjusting the initial slope

4.3.- PARAMETERS RESULTING FROM THE EXPERIMENTAL DATA

4.4.- PARAMETRIC ANALYSIS OF SF AND CNT

We will present the raw data curves together with the representative values and with a brief description of the specimens and its characteristics. They can be found in Annexes 1 to 4.

Chapter 4 - Lab Results

4.1.- Raw Data

When analyzing the data, there were some important observed phenomenon that, in order to have proper data, they need to be treated afterwards, because we need to be able to make a qualitative discussion about the results. Some of the issues are given by the nature of the materials, while others might come from the test procedure.

The most noticed issues are:

- On rare occasions, one of the extensometers for the test failed to record appropriate data. The apparent reason for it is experiencing a move provoked by the specimen or it can be bad placement of the extensometer. Also, there might happen that one of the extensometers is not well calibrated and it captures wrong data. On these occasions, we manually choose the extensometer we want to analyze and we discard using the other one for any comparison. An example of this situation can be seen below, where we will disregard the blue one.

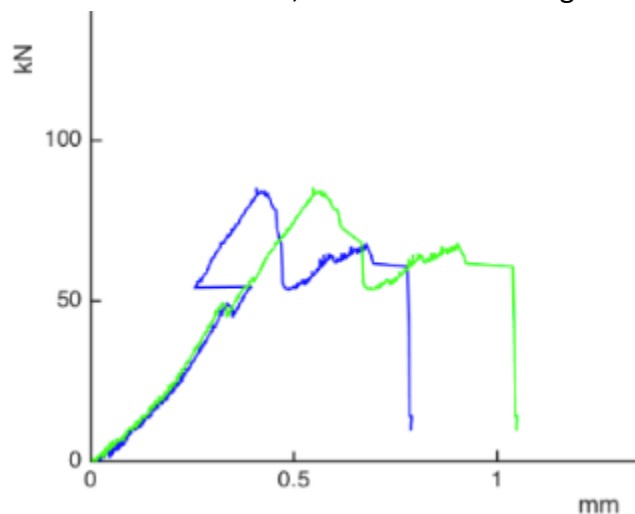


Figure 4-1 Example of one extensometer not recording correctly

- Half of our specimens were designed with steel fibers and the other half were designed without. We can see on the tests how quite a lot of the specimens without steel fibers have a fragile cracking when they reach the ultimate strength. After this peak point, all the data recorded is disruptive and undecryptable, so it needs to be eliminated, as it cannot be taken into account for the comparisons with other specimens, especially with those that have a post cracking behavior. An example of this phenomenon can be seen on the following picture.

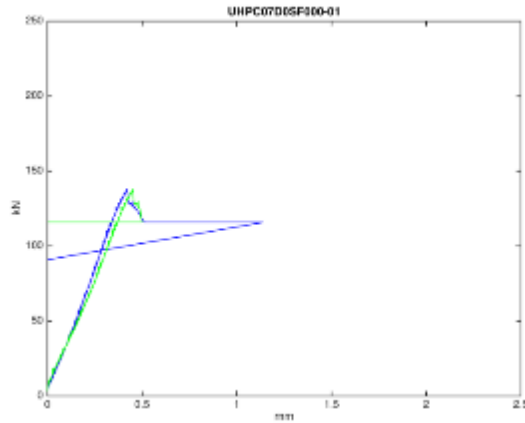


Figure 4-2 Example of disruptive post-peak data of a specimen without steel fibers

- Because of minor incidents in the laboratory, a few specimens were tested without the EpsilonTech extensometer and only with the LVDT from the loading machine. Even though the results were well obtained, there seems to be a recurrent/systematic error on the value/calibration of the strengths and displacement. By using a constant scale factor for all the specimens, the results can show greater similarity to the ones that were tested with extensometers. One specimen tested without extensometer can be seen below.

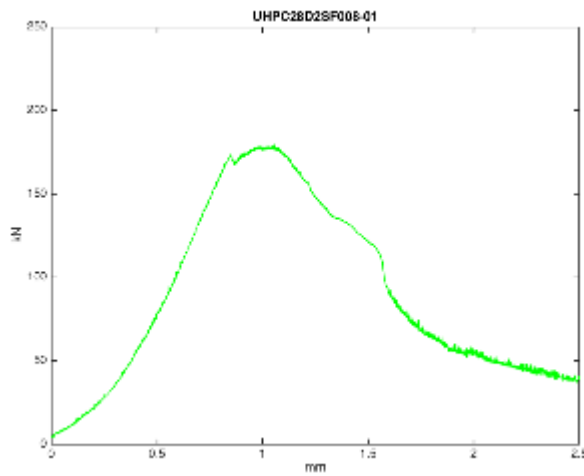


Figure 4-3 Specimen results obtained with the LVDT of the hydraulic press

- The initial slope of the curve is, in almost every specimen, increasing in the first stages of loading, which gives us the understanding that is caused by the accommodation between the specimen, the steel cylinder adapters and the plates of the loading machine settling with the initial increments of force, until it reaches the typical and real concrete constant slope. It can be seen on the example below.

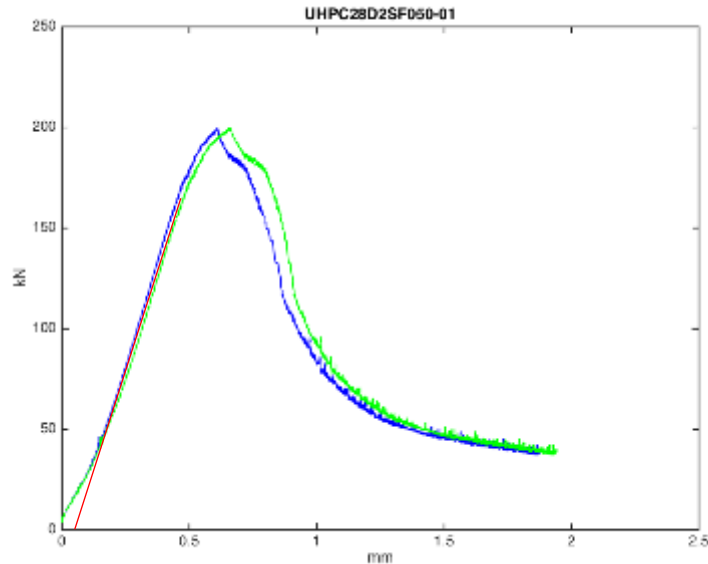


Figure 4-4 Force-displacement graph for UHPC28D2SF050-01 specimen

- On some specimens curve, we can see a sudden loss of strength just to increase again with the same slope than before the loss of strength. We hypothesize that this is due to a loss of the available loading area of the specimen that is proportionate to the loss of strength seen on the graph. However, the stress the specimen face is supporting will remain constant, as stress is F/A , and we are reducing both variables linearly by the same factor, having a smooth stress-strain curve. To prove this hypothesis, it would have been useful to weight specimens before and after tests, in order to calculate the loss of mass. This sudden loss of strength can be seen on the following example.

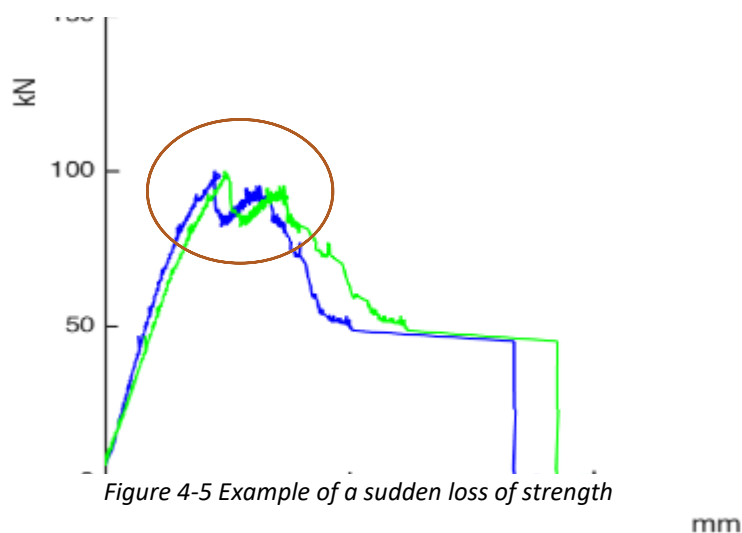


Figure 4-5 Example of a sudden loss of strength

4.2.- Pretreating of the data

4.2.1.- Filtering extensometers

The first issue that we tackled was choosing whether the data obtained was usable or if the extensometers failed to capture the correct values. In those cases where **extensometers deviate too much from one another**, and if we see clearly which one is the deviated extensometer, we remove from the analysis the deviated extensometer and we keep the accurate one, obtaining only one force- displacement curve that will be used to obtain the stress-strain curve. Otherwise, if both extensometers show more or less the same results, we will keep them both. On the case below, the red extensometer could not be used because it has a displacement that clearly is not physically capable of obtaining.

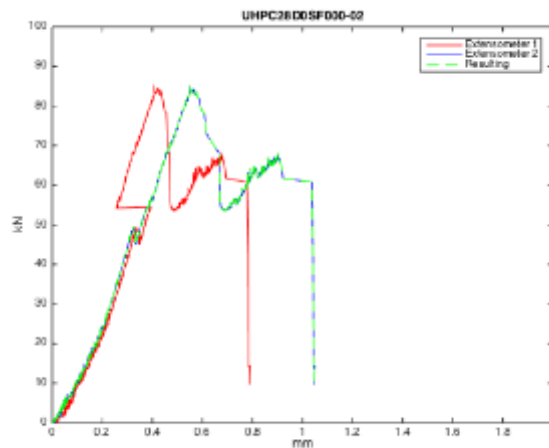


Figure 4-6 UHPC28D0SF000-02 Raw Data and resulting data after filtering wrong extensometer

Another example of one extensometer not recording the appropriate results can be seen below. In this case, the green extensometer has disruptive data around the peak strength, as well as at the end post-cracking section, so we use only the blue extensometer.

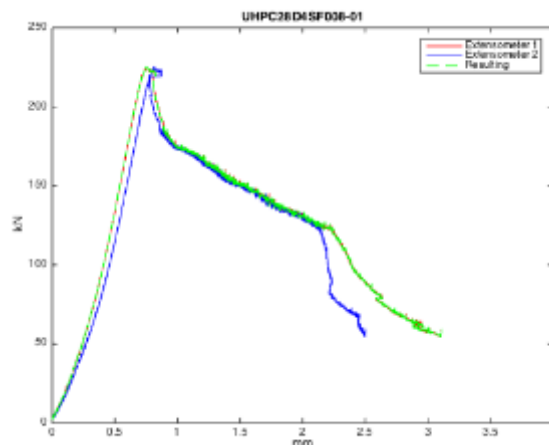


Figure 4-7 UHPC28D4SF008-01 Raw Data and resulting data after filtering wrong extensometer

All the process is made using programmed code in matlab that is interactive and allows the user to select the desired extensometers to be used from the desired specimen.

In case **both extensometers are usable**, we keep them both and we make the average of the strength results for each displacement, to obtain only one force-displacement curve that will be used to obtain the stress-strain curve. This averaging process can be seen in the next pictures.

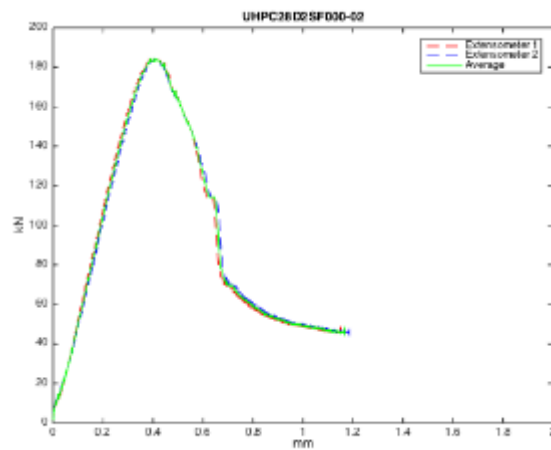


Figure 4-8 UHPC28D2SF000-02 Raw Data and averaged data of both extensometers

4.2.2.- Adjusting the initial slope

The initial slope of the concrete specimen test is a very important result of the test, as when changing the data to stress-strain curve, it will become the Elastic Modulus of the specimen. When testing specimens, there is an initial time period where there is a settling between the specimen and the loading plates, affecting at the contact faces between them. In our case, our specimens had to be polished manually to be flattened, increasing the problems on the initial settling. Until the load applied is not enough to eliminate the effect of the surface imperfections, we can't consider the initial slope as the Elastic Modulus of the specimen. Because we are looking for the Elastic Modulus constant, that comes from the initial constant slope, we will correct the initial settling behavior for matters of calculating the mechanical properties. When the first part of the curve is corrected, we will obtain a constant slope that will represent the Elastic Modulus on the stress-strain curve. It is important for the new initial constant slope to start at the origin, as we want to represent all the strength needed to deform the specimen, not counting the strength needed to adjust faces imperfections. The process is also computerized by matlab coding but it can be explained as a step by step process.

As an example, the steps of what the matlab code calculates can be showed with a few descriptive pictures.

We have a curve from one specimen obtained from the averaged data:

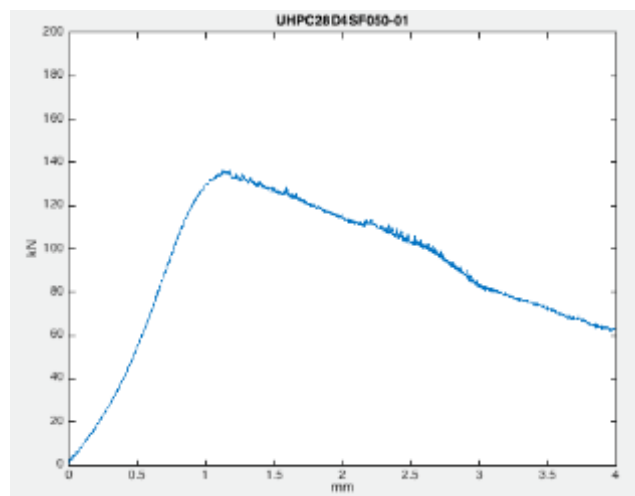


Figure 4-9 Averaged extensometers data of UHPC28D4SF050-01

On this specimens, we realize that there is a initial time period where the initial settling is occurring and we want to correct this behavior to use the data for mechanical properties calculations.

For this purpose, we need to decide which is the part where the settling occurs. The matlab code is programmed to find and compare the slopes between multiple consecutive segments of points on the initial part of the curve. Once the program finds consecutive sets of data that all have approximately the same slope, it modifies the curve so that it has a constant initial slope, without any settling disruptions, and it allows

us to obtain the strength without counting the force used on the settling process. A graphical example of the initial slope that we would obtain can be seen on figure 4-11.

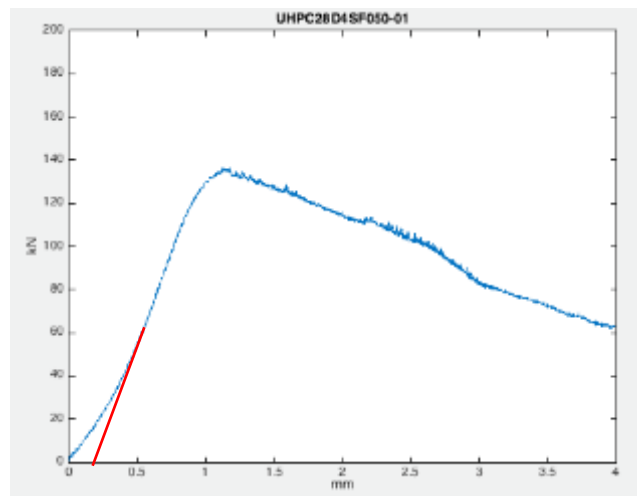


Figure 4-10 In red, the initial slope obtained with the Matlab code

As not all the curves have equal settling problems, and the code needs to accurately find the correct point where settling disruptions are over, we made it possible to adjust the quadratic error allowance, the amount of consecutive sets of points to be compared, and the amount of points in each set. In this way, we can always adjust the accuracy of the code taking into account the accuracy of the data.

Graphically it can be easily explained using the figure 4-12 below. We calculate iterations so that 4 (as example) consecutive segments of the curve have all the same slope, finding the time where settling ends. Knowing this time and the distance to the origin, we can set the real initial slope. The iterative process allows to find the first constant slope of the specimen data, which will be considered the elastic modulus of deformation.

We can see the first two iterations, in big scale, graphically represented. To obtain the initial settling time position, we would need to do more iterations until the program finds acceptable the quadratic error resulting from the comparison of curves.

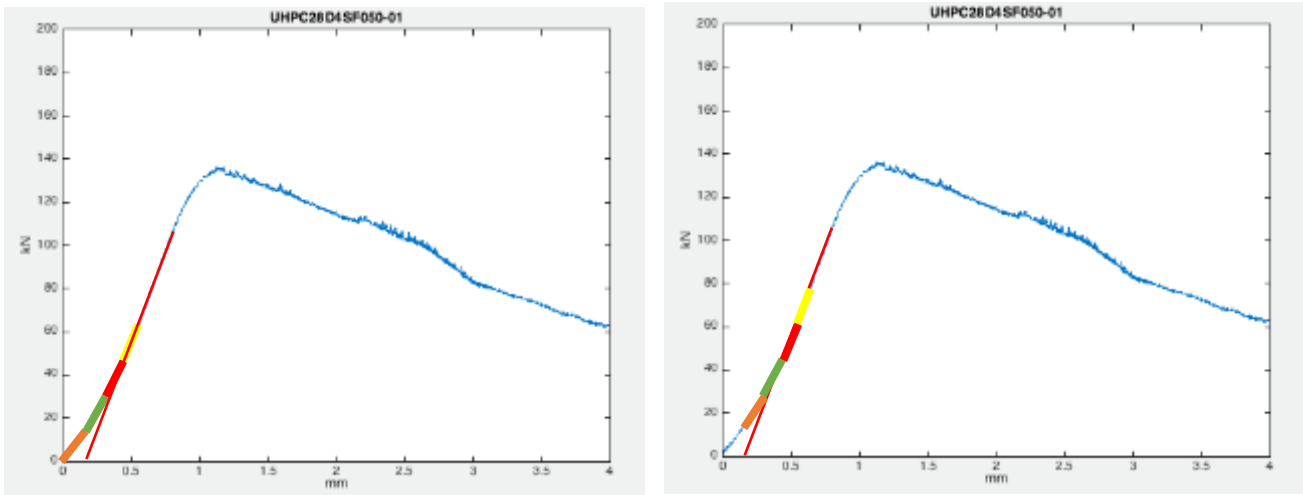


Figure 4-11 Simulation of the iteration performed by the code

The results after applying this algorithm are shown below.

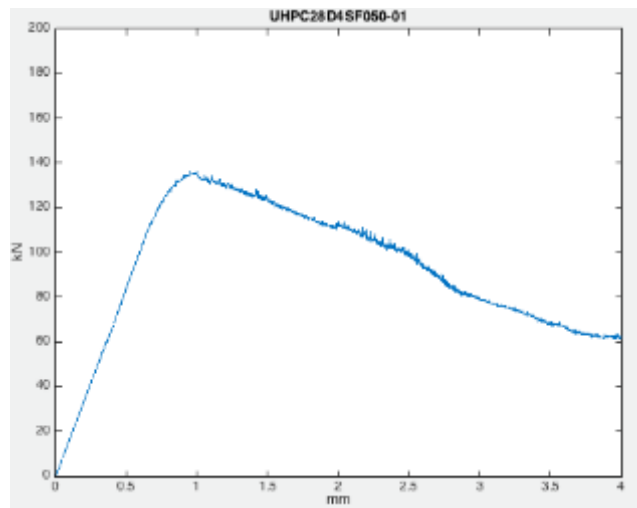


Figure 4-12 Final curve with the initial slope modified

Having our data pretreated with the filtering and adjust of the initial slope allows us to be prepared for calculating the objective of the tests, the parameters of the stress-strain curves. We are not modifying the force-displacement curve but removing the disruptive data, to depict it and deduce the stress-strain relationship. The filtering process applied has support in a physical reality and are identified in the laboratory (plates settling, contact faces with sand, etc).

4.3.- Parameters resulting from the experimental data

In this section, we will calculate the constitutive equation parameters that correspond to each one of the test results.

From direct observation of the test results, we obtain the values for E_c , f_c , ϵ_c , allowing us to formulate the first section of the constitutive equation. The rest of the parameters (σ_2/f_c , ϵ_2/ϵ_c , ϵ_3/ϵ_c) will be obtained by mathematical adjustment to the proposed constitutive equation using the method of the least squares. On the following table, we present the values for all the specimens.

Table 4-1 Summary table

7D	f_c (MPa)	ϵ_c	E_c (GPa)	E_c / E_s	σ_2/f_c	ϵ_2/ϵ_c	ϵ_3/ϵ_c	R^2	R^2 (<peak)	R^2 (>peak)
OSF000_1	70.3	0.0045	15.500	1.0000	0.9436	1.0163	2.9442	0.9993	0.9995	0.9999
OSF000_2	66.6	0.0036	19.100	1.0380	0.9199	1.1110	10.000	0.9992	0.9992	1.0000
OSF000_3	67.3	0.0037	21.976	1.2201	0.2601	1.5671	3.5392	0.9952	0.9993	0.9884
OSF008_1	47.5	0.0046	10.317	1.0000	0.2904	1.8519	3.6926	0.9772	0.9999	0.9865
OSF008_2	49.0	0.0034	20.065	1.3868	0.2591	1.7155	3.6930	0.9976	0.9978	1.0000
OSF008_3	53.7	0.0026	21.250	1.0225	0.6107	1.8175	10.000	0.9927	0.9998	0.9966
OSF050_1	43.0	0.0042	21.250	2.0597	0.6234	1.1715	2.5768	0.9633	0.9728	0.9975
OSF050_2	51.0	0.0025	24.718	1.1992	0.5198	2.1959	10.000	0.9840	0.9988	0.9923
2SF000_1	71.2	0.0073	11.637	1.1954	0.3811	2.0902	4.4842	0.9943	0.9998	0.9955
2SF000_2	85.8	0.0043	25.062	1.2535	0.5281	1.8500	6.3525	0.9901	0.9999	0.9922
2SF000_3	97.2	0.0051	24.973	1.3110	0.5063	2.1588	7.5593	0.9886	0.9999	0.9946
2SF008_1	92.1	0.0046	26.837	1.3325	0.3205	3.2435	9.7163	0.9939	0.9996	0.9968
2SF008_2	81.7	0.0052	23.565	1.5047	0.3589	2.6986	6.7019	0.9945	0.9991	0.9962
2SF008_3	79.5	0.0081	13.122	1.3371	0.3335	2.2134	4.4682	0.9956	0.9993	0.9967

28D	f_c (MPa)	ϵ_c	E_c (GPa)	E_c / E_s	ϵ_2/ϵ_c	σ_2/f_c	ϵ_3/ϵ_c	R^2	R^2 (<peak)	R^2 (>peak)
OSF000_1	58.0	0.0026	22.599	1.0234	0.5073	1.6618	3.6677	0.9986	0.9986	1.0000
OSF000_2	43.5	0.0050	8.843	1.0153	0.7000	1.3000	10.000	0.9783	0.9987	0.9887
OSF000_3	67.4	0.0042	17.880	1.1132	0.2523	1.5932	5.7189	0.9967	0.9975	0.9999
OSF008_1	55.7	0.0029	17.283	1.0000	0.6257	2.1046	4.8564	0.9978	0.9975	0.9999
OSF008_2	54.6	0.0078	10.093	1.4459	0.0000	1.5771	10.000	0.9715	0.9720	1.0000
OSF008_3	51.6	0.0037	14.099	1.0150	0.7543	1.3420	1.4539	0.9752	0.9997	0.9893
2SF000_1	58.4	0.0076	8.628	1.1178	0.4614	1.6211	3.6677	0.9939	0.9983	0.9983
2SF000_2	94.1	0.0041	25.911	1.1309	0.3241	1.8865	5.8086	0.9960	0.9998	0.9963
2SF000_3	89.9	0.0068	23.333	1.7682	0.3228	2.2366	5.7189	0.9888	0.9955	0.9977
2SF008_1	91.6	0.0082	15.021	1.3485	0.3345	1.8857	4.8564	0.9934	0.9991	0.9963
2SF008_2	111.0	0.0064	19.919	1.1462	0.2462	1.8251	10.000	0.9885	0.9996	0.9879
2SF008_3	79.3	0.0060	17.908	1.3489	0.2822	2.0232	4.8623	0.9950	0.9991	0.9952
2SF050_1	101.9	0.0058	20.485	1.1727	0.3267	1.7771	4.8907	0.9959	0.9998	0.9952
2SF050_2	105.6	0.0061	19.242	1.1110	0.2727	1.9013	5.2555	0.9884	0.9999	0.9856
2SF050_3	95.9	0.0057	20.267	1.2085	0.2229	1.9127	5.9176	0.9936	0.9986	0.9941
4SF000_1	118.9	0.0081	18.882	1.2847	0.4443	1.9908	4.4913	0.9950	0.9997	0.9965
4SF000_2	121.2	0.0058	22.817	1.0870	0.5982	2.1258	5.9780	0.9941	0.9999	0.9962
4SF000_3	130.7	0.0061	23.814	1.1036	0.3877	3.3562	7.0187	0.9955	1.0000	0.9967
4SF008_1	114.8	0.0060	20.128	1.0517	0.8283	1.2636	6.7285	0.9911	1.0000	0.9948
4SF008_2	137.3	0.0055	33.928	1.3550	0.3317	2.0827	5.4361	0.9958	0.9996	0.9973
4SF008_3	134.8	0.0071	22.293	1.1685	0.3161	2.0091	4.2739	0.9917	0.9997	0.9917
4SF050_1	69.6	0.0102	8.575	1.2623	0.5387	3.1477	9.6641	0.9968	0.9998	0.9987
4SF050_2	75.9	0.0055	22.893	1.6620	0.3514	3.0831	7.0202	0.9955	0.9985	0.9983

Where R^2 is the called "determination coefficient". R^2 is a statistic commonly used in the context of statistical models whose main purpose is to predict future results or test and hypothesis. The coefficient determines the quality of the model to replicate the results, and the proportion of variation of the results that can be explained by the model. It is the proportion of the variance in the dependent variable that is predictable from the independent variable. To understand how this coefficient works, we summarize a few concepts of statistics.

When we adjust a function to an experimental curve, the method of least squares takes the sum of the squared residuals as a measure of the error that is committed,

$$\sum_{i=1}^n e_i^2 = \sum_{i=1}^n (y_i - \hat{y}_i)^2 = \sum_{i=1}^n (y_i - f(x_i))^2 \quad (4.26)$$

That amount divided by n, the number of samples, is used as a measure of the goodness of fit.

In the case of linear functions (line, parabola, hyperbola, etc.), the average of the residuals is 0 (property 1), so the sum of the squares of the residuals divided by n is nothing other than the variance of the variable "e" and is called residual variance:

$$\frac{\sum_{i=1}^n e_i^2}{n} = \frac{\sum_{i=1}^n (e_i - \bar{e})^2}{n} = S_e^2 \quad (4.27)$$

Let's see the meaning of this residual variance:

$$e_i = y_i - \hat{y}_i \Rightarrow y_i = \hat{y}_i + e_i \Rightarrow S_y^2 = S_{\hat{y}}^2 + S_e^2 \quad (4.28)$$

The first term to the right of the equality is called "variance explained by the regression" and tells us to what extent the dependent variable (y) is explained by the adjustment model, being able to interpret the second summation -which is the "residual variance"- as a measure of what remains unexplained after having made the regression.

This residual variance presents the problem of determining from which values it is sufficiently small or large enough to admit a good or bad adjustment: the answer to this question will be given by the coefficient of determination R^2 .

$$R^2 = \frac{S_y^2}{S_y^2} = \frac{S_y^2 - S_e^2}{S_y^2} = 1 - \frac{S_e^2}{S_y^2} \quad (4.29)$$

The determination coefficient takes values between 0 and 1 ($0 \leq R^2 \leq 1$)

- It takes the value "0" when the regression does not explain anything about the variability of the observed values and therefore the obtained adjustment does not adequately (even minimally) model the relationship between variables.

$$R^2 = \frac{S_y^2}{S_y^2} = 0 \Rightarrow S_y^2 = 0 \Leftrightarrow S_y^2 = S_e^2 \quad (4.30)$$

- It takes the value "1" when the adjustment made collects all the variability of the original variable, and therefore the adjustment is perfect.

$$R^2 = \frac{S_y^2}{S_y^2} = 1 \Rightarrow S_y^2 = S_y^2 \Rightarrow S_e^2 = 0 \quad (4.31)$$

- For values between "0" and "1", the adjustment is the better the closer the coefficient of determination approaches 1. The adjustments are considered reasonable when $R^2 \geq 0.75$.

As we can see in the summary table 4-1, the values of the R^2 are greater than 0.99, which is considered an excellent approximation, confirming the goodness of our constitutive equation formulation. All the constitutive equation curves can be found in annex 3, in the same graph as adjusted experimental curves, to allow for a visual comparison.

4.4.- Parametric analysis of SF and CNT

On the previous section, we were able to get, from test results, the different parameters needed to define our constitutive equation, without comparing the different dosages between them. Following that, we will work on obtaining equations that could predict the outcome of any specimen with SF and CNT&GO particular quantities. We will compare and contrast each parameter for all specimens, and using different variables, we will obtain a universal equation that will define our UHPC parameters depending on the quantity of SF and CNT&GO.

To find the equation that simulates the effect of the quantitative change of steel fibers and/or carbon nanotubes, we will use a base parameter (e.g. the value of plain UHPC) and two multiplier factors.

These multiplier factors will be based on equations, mainly second-degree equations, which will model the observed change on the parameter with the increase or decrease of SF or CNT/GO. Obviously, this change is the different results we obtained from the tests on each dosage specimen.

Multiplying the plain UHPC parameter and the SF / CNT factors, we can obtain our specific dosage related parameter

The factors are defined as follows:

$$K_{SF} = ax^2 + bx + 1$$
$$K_{CNT} = cy^2 + dy + 1$$

Being:

a, b, c, d: different values to be found for each factor of each material property parameter calculation.

x: the concentration of steel fibers, expressed on % by volume

y: the concentration of CNT, expressed on % weight material/weight cement

The calculation of “a, b, c, d”, and the calculation of the factors, will be done by fitting for the best values by least squared errors method. The least squared errors are calculated as the difference between results obtained through the proposed equations and their equivalent test result parameter.

For each parameter, the factors K_{SF} and K_{CNT} will be calculated and they will most likely be different. In addition, for null concentrations of steel fibers and/or CNT, the factors are indeed equal to one, making the parameter equal to that of the plain UHPC.

After detailed mathematical work, the formulation that we will be using for each parameter, and that most accurately represents our test results, is the following:

$$E_c(UHPC, \%SF, \%CNT) = E_c(UHPC, 0, 0) \cdot (0.016 \cdot x^2 - 0.021 \cdot x + 1) \cdot (3.977 \cdot y^2 - 1.827 \cdot y + 1)$$

$$f_c(UHPC, \%SF, \%CNT) = f_c(UHPC, 0, 0) \cdot (-0.007 \cdot x^2 + 0.301 \cdot x + 1) \cdot (-1.796 \cdot y^2 + 0.632 \cdot y + 1)$$

$$\varepsilon_c(UHPC, \%SF, \%CNT) = \varepsilon_c(UHPC, 0, 0) \cdot (-0.008 \cdot x^2 + 0.208 \cdot x + 1) \cdot (-1.276 \cdot y^2 + 0.731 \cdot y + 1)$$

$$\frac{\sigma_2}{f_c}(UHPC, \%SF, \%CNT) = \frac{\sigma_2}{f_c}(UHPC, 0, 0) \cdot (0.073 \cdot x^2 - 0.376 \cdot x + 1) \cdot (8.011 \cdot y^2 - 4.462 \cdot y + 1)$$

$$\frac{\varepsilon_2}{\varepsilon_c}(UHPC, \%SF, \%CNT) = \frac{\varepsilon_2}{\varepsilon_c}(UHPC, 0, 0) \cdot (0.129 \cdot x + 1) \cdot (-2.338 \cdot y^2 + 1.568 \cdot y + 1)$$

$$\frac{\varepsilon_3}{\varepsilon_c}(UHPC, \%SF, \%CNT) = \frac{\varepsilon_3}{\varepsilon_c}(UHPC, 0, 0) \cdot (0.009 \cdot x^2 + 0.086 \cdot x + 1) \cdot (1.597 \cdot y^2 - 0.328 \cdot y + 1)$$

With these equations, and although the results are not as clear as it would have been desirable, we are already in a position to have a basic parametric study, where we can compare different dosages and the expected results to be obtained. More importantly, we will be able to mathematically optimize a dosage to obtain the best performance by the described parameters and equations.

Annex 4 shows graphs for each parameter for different dosages, both for the original data points and the parametric curve obtained with the previous equations.

Chapter 5 - Finite Element Model for a Biaxial Stress on UHPC

5.1.- MATHEMATICAL FORMULATION FOR BIAXIAL UHPC CONSTITUTIVE EQUATIONS

5.1.1.- Uniaxial Constitutive Relationships

5.1.2.- Biaxial Constitutive Relationships

5.2.- PROPOSED UMAT (ABAQUS) SUBROUTINE

5.2.1.- Pseudocode for UMAT Subroutine

5.2.1.1.- Inputs

5.2.1.2.- Outputs

5.2.1.3.- Local Variables

5.2.1.4.- External Process

5.2.1.5.- Process

5.2.2.- Pseudocode for SLOPE Subroutine

5.2.2.1.- Inputs

5.2.2.2.- Outputs

5.2.2.3.- Local Variables

5.2.2.4.- Process

5.3.- FORTRAN CODE FOR ORTHOTROPIC BIAXIAL NONLINEAR MODEL FOR UHPC

5.3.1.- UMAT4UHPC SUBROUTINE

5.3.2.- Subroutine SWAP(A,B)

5.3.3.- Subroutine SLOPE

5.4.- CHECKING THE GOODNESS OF THE PROPOSED MODEL

5.4.1.- Model geometry

5.4.2.- Material properties

5.4.3.- Load application and measurement of results

5.4.4.- Presentation of results of the FEM for UHPC

In this chapter, the finite element model for Biaxial Compression Test on our UHPC is explained and implemented.

Chapter 5 - Finite Element Model for a Biaxial Stress on UHPC

The aims of this chapter is the numerical simulation of the mechanical performance of ultra-high performance concrete UHPC with additions: graphene oxide, carbon nanotubes and/or steel fibers.

In order to achieve such purpose, it was used a computational support that was developed in the ABAQUS development environment, on the basis of the finite element method on the orthotropic biaxial framework and nonlinear constitutive relationships for concrete, obtained from experimental results, as explained in previous chapters.

Specific UMAT (User Material subroutines in ABAQUS context) has been designed and coded, formulating both axisymmetric stress and plane stress models, and compared with the fulfilled compressive cylinder test.

The numerical analysis was performed on an incremental iterative procedure and finite element approach adopting the orthotropic nonlinear formulation proposed by KWAK and FILIPPOU [112], from which the constitutive matrix is defined through the equivalent strains “ ε_{ei} ”, that are given by:

$$\varepsilon_{ei} = \varepsilon_i + D_{ij}\varepsilon_j / D_{ii} \quad (5.1)$$

The “ i ” and “ j ” indexes refer to principal plane direction. The “ D_{ij} ” parameters represent the constitutive matrix elements.

5.1.- Mathematical formulation for Biaxial UHPC constitutive equations

5.1.1.- Uniaxial Constitutive Relationships

For the simulation of concrete in **uniaxial tension and compression** it was adopted the constitutive relationships proposed in previous chapter 4, as illustrated in figures from Annex 3, represented by the formulas:

$$\sigma(x = \varepsilon/\varepsilon_c) = f_c \cdot \begin{cases} \left(1 - \frac{E_c}{E_s}\right) \cdot x^{\frac{E_c}{E_s - E_c}} + \frac{E_c}{E_s} \cdot x, & x \leq 1 \\ (\sigma_2/f_c - 1) \cdot \left[\frac{(x-1)}{(\varepsilon_2/\varepsilon_c - 1)}\right]^{\frac{E_c}{E_s}} + 1, & 1 < x \leq \varepsilon_2/\varepsilon_c \\ \sigma_2/f_c \cdot \frac{(\varepsilon_3/\varepsilon_c - x)}{(\varepsilon_3 - \varepsilon_2)/\varepsilon_c}, & \varepsilon_2/\varepsilon_c < x \end{cases} \quad (5.2)$$

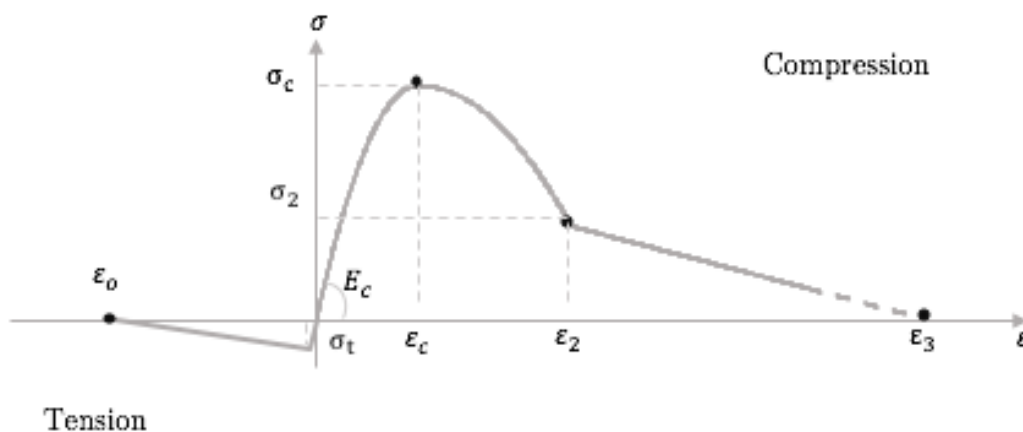


Figure 5-1 Proposed constitutive relationships

We define unitary stress, unitary strain and unitary elasticity modulus as:

Unitary stress

$s = \sigma/\sigma_p$	$s_2 = \sigma_2/\sigma_p$	$s_t = \sigma_t/\sigma_p$
-----------------------	---------------------------	---------------------------

Unitary strain

$e = \varepsilon/\varepsilon_p$	$e_2 = \varepsilon_2/\varepsilon_p$	$e_u = \varepsilon_u/\varepsilon_p$	$e_t = s_t/E$	$e_o = \varepsilon_o/\varepsilon_p$
---------------------------------	-------------------------------------	-------------------------------------	---------------	-------------------------------------

Unitary elasticity modulus

$E = E_c \cdot \varepsilon_p/\sigma_p$
--

Then the stress-strain relationship $s = s(e)$ is to be defined by sections:

$e \leq e_0$	>	$s = 0$
$e_0 < e \leq e_t$	>	$s = s_t \cdot (e - e_0) / (e_t - e_0)$
$e_t < e \leq 0$	>	$s = E \cdot e$
$0 < e \leq 1$	>	$s = E \cdot e - (E - 1) \cdot e^{(E/(E-1))}$
$1 < e \leq e_2$	>	$s = 1 + (s_2 - 1) \cdot [(e - 1) / (e_2 - 1)]^E$
$e_2 < e \leq e_u$	>	$s = s_2 \cdot (e - e_u) / (e_2 - e_u)$
$e_u < e$	>	$s = 0$

The parameters in these formulas represent, beyond every principal direction:

- E_c the initial concrete deformation module,
- σ_p the concrete peak stress in compression and
- ϵ_p the correspondent strain at peak stress,
- σ_2 and ϵ_2 the second point of stress-strain when softening in compression,
- ϵ_u the ultimate strain in compression,
- σ_t the concrete peak stress in tension,
- ϵ_o the ultimate strain in tension

All of them can be easily deducted from simple tests procedures (uniaxial compression test and splitting tensile strength test on concrete cylinders)

5.1.2.- Biaxial Constitutive Relationships

To study the behavior of a concrete structure, no matter how simple it is (eg, specimen subject to uniaxial compression with constrained transversal displacements), we need to know the behavior of concrete in a biaxial state of stress: flat deformation (eg, beams), flat stress (eg, slabs) or axisymmetric stress (eg, cylinders).

As we have only had gotten to know the behavior of the UHPC in uniaxial compression, in order to simulate the behavior of concrete in a biaxial state of stresses, the failure envelope proposed by Kupfer and Gerstle [94], figure 5-2, will be adopted.

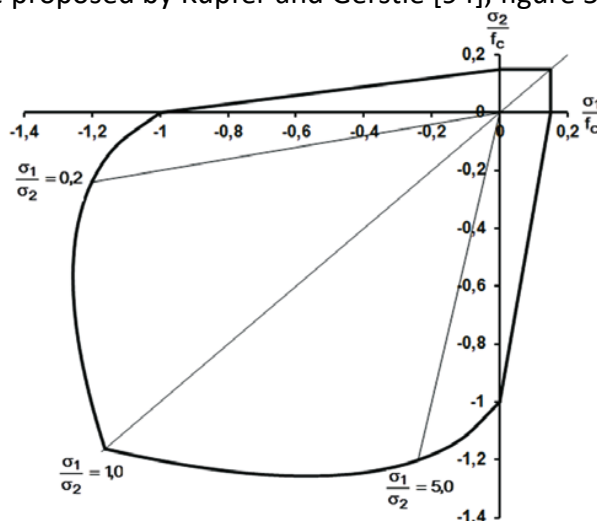


Figure 5-2 Failure envelope to the biaxial state of stresses of concrete [127]

Being the unitary stresses on the principal directions:

$$s_I = \sigma_I/\sigma_p \quad \text{and} \quad s_{II} = \sigma_{II}/\sigma_p \quad (\text{where } s_I \leq s_{II}) \quad (5.3)$$

and defining

$$\alpha = s_I/s_{II} \quad (5.4)$$

the equivalent biaxial concrete peak stresses, to be used instead of σ_p , on the principal directions, would be given by:

$$s_I \leq s_{II} \leq 0 \quad \rightarrow \quad \sigma_{IIp} = \sigma_{Ip} = \sigma_p \quad (5.5)$$

$$s_I \leq 0 < s_{II} \quad \rightarrow \quad \sigma_{IIp} = \frac{s_t}{(s_t - \alpha)} \cdot \sigma_p \quad ; \quad \sigma_{Ip} = \sigma_p \quad (5.6)$$

$$0 < s_I \leq s_{II} \quad \rightarrow \quad \sigma_{IIp} = \frac{1+3.65 \cdot \alpha}{(1+\alpha)^2} \cdot \sigma_p \quad ; \quad \sigma_{Ip} = \alpha \cdot \sigma_{IIp} \quad (5.7)$$

and the equivalent biaxial concrete strain corresponding to the compressive peak stress, to be used instead of ε_p , on the principal directions, would be obtained from the expressions:

$$\varepsilon_{IIp} = \varepsilon_p \cdot (3 \cdot s_{IIp} - 2) \quad (\text{where } s_{IIp} = \sigma_{IIp}/\sigma_p) \quad (5.8)$$

$$\varepsilon_{Ip} = \varepsilon_p \cdot (0.35 \cdot s_{Ip} + 2.25 \cdot s_{Ip}^2 - 1.60 \cdot s_{Ip}^3) \quad (\text{where } s_{Ip} = \sigma_{Ip}/\sigma_p) \quad (5.9)$$

6.1.3.- Orthotropic constitutive matrix

For concrete subjected to **biaxial state of stresses**, it was adopted the constitutive relationship on incremental form proposed by Desai and Siriwardance [93], according the equation:

$$\begin{bmatrix} \Delta\sigma_I \\ \Delta\sigma_{II} \\ \Delta\tau \end{bmatrix} = \frac{1}{(1-\nu^2)} \cdot \begin{bmatrix} E_I & \nu\sqrt{E_I E_{II}} & 0 \\ \nu\sqrt{E_I E_{II}} & E_{II} & 0 \\ 0 & 0 & 0.25[(E_I + E_{II}) - 2\nu\sqrt{E_I E_{II}}] \end{bmatrix} \cdot \begin{bmatrix} \Delta\varepsilon_I \\ \Delta\varepsilon_{II} \\ \Delta\gamma \end{bmatrix} \quad (5.10)$$

The $\Delta\sigma_I$, $\Delta\sigma_{II}$, and $\Delta\tau$ parameters presented on equation xxx are the stress increments on the principal directions. The $\Delta\varepsilon_I$, $\Delta\varepsilon_{II}$, and $\Delta\gamma$ parameters are the strain increments on the principal directions. The E_I and E_{II} parameters are the tangent deformation

modules relating to such directions and ν is the Poisson's ratio, considered the same in all directions.

The "Ei's" parameters to be obtained as the derivatives of the constitutive relationship applied for each principal direction:

Where for:

$$\begin{array}{ll}
 e \leq e_o & > & s' = 0 \\
 e_o < e \leq e_t & > & s' = s_t / (e_t - e_o) \\
 e_t < e \leq 0 & > & s' = E \\
 0 < e \leq 1 & > & s' = E \cdot (1 - e^{(1/(E-1))}) \\
 1 < e \leq e_2 & > & s' = E \cdot [(s_2 - 1) / (e_2 - 1)] \cdot [(e - 1) / (e_2 - 1)]^{(E-1)} \\
 e_2 < e \leq e_u & > & s' = s_2 / (e_2 - e_u) \\
 e_u < e & > & s' = 0
 \end{array}$$

Analogously, the constitutive relationship for an **axisymmetric orthotropic incremental model** would be obtained:

$$\begin{bmatrix} \Delta\sigma_z \\ \Delta\sigma_r \\ \Delta\sigma_\theta \\ \Delta\tau \end{bmatrix} = \frac{1}{(1 + \nu)(1 - 2\nu)} \begin{bmatrix} (1-\nu)E_I & \nu\sqrt{E_I E_{II}} & \nu\sqrt{E_I E_{II}} & 0 \\ \nu\sqrt{E_I E_{II}} & (1-\nu)E_{II} & \nu E_{II} & 0 \\ \nu\sqrt{E_I E_{II}} & \nu E_{II} & (1-\nu)E_{II} & 0 \\ 0 & 0 & 0 & 0.25[(1-\nu)(E_I + E_{II}) - 2\nu\sqrt{E_I E_{II}}] \end{bmatrix} \begin{bmatrix} \Delta\varepsilon_z \\ \Delta\varepsilon_r \\ \Delta\varepsilon_\theta \\ \Delta\gamma \end{bmatrix} \quad (5.11)$$

5.2.- Proposed UMAT (ABAQUS) Subroutine

Furthermore, we will present the code used for computing the numerical simulation of the mechanical performance of our UHPC with additions. Firstly, the subroutine is explained and later, the code is presented.

5.2.1.- Pseudocode for UMAT Subroutine

(to evaluate incremental stress due to an increment of strain, in biaxial UHPCConcrete)

5.2.1.1.- Inputs

- number of stress/strain components (3-plane stress or 4-axisymmetric, others NO)
- actual stresses (vector)
- actual strains (vector)
- increment of strains $\Delta\varepsilon$ (vector)
- UHPCConcrete properties vector($E_c, \sigma_p, \varepsilon_p, s_2, e_2, e_u, s_t, e_o$)

5.2.1.2.- Outputs

- Increment of stresses $\Delta\sigma$ (vector)

5.2.1.3.- Local Variables

- UHPC properties for principal directions, i.e. 2 vectors ($E_c, \sigma_p, \varepsilon_p, s_2, e_2, e_u, s_t, e_o$)
- Stiffness matrix D(3x3 or 4x4)

5.2.1.4.- External Process

UMAT will call external subroutine SLOPE to evaluate the slope of the concrete constitutive relationship curve for a given strain.

5.2.1.5.- Process

1. If not (plane or axisymmetric model) then end
2. Get initialized UHPC properties in local vectors
3. Get normal stresses and Calculate s_I and s_{II} , unitary normal stresses
4. If $s_I > s_{II}$ then swap (s_I, s_{II})
5. if not($s_I \leq 0$ and $s_{II} \leq 0$) then Calculate $\alpha = s_I / s_{II}$;
6. if $s_I \leq 0$ and $0 < s_{II}$ then Calculate $\sigma_{IIp} = \frac{s_t}{(s_t - \alpha)} \cdot \sigma_p$
else Calculate $\sigma_{IIp} = \frac{1+3.65\cdot\alpha}{(1+\alpha)^2} \cdot \sigma_p$; $\sigma_{Ip} = \alpha \cdot \sigma_{IIp}$
7. Calculate $s_{Ip} = \sigma_{Ip} / \sigma_p$; $s_{IIp} = \sigma_{IIp} / \sigma_p$
8. Calculate $\varepsilon_{Ip} = \varepsilon_p \cdot (0.35 \cdot s_{Ip} + 2.25 \cdot s_{Ip}^2 - 1.60 \cdot s_{Ip}^3)$; $\varepsilon_{IIp} = \varepsilon_p \cdot (3 \cdot s_{IIp} - 2)$
9. If (s was swapped) then swap($\sigma_{Ip}, \sigma_{IIp}$); swap($\varepsilon_{Ip}, \varepsilon_{IIp}$)
10. Update $\sigma_{Ip}, \sigma_{IIp}$ and $\varepsilon_{Ip}, \varepsilon_{IIp}$ in the corresponding UHPC properties local vectors

11. Get ε_i and ε_{II} , normal strains
12. Evaluate SLOPE(E_i , ε_i , UHPCprops_i)
13. Evaluate SLOPE(E_{II} , ε_{II} , UHPCprops_{II})
14. If (plane stress) then Calculate and fill stiffness matrix D(3x3) (eq.xx3)
 else Calculate and fill stiffness matrix D(4x4) (eq.xx4)
15. Calculate $\Delta\sigma=D\cdot\Delta\varepsilon$
16. end

5.2.2.- Pseudocode for SLOPE Subroutine

(to evaluate slope of the concrete constitutive relationship curve for a given strain)

5.2.2.1.- Inputs

- actual strain ε
- UHPCConcrete properties vector($E_c, \sigma_p, \varepsilon_p, s_2, e_2, e_u, s_t, e_o$)

5.2.2.2.- Outputs

- Slope of the curve for the actual strain value E_{slope}

5.2.2.3.- Local Variables

- UHPC properties $E_c, \sigma_p, \varepsilon_p, s_2, e_2, e_u, s_t, e_o$

5.2.2.4.- Process

1. Get UHPC properties in local variables
2. Calculate $e = \varepsilon / \varepsilon_p$; $E = E_c \cdot \varepsilon_p / \sigma_p$; $e_t = s_t / E$
3. In case of

$e \leq e_o$	>	slope = 0
$e_o < e \leq e_t$	>	slope = $s_t / (e_t - e_o)$
$e_t < e \leq 0$	>	slope = E
$0 < e \leq 1$	>	slope = $E \cdot (1 - e^{(1/(E-1))})$
$1 < e \leq e_2$	>	slope = $E \cdot [(s_2 - 1) / (e_2 - 1)] \cdot [(e - 1) / (e_2 - 1)]^{(E-1)}$
$e_2 < e \leq e_u$	>	slope = $s_2 / (e_2 - e_u)$
$e_u < e$	>	slope = 0
other	>	slope = 0

4. Calculate $E_{\text{slope}} = \text{slope} \cdot \sigma_p / \varepsilon_p$
5. end

5.3.- Fortran Code for Orthotropic Biaxial nonlinear model for UHPC

5.3.1.- UMAT4UHPC SUBROUTINE

```
C
C UMAT4UHPC SUBROUTINE (for ABAQUS)
C to evaluate increment stress due to increment of strain, in UHPConcrete
C
  SUBROUTINE UMAT(STRESS,STATEV,DDSDDE,SSE,SPD,SCD,
1 RPL,DDSDDT,DRPLDE,DRPLDT,
2 STRAN,DSTRAN,TIME,DTIME,TEMP,DTEMP,PREDEF,DPRED,CMNAME,
3 NDI,NSHR,NTENS,NSTATV,PROPS,NPROPS,COORDS,DROT,PNEWDT,
4 CELENT,DFGRD0,DFGRD1,NOEL,NPT,LAYER,KSPT,JSTEP,KINC)
C
  INCLUDE 'ABA_PARAM.INC'
C
  CHARACTER*80 CMNAME
  DIMENSION STRESS(NTENS),STATEV(NSTATV),
1 DDSDDE(NTENS,NTENS),DDSDDT(NTENS),DRPLDE(NTENS),
2 STRAN(NTENS),DSTRAN(NTENS),TIME(2),PREDEF(1),DPRED(1),
3 PROPS(NPROPS),COORDS(3),DROT(3,3),DFGRD0(3,3),DFGRD1(3,3),
4 JSTEP(4)
C
C UHPC properties for principal directions (Ec,σp,εp,s2,e2,eu,st,eo,v)
  DOUBLEPRECISION PROPSI(NPROPS),PROPSII(NPROPS)
C
  LOGICAL SWAPPED
  DOUBLEPRECISION SI,SII,SIP,SIIP,STRESIP,STRESIIP
  DOUBLEPRECISION STRANIP,STRANIIP
  DOUBLEPRECISION ALFA,E1,E2,ANU,ANU2
  PARAMETER (ZERO=0.0D0, ONE=1.0D0, TWO=2.0D0)
C
C1 If not (plane or axisymmetric model) then end
  IF (NTENS.NE.3.AND.NTENS.NE.4) RETURN
C
C2 Get initialized UHPC properties in local vectors
  DO I=1,NPROPS
    PROPSI(I) =PROPS(I)
    PROPSII(I)=PROPS(I)
  ENDDO
C
C3 Get normal stresses and Calculate sI and sII, unitary normal stresses
  STRESIP =PROPS(2)
  STRESIIP=PROPS(2)
  SI =STRESS(1)/STRESIP
  SII=STRESS(2)/STRESIIP
C
C4 If sI > sII then swap (sI,sII)
  SWAPPED=.FALSE.
  IF (SI.GT.SII) THEN
    CALL SWAP(SI,SII)
    SWAPPED=.TRUE.
  ENDIF
C
C5 if not(sI ≤ 0 and sII ≤ 0) then Calculate α=sI/sII and calculate σIIp, σIp
  IF (.NOT.(SI.LE.ZERO.AND.SII.LE.ZERO)) THEN
    ALFA=SI/SII
    IF (SI.LE.ZERO.AND.SII.GT.ZERO) THEN
      STRESIIP=PROPS(2)*PROPS(7)/(PROPS(7)-ALFA)
    ELSE
```

```

                STRESIIP=PROPS(2)*(ONE+3.65D0*ALFA)/(ONE+ALFA)**2
                STRESIP=ALFA*STRESIIP
            ENDIF
        ENDIF
    C
    C6 Calculate sIp =  $\sigma_{Ip}/\sigma_p$  ; sIIP =  $\sigma_{IIP}/\sigma_p$ 
        SIP =STRESIP/PROPS(2)
        SIIP=STRESIIP/PROPS(2)
    C
    C7 Calculate  $\epsilon_{Ip}=\epsilon_p\cdot(0.35\cdot s_{Ip} + 2.25\cdot s_{Ip}^2 - 1.60\cdot s_{Ip}^3)$ ;  $\epsilon_{IIP}=\epsilon_p\cdot(3\cdot s_{IIP} - 2)$ 
        STRANIP =PROPS(3)*(0.35D0*SIP+2.25D0*SIP**2-1.60D0*SIP**3)
        STRANIIP=PROPS(3)*(3.00D0*SIIP-2.00D0)
    C
    C8 If(s was swapped) then swap( $\sigma_{Ip}$ ,  $\sigma_{IIP}$ ); swap( $\epsilon_{Ip}$ , $\epsilon_{IIP}$ )
        IF (SWAPPED.EQV..TRUE.) THEN
            CALL SWAP(STRESIP,STRESIIP)
            CALL SWAP(STRANIP,STRANIIP)
        ENDIF
    C
    C9 Update  $\sigma_{Ip}$ ,  $\sigma_{IIP}$  and  $\epsilon_{Ip}$ , $\epsilon_{IIP}$  in the UHPC props local vectors
        PROPSI(2)=STRESIP
        PROPSI(3)=STRANIP
        PROPSII(2)=STRESIIP
        PROPSII(3)=STRANIIP
    C
    C10 Evaluate SLOPE(EI, $\epsilon_I$ ,UHPCpropsI)
        CALL SLOPE(E1,STRAN(1),NPROPS,PROPSI)
        CALL SLOPE(E2,STRAN(2),NPROPS,PROPSII)
        ANU=PROPS(9)
        ANU2=ZERO
    C13 Calculate and fill stiffness matrix D(3x3)or(4x4)
        DO I=1,NTENS
            DO J=1,NTENS
                DDSDDE(I,J)=ZERO
            ENDDO
        ENDDO
        IF (NTENS.EQ.3) THEN
            ANU2=ONE-ANU**2
            DDSDDE(1,1)=E1/ANU2
            DDSDDE(1,2)=ANU*SQRT(E1*E2)/ANU2
            DDSDDE(2,1)=DDSDDE(1,2)
            DDSDDE(2,2)=E2/ANU2
            DDSDDE(3,3)=0.25D0*(E1+E2-TWO*ANU*SQRT(E1*E2))/ANU2
        ELSE
            ANU2=(ONE+ANU)*(ONE-TWO*ANU)
            DDSDDE(1,1)=(ONE-ANU)*E1/ANU2
            DDSDDE(1,2)=ANU*SQRT(E1*E2)/ANU2
            DDSDDE(1,3)=ANU*SQRT(E1*E2)/ANU2
            DDSDDE(2,1)=DDSDDE(1,2)
            DDSDDE(2,2)=(ONE-ANU)*E2/ANU2
            DDSDDE(2,3)=ANU*E2/ANU2
            DDSDDE(3,1)=DDSDDE(1,3)
            DDSDDE(3,2)=DDSDDE(2,3)
            DDSDDE(3,3)=(ONE-ANU)*E2/ANU2
            DDSDDE(4,4)=0.25D0*((ONE-ANU)*(E1+E2)-TWO*ANU*SQRT(E1*E2))/ANU2
        ENDIF
    C
    C14 Calculate  $\Delta\sigma=D\cdot\Delta\epsilon$ 
        DO I=1,NTENS

```

```
        DO J=1,NTENS
          STRESS(I)=STRESS(I)+DDSDDE(I,J)*DSTRAN(J)
        ENDDO
      ENDDO
C
      RETURN
      END
```

5.3.2.- Subroutine SWAP(A,B)

```
C
C Subroutine SWAP(A,B)
C to swap two values
C
      SUBROUTINE SWAP(AAAA,BBBB)
      DOUBLEPRECISION AAAA,BBBB,TEMP
      TEMP=AAAA
      AAAA=BBBB
      BBBB=TEMP
      RETURN
      END
```

5.3.3.- Subroutine SLOPE

```
C
C Subroutine SLOPE(ESLOPE, ε, nprops, Ec, σp, εp, s2, e2, eu, st, eo, v)
C to evaluate the slope of the concrete constitutive relationship curve for a
given strain
C
C     SUBROUTINE SLOPE(ESLOPE,STRAN,NPROPS,PROPS)
C
C     DOUBLEPRECISION ESLOPE,STRAN
C     DOUBLEPRECISION EC,STRESP,STRANP,S2,E2,EU,ST,E0,ANU
C     DOUBLEPRECISION EE,E,ET,SL
C     DIMENSION PROPS(NPROPS)
C
C     PARAMETER (ZERO=0.0D0, ONE=1.0D0, TWO=2.0D0)
C
C1 Get UHPC properties in local variables
C     EC=PROPS(1)
C     STRESP=PROPS(2)
C     STRANP=PROPS(3)
C     S2=PROPS(4)
C     E2=PROPS(5)
C     EU=PROPS(6)
C     ST=PROPS(7)
C     E0=PROPS(8)
C     ANU=PROPS(9)
C
C2 Calculate  $e=\epsilon/\epsilon_p$  ;  $E=E_c \cdot \epsilon_p/\sigma_p$  ;  $et=st/E$ 
C     EE=STRAN/STRANP
C     E=EC*STRANP/STRESP
C     ET=ST/E
C
C3 Calculate slope by section
C     SL=ZERO
C     IF (EE.LE.E0) THEN
C         SL=ZERO
C     ELSE IF (EE.LE.ET) THEN
C         SL=ST/(ET-E0)
C     ELSE IF (EE.LE.ZERO) THEN
C         SL=E
C     ELSE IF (EE.LE.ONE) THEN
C         SL=E*(ONE-EE**((ONE/(E-ONE))))
C     ELSE IF (EE.LE.E2) THEN
C         SL=E*(S2-ONE)/(E2-ONE)*((EE-ONE)/(E2-ONE))**(E-ONE)
C     ELSE IF (EE.LE.EU) THEN
C         SL=S2/(E2-EU)
C     ELSE
C         SL=ZERO
C     ENDIF
C
C4 Calculate  $Eslope=sl \cdot \sigma_p/\epsilon_p$ 
C     ESLOPE=SL*STRESP/STRANP
C
C     RETURN
C     END
```


5.4.- Checking the goodness of the proposed model

In order to verify the performance of the proposed constitutive equation, the reliability of the built Finite Element Model and the specifically developed UMAT routines, we simulate numerically an uniaxial cylinder compressive test.

The results of applying our numerical simulation are consistent with the experimental results, so we can conclude that the proposed formulation can be used with confidence to simulate the behavior of UHPC structures in plane stress or axisymmetric stress states.

5.4.1.- Model geometry

As it was explained in chapter 3, to be able to record the specimens' results, with the available instrumentation, while performing the compression tests, we had to interpose two steel adapter cylinders between specimens and loading plates, altering slightly the application conditions of the loads. Hence, we must consider these adapters in the numerical model and discretize the steel cylinders in it.

We will take advantage of the axial symmetry of the compression test to use an axisymmetric model, so that we will need to detail only a section of it.

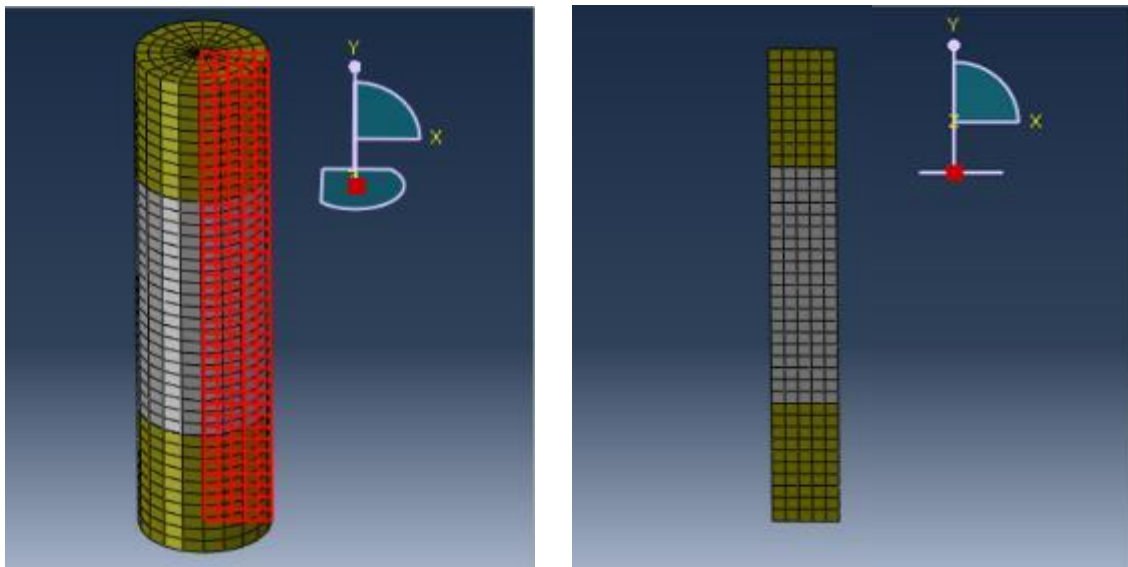


Figure 5-3 Section of the model. 3D (left); Axisymmetric (right)

For the discretization of both the specimen and the steel cylinders, we will use the abaqus standard finite element CAX4, which is a 4-nodes bilinear axisymmetric quadrilateral element, with dimensions 5x5 mm, so once assembled will result in a mesh of 100 elements and 400 nodes for the UHPC specimen and 50 elements and 200 nodes for each steel cylinder.

To ensure continuity between the combined pieces, the interaction between the specimens and steel cylinders contact surfaces will be considered as a solidary union without any possible separation nor gliding.

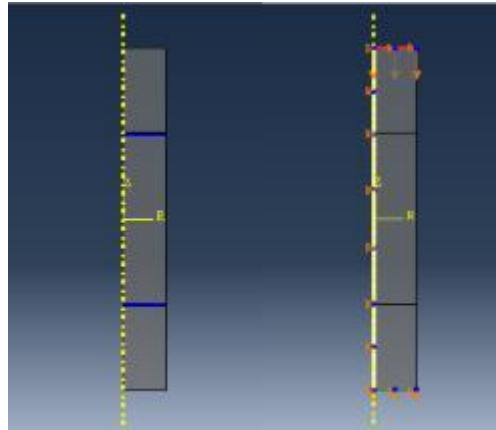


Figure 5-4 Interaction between specimen and steel cylinders (left); Displacements conditions between steel cylinders and loading plates and centre of specimen (right)

In the same way, the contact between the press and the steel adapter cylinders will be supposed without any possible tangential gliding and therefore, because the rigidity of the loading plates can be considered infinitely higher than the steel cylinders, on these two contact surfaces we will impose a null horizontal displacement range with the corresponding boundary conditions.

Our test was carried on a displacement-controlled load method, so we need to simulate that on our finite element method. For that, we will impose a displacement on one loading plate while we keep the other one without displacement. In the real tests, the bottom plate had vertical displacements while the top plate hold no vertical displacement. On the FEM simulation, we will do the opposite, as we will obviously obtain the same result but it is easier to visualize graphically.

In other words, the top surface of the top steel adapter cylinder (in contact with the top loading plate), will get the imposed vertical displacements, while the bottom surface of the bottom steel cylinder (in contact with the bottom loading plate), will be supposed as being supported on a firm surface, therefore without vertical displacement.

5.4.2.- Material properties

The material of the sections corresponding to the adapter cylinders will be supposed as conventional steel, elastic and isotropic, the properties of which are presented in table 5-1.

The source specimen that we will use to demonstrate the good performance of the finite element model corresponds with the specimens UHPC28D4SF008_1-3, presented in figure 5-5, which mechanical properties are presented in chapter 4 section 3 together with the adjusted Initial slope curves in annex 2.

It is important to mention that tensile characteristic mechanical properties are not obtained from our experimental campaign, because we were not able to do them, and thus we are using calculated values for the purpose of completing the model. We are using for the tensile characteristic strength, $f_t = f_c/10$, which gives consistent values with the observed in the literature reviewed for a UHPFRC with a 4% of steel fibers.

The mechanical properties for the steel cylinders are those given to us by the factory that produced them.

Table 5-1 Average mechanical properties constants values

Mechanical Properties for UHPC28D4SF008_K	Mechanical Properties for Steel
E_c	24.85 GPa
f_c	-128.88 Mpa
ϵ_c	-0.00635
σ_2/σ_c	0.47
ϵ_2/ϵ_c	1.98
ϵ_3/ϵ_c	5.25
f_t	12.89
ϵ_t	0.00635
Poisson ratio, ν	0.2
	0.3

$[\sigma_2/\sigma_c, \epsilon_2/\epsilon_c, \epsilon_3/\epsilon_c]$ they are all input as a proportion of f_c or ϵ_c , accordingly, and the tensile constants are taken as an approximation due to lack of tests for tensile strength.

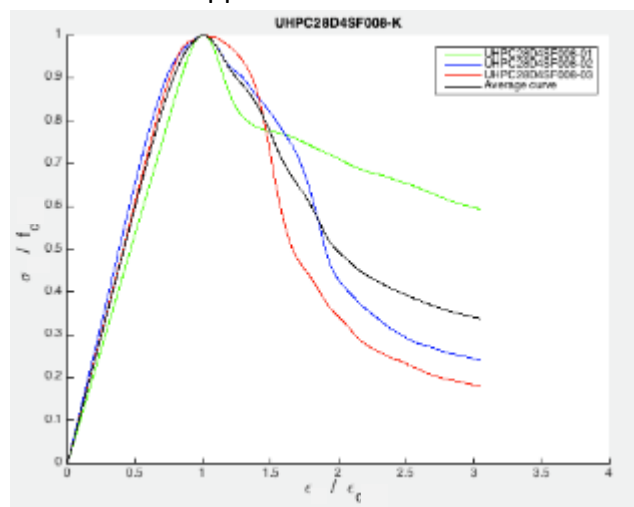


Figure 5-5 Test used to compare the finite element model with the experimental results

5.4.3.- Load application and measurement of results

The uniaxial compression test was performed by the application of small successive variations of the load but with a closed-loop control method (displacement-controlled load) of the vertical displacements, by means of an extensometer applied between the edges of the UHPC specimen, to obtain a complete curve of the concrete behavior, including not only the increasing resistance section but also the part of the curve after the maximum resistance, also called post-peak behavior.

On the numerical model, we will impose consecutive vertical displacements on the top surface of the top adapter cylinder, until reaching 2 mm, which corresponds to the maximum deformation registered on the actual test.

The results to be obtained from the model, and that will be considered as equivalent to those obtain on the tests, will be:

- The displacement imposed in each loading step, that will correspond to the measure of displacement between loading.
- The total reaction forces on the bottom surface of the bottom adapter cylinder, that will correspond to the load applied by the press.
- The displacements between the top and bottom surfaces of the specimen, that will correspond to the displacements obtained by the extensometers.
- The stress-strain curve in the middle interior point, that will correlate with the proposed constitutive curve.

5.4.4.- Presentation of results of the FEM for UHPC

Once the model is assembled, with the described material characteristics, we proceed to impose a sequence of increments of vertical displacements on the top surface of the model, obtaining a succession of stress states that will lead to a deformations field compatible with the one observed experimentally.

The Monitor Data file, which contains printed output of the model and history definition generated by the analysis input file processor, and the Monitor Message file, which contains diagnostic or informative messages about the progress of the solution, can be found in the Annex 4 and Annex 5, respectively.

They are both very useful to double check any problem that might had occurred.

The results processed through visualization capabilities offer us different graphical solutions that will allow for visual comparison with the experimental results.

We can graphically obtain the incremental succession of different values. On this regard, we represent the consecutive steps of the vertical strain E22 in the following figure. Note that the red color in the specimen corresponds to tensile strains due from Poisson effect.

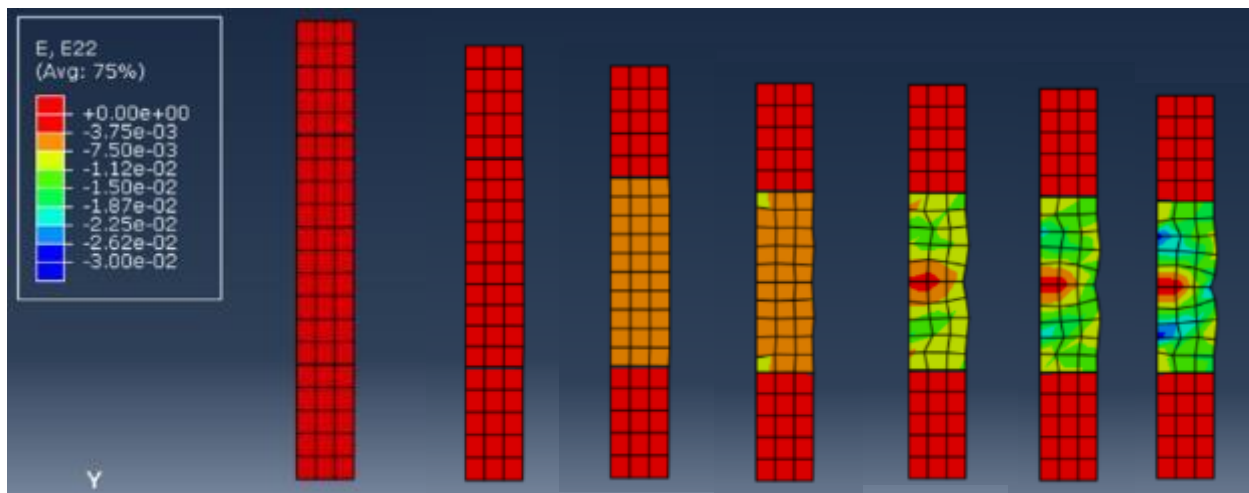


Figure 5-6 Simulation of the consecutive steps of the vertical strain of the compressive test

A 3D representation of the vertical stresses can be seen in figure 5-7. It can be observed how the stresses on the outer part of the specimen are higher than those in the center, tending to form vertical stress isolines, which was observed as well in the experimental tests.

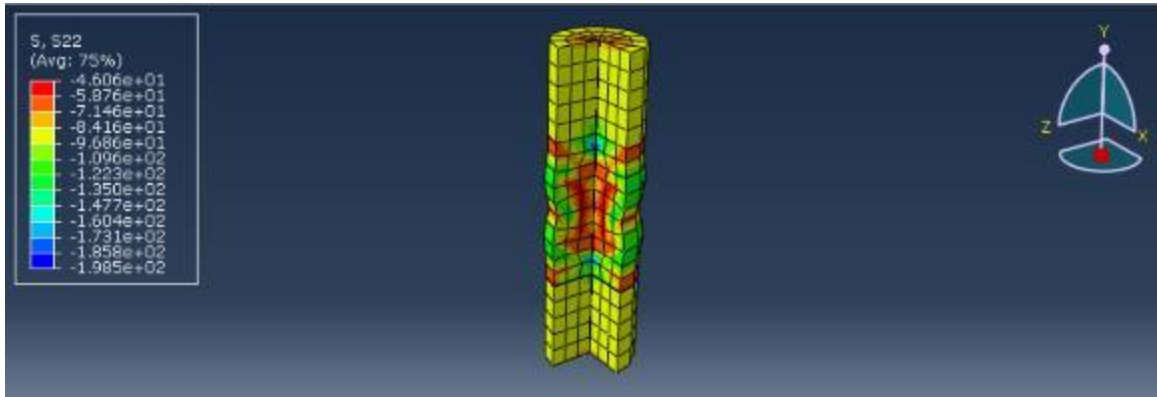


Figure 5-7 Vertical Stress 3D simulation of the compressive tests

The stress-strain curve can also be obtained, equivalent to the original experimental test curve, and it is shown in the following figure. The comparison between the two curves, with their numerical values, will be done in the discussion for the results, in chapter 6.

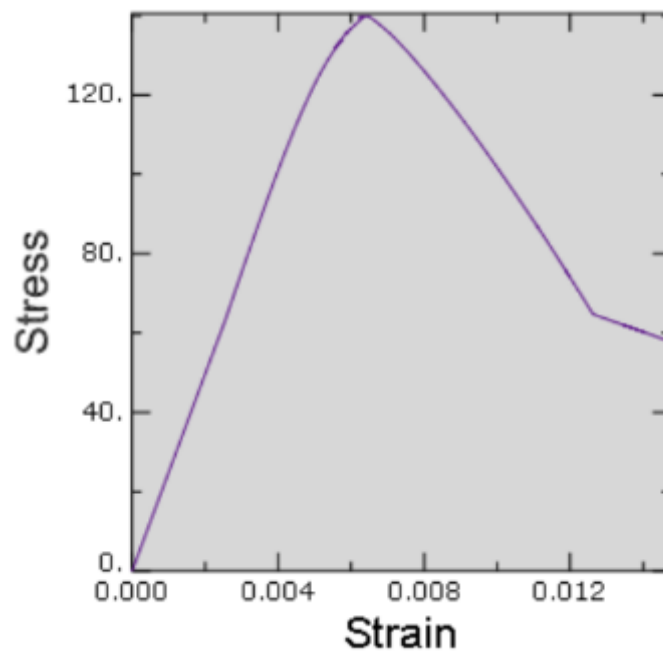


Figure 5-8 Stress-Strain curve obtained with the FEM

It is also interesting to obtain the force displacement curve to compare it with the original raw data curves and check whether the maximum forces are reached on the numerical model. It can be seen in the following figure 5-9 that maximum strength is in the order of 220 kN, being equivalent to the one obtained on the experimental tests, which can be seen in Annex 1.

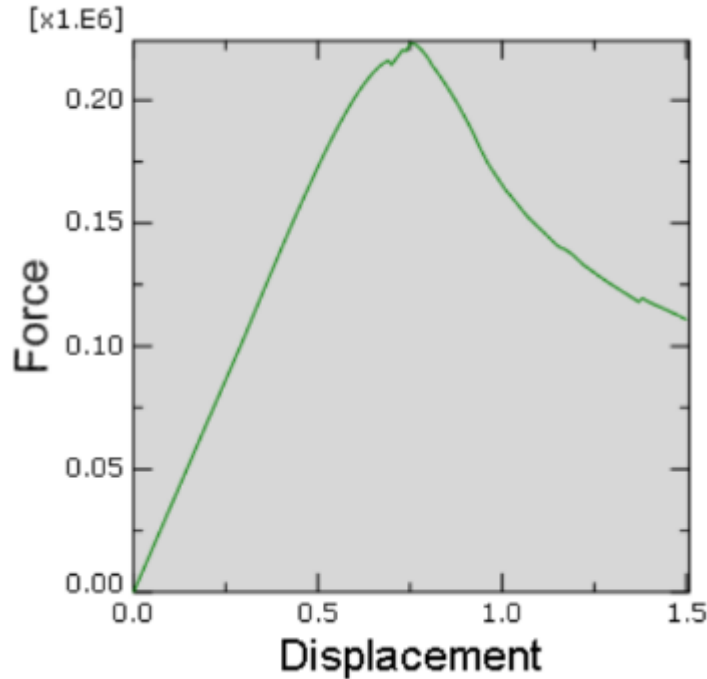


Figure 5-9 Force-Displacement curve obtained with the FEM

The values of the displacement, force, strain and stress of some representative steps can be seen on the following table.

Table 5-2 Values from FEM results

Displacement [mm]	Force [kN]	Strain	Stress [Mpa]
0	0.000	0.000000	0.000
0.1	-34.563	-0.000850	-21.141
0.2	-69.127	-0.001700	-42.217
0.3	-103.536	-0.002544	-63.002
0.4	-139.331	-0.003362	-84.877
0.5	-172.803	-0.004211	-106.018
0.6	-201.035	-0.005067	-123.920
0.7	-214.494	-0.005539	-131.706
0.8	-216.833	-0.006679	-138.476
0.9	-192.786	-0.008320	-122.439
1	-165.561	-0.010532	-94.609
1.1	-148.102	-0.011646	-79.093
1.2	-135.995	-0.012137	-71.973
1.3	-124.754	-0.013153	-62.999
1.4	-117.846	-0.013598	-61.556
1.5	-110.778	-0.014685	-58.035

Chapter 6 - Discussion of results

- 6.1.- EFFECT OF THE INCIDENTS IN THE TESTS ON THE RAW RESULTS
- 6.2.- INFLUENCE OF CNT AND SF DOSAGE ON THE UHPC'S MECHANICAL CHARACTERISTICS
- 6.3.- INFLUENCE OF CURING TIME IN UHPC WITH CNT&GO ADDITIONS
- 6.4.- RELIABILITY OF THE PROPOSED FINITE ELEMENT MODEL

This section analyses experimental and parametric results and discuss the possible arguments for the expected and unexpected results.

Chapter 6 - Discussion of results

In this section we will evaluate the research and discuss our expectations of possible causes and consequences of the results, analyze the possible limitations we encountered and provide suggestions for follow-up research. The research design followed in this thesis, from raw materials to the finite element model, represents the standard methodology of any study focusing on material properties.

6.1.- Effect of the incidents in the tests on the raw results

As described in detail in the corresponding chapters, the tests were limited to small size specimens causing difficulties in their execution and a large dispersion of results for specimens of equivalent dosages.

Due to capacity constraints in the laboratories, economic limitations and the developing time of the thesis itself, it was renounced to explore variations in the dosage of graphene oxide that remained fixed at 0.04%. For the same reasons, we restricted to only two cases the possible dosages of carbon nanotubes (0.08% and 0.50%) and steel fibers (2% and 4%), which will not allow us to reach decisive conclusions.

To adapt the test press and the extensometers available to the special sample size (ϕ 50x100mm), interposed metal rings were used, so that, on occasions, the records obtained denoted significant measurement errors.

It is remarkable the effect indicated, and corrected, in 4.2, about the determination of the initial modulus of elasticity, which has been interpreted as the consequence of an adaptation process between press-rings-specimen contact faces and the settlement of extensometers' fixation tips. This phenomenon could have been avoided, in part, by means of a process of preloading and discharging up to 30% of the expected resistance, which could be applied only in the last tests, obtaining much more coherent results.

Another possible consequence of interposing the adaptation rings is the disappearance of the confinement effect in the press-specimen contact, which has led to breaks in slabs parallel to the test-tube axis, instead of the typical breaks in opposite cones. In extreme cases, we observed a detachment of part of the effective resistant section of the specimen while simultaneously registering a significant drop in the resistive load for a given deformation. To assess the impact of this effect, it would have been advisable to weigh the specimens also after the test, to approximately evaluate what was the loss of resistant area and to try to correlate it with the loss of apparent resistance.

It has been tried to modify the records where these abrupt falls of resistance had been detected, assuming a loss of equivalent resistant area.

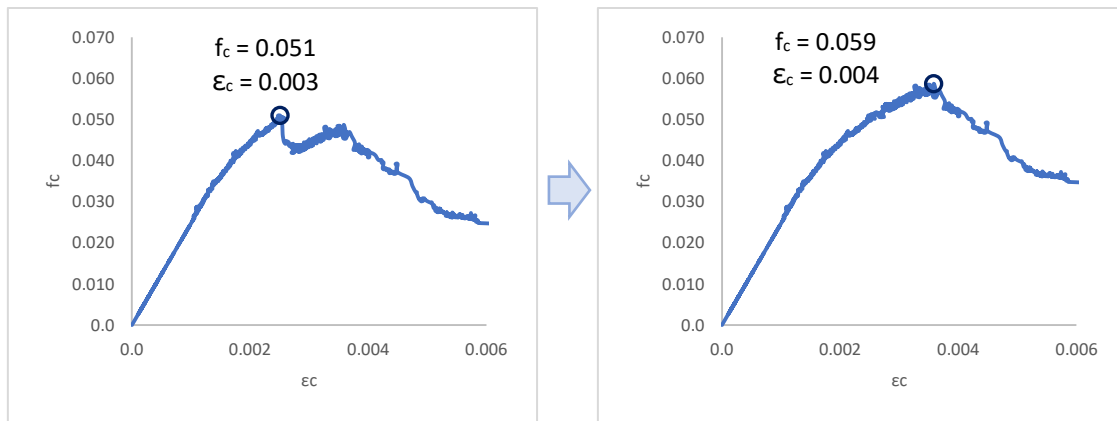


Figure 6-1 Adjusting the loss of effective resistant area

The resulting graphs seem suitable as we recover the continuity of the curve and could be used as real results in the corresponding stress / strain field. However, since we do not have the weight of the post-test specimens, this hypothesis can not be confirmed and, therefore, we use the original records.

As it can be observed in figure 6-1, if we accept the hypothesis arguing that the loss of resisted strength is due to a reduction of the effective resistant area, the resulting values for both peak strength and peak deformation increase with the applied changes. The resulting values of some other tested specimens would be changed, thus conclusions of the parametric study might suffer modifications. This issue should be examined in future researches, where they might experience the same cracking pattern and strength-deformation curve, to deepen in this phenomenon probably caused as a consequence of using additional testing rings. For that, we recommend checking the loss of weight of the specimen after tests.

6.2.- Influence of CNT and SF dosage on the UHPC's mechanical characteristics

Before we had the results, the promising outcomes of different nanomaterials studies suggested that mixing them with concrete might turn up in improving several properties of this construction material. Moreover, there were expectations of synergies when working together with carbon nanotubes and graphene oxide, even though they were never mixed together with concrete. As nanomaterials' technology grew and developed, also the hopes around using them together with concrete, and so it was expected to have optimal results.

From the parametric analysis of the compressive strength, figure 6-2 and 6-3, we can conclude that more steel fibers increase the compressive strength, although we should have more tests with different dosages to deduce the optimal amount of steel fibers. On the other side, we cannot say that increasing the CNT content is increasing the compressive strength for any dosage, as we see that we have the higher values for the 0.07% concentration. However, there are some differences in value between similar specimens, which could lead to other conclusions, caused by mixing and curing process problems, where the lack of expertise of the people involved and the lack of help, added to problems with the machinery and curing places, probably affected the final result.

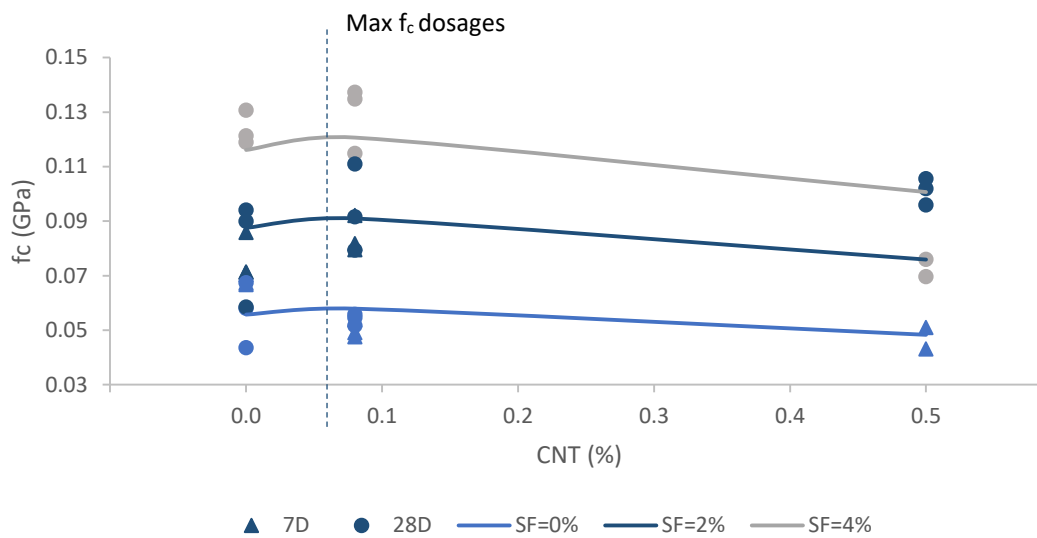


Figure 6-2 f_c parametric curves and experimental values by CNT dosage

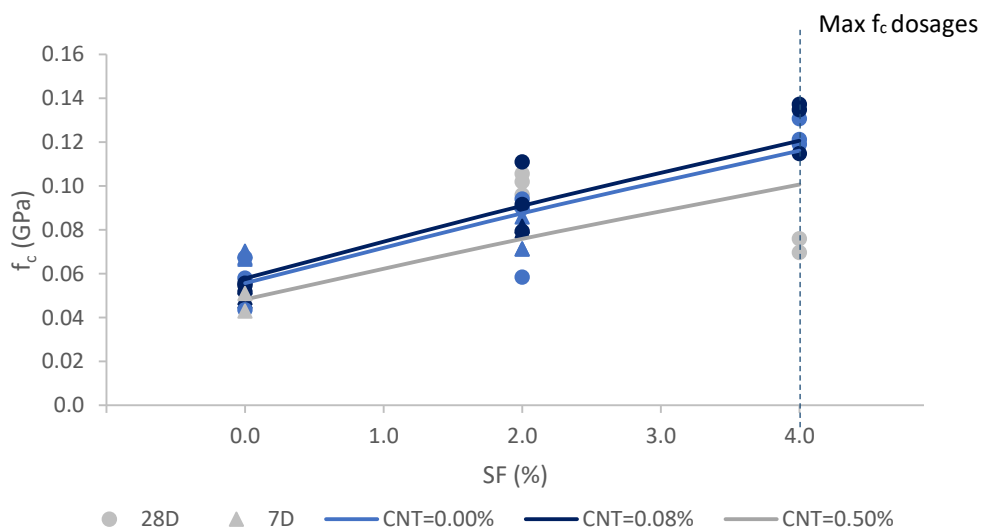


Figure 6-3 f_c parametric curves and experimental values by SF dosage

The maximum deformation the concrete is able to stand before failure, related to the characteristic strain value, was expected to be higher with the addition of carbon nanotubes, as it was explained that they create bonds at nano level, and it aids to determine the feasibility of these materials for construction. From figure 6-2, we can actually see specimens with 0.08%wt and 0.5%wt of CNT concentration tend to have characteristic strain values higher than plain UHPCs, for all concentrations of steel fibers. However, it also seems to indicate that adding too many carbon nanotubes doesn't help on creating more bonding, remaining the same. On the contrary, as we can also see in figure 6-4 and 6-5, the characteristic strain is directly dependant on the content of steel fibers, been the higher values for the 4% steel fiber specimens.

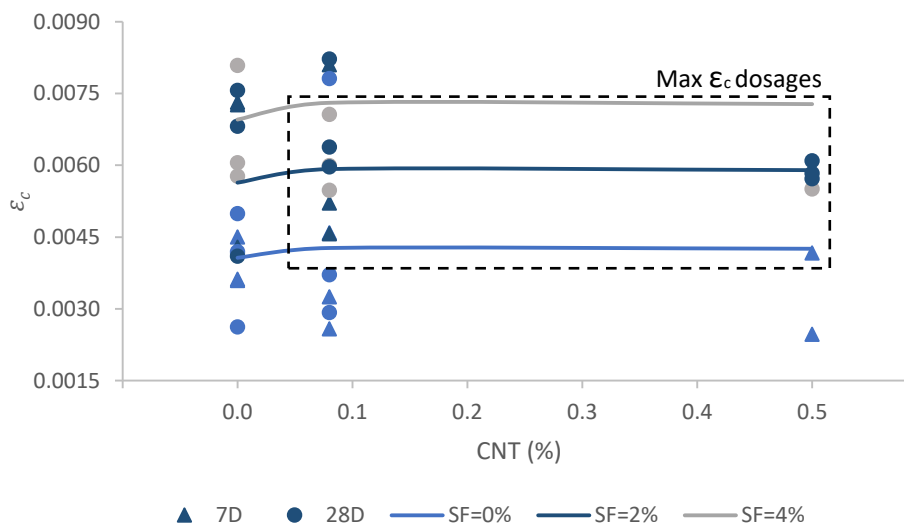


Figure 6-4 ϵ_c parametric curves and experimental values by CNT dosage

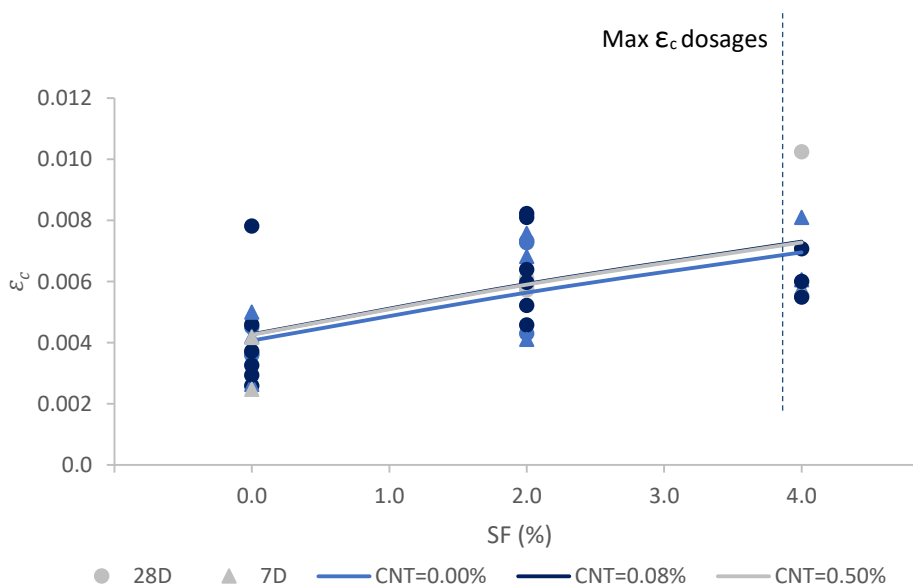


Figure 6-5 ϵ_c parametric curves and experimental values by SF dosage

The elastic modulus parametric analysis shows that by adding SF 2% the increase is minimal, however, when adding up to 4% steel fibers, the elastic modulus is increased. Although we obtain these results, further tests should be made with different steel fiber dosages for assurance.

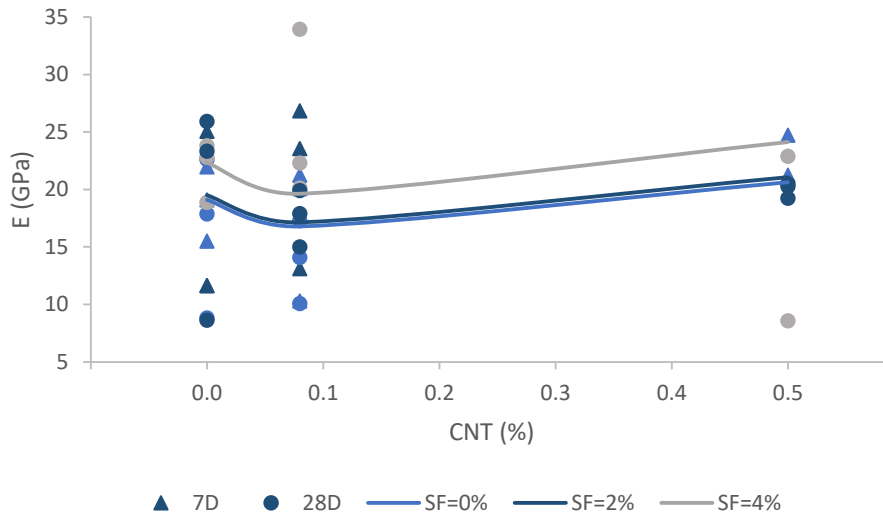


Figure 6-6 E parametric curves and experimental values by CNT dosage

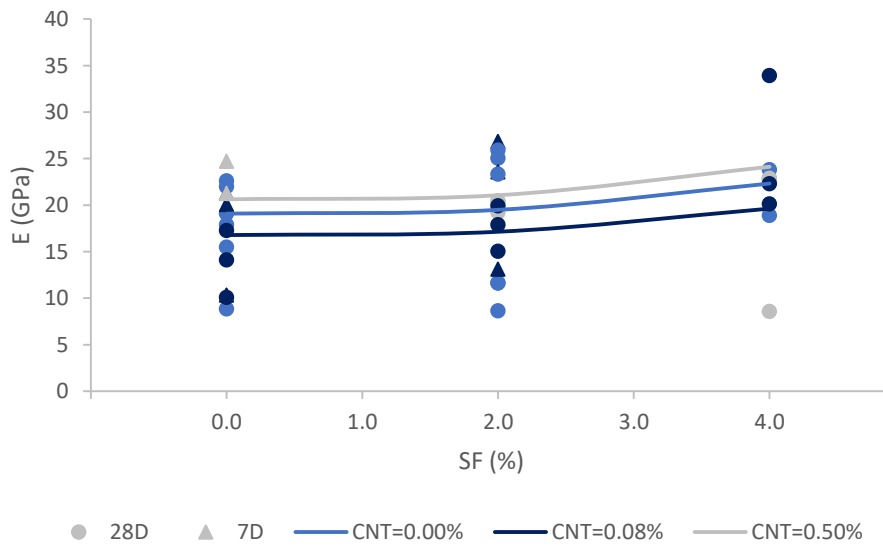


Figure 6-7 E parametric curves and experimental values by SF dosage

The post-peak behavior on the specimens is, as expected, only present on those specimens using steel fibers. Even though some specimens without SF might have post-peak values, they are not representative of the dosage. Specimens' behavior differs slightly when using carbon nanotubes, with a tendency to have lower σ_2 values compared to the respective f_c . These results must be discussed providing the respective $\varepsilon_2/\varepsilon_c$ value, both presented on figures 6-8, 6-9, 6-10 and figure 6-11, in order to fully understand the behavior of the specimen.

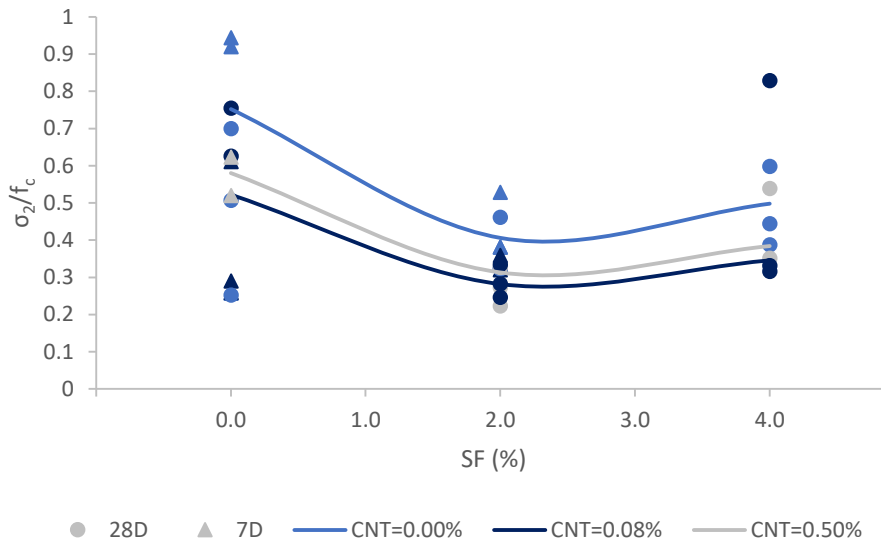


Figure 6-8 σ_2/f_c parametric curves and experimental values by SF dosage

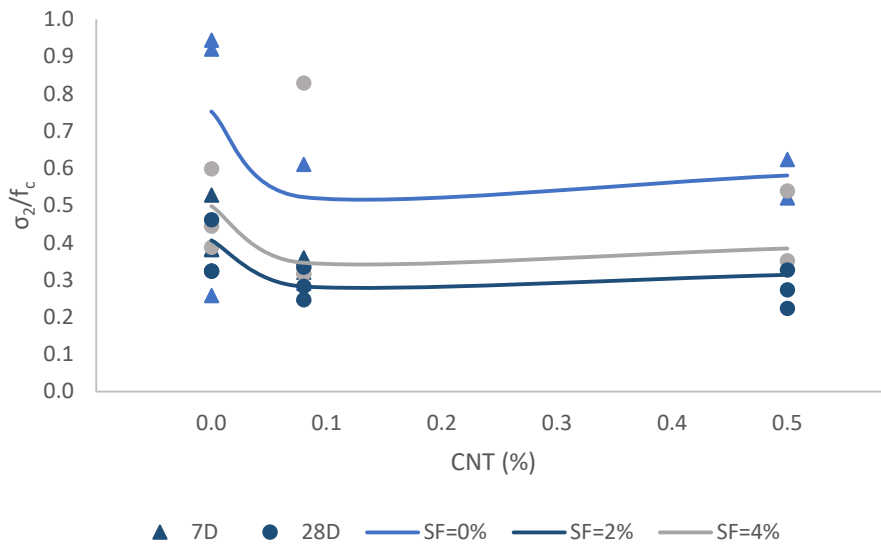


Figure 6-9 σ_2/f_c parametric curves and experimental values by CNT dosage

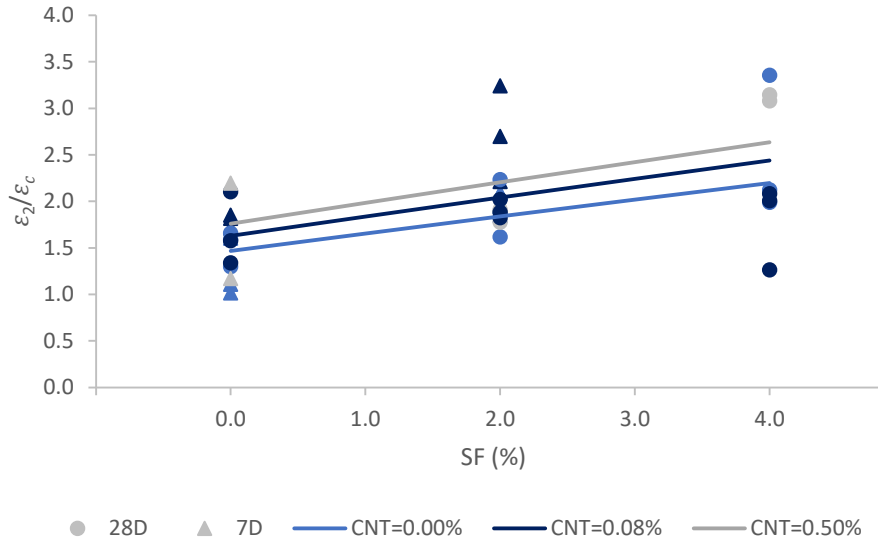


Figure 6-10 $\varepsilon_2/\varepsilon_c$ parametric curves and experimental values by SF dosage

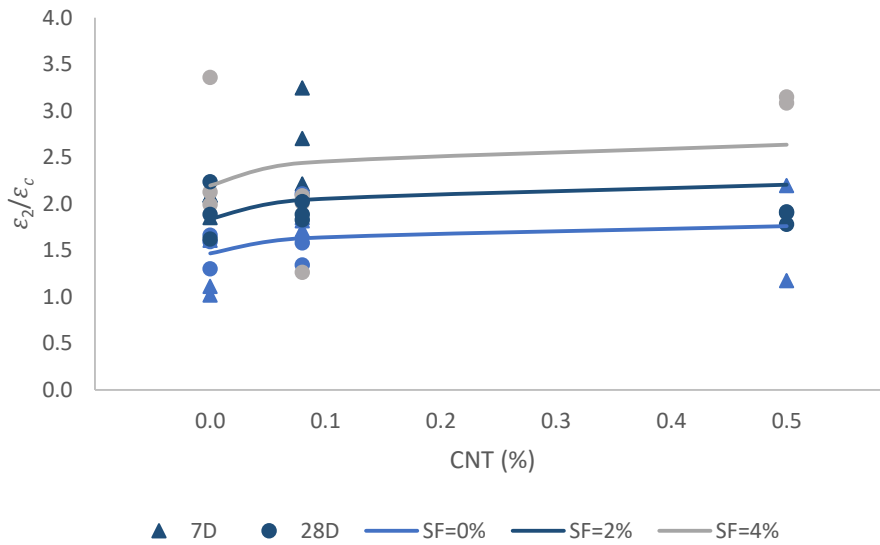


Figure 6-11 $\varepsilon_2/\varepsilon_c$ parametric curves and experimental values by CNT dosage

As explained in chapter 2, σ_2/f_c , $\varepsilon_2/\varepsilon_c$ are the stress and strain points where the stress strain curve has a change of slope on the post-peak section. They are determined numerically from experimental data to optimize the adjustment of the proposed equation.

It can be seen that σ_2/f_c value, representing the loss of compressive strength from peak strength before stabilizing in a remnant strength level, gets reduced when adding CNT, in particular when adding CNT on a 0.08 %wt concentration. On the contrary, the $\varepsilon_2/\varepsilon_c$ value, that represents the strain increase until reaching σ_2 point, it increases when the CNT is increased.

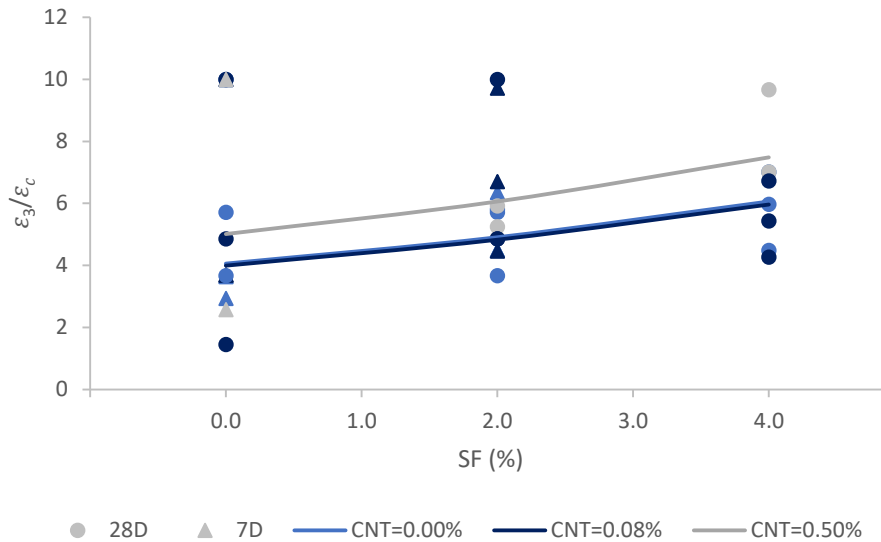


Figure 6-12 ϵ_3/ϵ_c parametric curves and experimental values by SF dosage

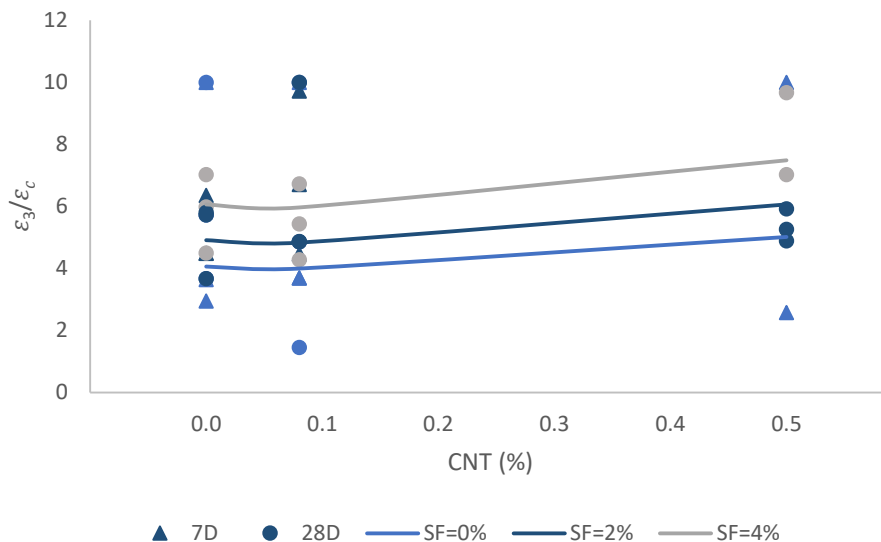


Figure 6-13 ϵ_3/ϵ_c parametric curves and experimental values by SF dosage

For the parameter ϵ_3/ϵ_c , representing the strain of the specimen when it can not hold any more stress, we can observe that it is increasing with both the content of steel fibers and the content of CNT, especially when using the 0.50% CNT dosage.

6.3.- Influence of curing time in UHPC with CNT&GO additions

Because of the different difficulties encountered during the research, we have available only two pairs of UHPC with CNT&GO admixture to compare between curing times of 7 days and 28 days (i.e. specimens with 0%/2% steel fibers and 0.08% CNT).

Analyzing these specimens (figure 6-14), we can observe there is indeed an increase on the compressive strength at 28 days, being the relation between 7 days and 28 days a factor of 0.9 (i.e. 7 days compressive strength is 90% of 28 days compressive

strength). Even though this value could seem high in relation to conventional concrete (0.65 - 0.75), it is a normal value in ultra high performance concretes, so it does not seem that CNT&GO addition modified this behavior.

More research should be done on the difference of compressive strength in UHPC with additions of different CNT&GO dosages, although it does not seem to be a relevant factor.

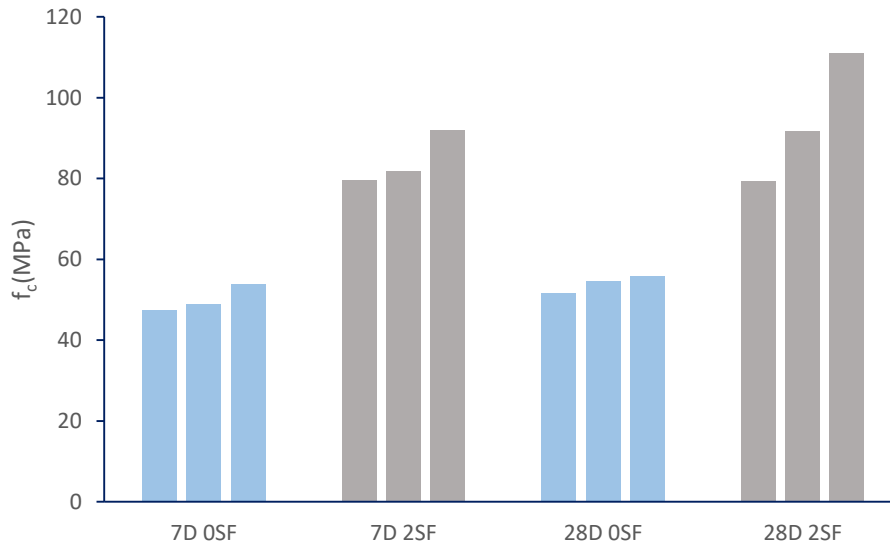


Figure 6-14 Variation of f_c on UHPC specimens with 0.08% CNT dosage

Regarding peak deformation results, we can perceive variations similar to what is observed in the compressive strength results, so similar conclusion can be extracted. The results are shown in figure 6-15.

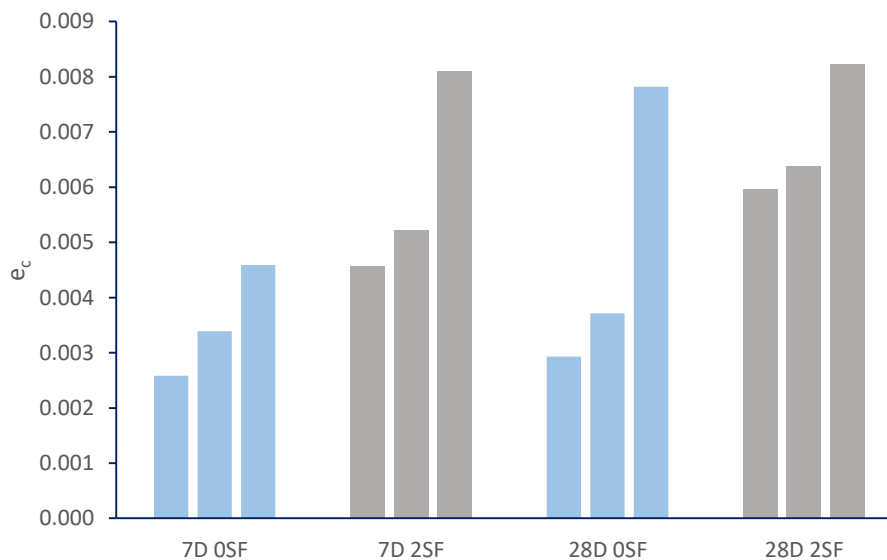


Figure 6-15 Variation of e_c on UHPC specimens with 0.08% CNT dosage

6.4.- Reliability of the proposed finite element model

For the finite element model evaluation, we focused on the stress-strain curve obtained from both the numerical program and the experimental tests. The purpose of a FE model should be to do a more parametric study, however our thesis limited the scope to the evaluation of the compression behavior and we don't have tensile or flexural behavior, thus the tensile curve is approximate and should be studied in future researches to be able to do a parametric study of the material.

With the tensile assumptions, we can compare the obtained stress-strain curve on the finite element model and the curve obtained through the experimental tests.

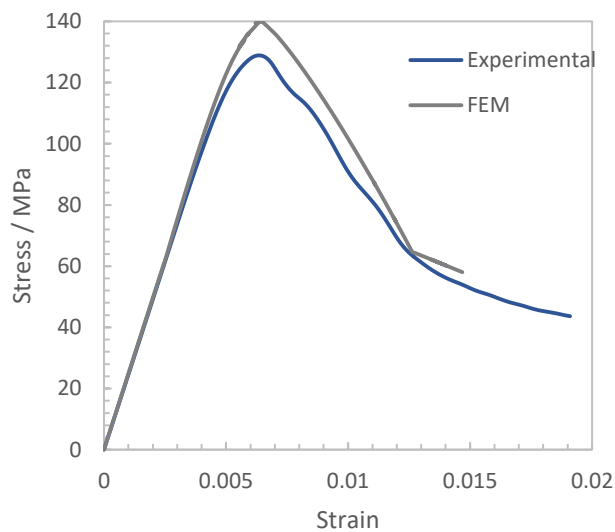


Figure 6-16 Stress-Strain curves of both FEM and Experimental results

As we can see on the curve comparison, our equation approaches correctly the initial slope.

There is a difference between the slopes occurring approaching the peak strength. The maximum difference between curves is 8%, which is an acceptable error range, especially since the tensile behavior is assumed.

This difference will be solved in our equation's general approach and simplification to simulate all the different curves with simple data obtained from experimental tensile tests, without having to adapt the equation for every specific case.

The squared error calculation results [0.997], giving us the assurance of a correct formulation of our equation and its implementation in a finite element model, as well as the correct definition of the material behavior in numerical analysis.

On the figure below we can see how the model reproduces sufficiently the phenomena of the experimental tests, exemplified with the force-displacement curves, being SP# the different specimens of the same UHPC4SF28D008 dosage.

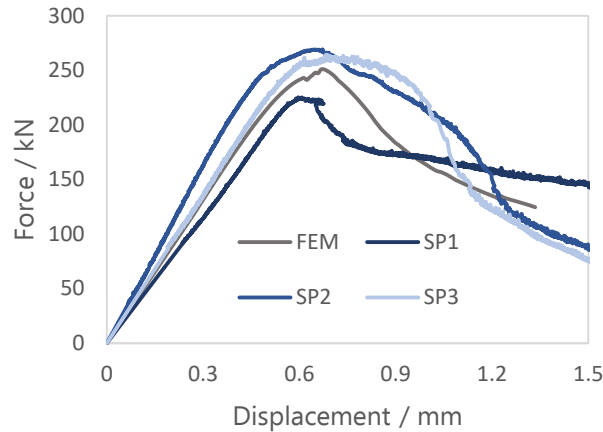


Figure 6-17 Force - displacement comparison curve

The finite element model curve and the experimental test curve are, as expected, similar, and the FEM curve represents assuredly the experimental test curve.

Noting that:

- A working numerical model was constructed
- It includes all the relevant aspects
- It was proved with the performed tests but can be presumably used for any other case with plane stress or axisymmetric.
- The obtained results certainly manifest the results of the experimental lab tests
- In case of extending its use to other types of structures, it would be necessary to perform the corresponding 4-point bending tests to calibrate and adjust the numerical model, if required.

A future modification of the finite element model might come from adding the tensile properties on the material behavior level, which will improve the model and equip it with capabilities towards tensile behavior characterization.

Chapter 7 - Conclusions

This research lays in the study of UHPC with admixtures, obtaining a better knowledge of their dosing, mixing and commissioning conditions as well as to identify the stress-strain characteristics of the UHPCs obtained from CNT & GO cement composites with aggregated (or not) steel fibers. The properties of these new UHPCs were then identified and reproduced in a finite element model to facilitate the study and its use in future researches and the calculation of real structures.

The state of the art research showed a clear tendency towards using nanomaterials in cement composites to enhance some of its weaker characteristics, especially the tension behavior of concrete. However, in the case of carbon nanotubes and graphene oxide, there has not been an agreement on the optimal dosage of neither of them, and more research with different dosages should be made.

As it was reviewed in chapter 2, nanomaterials are undoubtedly the future of many new material composites. However, there should be further studies to produce them at industrial scale and to quantify the improvement on concrete composites.

Regarding this improvement, materials' cost is a significant limitation for the quantity to use and it is important to delve into the different concrete dosages in future researches. Costs are supposed to get lower as technology develops and as the restraining materials (CNT and GO) achieve more importance in future composites.

A comparison on the costs show that UHPC with CNT and GO costs between 7 to 17 times more than regular UHPC. In contrast, the addition of steel fibers in plain UHPC increases the cost by only 7% delivering an adequate improvement/cost ratio.

Numerical models allow us to test different material options or structural typologies to analyze and compare different solutions without requiring costly and complicated laboratory tests. There are different discretization methods for a numerical model to represent a test, however, we came to the conclusion that finite element method with Abaqus software and ad-hoc Fortran modules would be the best fitted solution as they are widely used in the university and there is a wide range of support documents.

Regarding the materials characterization and mixing procedure analyzed in chapter 3, we experienced the whole mixing process should be accurate and focus mostly on the timing of the mixing so that concrete stays moist. It is very important the compaction process by vibration table, especially with small specimens, which required longer times of application than in the literature reviewed. It is important to make sure the good quality of materials and the homogeneous creation of all the batches with comparable dosages.

A critical consideration when mixing CNT and GO dosages is that it is useful to use the nanomaterials dispersed in water for correct mixing with cement composites, although the water used must be calculated and be within concrete standard limits.

To mix these nanomaterials with water, especially CNT, the standard method used in all the literature reviewed is the sonication process. When mixing the CNT and GO dispersed in water, it is necessary to use high-range water reducer (HRWR) products to obtain the desired solution, otherwise the quantity of water needed only for this process would be more than the appropriate for UHPC.

The testing procedure has highlighted the importance of the size factor in specimens, being small specimens more prone to irregularities. Due to high materials costs, all researchers tend to use small specimens, entailing an obligation to pay extra attention to the manufacturing, mixing, curing and testing processes as well as test equipment, as it is not usual to have the adequate instrumentation for this kind of tests and it can not be done with guarantees in a conventional testing lab.

There are no comparable studies before this one where they add both carbon nanotubes and graphene oxide to ultra-high performance concrete, and although direct comparison cannot be made, test results incline to low performance of the nanomaterials admixtures.

As expected, those specimens with steel fibers experienced a post-cracking resistance and a tendency for greater strengths. However, the presence of different quantities of carbon nanotubes and graphene oxide on the mixing were not able to increase the maximum compressive strength of the concrete. Future research should address this issue by selecting and comparing more dosages.

In extreme cases, we observed a detachment of part of the effective resistant section of the specimen while simultaneously registering a significant drop in the resistive load for a given deformation. To assess the impact of this effect, it would have been advisable to weigh the specimens also after the test, to approximately evaluate what was the loss of resistant area and to try to correlate it with the loss of apparent resistance.

In addition to that, specimens with added nanomaterials experienced more brittle behaviors, being imperative the addition of steel fibers to limit fragility. On future researches, this behavior must be analyzed and proved by bending tests, but in any case, we can conclude that UHPC should always include steel fibers as admixtures because the addition of only CNT&GO could lead to poor performances in the concrete.

From the parametric results observation, we can deduce that for high CNT dosages, the compressive strength does not increase significantly. On the contrary, the elastic modulus is increased by the CNT amount.

Analyzing the test results, we obtained a set of relationships that will define our UHPC parameters depending on the quantity of SF and CNT&GO, allowing us to get close to the optimal dosage that would give a desired value on any parameter.

The results were able to provide a base to define a constitutive equation that characterizes the material properties and will be of use on future researches.

This equation is built by using variables that are easily obtained from lab tests, and therefore, these variables have a physical meaning. They are not random parameters used to adjust the curve so it fits.

With this equation, we carried out the numerical simulation through a finite element model and compared the numerical results with the real test results. Using the Abaqus program for the calculations, we were able to compare both results without any significant difference, confirming that the constitutive equation and finite element model fairly represent the behavior of the concrete specimens.

Resolving the feasibility for commercial use of these admixtures will be key in future researches. The main focus should be on testing more specimens and increasing the number of dosages, as well as researching on other varieties of nanomaterials, especially on different CNT.

It would be useful for future studies to add a fourth CNT and a fourth SF dosage, e.g. 0.25% and 3%, which would allow interpolation of more accurate curves to discover the optimal CNT and SF dosages for each of the parameters. In addition, different dosages of GO should be tested, as this study used only one dosage, allowing for an additional parametric study of UHPC with GO as admixture.

New studies should also aim to study differences in properties by curing time, as we are not able to extract relevant conclusions from our research. Different curing times (e.g. 7 days, 14 days, 28 days and 90 days) should be tested with each different dosage and compare between results for each parameter.

On the numerical modeling aspect, this dissertation's scope is focused on the evaluation of the compressive strength behavior on both pre and post-cracking. To comply with the main purpose of the finite element modeling, which is doing a full parametric study, next studies should research on tensile and flexural behavior to obtain a complete model of the material.

References

- [1] Mohammed S. et al., Trends and developments in green cement and concrete technology, *International Journal of Sustainable Built Environment*, December 2012, 1(2):194–216
- [2] Zhang T et al., Effectiveness of novel and traditional methods to incorporate industrial wastes in cementitious materials – An overview, *Resources, Conservation and Recycling*, 2013, 74:134–143.
- [3] Tang J H, Cai J W, Zhou M K. The status of researching and developing in high performance concrete, *Science and Technology of Overseas Building Materials*, 2006, 27(3): 11-15.
- [4] Association Française de Génie Civil, Paris, France, Ultra High Performance Fibre-Reinforced Concretes-Interim Recommendations (2002).
- [5] Boulekbache B, Hamrat M, Chemrouk M, et al. Influence of yield stress and compressive strength on direct shear behaviour of steel fibre-reinforced concrete, *Construction and Building Materials*, 2012, 27(1): 6-14.
- [6] Sun M, Liu Q, Li Z, et al. A study of piezoelectric properties of carbon fiber reinforced concrete and plain cement paste during dynamic loading, *Cement and Concrete Research*, 2000, 30(10):1593-1595.
- [7] Federal Highway Administration, Ultra-High Performance Concrete: A State-of-the-Art Report for the Bridge Community, FHWA-HRT-13-060: Federal Highway Administration. June 2013.
- [8] C. D. Johnston, *Fiber reinforced cements and concrete*, Taylor and Francis, 2001.
- [9] Kay Wille and Kenneth J. Loh, Nanoengineering Ultra-High-Performance Concrete with Multiwalled Carbon Nanotubes, *Transportation Research Record: Journal of the Transportation Research Board*, No. 2142, 2010, 119–126.
- [10] Jun Xia, *Ultra-high performance fiber reinforced concrete in bridge deck applications*, University of Central Florida, 2011.
- [11] R. Yu et al., Mix design and properties assessment of Ultra-High Performance Fibre Reinforced Concrete (UHPRFC), *Cement and Concrete Research*, 2014, 56: 29–39
- [12] In-Hwan Yang et al., Flexural strength of large-scale ultra high performance concrete prestressed T-beams, *Can. J. Civ. Eng.*, 2011, 38: 1185–1195
- [13] Graybeal, B., “Material Property Characterization of Ultra - High Performance Concrete,” FHWA, U.S. Department of Transportation, Report No. FHWA-HRT-06-103, McLean, VA, 2006.
- [14] Libya Ahmed Sbia, Amirpasha Peyvandi, Parviz Soroushian and Anagi M. Balachandra, Optimization of ultra-high-performance concrete with nano- and micro-scale reinforcement, *Cogent Engineering*, 2014, 2: 990673.
- [15] D'mello, Sandhya, Explosion resistant cement in UAE. *Khaleej Times*. 2005
- [16] Kowald T., Influence of Surface-Modified Carbon Nanotubes on Ultra-High Performance Concrete. *Proceedings of International Symposium on Ultra High Performance Concrete*, Kassel, Germany, 2004, pp. 195–202.
- [17] Kowald T., R. Trettin, N. Dorbaum, T. Stadler, and X. Jian. Influence of Carbon Nanotubes on the Micromechanical Properties of a Model System for Ultra-High Performance Concrete. *Proc., 2nd International Symposium on Ultra High Performance Concrete*, 2008, pp. 129–134.
- [18] Yuliarti K. et al., UHPC compressive strength test specimens: Cylinder or cube?, *Procedia Engineering*, 125 (2015) 1076 – 1080
- [19] C 109/C 109M – 02, Standard Test Method for Compressive Strength of Hydraulic Cement Mortars
- [20] C 348 – 02, Standard Test Method for Flexural Strength of Hydraulic-Cement Mortars
- [21] Zollo R.F., Fiber-reinforced concrete: an overview after 30 years of development, *Cement and Concrete Composites*, 1997, 19(2):107–22.
- [22] Qian CX, Stroeven P. Development of hybrid polypropylene-steel fibre-reinforced concrete, *Cement and Concrete Research*, 2000, 30(1):63–9.
- [23] Hamoush S, Abu-Lebdeh T, Cummins T. Deflection behavior of concrete beams reinforced with PVA micro-fibers, *Construction and Building Materials*, 2010, 24(11):2285–93.
- [24] Wichmann MHG, Schulte K, Wagner HD. On nanocomposite toughness, *Composites Science and Technology*, 2008, 68(1):329–31.
- [25] S. Chuah et al., Nano reinforced cement and concrete composites and new perspective from graphene oxide, *Construction and Building Materials*, 2014, 73:113–124.

- [26] S. Musso, M. Tulliani, G. Ferro, and A. Tagliaferro, Influence of carbon nanotubes structure on the mechanical behavior of cement composites, *Composites Science and Technology*, 2009, 69(11-12):1985–1990.
- [27] Raki L et al. Cement and concrete nanoscience and nanotechnology. *Materials* 2010;3(2):918–42.
- [28] Sanchez F. and Sobolev K., Nanotechnology in concrete – a review, *Construction and Building Materials*, 2010, 24(11):2060–71.
- [29] Bjornstrom J, Martinelli A, Matic A, Borjesson L, Panas I. Accelerating effects of colloidal nano-silica for beneficial calcium–silicate–hydrate formation in cement. *Chem Phys Lett* 2004;392(1–3):242–8.
- [30] J T. Preliminary study on the water permeability and microstructure of concrete incorporating nano-SiO₂. *Cem Concr Res* 2005;35(10):1943–7.
- [31] Li H, Zhang M-h, Ou J-p. Abrasion resistance of concrete containing nano -particles for pavement. *Wear* 2006;260(11–12):1262–6.
- [32] Li H, Zhang M-h, Ou J-p. Flexural fatigue performance of concrete containing nano-particles for pavement. *Int J Fatig* 2007;29(7):1292–301.
- [33] Li H, Xiao H-g, Ou J-p. A study on mechanical and pressure-sensitive properties of cement mortar with nanophase materials. *Cem Concr Res* 2004;34(3):435–8.
- [34] Li Z, Wang H, He S, Lu Y, Wang M. Investigations on the preparation and mechanical properties of the nano-alumina reinforced cement composite. *Mater Lett* 2006;60(3):356–9.
- [35] Chang T-P, Shih J-Y, Yang K-M, Hsiao T-C. Material properties of portland cement paste with nanomontmorillonite. *J Mater Sci* 2007;42(17):7478–87.
- [36] Jo B-W et al. Characteristics of cement mortar with nano-SiO₂ particles. *Constr Build Mater* 2007;21(6):1351–5.
- [37] Nazari A, Riahi S. The effects of SiO₂ nanoparticles on physical and mechanical properties of high strength compacting concrete. *Compos Part B: Eng* 2011;42(3):570–8.
- [38] Li H, Xiao H-g, Yuan J, Ou J. Microstructure of cement mortar with nano-particles. *Compos B Eng* 2004;35(2):185–9.
- [39] Sobolev K, Engineering of SiO₂ nanoparticles for optimal performance in nano cement- based materials, 2009
- [40] Kong D et al. Influence of nano-silica agglomeration on microstructure and properties of the hardened cement-based materials. *Constr Build Mater* 2012;37:707–15.
- [41] Murata Y et al. Air purifying pavement: development of photocatalytic concrete blocks. *J Adv Oxidat Technol* 1999;4(2):227–30.
- [42] Makar JMet al. Carbon nanotube/cement composites – early results and potential applications. Proceedings of 3rd international conference on construction materials: performance, innovations and structural implications. 2005 , p. 1–10.
- [43] Cwirzen A, et al. Surface decoration of carbon nanotubes and mechanical properties of cement/carbon nanotube composites. *Adv Cem Res* 2008;20(2):65–73.
- [44] Hyukjin Choi et al., Effect of Some Parameters on the Compressive Strength of MWCNT-Cement Composites, *Advances in Materials Science and Engineering*, 2015.
- [45] Josef Foldyna et al., Dispersion of carbon nanotubes for application in cement composites, *Procedia Engineering*, 2016, 149:94–99.
- [46] M. S. Morsy et al. “Hybrid effect of carbon nanotube and nano-clay on physico-mechanical properties of cement mortar,” *Construction and Building Materials*, vol. 25, no. 1, pp. 145–149, 2011.
- [47] Su-Tae Kang, Jun-Yeong Seo, and Sun-Hong Park, The Characteristics of CNT/Cement Composites with Acid-Treated MWCNTs, *Advances in Materials Science and Engineering*, 2015.
- [48] Zou B, Chen SJ, Korayem AH, Collins F, Wang CM, Duan WH, Effect of ultrasonication energy on engineering properties of carbon nanotube reinforced cement pastes, *Carbon*, 2015, 85:212-220.
- [49] Abu Al-Rub RKet al., Mechanical Properties of Nanocomposite Cement Incorporating Surface-Treated and Untreated Carbon Nanotubes and Carbon Nanofibers, *Journal of Nanomechanics and Micromechanics*, 2012, 2(1):1-6.
- [50] G. Y. Li, P. M. Wang, and X. Zhao, Mechanical behavior and microstructure of cement composites incorporating surface- treated multi-walled carbon nanotubes, *Carbon*, 2005, 43(6):1239–1245.
- [51] S. Kumar, P. Kolay, S. Malla, and S. Mishra, “Effect of multi-walled carbon nanotubes on mechanical strength of cement paste,” *Journal of Materials in Civil Engineering*, vol. 24, no. 1, pp. 84–91, 2012.

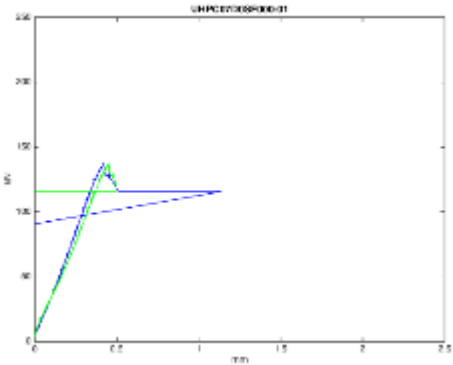

- [52] G. Ferro et al., Carbon nanotubes cement composites, 2011
- [53] A. Chaipanich et al., "Compressive strength and microstructure of carbon nanotubes-fly ash cement composites," *Materials Science and Engineering A*, vol. 527, no. 4-5, pp. 1063–1067, 2010.
- [54] Chan LY, Andrawes B. Finite element analysis of carbon nanotube/cement composite with degraded bond strength. *Comput Mater Sci* 2010;47(4):994–1004.
- [55] Konsta-Gdoutos MS, Metaxa ZS, Shah SP. Multi-scale mechanical and fracture characteristics and early-age strain capacity of high performance carbon nanotube/cement nanocomposites. *Cem Concr Compos* 2010;32(2):110–5.
- [56] Metaxa ZS et al. Highly concentrated carbon nanotube admixture for nano- fiber reinforced cementitious materials. *Cem Concr Compos* 2012;34(5):612–7.
- [57] Konsta-Gdoutos MS, Metaxa ZS, Shah SP. Highly dispersed carbon nanotube reinforced cement based materials. *Cem Concr Res* 2010;40(7):1052–9.
- [58] Wang B, Han Y, Liu S. Effect of highly dispersed carbon nanotubes on the flexural toughness of cement-based composites. *Constr Build Mater* 2013;46:8–12.
- [59] Sobolkina A et al. Dispersion of carbon nanotubes and its influence on the mechanical properties of the cement matrix. *Cem Concr Compos* 2012;34(10):1104–13.
- [60] Camacho M , "Mechanical properties and durability of CNT cement composites," *Materials*, vol. 7, no. 3, pp. 1640–1651, 2014.
- [61] Morsy MS, Alsayed SH, Aqel M. Hybrid effect of carbon nanotube and nanoclay on physico-mechanical properties of cement mortar. *Constr Build Mater* 2011;25(1):145–9.
- [62] Qiu L et al. Dispersing carbon nanotubes with graphene oxide in water and synergistic effects between graphene derivatives. *Chem – Eur J* 2010;16(35):10653–8.
- [63] Wu YH, Yu T, Shen ZX. Two-dimensional carbon nanostructures: fundamental properties, synthesis, characterization, and potential applications. *J Appl Phys* 2010;108(7):071301.
- [64] Park S, Ruoff RS. Chemical methods for the production of graphenes. *Nat Nanotechnol* 2009;4:217–24.
- [65] Cong Lu, Zeyu Lu , Zongjin Li, Christopher K.Y. Leung, Effect of graphene oxide on the mechanical behavior of strain hardening cementitious composites, *Construction and Building Materials*, 2016, 120:457–464.
- [66] Mohammed A. et al., Incorporating graphene oxide in cement composites: A study of transport properties, *Construction and Building Materials*, 2015, 84:341–347.
- [67] Gong K et al., Reinforcing effects of graphene oxide on portland cement paste, *Journal of Materials in Civil Engineering*, 2014.
- [68] Shenghua Lv et al., Effect of graphene oxide nanosheets of microstructure and mechanical properties of cement composites, *Construction and Building Materials*, 2013, 49: 121–127.
- [69] Z. Pan et al., Mechanical properties and microstructure of a graphene oxide–cement composite, *Cement Concr. Compos.* 58 (2015) 140–147.
- [70] M Wang et al., Study on the three dimensional mechanism of modified graphene oxide nanosheets. *Cement, construction and Building Materials* 126 (2016) 730–739
- [71] Qin Wang et al., Influence of graphene oxide additions on the microstructure and mechanical strength of cement, *New Carbon Materials*, 2015, 30(4): 349–356
- [72] L. J. Cote, F. Kim, J. X. Huang, *J. Am. Chem. Soc.* 2009, 131, 1043.
- [73] C. G. Salzmann, S. A. Llewellyn, G. Tobias, M. A. H. Ward, Y. Huh, M. L. H. Green, *Adv. Mater.* 2007,
- [74] Xueguang Li et al., Co-effects of graphene oxide sheets and single wall carbon nanotubes on mechanical properties of cement, *Journal of Physics and Chemistry of Solids*, 2015, 85: 39–43.
- [75] Ali A. Abbas et al., A simplified finite element model for assessing steel fiber reinforced concrete structural performance, *Computers and Structures*, 2016, 173: 31–49
- [76] Faezeh Faghieh et al., Finite Element Modeling of Carbon Nanofiber Concrete Structural Members, *Structures Congress*, 2014, 1048-1058.
- [77] Lai Yin Christina Chan et al., Numerical Modeling of Flexural Enhancement in Carbon Nanotube/Cement Composite, *Structures* 2009: Don't Mess with Structural Engineers, 2009, 2686-2693.
- [78] R. Hamzaoui, A. Bennabi, S. Guessasma, M. R. Khelifa, and N. Leklou, "Optimal carbon nanotubes concentration incorporated in mortar and concrete," *Advanced Materials Research*, vol. 587, no. 10, pp. 107–110, 2012.

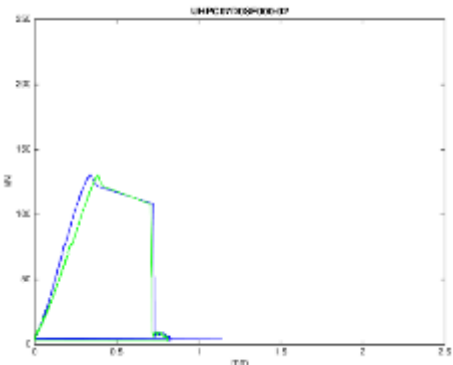

- [79] Metaxa ZS, Konsta-Gdoutos MS, Shah SP. Carbon nanofiber cementitious composites: effect of debulking procedure on dispersion and reinforcing efficiency. *Cem Concr Compos* 2013;36:25–32.
- [80] Nasibulina LI et al. Effect of carbon nanotube aqueous dispersion quality on mechanical properties of cement composite. *J Nanomater* 2012;2012.
- [81] Kim HK, Nam IW, Lee HK. Enhanced effect of carbon nanotube on mechanical and electrical properties of cement composites by incorporation of silica fume. *Compos Struct* 2014;107:60–9.
- [82] Melo VS et al. Macro- and micro-characterization of mortars produced with carbon nanotubes. *ACI Mater J* 2011;108(3):327–32.
- [83] F. Torabian Isfahani et al., Dispersion of multi-walled carbon nanotubes and its effects on the properties of cement composites, *Cement and Concrete Composites* 74 (2016) 154-163
- [84] Tyson B.M. et al., Carbon Nanotubes and Carbon Nanofibers for Enhancing the Mechanical Properties of Nanocomposite Cementitious Materials, *J. Mater. Civ. Eng.*, 2011, 23(7): 1028-1035
- [85] Choi. H et al., Effect of Some Parameters on the Compressive Strength of MWCNT-Cement Composites, *Advances in Materials Science and Engineering*, 2015
- [86] Hunashyal A et al., Experimental investigation of the effect of carbon nanotubes and carbon fibres on the behaviour of plain cement composite beams. *IES J Part A: Civil Struct Eng* 2011;4(1):29–36.
- [87] Campillo I, Dolado J, Porro A., High-performance nanostructured materials for construction., *Special Pub-R Soc Chem*, 2004;292:215–26.
- [88] Collins F, Lambert J, Duan WH. The influences of admixtures on the dispersion, workability, and strength of carbon nanotube-OPC paste mixtures. *Cem Concr Compos*, 2012;34(2):201–7.
- [89] K. J. Bathe, *Finite Element Procedures*, Prentice Hall, 2nd edition, 1995.
- [90] O. C. Zienkiewicz, R. L. Taylor, *El Método de los Elementos Finitos*, CIMNE-Mc Graw Hill, 1994, 1&2.
- [91] E. Oñate, *Cálculo de Estructuras por el Método de los Elementos Finitos*, CIMNE, Barcelona, 1995.
- [92] J. J. Benito Muñoz et al., *Introducción al Método de los Elementos Finitos*, 2014.
- [93] C. S. Desai and H. J. Siriwardane, *Constitutive laws for engineering materials: with emphasis on geologic materials*, Prentice-Hall, Inc., 1984
- [94] Kupfer, H.B.; Gerstle, K.H. Behaviour of Concrete under Biaxial Stresses. *Journal of Engineering Mechanics*, [S.l.], vol. 99, n. 4, p. 853-866, 1973.
- [95] Oñate, E. et al., A local constitutive model for the discrete element method: application to geomaterials and concrete. *Computational particle mechanics*, June 2015, vol. 2, num. 2, p. 139-160.
- [96] Abaqus 6.13 User Manual, Simulia
- [97] Mier, J. G. M., et al., Strain-softening of concrete in uniaxial compression, *Materials and Structures*, vol. 30, May 1997.
- [98] Jansen, D. C., et al., Stress-Strain Results of Concrete from Circumferential Strain Feedback Control Testing, *ACI Materials Journal*, V. 92, No. 4, July-August 1995, pp. 419-428.
- [99] Okubo, S. and Nishimatsu, Y., Uniaxial Compression Testing Using a Linear Combination of Stress and Strain as the Control Variable, *Int. J. Rock Mech., Min. Sci. and Geomech. Abstr.*, V. 22, No. 5, 1985, pp. 323-330.
- [100] Thomas Telford, Comité Euro-International du Béton. CBE-FIP Model Code 90, 1991.
- [101] Ritter, K. W. (1899). Die Bauweise Hennebique. *Schweizerische Bauzeitung*, 33(7): 59-61.
- [102] Smith, G. M. y Young, L. E. (1956). Ultimate flexural analysis on stress-strain curves for cylinders. *ACI Journal Proceedings*, 53(12): 597-609.
- [103] Kachanov, L. M. (1958). On the time to rupture under creep conditions. *Izv. Akad. Nauk SSSR. Otd. Tekhn. Nauk*, 8: 26-31.
- [104] Rabotnov, Y.N. (1959). A mechanism of a long time failure, *Creep Problems in Structural Members*, USSR Academy of Sci. Publ., Moscow.
- [105] Collins, M. P., Mitchell, D. y MacGregor, J. G. (1993). Structural design considerations for high-strength concrete. *Concrete International: Design and Construction*, 15(5): 27-34.
- [106] Weibull, W. (1951). A statistical distribution function of wide applicability. *J. Appl. Mech.*, 18:293-297.
- [107] Lim, T.Y., Paramasivam, P. et al. (1988), Bending Behaviour of Steel-Fiber Concrete Beams. *ACI Journal*, Vol. 84, p. 524-536
- [108] Lok, T.S. y Xiao, L. (1998). Tensile behaviour and moment - curvature relationship of steel reinforced concrete. *Magazine of Concrete Research*, Vol. 50, no 4, p. 359 – 368.

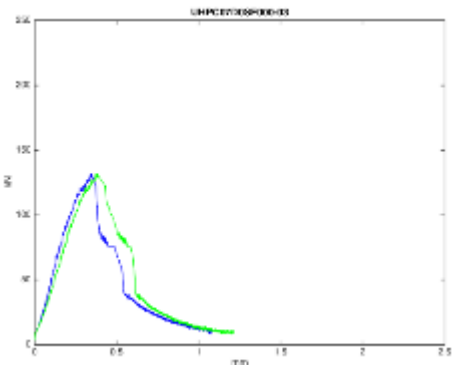

- [109] Rilem TC-162 TDF (2002), Test and design methods for steel fibre reinforced concrete: Bending test. *Materials and Structures*, Vol. 35, p. 579-582.
- [110] Dupont, D. (2003). Modelling and experimental validation of constitutive law and cracking behaviour of steel fibre reinforced concrete. Doctoral Thesis. Katholieke University Leuven. ISBN 90-5682-424-4
- [111] ASTM C469 / C469M-14, Standard Test Method for Static Modulus of Elasticity and Poisson's Ratio of Concrete in Compression, ASTM International, West Conshohocken, PA, 2014, www.astm.org
- [112] KWAK, H.G. and FILIPPOU, F.C. Finite Elements Analysis of Reinforced Concrete Structures under Monotonic Loads. Report UCB/SEMM-90/14, Berkeley, California. 1990.
- [113] Global Carbon Nanotubes Market Size Analysis, 2018-2028, Bekryl, Apr 2018
- [114] Graphenea Blog
- [115] Future Markets, Inc, Global Market for Carbon Nanotubes 2018-2023, Jan 2018
- [116] Simon Paonessa, Reducing Signal Noise in Practice, The Current Quandary
- [117] Craven, P. & Wahba, Smoothing noisy data with spline functions, *G. Numer. Math.* (1978) 31: 377
- [118] Matlab Manual
- [119] Yuan Gao et al., Influence of ultrasonication on the dispersion and enhancing effect of graphene oxide-carbon nanotube hybrid nanoreinforcement in cementitious composite, *Composites Part B: Engineering*, Vol. 164, May 2019, p. 45-53
- [120] Taher A. Tawfik et al., (2018) Influence of nanoparticles on mechanical and nondestructive properties of high- performance concrete, *Journal of the Chinese Advanced Materials Society*, 6:4, 409-433
- [121] Lim, J. et al., R. Autogenous Shrinkage, Microstructure, and Strength of Ultra-High Performance Concrete Incorporating Carbon Nanofibers. *Materials* 2019, 12, 320
- [122] Dimitar Dimov et al., Ultrahigh Performance Nanoengineered Graphene-Concrete Composites for Multifunctional Applications, *Advanced Functional Materials*, Vol. 28-23, June 2018
- [123] Sanchez Carrillo (2015), Ensayos de Compresión, Blog
- [124] Charif, Abdelhamid. (2014). Developing Structural Lightweight Concrete Using Volcanic Scoria Available in Saudi Arabia. *Arabian Journal For Science And Engineering*. 12 pages.
- [125] Bezerra, U. T., et al. (2016). Hourglass-shaped specimen: compressive strength of concrete and mortar (numerical and experimental analyses). *Revista IBRACON de Estruturas e Materiais*, 9(4), 510-524
- [126] Ediciones Santillana 3º ESO, *Materiales de Construcción*
- [127] Madureira, E. L., Siqueira, T. M., & Rodrigues, E. C.. (2013). Creep strains on reinforced concrete columns. *Revista IBRACON de Estruturas e Materiais*, 6(4), 537-560

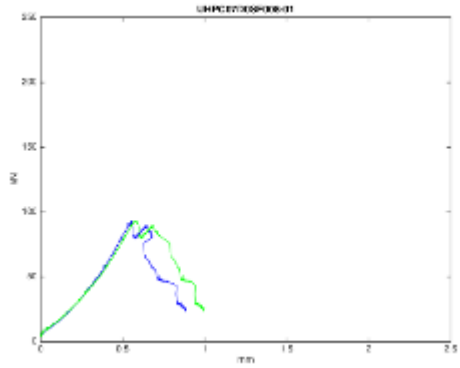

Annex 1 Raw data and test annotations

07 Days

UHPC07D0SF000_01		
<p>Curing: 7 Days Steel Fibers: NO / 0 CNT&GO: NO / 0% Height: 96.5 mm Ø: 50 mm</p>		
<p>Notes: Small holes of 6 mm, no cracks. 2 extensometers.</p>	<p>Remarks: Initial settling specimen-plate. After reaching peak strength, extensometers' data not usable.</p>	

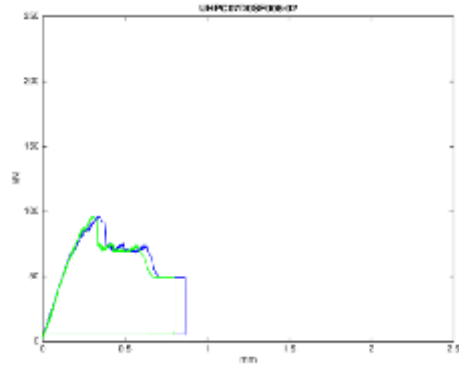
UHPC07D0SF000_02		
<p>Curing: 7 Days Steel Fibers: NO / 0% CNT&GO: NO / 0% Height: 97 mm Ø: 50 mm</p>		
<p>Notes: Very small holes, no cracks. 2 extensometers.</p>	<p>Remarks: Initial settling specimen-plate. After reaching peak strength, extensometers' data not usable.</p>	

UHPC07D0SF000_03		
<p>Curing: 7 Days Steel Fibers: NO / 0% CNT&GO: NO / 0% Height: 97 mm Ø: 50 mm</p>		
<p>Notes: No important holes or cracks. 2 extensometers.</p>	<p>Remarks: Initial settling specimen-plate. Data after the peak very disassociated.</p>	

UHPC07D0SF008_01		
<p>Curing: 7 Days Steel Fibers: NO / 0% CNT&GO: 0.08% wt% Height: 97 mm Ø: 50 mm</p>		
<p>Notes: No important holes or cracks. 2 extensometers.</p>	<p>Remarks: Initial settling specimen-plate. Sudden loss of loading area at 0.7 mm. After reaching peak strength, extensometers' data not usable.</p>	

UHPC07D0SF008_02

Curing: 7 Days
Steel Fibers: NO / 0%
CNT&GO: 0.08% wt%
Height: 97 mm
Ø: 50 mm



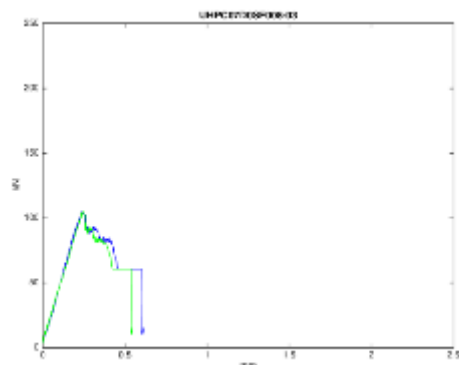
Notes: No important holes or cracks. 2 extensometers.

Remarks: Initial settling specimen-plate. Sudden loss of loading area at 0.4 and 0.51 mm. After reaching peak strength, extensometers' data not usable.



UHPC07D0SF008_03

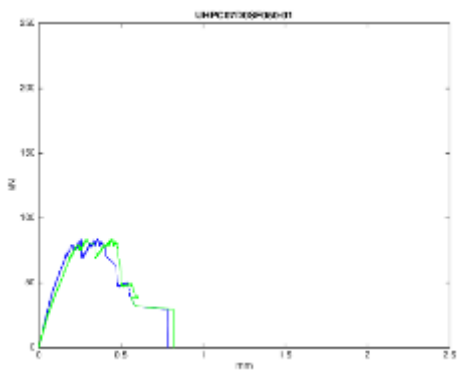

Curing: 7 Days
Steel Fibers: NO / 0%
CNT&GO: 0.08% wt%
Height: 97 mm
Ø: 50 mm

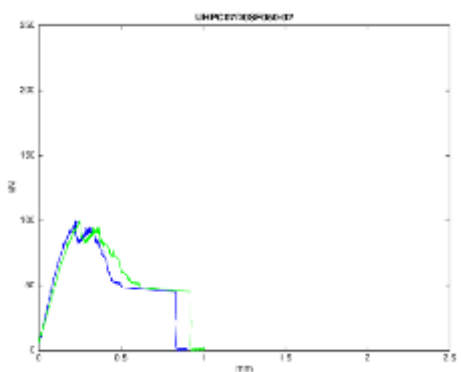



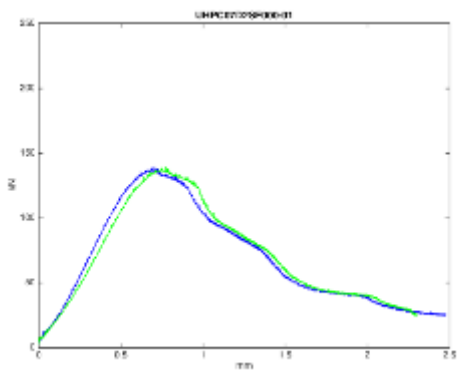

Notes: No important holes or cracks. 2 extensometers.

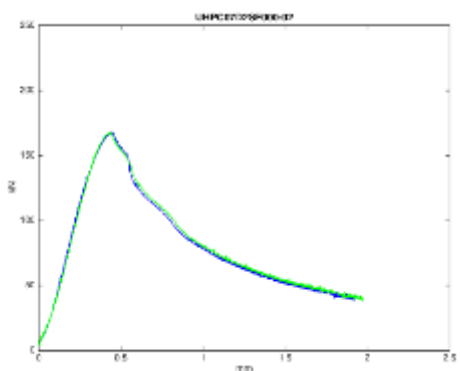

Remarks: Slight settling specimen-plate. After reaching peak strength, extensometers' data not usable.

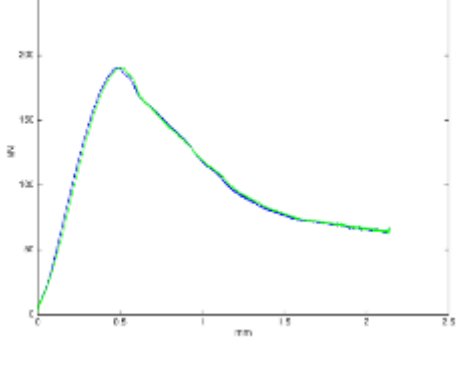



UHPC07D0SF050_01		
<p>Curing: 7 Days Steel Fibers: NO / 0% CNT&GO: 0.50% wt% Height: 97 mm Ø: 50 mm</p>	<p>Notes: No important holes or cracks. 2 extensometers.</p>	<p>Remarks: Initial settling specimen-plate. Sudden loss of loading area at 0.3 mm. Data slightly unpaired between extensometers. After reaching peak strength, extensometers' data not usable.</p>

UHPC07D0SF050_02		
<p>Curing: 7 Days Steel Fibers: NO / 0% CNT&GO: 0.50% wt% Height: 97 mm Ø: 50 mm</p>	<p>Notes: No important holes or cracks. 2 extensometers.</p>	<p>Remarks: Initial settling specimen-plate. Sudden loss of loading area at 0.3 mm. After reaching peak strength, extensometers' data not usable.</p>

UHPC07D2SF000_01		
<p>Curing: 7 Days Steel Fibers: ~2% CNT&GO: NO / 0% Height: 95 mm Ø: 50 mm</p>	<p>Notes: No important holes or cracks. 2 extensometers.</p>	<p>Remarks: Initial settling specimen-plate. Good post-cracking data.</p>

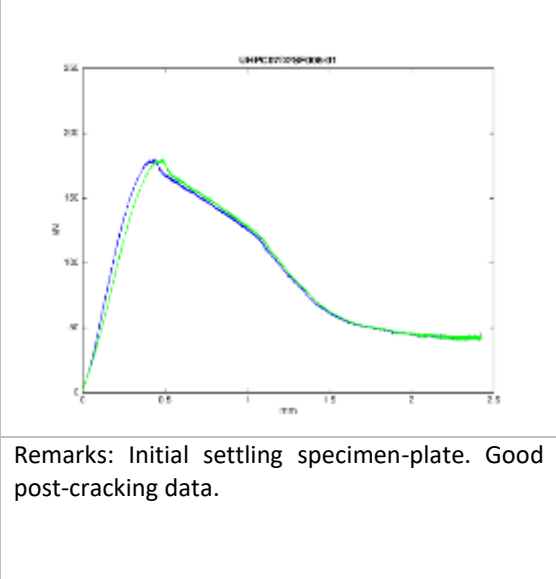
UHPC07D2SF000_02		
<p>Curing: 7 Days Steel Fibers: ~2% CNT&GO: NO / 0% Height: 97 mm Ø: 50 mm</p>	<p>Notes: No important holes or cracks. 2 extensometers.</p>	<p>Remarks: Initial settling specimen-plate. Good post-cracking data.</p>

UHPC07D2SF000_03		
<p>Curing: 7 Days Steel Fibers: ~2% CNT&GO: NO / 0% Height: 97 mm Ø: 50 mm</p>	<p>Notes: No important holes or cracks. 2 extensometers.</p>	<p>Remarks: Initial settling specimen-plate. Good post-cracking data.</p>

UHPC07D2SF008_01

Curing: 7 Days
 Steel Fibers: ~2%
 CNT&GO: 0.08% wt%
 Height: 97 mm
 Ø: 50 mm

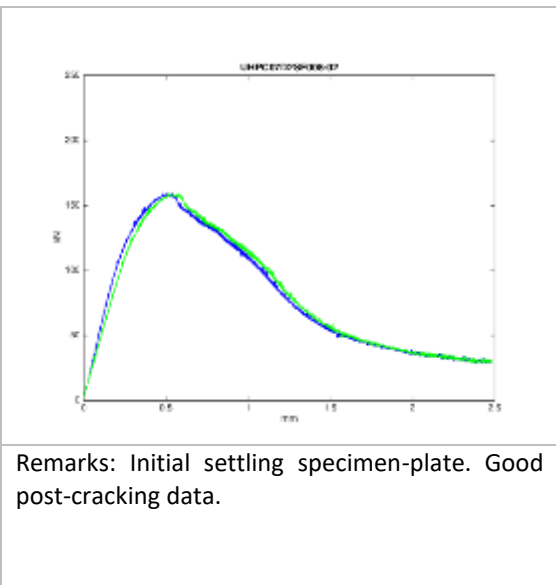
Notes: No important holes or cracks. 2 extensometers.



UHPC07D2SF008_02

Curing: 7 Days
 Steel Fibers: ~2%
 CNT&GO: 0.08% wt%
 Height: 97 mm
 Ø: 50 mm

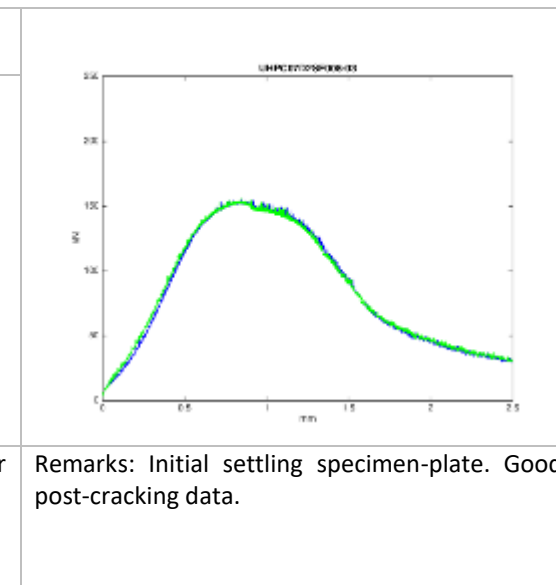
Notes: No important holes or cracks. 2 extensometers.



UHPC07D2SF008_03

Curing: 7 Days
 Steel Fibers: ~2%
 CNT&GO: 0.08% wt%
 Height: 97 mm
 Ø: 50 mm

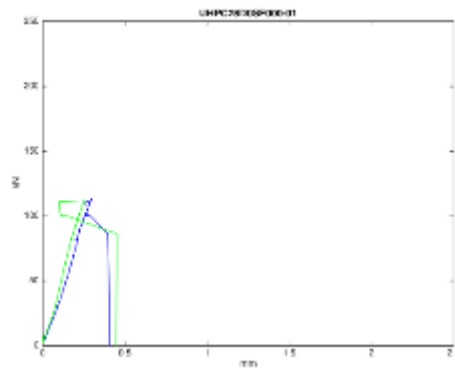
Notes: No important holes or cracks. 2 extensometers.



28 Days

UHPC28D0SF000_01

Curing: 28 Days
 Steel Fibers: NO / 0%
 CNT&GO: NO / 0%
 Height: 97 mm
 Ø: 50 mm

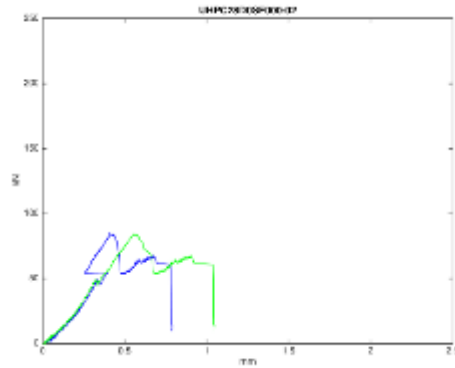


Notes: No important holes or cracks. 2 extensometers.

Remarks: Initial settling specimen-plate. After reaching peak strength, extensometers' data not usable.

**UHPC28D0SF000_02**

Curing: 28 Days
 Steel Fibers: NO / 0%
 CNT&GO: NO / 0%
 Height: 97 mm
 Ø: 50 mm

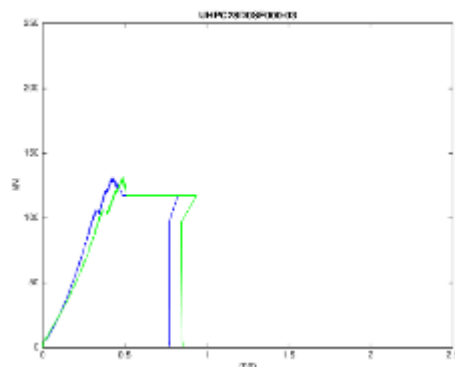


Notes: No important holes or cracks. 2 extensometers.

Remarks: Initial settling specimen-plate. Sudden loss of loading area at 0.6 mm. After reaching peak strength, extensometers' data not usable. "Blue" extensometer unpaired.

**UHPC28D0SF000_03**

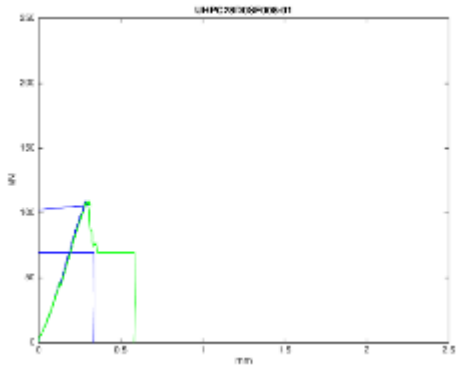

Curing: 28 Days
 Steel Fibers: NO / 0%
 CNT&GO: NO / 0%
 Height: 96 mm
 Ø: 50 mm

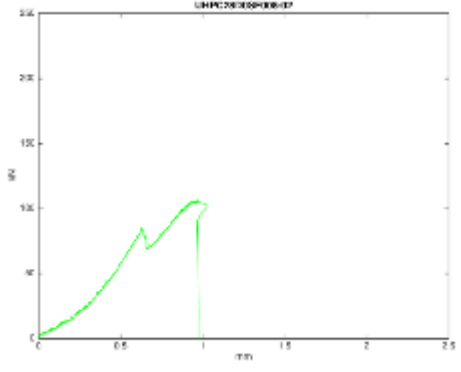



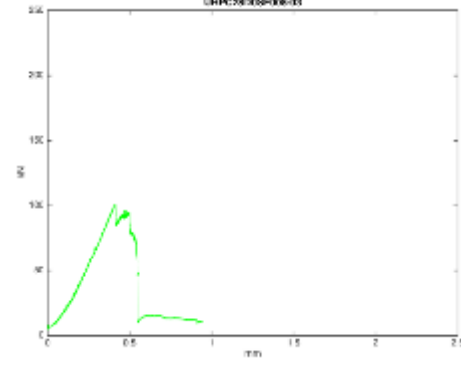

Notes: No important holes or cracks. 2 extensometers.

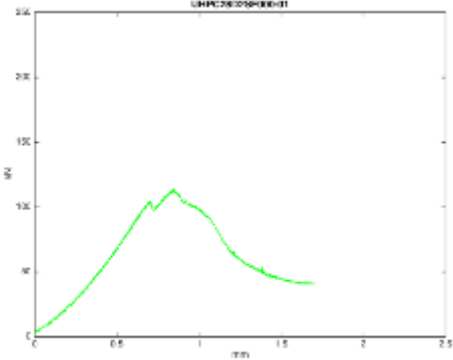

Remarks: Initial settling specimen-plate. Data after the peak very disassociated.



UHPC28D0SF008_01		
<p>Curing: 28 Days Steel Fibers: NO / 0% CNT&GO: 0.08% wt% Height: 97 mm \varnothing: 50 mm</p>		
<p>Notes: No important holes or cracks. 2 extensometers.</p>	<p>Remarks: Initial settling specimen-plate. After reaching peak strength, extensometers' data not usable.</p>	

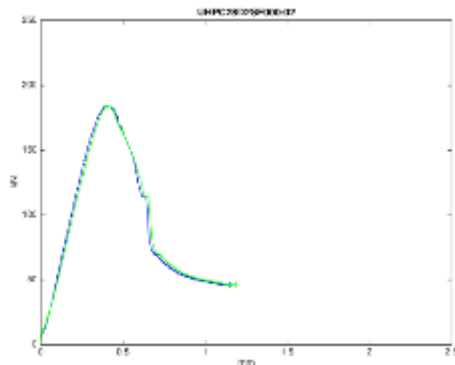
UHPC28D0SF008_02		
<p>Curing: 28 Days Steel Fibers: NO / 0% CNT&GO: 0.08% wt% Height: 97 mm \varnothing: 50 mm</p>		
<p>Notes: No important holes or cracks. 1 extensometer.</p>	<p>Remarks: Initial settling specimen-plate. Sudden loss of loading area at 0.6 mm. After reaching peak strength, extensometers' data not usable.</p>	

UHPC28D0SF008_03		
<p>Curing: 28 Days Steel Fibers: NO / 0% CNT&GO: 0.08% wt% Height: 97 mm \varnothing: 50 mm</p>		
<p>Notes: No important holes or cracks. 1 extensometer.</p>	<p>Remarks: Slight settling specimen-plate. Sudden loss of loading area at 0.4 mm. After reaching peak strength, extensometers' data not usable.</p>	

UHPC28D2SF000_01		
<p>Curing: 28 Days Steel Fibers: ~2% CNT&GO: NO / 0% Height: 96.5 mm Ø: 50 mm</p>		
<p>Notes: Small holes, no cracks. Defect on one edge of one face. 1 extensometer.</p>	<p>Remarks: Initial settling specimen-plate. Sudden loss of loading area at 0.75 mm. Good post-cracking data.</p>	

UHPC28D2SF000_02

Curing: 28 Days
Steel Fibers: ~2%
CNT&GO: NO / 0%
Height: 96 mm
Ø: 50 mm



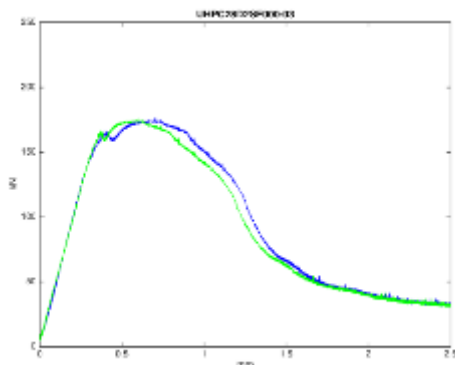
Notes: No important holes or cracks. 2 extensometers.

Remarks: Initial settling specimen-plate. Good post-cracking data.



UHPC28D2SF000_03


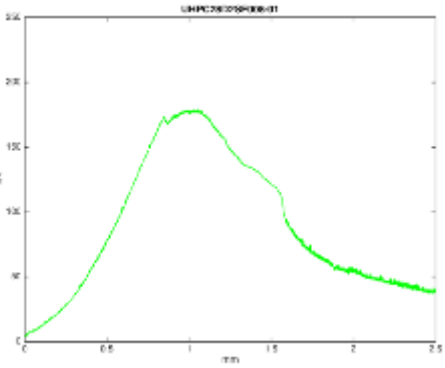
Curing: 28 Days
Steel Fibers: ~2%
CNT&GO: NO / 0%
Height: 95.5 mm
Ø: 50 mm


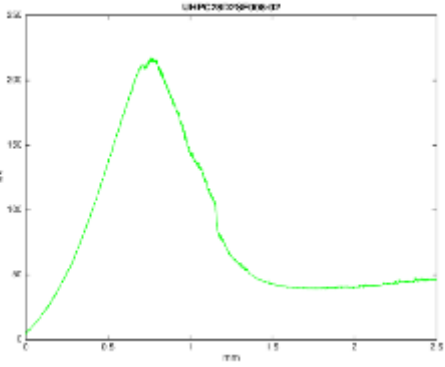



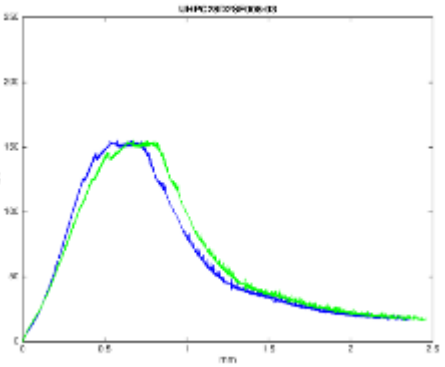
Notes: No important holes or cracks. Faces needed to be polished thoroughly. 2 extensometers.

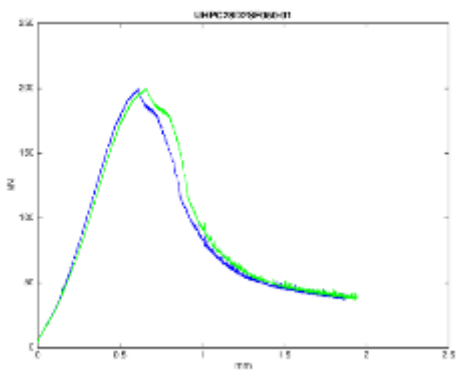

Remarks: Initial settling specimen-plate. Sudden loss of loading area at 0.45 mm. Extensometers slightly unpaired afterwards. Good post-cracking data.

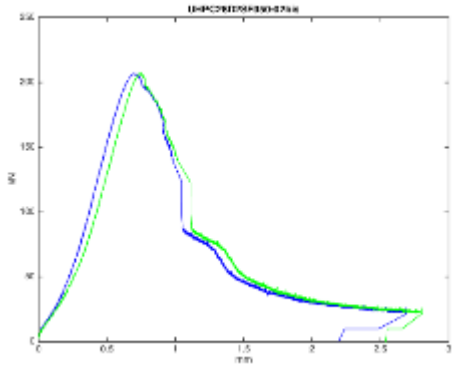



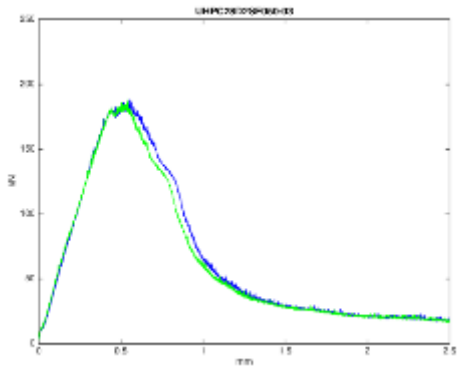

UHPC28D2SF008_01		
Curing: 28 Days Steel Fibers: ~2% CNT&GO: 0.08% wt% Height: 96.5 mm \varnothing : 50 mm		
Notes: No important holes or cracks. 1 extensometer.	Remarks: Initial settling specimen-plate. Sudden loss of loading area at 0.8 mm. Good post-cracking data.	

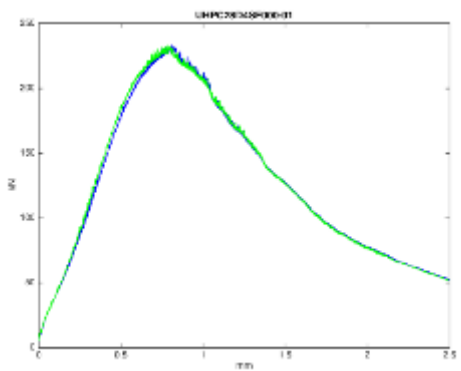

UHPC28D2SF008_02		
Curing: 28 Days Steel Fibers: ~2% CNT&GO: 0.08% wt% Height: 97.5 mm \varnothing : 50 mm		
Notes: Medium hole on one face' edge of 0.7 mm, no cracks. 1 extensometer.	Remarks: Important initial settling specimen-plate. Sudden loss of loading area at 0.75 mm. Good post-cracking data.	

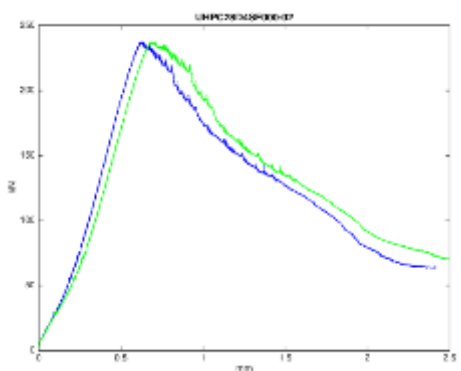

UHPC28D2SF008_03		
Curing: 28 Days Steel Fibers: ~2% CNT&GO: 0.08% wt% Height: 96.5 mm \varnothing : 50 mm		
Notes: : Medium hole on one face of 0.7 mm diameter, no cracks. 2 extensometers.	Remarks: Initial settling specimen-plate. Good post-cracking data. Sudden loss of loading area at 0.5 mm.	

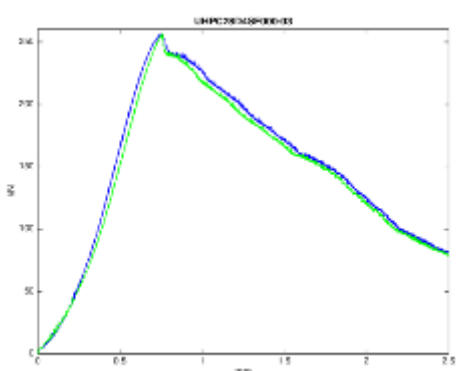

UHPC28D2SF050_01		
<p>Curing: 28 Days Steel Fibers: ~2% CNT&GO: 0.08% wt% Height: 97 mm Ø: 50 mm</p>	<p>Notes: Two big holes, no cracks. 2 extensometers.</p>	<p>Remarks: Initial settling specimen-plate. Good post-cracking data.</p>

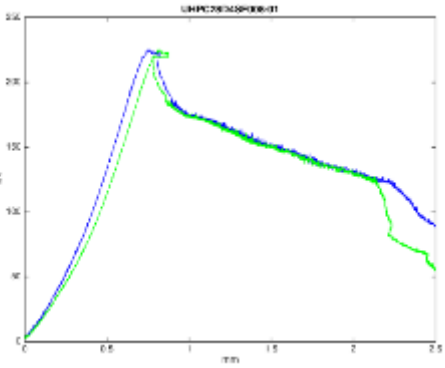

UHPC28D2SF050_02		
<p>Curing: 28 Days Steel Fibers: ~2% CNT&GO: 0.08% wt% Height: 96.7 mm Ø: 50 mm</p>	<p>Notes: Big holes of more than 1 cm, no cracks. 2 extensometers.</p>	<p>Remarks: Initial settling specimen-plate. Good post-cracking data.</p>

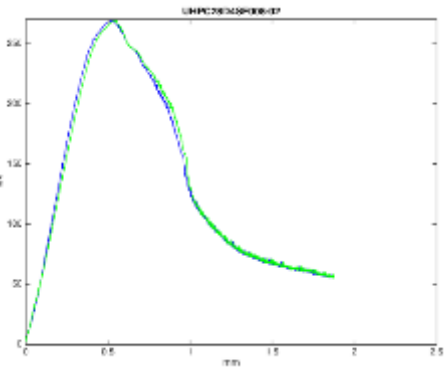

UHPC28D2SF050_03		
<p>Curing: 28 Days Steel Fibers: ~2% CNT&GO: 0.08% wt% Height: 96.9 mm Ø: 50 mm</p>	<p>Notes: Big holes of more than 1 cm, no cracks. 2 extensometers.</p>	<p>Remarks: Initial settling specimen-plate. Sudden loss of strength at 0.45 mm. Good post-cracking data.</p>

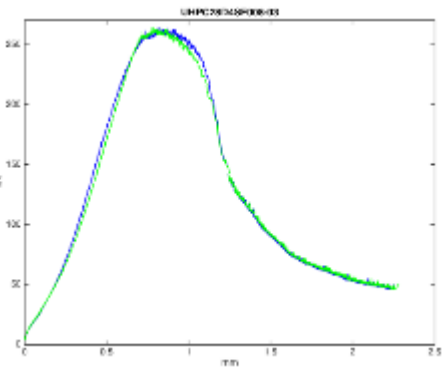

UHPC28D4SF000_01		
<p>Curing: 28 Days Steel Fibers: 4% CNT&GO: NO / 0% Height: 96.7 mm Ø: 50 mm</p>	<p>Notes: Big holes of more than 2 cm, no cracks. 2 extensometers.</p>	<p>Remarks: Initial settling specimen-plate. Good post-cracking data.</p>

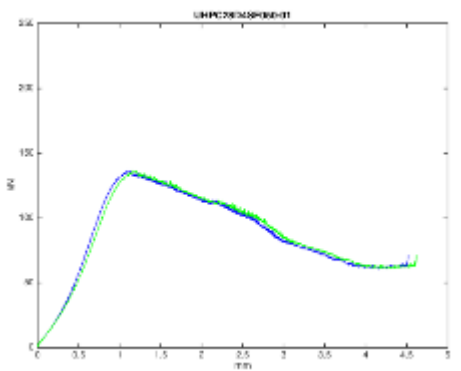

UHPC28D4SF000_02		
<p>Curing: 28 Days Steel Fibers: 4% CNT&GO: NO / 0% Height: 95.7 mm Ø: 50 mm</p>	<p>Notes: Big holes, no cracks. 2 extensometers.</p>	<p>Remarks: Initial settling specimen-plate. Good post-cracking data. Extensometers slightly unpaired.</p>

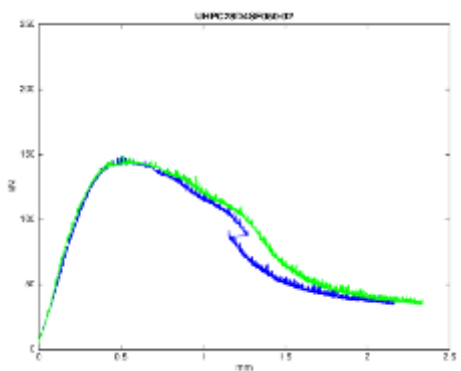

UHPC28D4SF000_03		
<p>Curing: 28 Days Steel Fibers: 4% CNT&GO: NO / 0% Height: 95.2 mm Ø: 50 mm</p>	<p>Notes: Big holes and notches, no cracks. 2 extensometers.</p>	<p>Remarks: Initial settling specimen-plate. Good post-cracking data.</p>

UHPC28D4SF008_01		
<p>Curing: 28 Days Steel Fibers: 4% CNT&GO: 0.08% wt% Height: 95.9 mm Ø: 50 mm</p>	<p>Notes: Holes, notches and cracks. 2 extensometers.</p>	<p>Remarks: Initial settling specimen-plate. Disruptions at peak strength / 0.8 mm. Good post-cracking data until 2.2 mm.</p>

UHPC28D4SF008_02		
<p>Curing: 28 Days Steel Fibers: 4% CNT&GO: 0.08% wt% Height: 97.2 mm Ø: 50 mm</p>	<p>Notes: Holes, notches and cracks. 2 extensometers.</p>	<p>Remarks: Initial settling specimen-plate. Good post-cracking data.</p>

UHPC28D4SF008_03		
<p>Curing: 28 Days Steel Fibers: 4% CNT&GO: 0.08% wt% Height: 96.5 mm Ø: 50 mm</p>	<p>Notes: Holes, notches and large cracks. 2 extensometers.</p>	<p>Remarks: Initial settling specimen-plate. Good post-cracking data.</p>

UHPC28D4SF050_01		
<p>Curing: 28 Days Steel Fibers: 4% CNT&GO: 0.08% wt% Height: 96.6 mm Ø: 50 mm</p>	<p>Notes: Holes, notches and large cracks. 2 extensometers.</p>	<p>Remarks: Initial settling specimen-plate. Good post-cracking data.</p>

UHPC28D4SF050_02		
<p>Curing: 28 Days Steel Fibers: 4% CNT&GO: 0.08% wt% Height: 94.7 mm Ø: 50 mm</p>	<p>Notes: Big holes, no cracks. 2 extensometers.</p>	<p>Remarks: Initial settling specimen-plate. Post-cracking data for "blue" extensometer disassociated.</p>

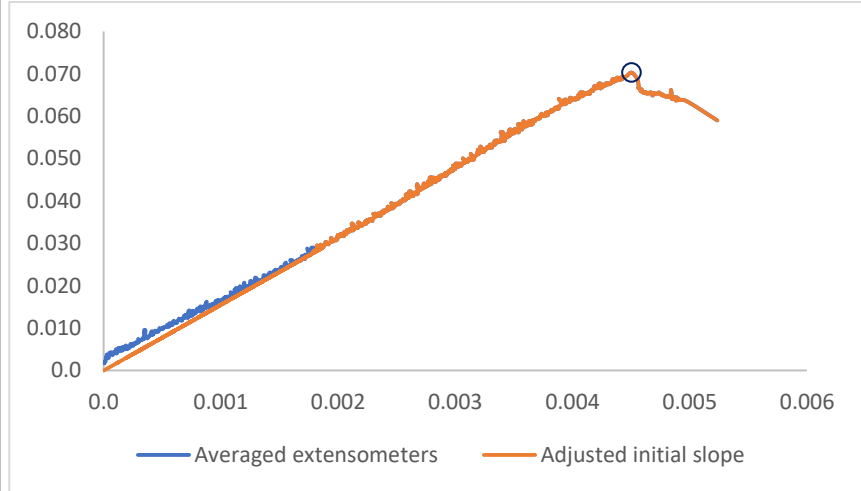
Annex 2 Pretreated data

7 DAYS

Pretreated data

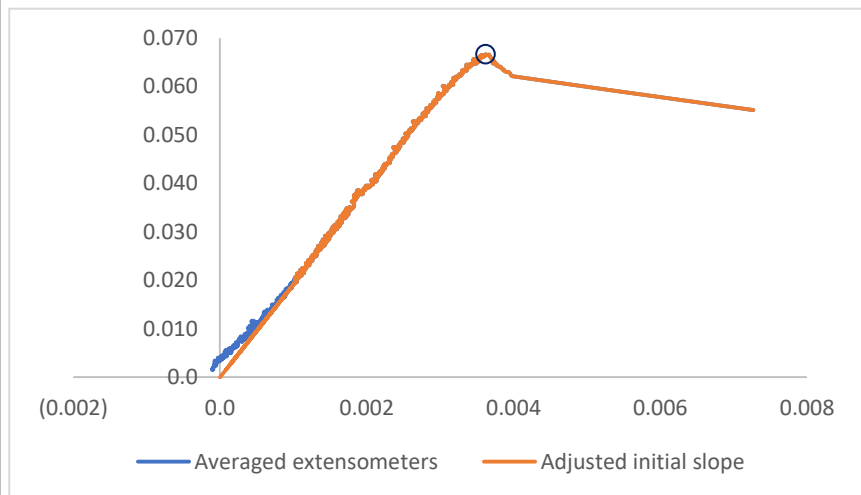
UHPC07D0SF000_1

f_c	70.3 Mpa
ε_c	0.0045
E_c	15.5 Gpa



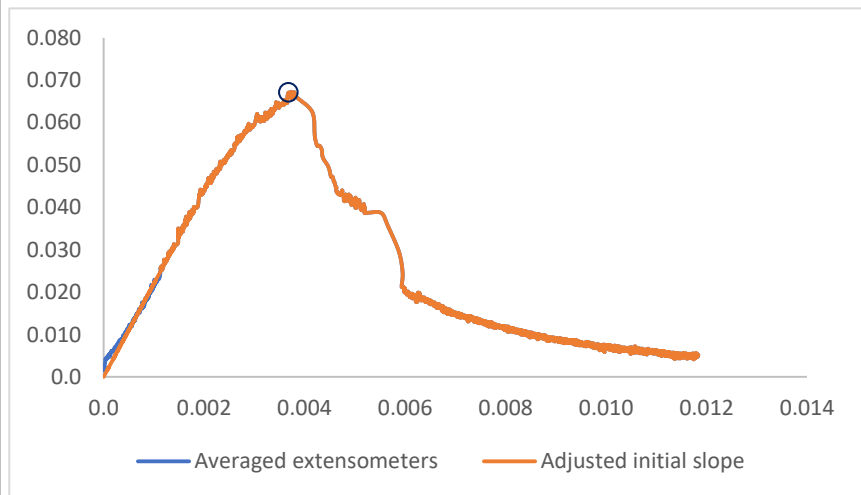
UHPC07D0SF000_2

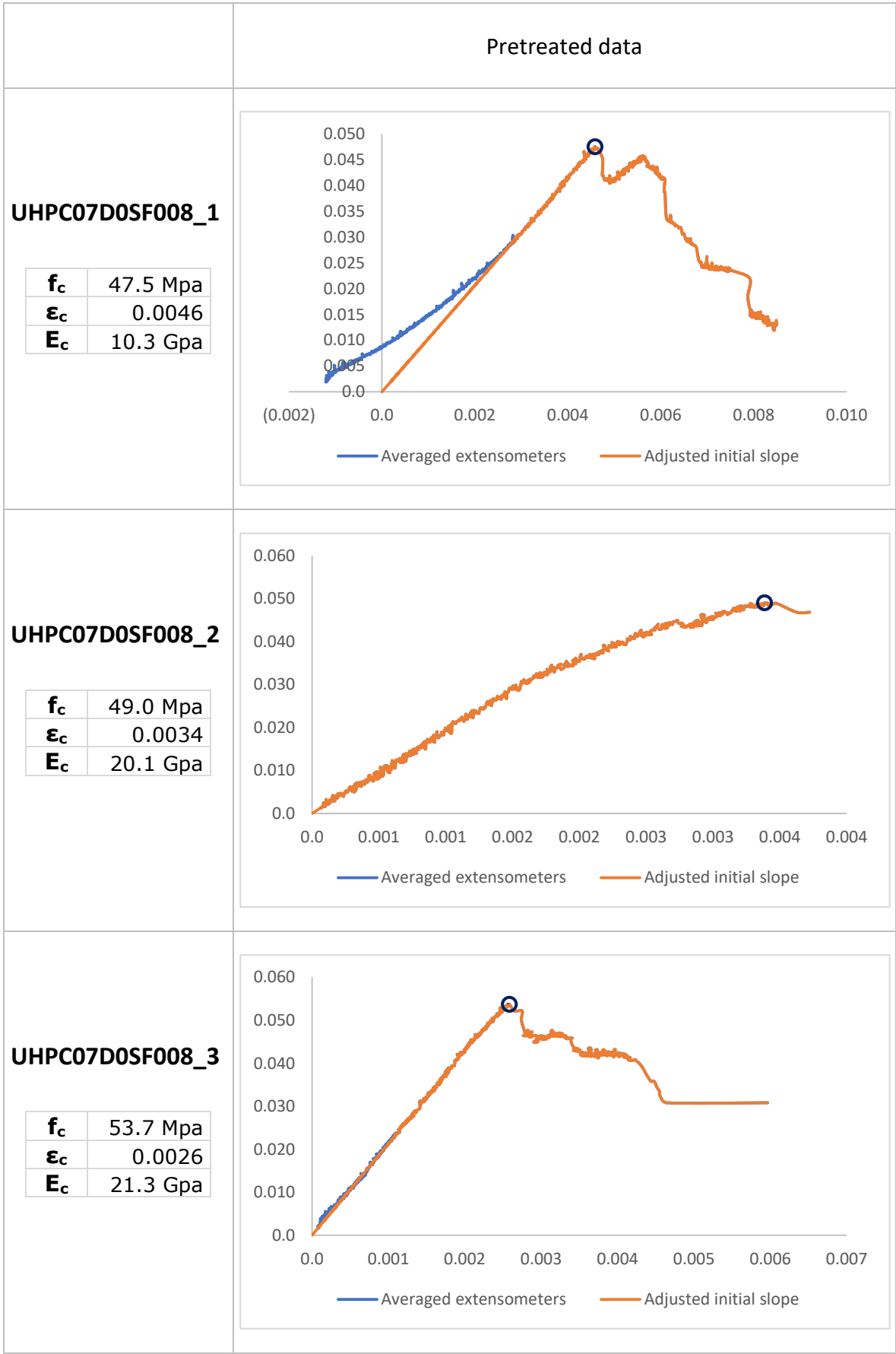
f_c	66.6 Mpa
ε_c	0.0036
E_c	19.1 Gpa

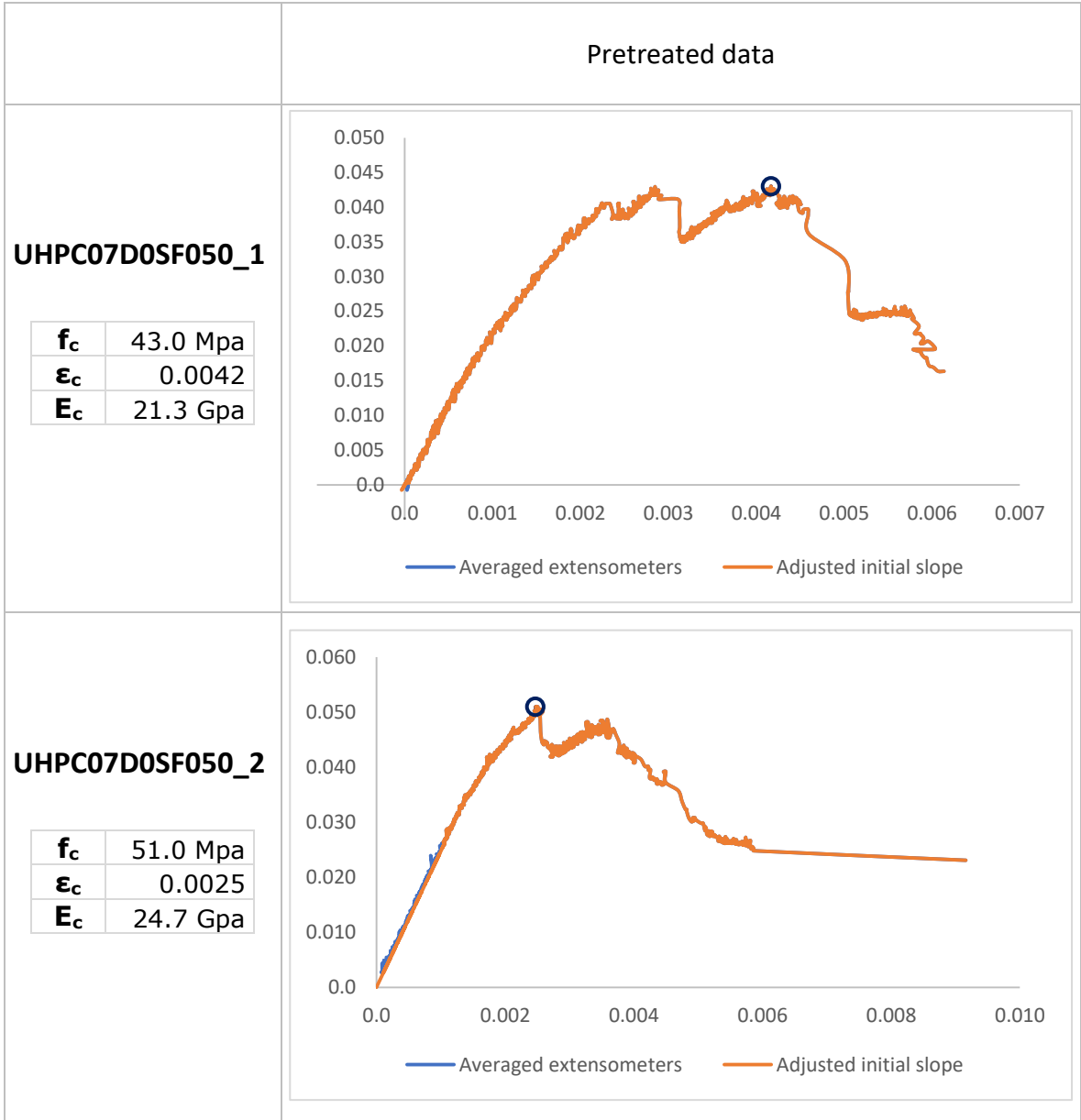


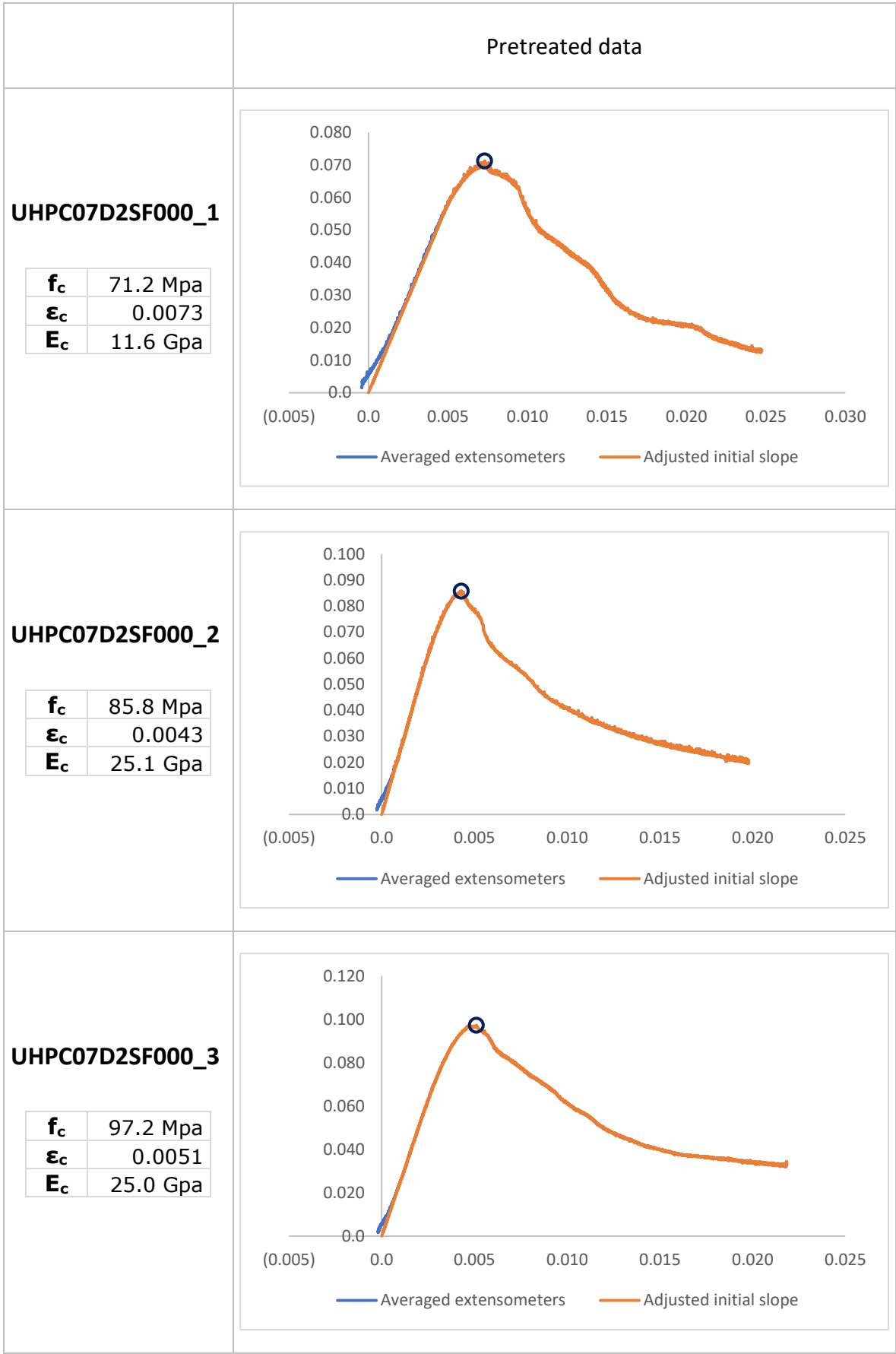
UHPC07D0SF000_3

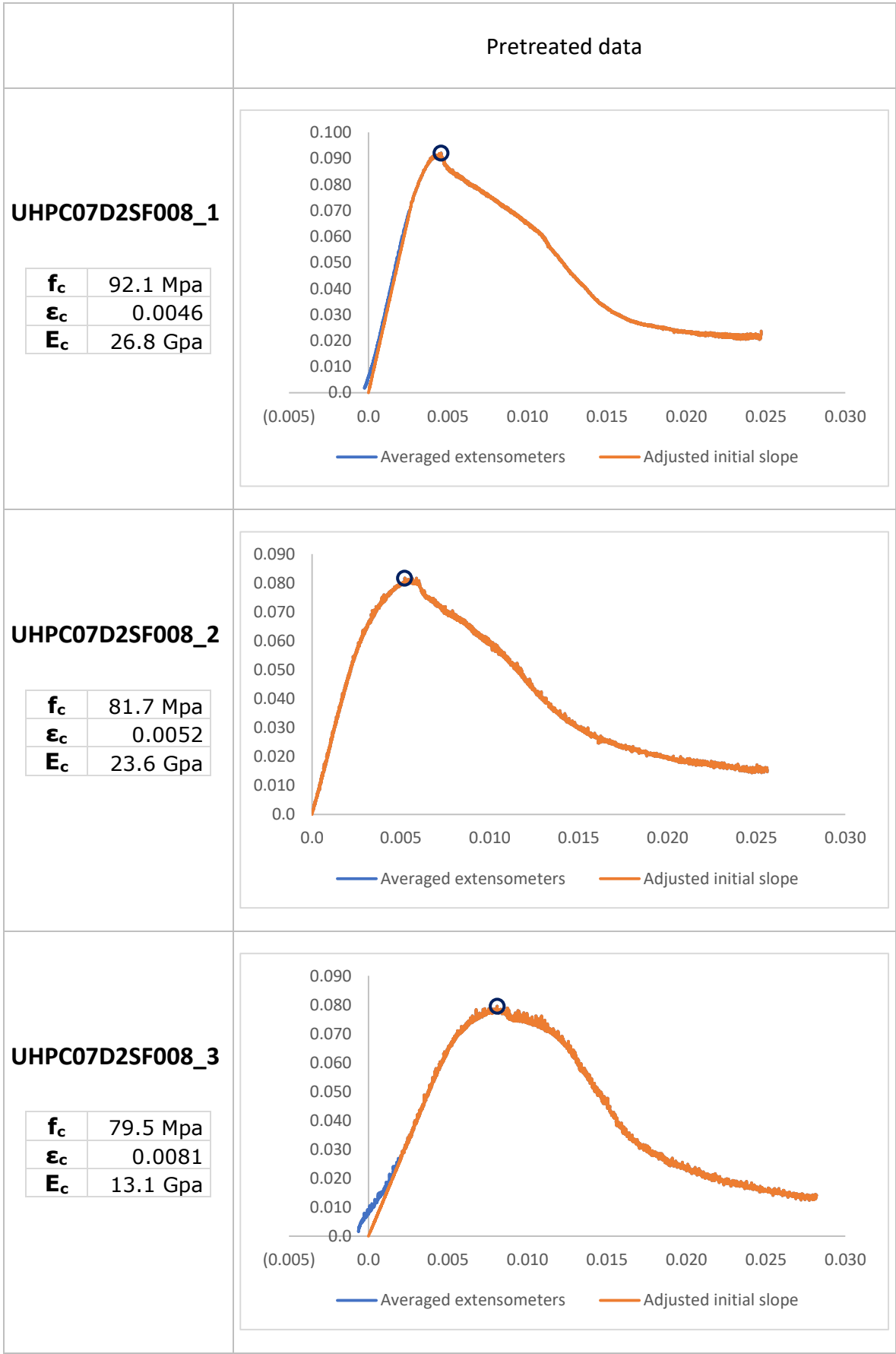
f_c	67.3 Mpa
ε_c	0.0037
E_c	22.0 Gpa









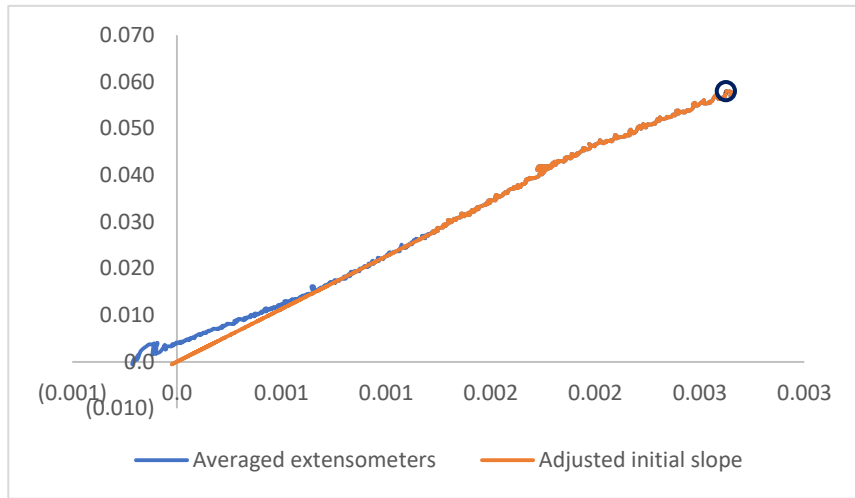


28 DAYS

Pretreated data

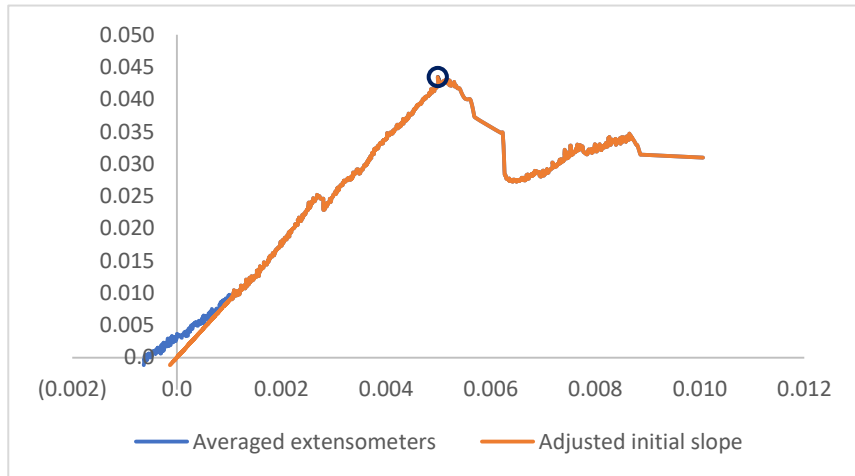
UHPC28D0SF000_1

f_c	58.0 Mpa
ε_c	0.0026
E_c	22.6 Gpa



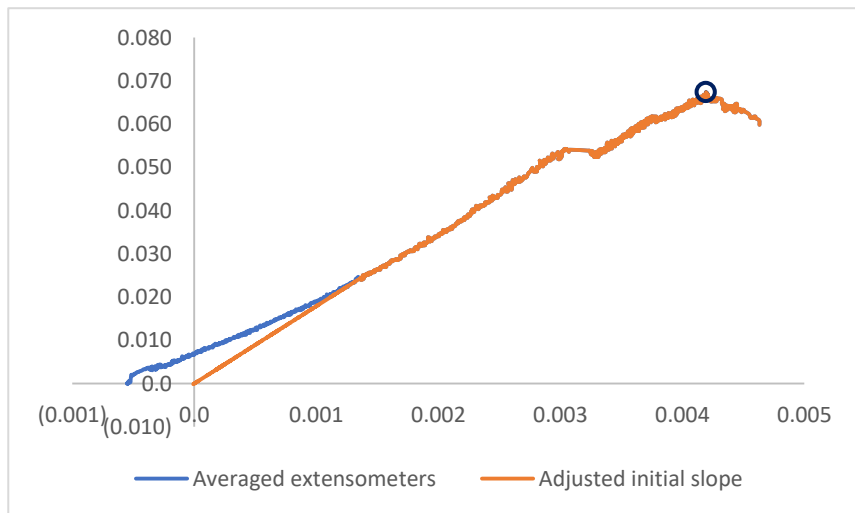
UHPC28D0SF000_2

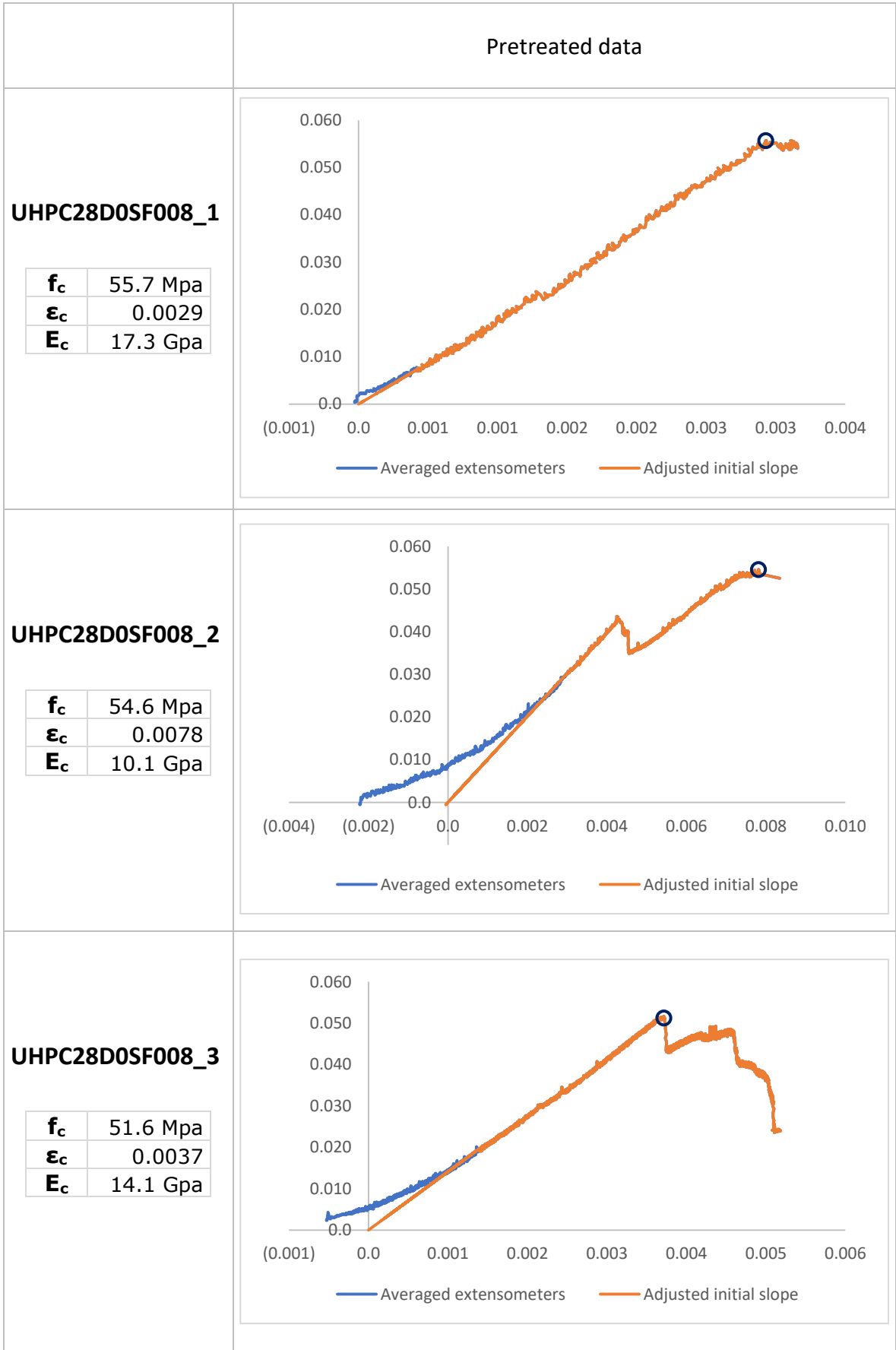
f_c	43.5 Mpa
ε_c	0.0050
E_c	8.8 Gpa



UHPC28D0SF000_3

f_c	67.4 Mpa
ε_c	0.0042
E_c	17.9 Gpa

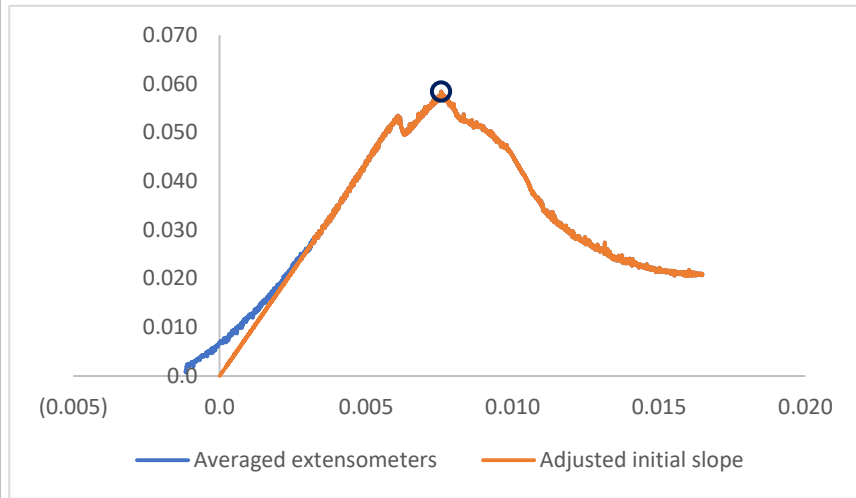




Pretreated data

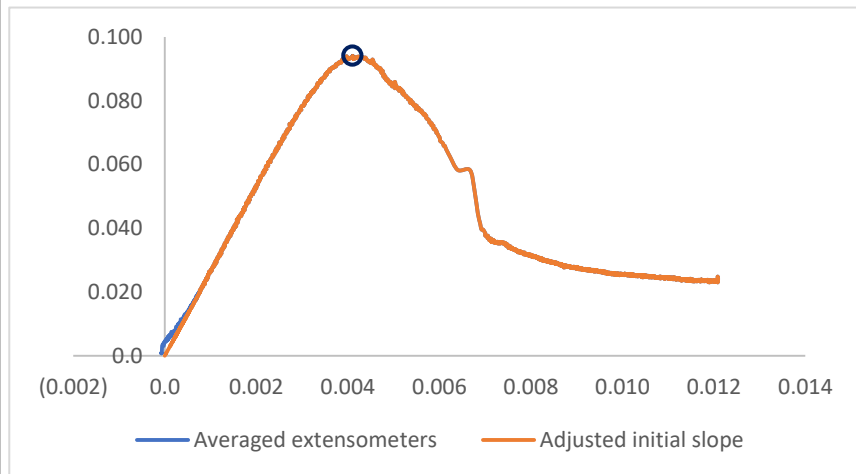
UHPC28D2SF000_1

f_c	58.4 Mpa
ε_c	0.0076
E_c	8.6 Gpa



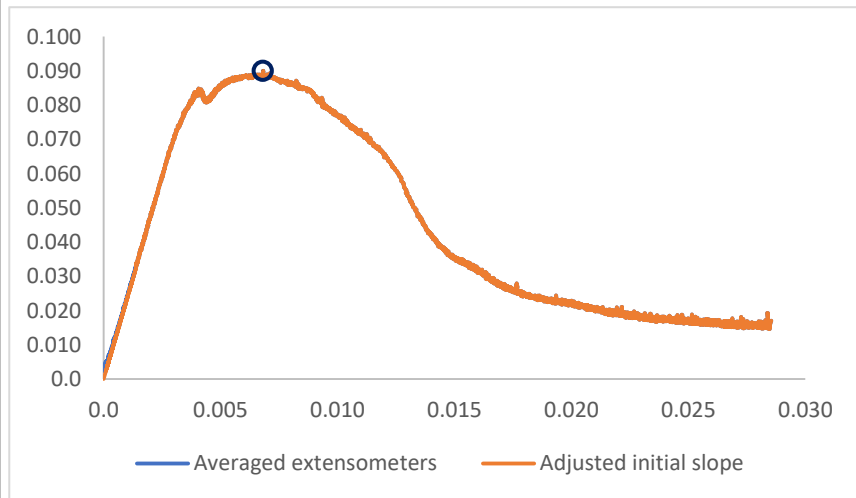
UHPC28D2SF000_2

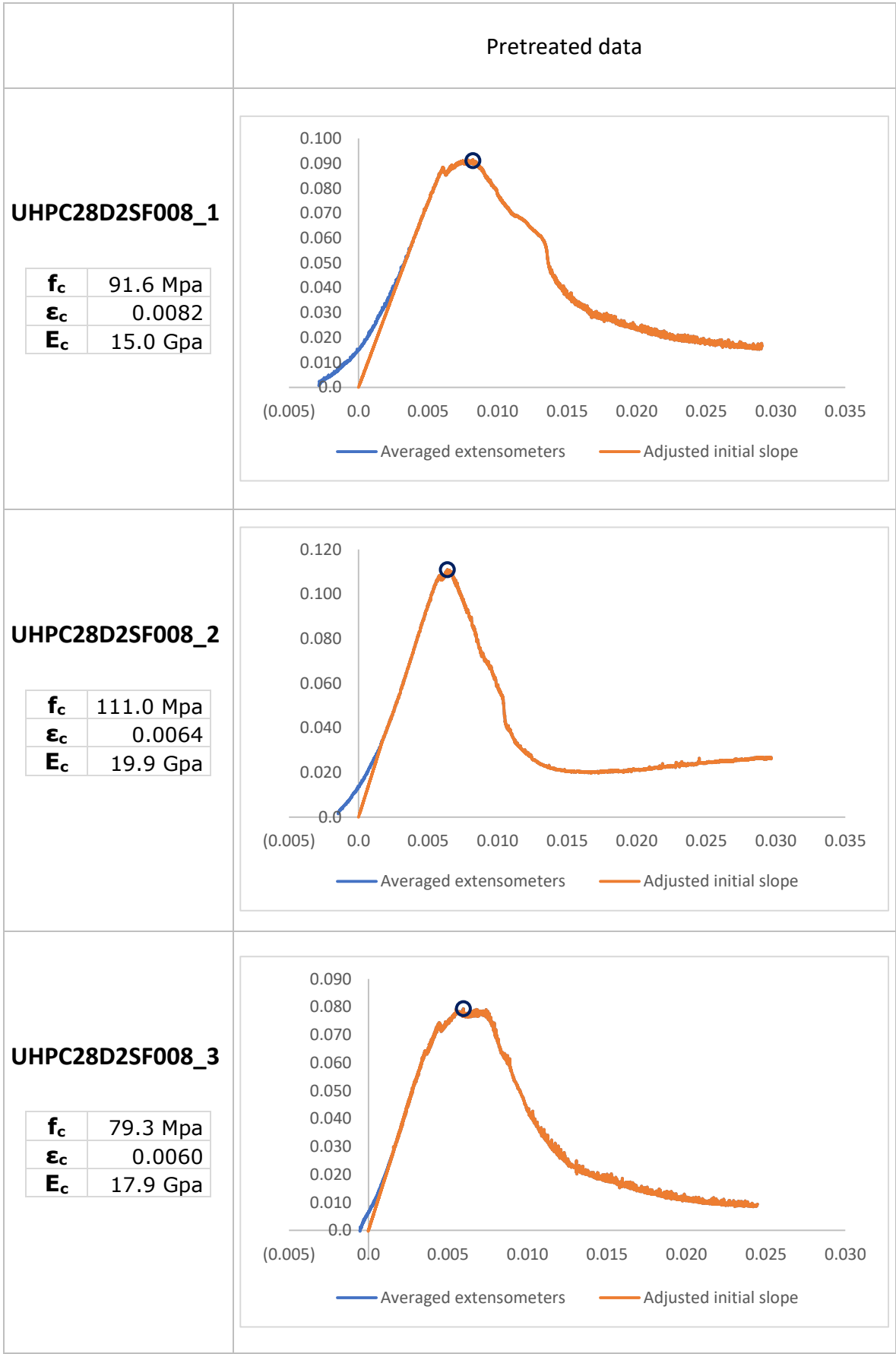
f_c	94.1 Mpa
ε_c	0.0041
E_c	25.9 Gpa

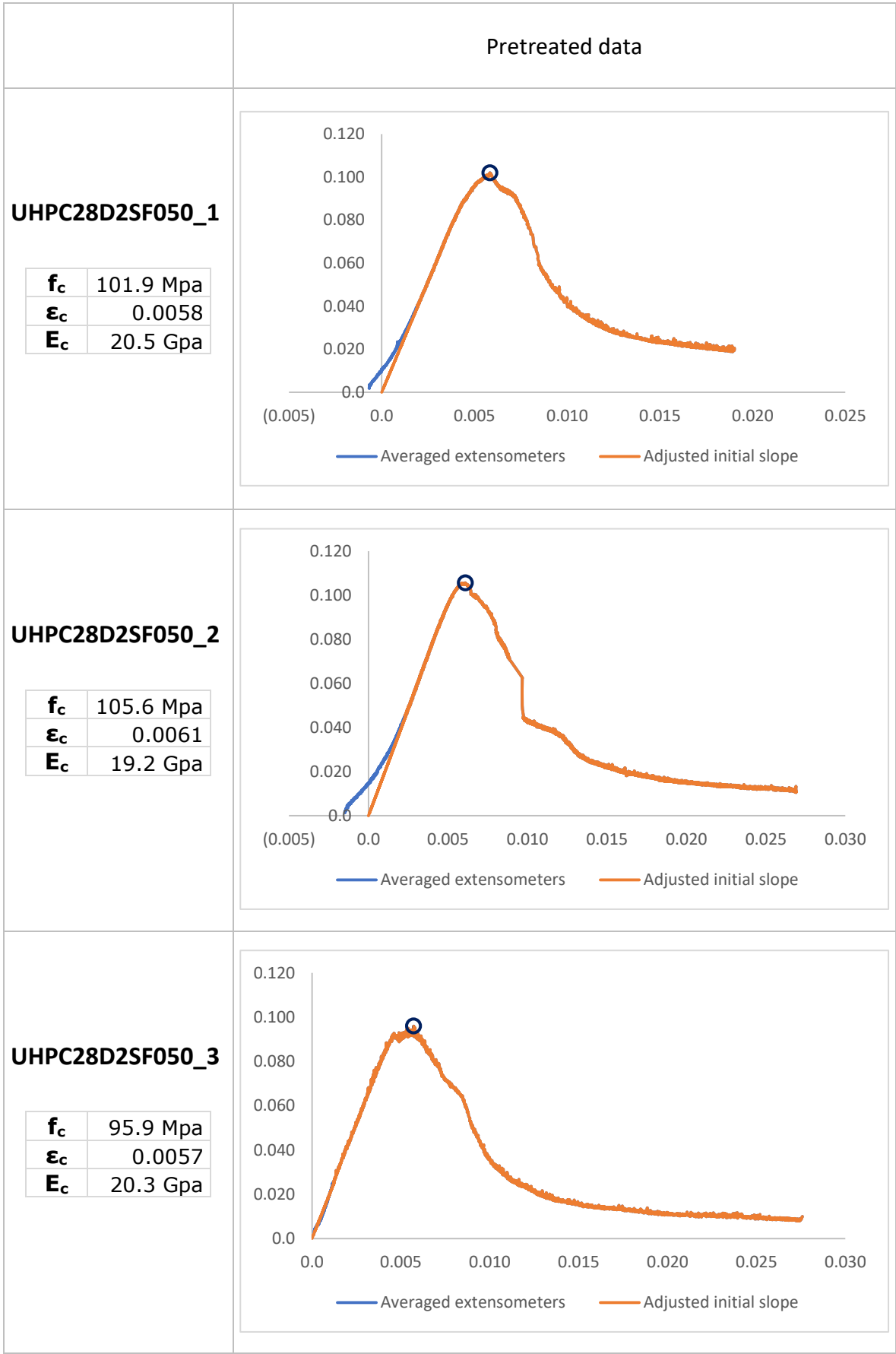


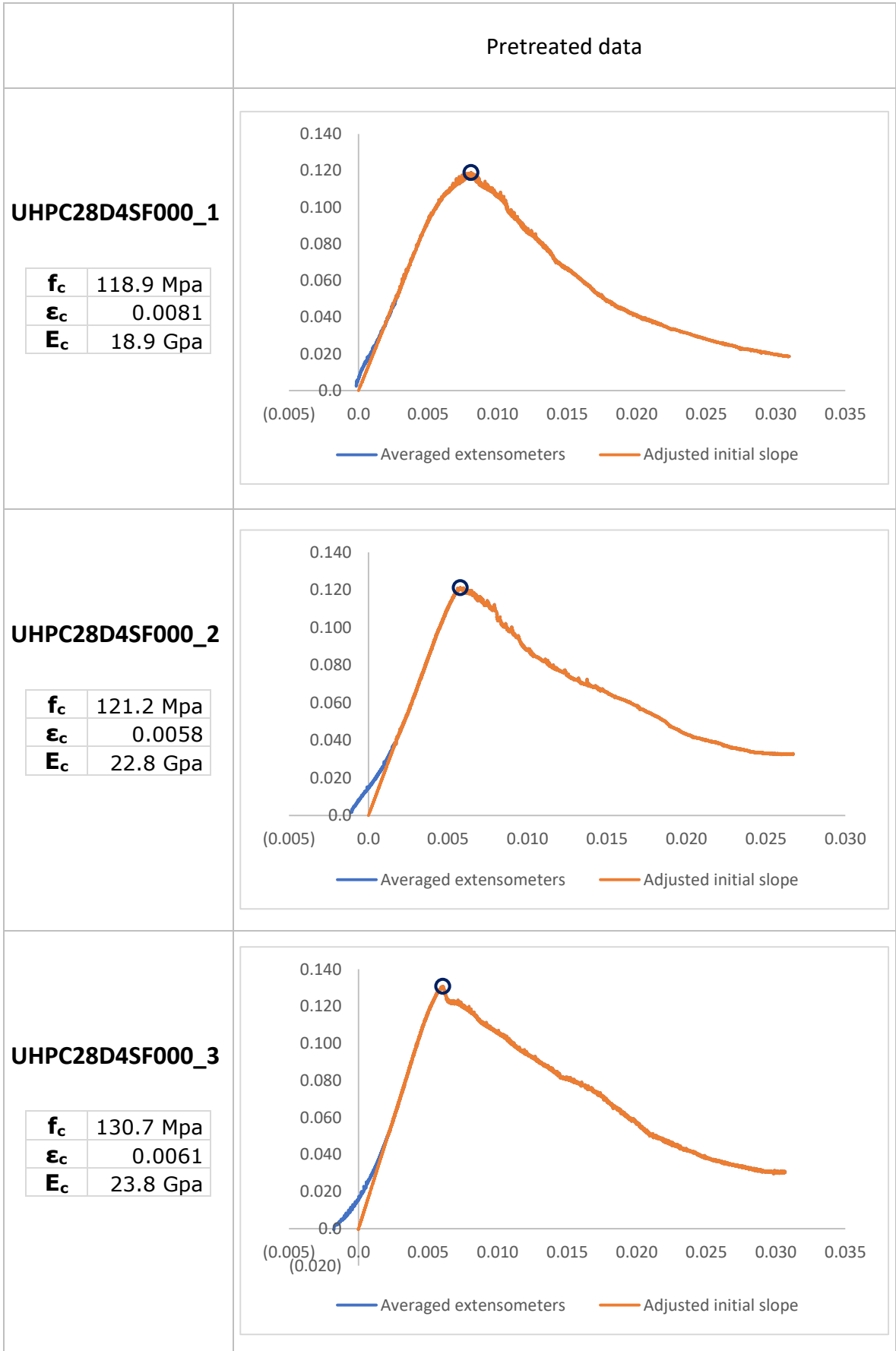
UHPC28D2SF000_3

f_c	89.9 Mpa
ε_c	0.0068
E_c	23.3 Gpa





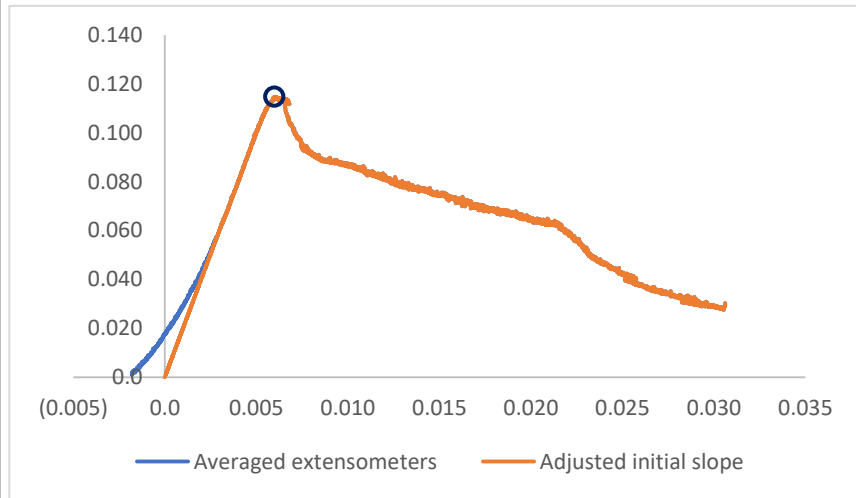




Pretreated data

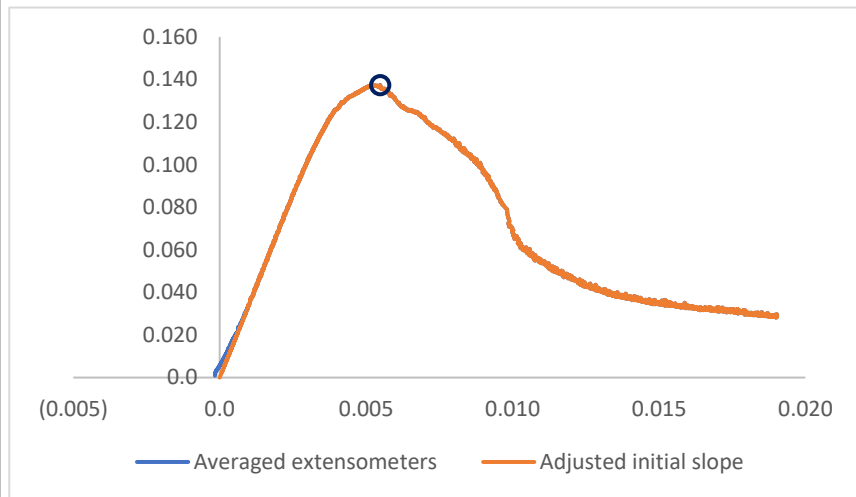
UHPC28D4SF008_1

f_c	114.8 Mpa
ε_c	0.0060
E_c	20.1 Gpa



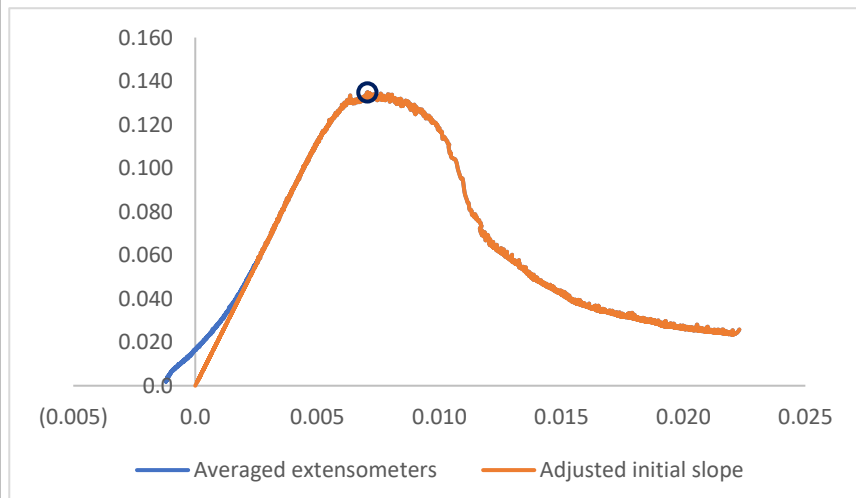
UHPC28D4SF008_2

f_c	137.3 Mpa
ε_c	0.0055
E_c	33.9 Gpa



UHPC28D4SF008_3

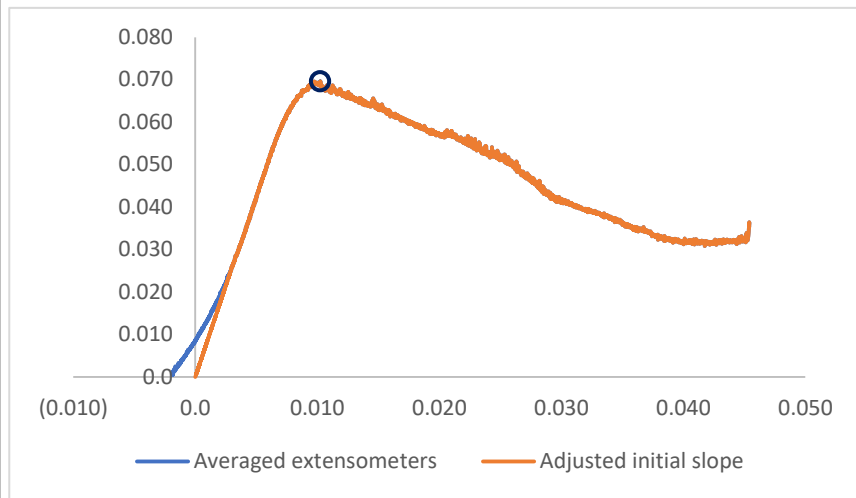
f_c	134.8 Mpa
ε_c	0.0071
E_c	22.3 Gpa



Pretreated data

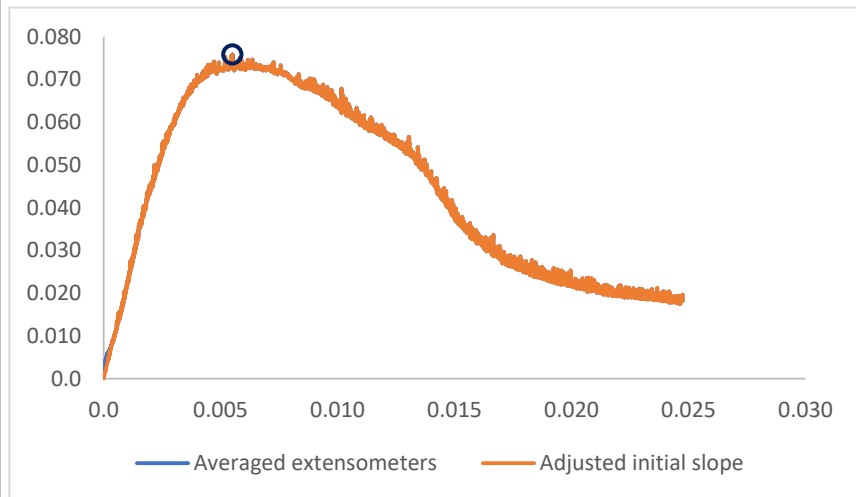
UHPC28D4SF050_1

f_c	69.6 Mpa
ε_c	0.0102
E_c	8.6 Gpa



UHPC28D4SF050_2

f_c	75.9 Mpa
ε_c	0.0055
E_c	22.9 Gpa



Annex 3 Parameters resulting from the experimental data

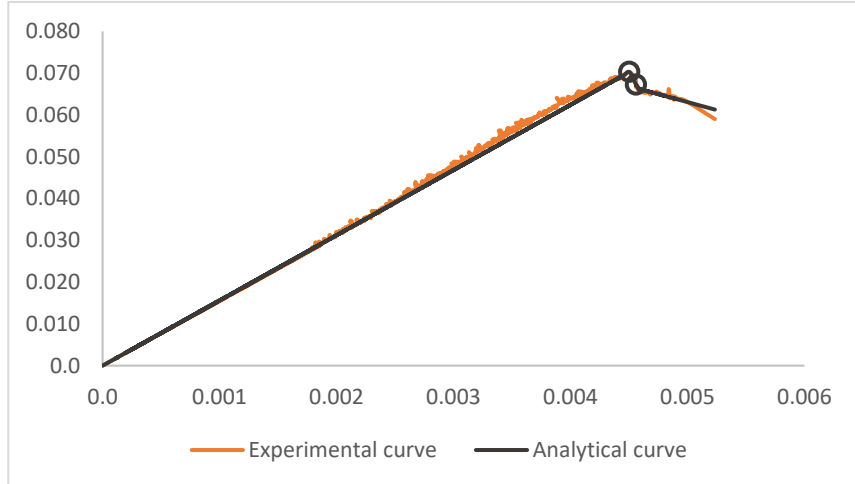
7 DAYS

Parameters resulting from the experimental data

UHPC07D0SF000_1

f_c	70.3 Mpa
ε_c	0.0045
E_c	15.5 Gpa
σ₂	0.944 · f _c
ε₂	1.016 · ε _c
σ₃	0 MPa
ε₃	2.944 · ε _c

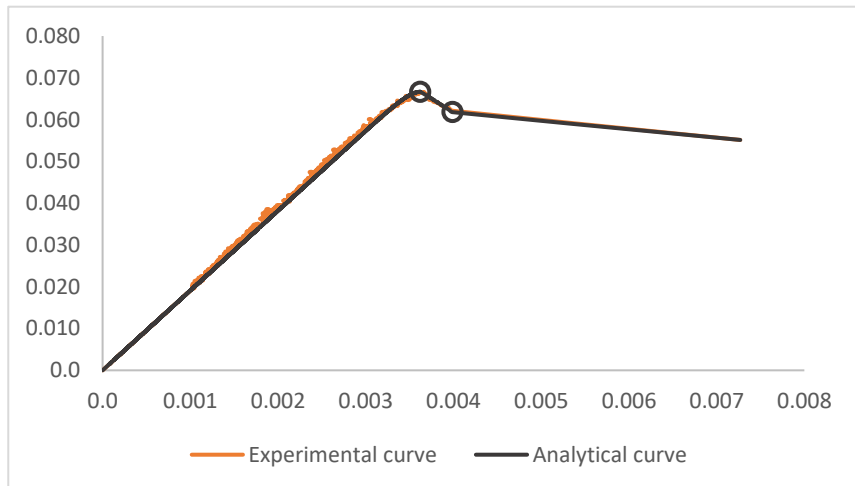
R²	0.9993
----------------------	--------



UHPC07D0SF000_2

f_c	66.6 Mpa
ε_c	0.0036
E_c	19.1 Gpa
σ₂	0.920 · f _c
ε₂	1.111 · ε _c
σ₃	0 MPa
ε₃	10.000 · ε _c

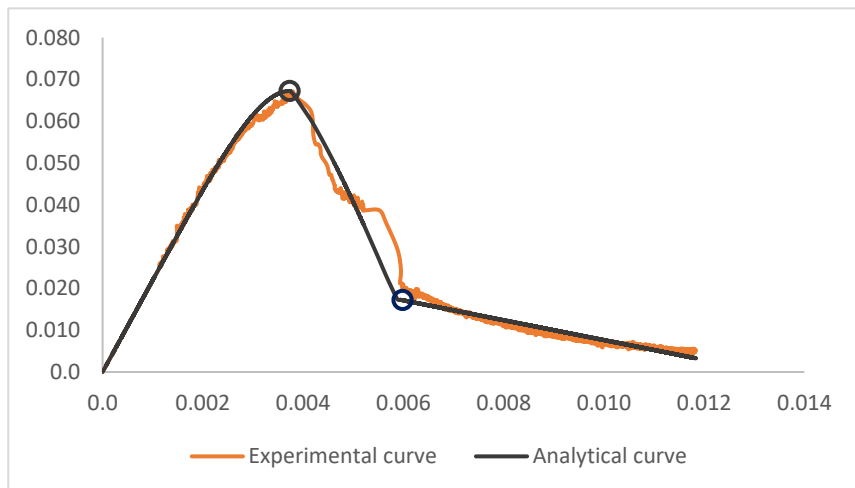
R²	0.9992
----------------------	--------



UHPC07D0SF000_3

f_c	67.3 Mpa
ε_c	0.0037
E_c	22.0 Gpa
σ₂	0.260 · f _c
ε₂	1.567 · ε _c
σ₃	0 MPa
ε₃	3.539 · ε _c

R²	0.9952
----------------------	--------

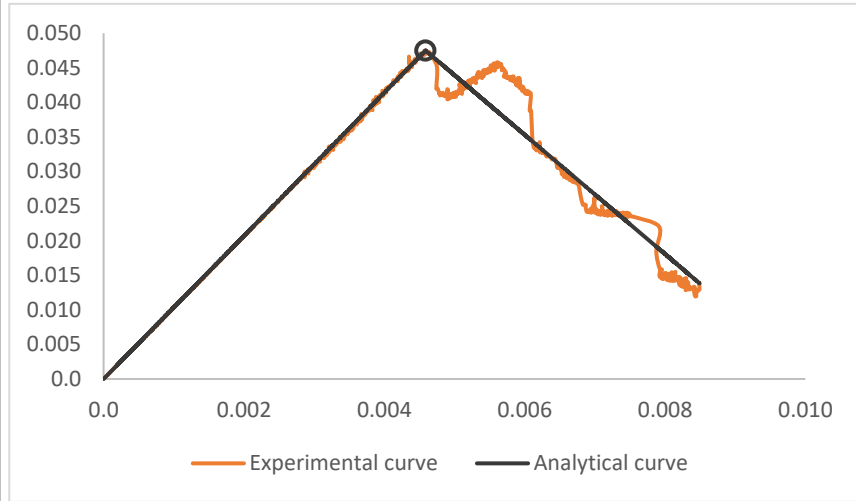


Parameters resulting from the experimental data

UHPC07D0SF008_1

f_c	47.5 Mpa
ε_c	0.0046
E_c	10.3 Gpa
σ₂	0.290 · f _c
ε₂	1.852 · ε _c
σ₃	0 MPa
ε₃	3.693 · ε _c

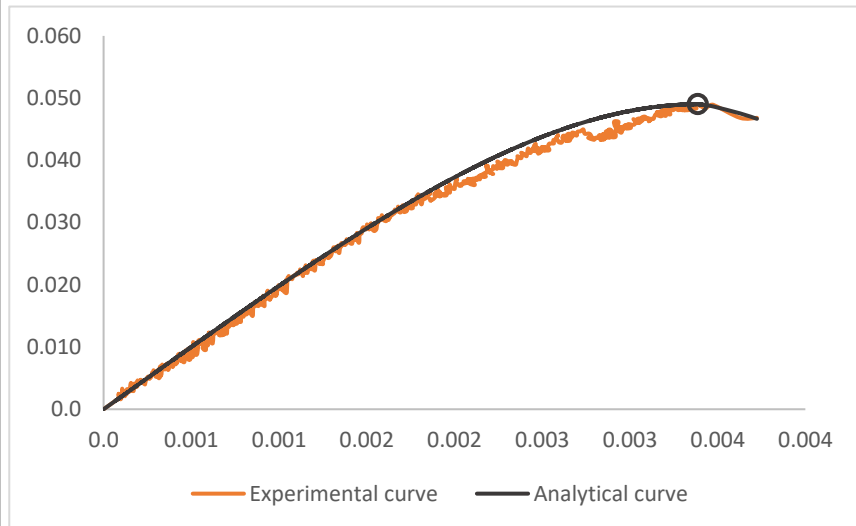
R²	0.9772
----------------------	--------



UHPC07D0SF008_2

f_c	49.0 Mpa
ε_c	0.0034
E_c	20.1 Gpa
σ₂	0.259 · f _c
ε₂	1.716 · ε _c
σ₃	0 MPa
ε₃	3.693 · ε _c

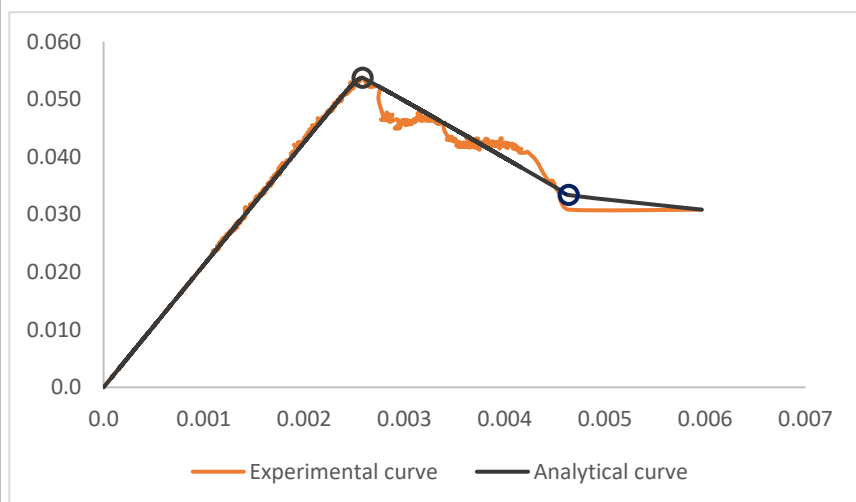
R²	0.9976
----------------------	--------



UHPC07D0SF008_3

f_c	53.7 Mpa
ε_c	0.0026
E_c	21.3 Gpa
σ₂	0.611 · f _c
ε₂	1.817 · ε _c
σ₃	0 MPa
ε₃	10.000 · ε _c

R²	0.9927
----------------------	--------

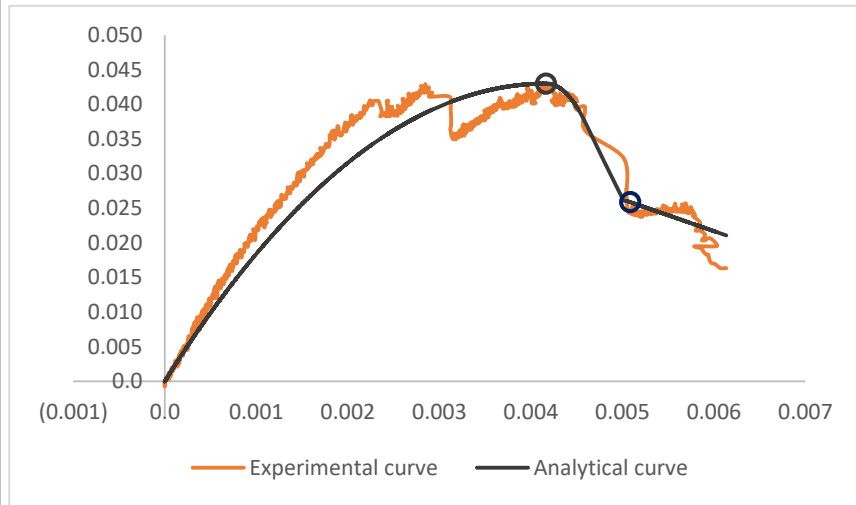


Parameters resulting from the experimental data

UHPC07D0SF050_1

f_c	43.0 Mpa
ε_c	0.0042
E_c	21.3 Gpa
σ₂	0.623 · f _c
ε₂	1.172 · ε _c
σ₃	0 MPa
ε₃	2.577 · ε _c

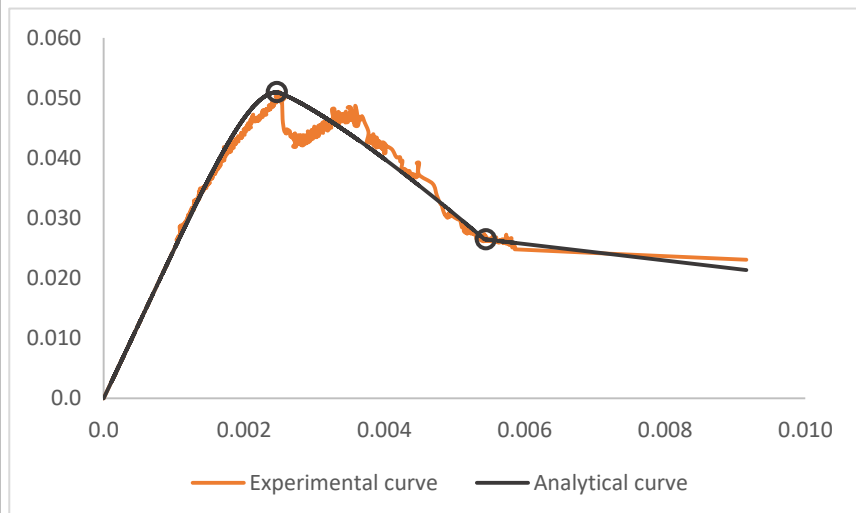
R²	0.9633
----------------------	--------



UHPC07D0SF050_2

f_c	51.0 Mpa
ε_c	0.0025
E_c	24.7 Gpa
σ₂	0.520 · f _c
ε₂	2.196 · ε _c
σ₃	0 MPa
ε₃	10.000 · ε _c

R²	0.9840
----------------------	--------

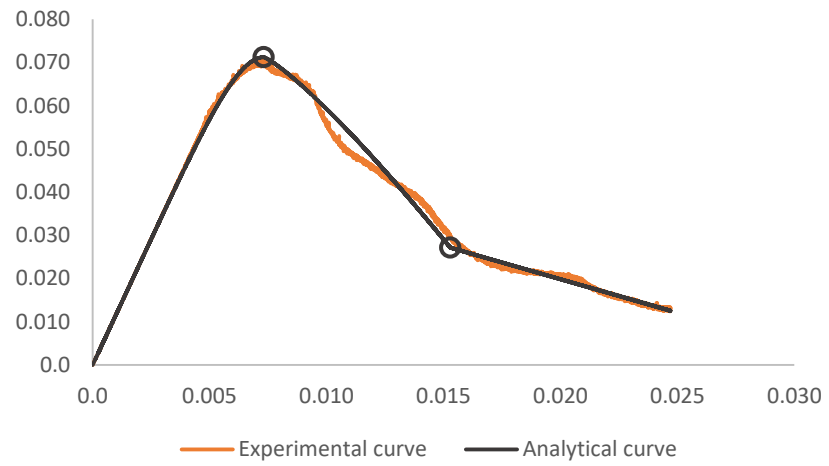


Parameters resulting from the experimental data

UHPC07D2SF000_1

f_c	71.2 Mpa
ε_c	0.0073
E_c	11.6 Gpa
σ₂	0.381 · f _c
ε₂	2.090 · ε _c
σ₃	0 MPa
ε₃	4.484 · ε _c

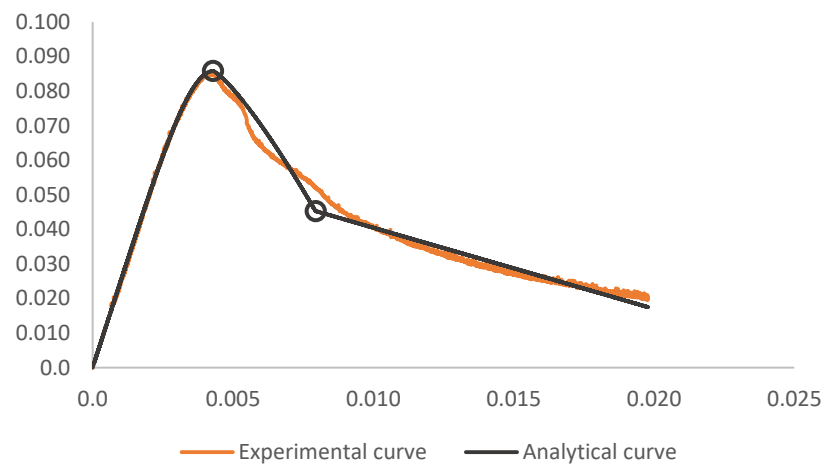
R²	0.9943
----------------------	--------



UHPC07D2SF000_2

f_c	85.8 Mpa
ε_c	0.0043
E_c	25.1 Gpa
σ₂	0.528 · f _c
ε₂	1.850 · ε _c
σ₃	0 MPa
ε₃	6.352 · ε _c

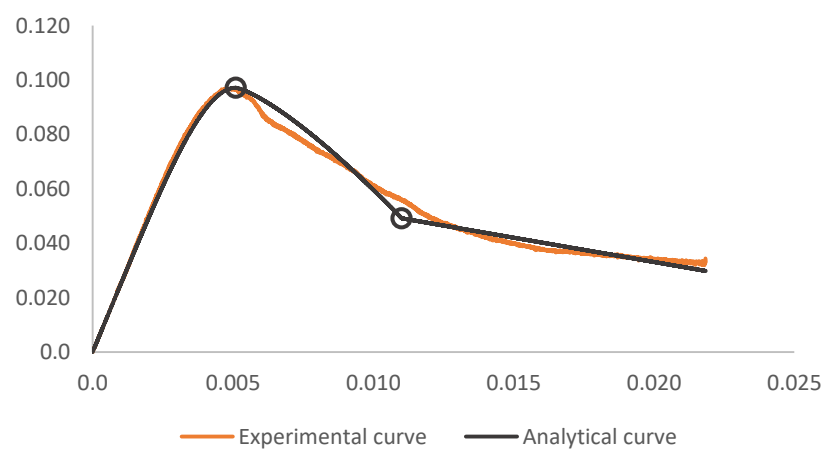
R²	0.9901
----------------------	--------



UHPC07D2SF000_3

f_c	97.2 Mpa
ε_c	0.0051
E_c	25.0 Gpa
σ₂	0.506 · f _c
ε₂	2.159 · ε _c
σ₃	0 MPa
ε₃	7.559 · ε _c

R²	0.9886
----------------------	--------

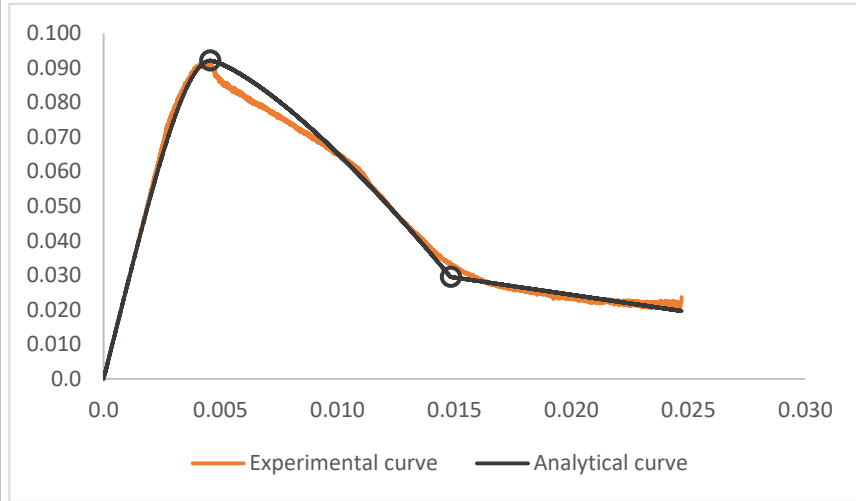


Parameters resulting from the experimental data

UHPC07D2SF008_1

f_c	92.1 Mpa
ε_c	0.0046
E_c	26.8 Gpa
σ₂	0.320 · f _c
ε₂	3.243 · ε _c
σ₃	0 MPa
ε₃	9.716 · ε _c

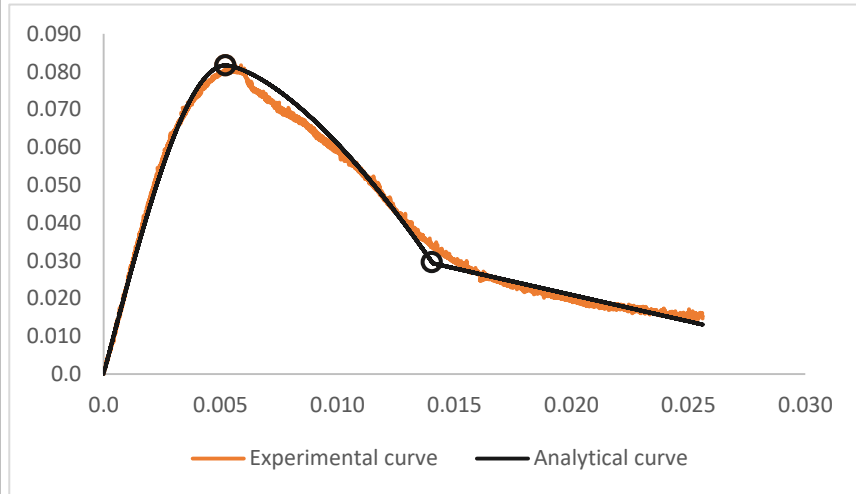
R²	0.9939
----------------------	--------



UHPC07D2SF008_2

f_c	81.7 Mpa
ε_c	0.0052
E_c	23.6 Gpa
σ₂	0.359 · f _c
ε₂	2.699 · ε _c
σ₃	0 MPa
ε₃	6.702 · ε _c

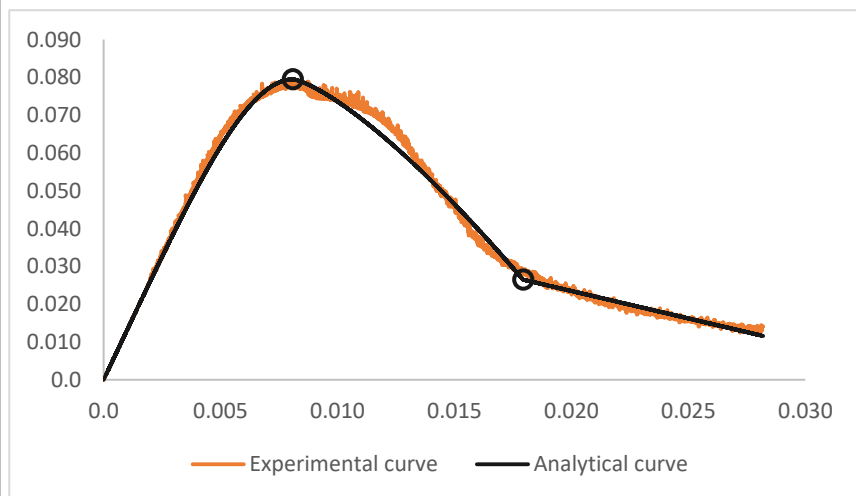
R²	0.9945
----------------------	--------



UHPC07D2SF008_3

f_c	79.5 Mpa
ε_c	0.0081
E_c	13.1 Gpa
σ₂	0.333 · f _c
ε₂	2.213 · ε _c
σ₃	0 MPa
ε₃	4.468 · ε _c

R²	0.9956
----------------------	--------



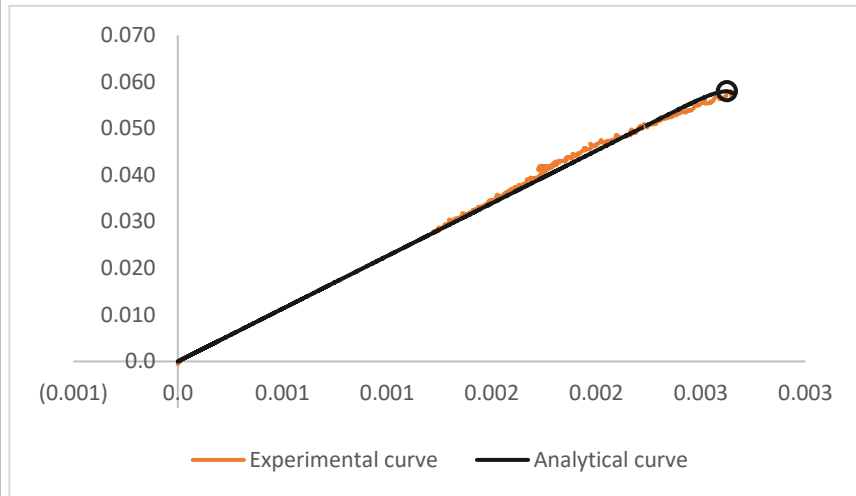
28 DAYS

Parameters resulting from the experimental data

UHPC28D0SF000_1

f_c	58.0 Mpa
ε_c	0.0026
E_c	22.6 Gpa
σ₂	0.507 · f _c
ε₂	1.662 · ε _c
σ₃	0 MPa
ε₃	3.668 · ε _c

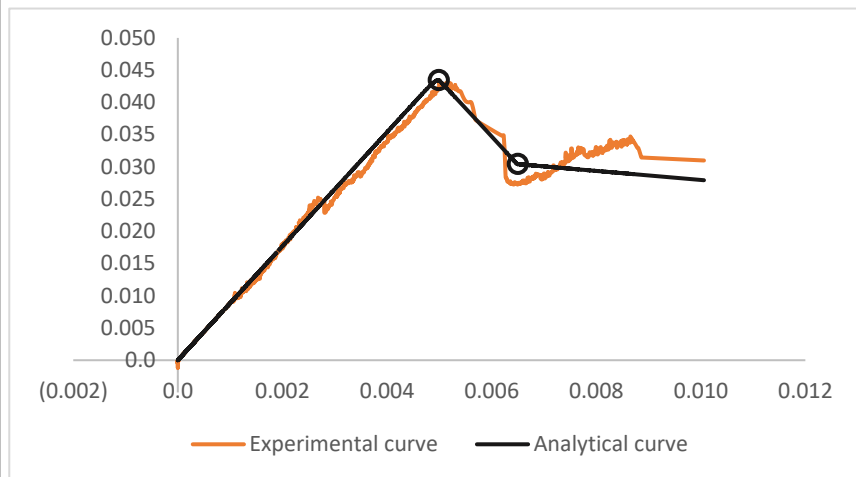
R²	0.9986
----------------------	--------



UHPC28D0SF000_2

f_c	43.5 Mpa
ε_c	0.0050
E_c	8.8 Gpa
σ₂	0.700 · f _c
ε₂	1.300 · ε _c
σ₃	0 MPa
ε₃	10.000 · ε _c

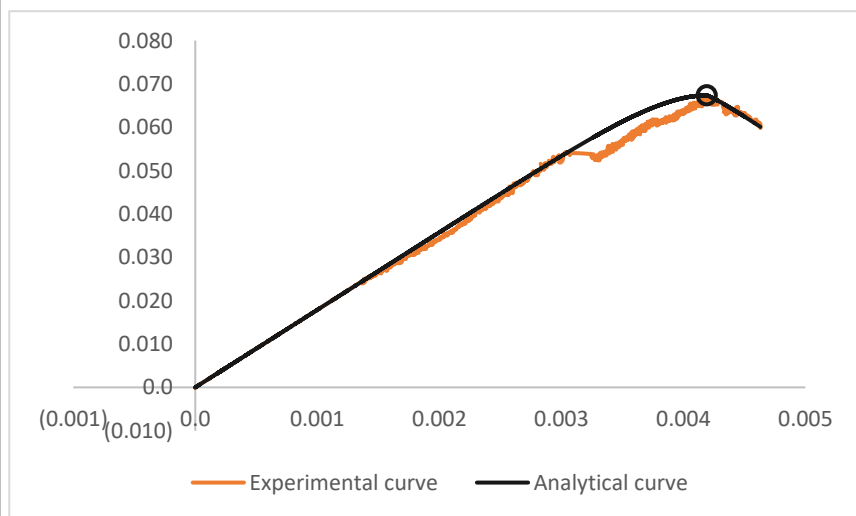
R²	0.9783
----------------------	--------



UHPC28D0SF000_3

f_c	67.4 Mpa
ε_c	0.0042
E_c	17.9 Gpa
σ₂	0.252 · f _c
ε₂	1.593 · ε _c
σ₃	0 MPa
ε₃	5.719 · ε _c

R²	0.9967
----------------------	--------

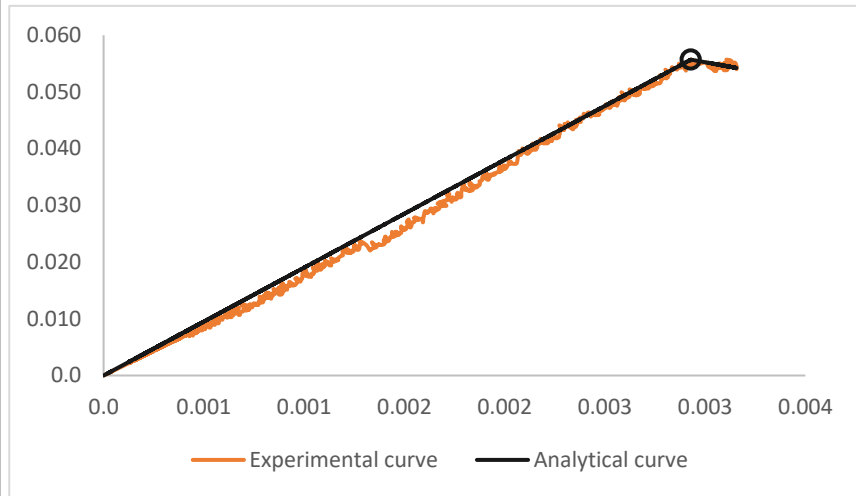


Parameters resulting from the experimental data

UHPC28D0SF008_1

f_c	55.7 Mpa
ε_c	0.0029
E_c	17.3 Gpa
σ₂	0.626 · f _c
ε₂	2.105 · ε _c
σ₃	0 MPa
ε₃	4.856 · ε _c

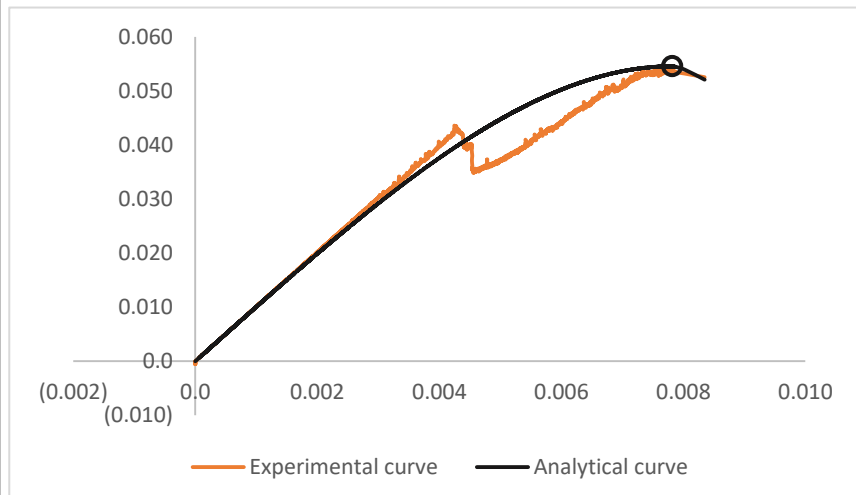
R²	0.9978
----------------------	--------



UHPC28D0SF008_2

f_c	54.6 Mpa
ε_c	0.0078
E_c	10.1 Gpa
σ₂	0.000 · f _c
ε₂	1.577 · ε _c
σ₃	0 MPa
ε₃	10.000 · ε _c

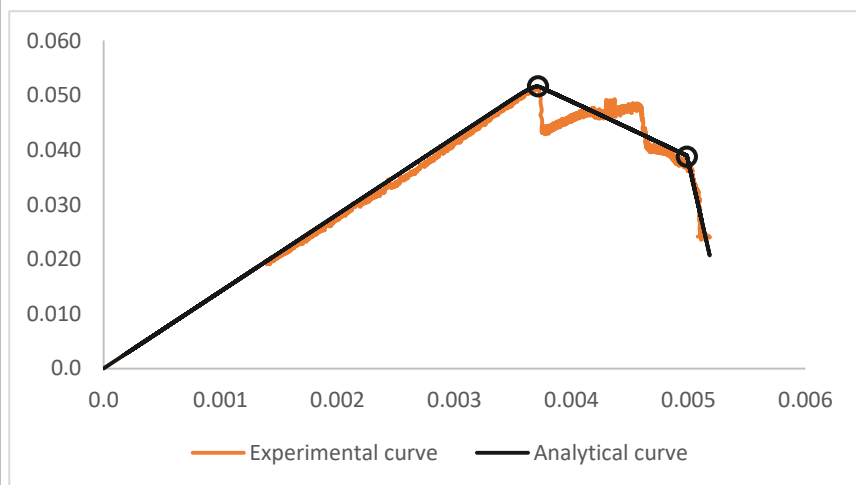
R²	0.9715
----------------------	--------



UHPC28D0SF008_3

f_c	51.6 Mpa
ε_c	0.0037
E_c	14.1 Gpa
σ₂	0.754 · f _c
ε₂	1.342 · ε _c
σ₃	0 MPa
ε₃	1.454 · ε _c

R²	0.9752
----------------------	--------

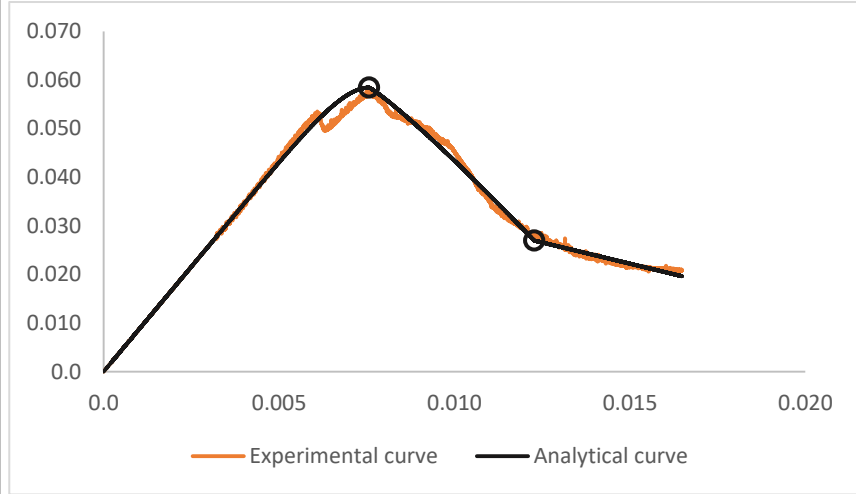


Parameters resulting from the experimental data

UHPC28D2SF000_1

f_c	58.4 Mpa
ε_c	0.0076
E_c	8.6 Gpa
σ₂	0.461 · f _c
ε₂	1.621 · ε _c
σ₃	0 MPa
ε₃	3.668 · ε _c

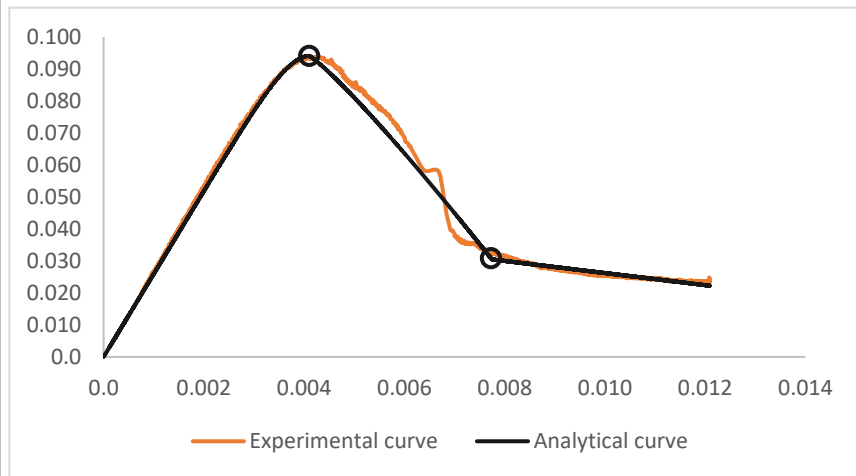
R²	0.9939
----------------------	--------



UHPC28D2SF000_2

f_c	94.1 Mpa
ε_c	0.0041
E_c	25.9 Gpa
σ₂	0.324 · f _c
ε₂	1.886 · ε _c
σ₃	0 MPa
ε₃	5.809 · ε _c

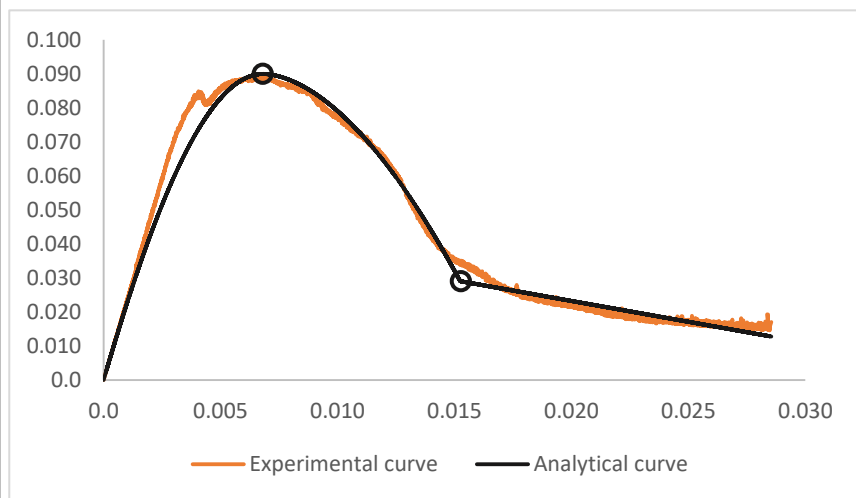
R²	0.9960
----------------------	--------



UHPC28D2SF000_3

f_c	89.9 Mpa
ε_c	0.0068
E_c	23.3 Gpa
σ₂	0.323 · f _c
ε₂	2.237 · ε _c
σ₃	0 MPa
ε₃	5.719 · ε _c

R²	0.9888
----------------------	--------

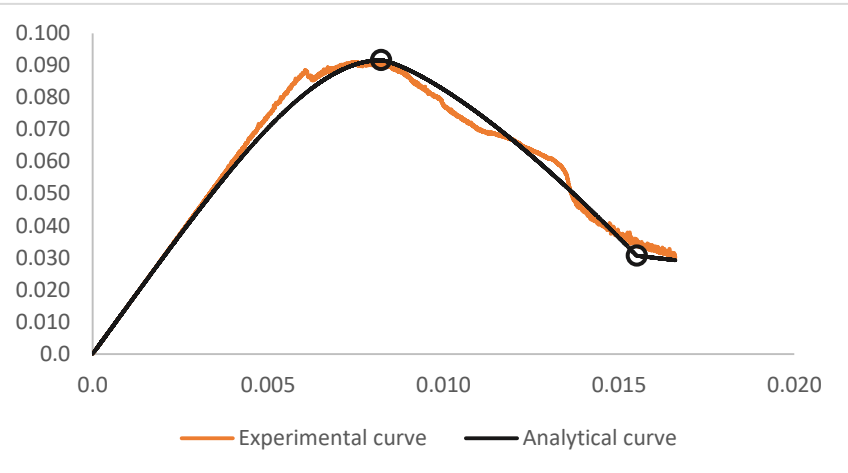


Parameters resulting from the experimental data

UHPC28D2SF008_1

f_c	91.6 Mpa
ϵ_c	0.0082
E_c	15.0 Gpa
σ_2	$0.335 \cdot f_c$
ϵ_2	$1.886 \cdot \epsilon_c$
σ_3	0 MPa
ϵ_3	$4.856 \cdot \epsilon_c$

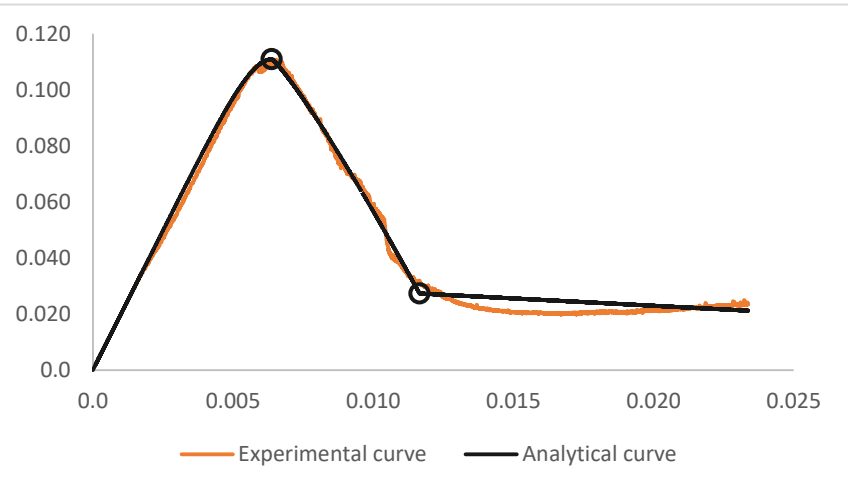
R^2	0.9934
-------	--------



UHPC28D2SF008_2

f_c	111.0 Mpa
ϵ_c	0.0064
E_c	19.9 Gpa
σ_2	$0.246 \cdot f_c$
ϵ_2	$1.825 \cdot \epsilon_c$
σ_3	0 MPa
ϵ_3	$10.000 \cdot \epsilon_c$

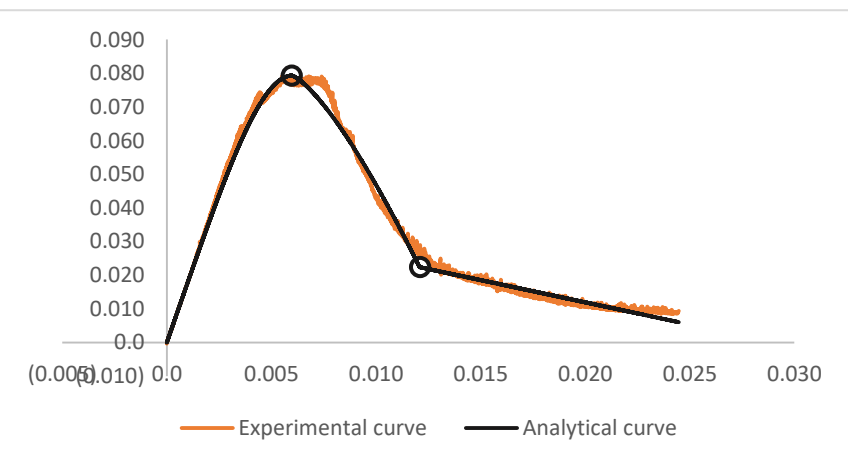
R^2	0.9885
-------	--------



UHPC28D2SF008_3

f_c	79.3 Mpa
ϵ_c	0.0060
E_c	17.9 Gpa
σ_2	$0.282 \cdot f_c$
ϵ_2	$2.023 \cdot \epsilon_c$
σ_3	0 MPa
ϵ_3	$4.862 \cdot \epsilon_c$

R^2	0.9950
-------	--------

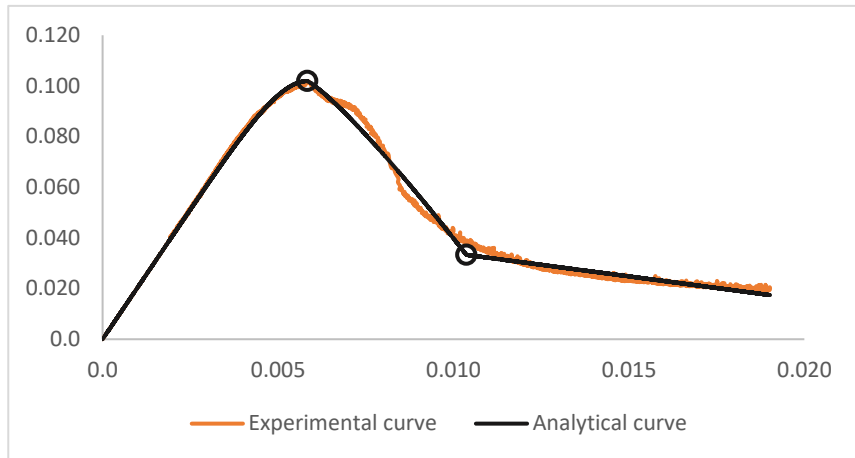


Parameters resulting from the experimental data

UHPC28D2SF050_1

f_c	101.9 Mpa
ε_c	0.0058
E_c	20.5 Gpa
σ₂	0.327 · f _c
ε₂	1.777 · ε _c
σ₃	0 MPa
ε₃	4.891 · ε _c

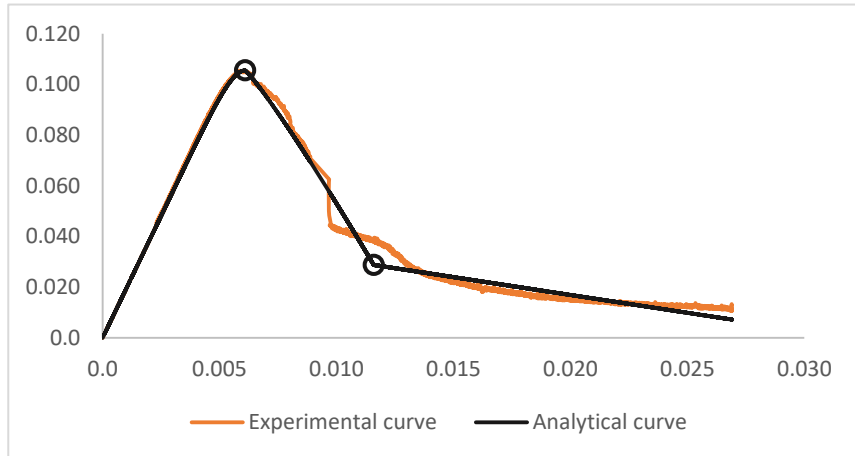
R²	0.9959
----------------------	--------



UHPC28D2SF050_2

f_c	105.6 Mpa
ε_c	0.0061
E_c	19.2 Gpa
σ₂	0.273 · f _c
ε₂	1.901 · ε _c
σ₃	0 MPa
ε₃	5.255 · ε _c

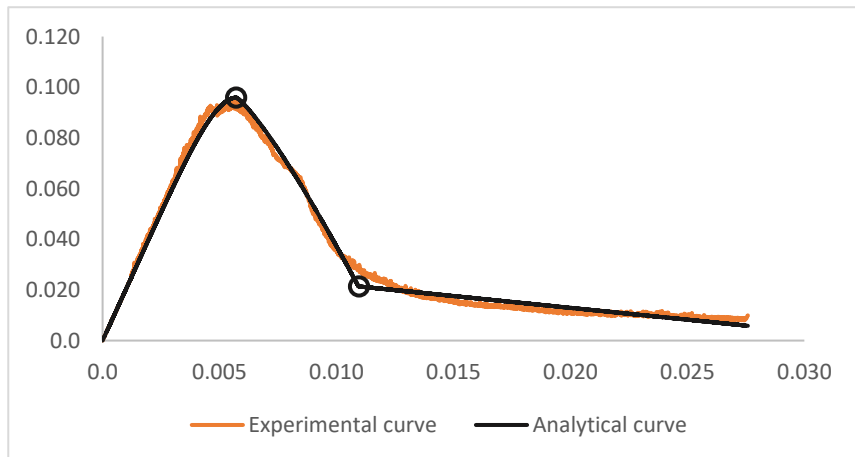
R²	0.9884
----------------------	--------



UHPC28D2SF050_3

f_c	95.9 Mpa
ε_c	0.0057
E_c	20.3 Gpa
σ₂	0.223 · f _c
ε₂	1.913 · ε _c
σ₃	0 MPa
ε₃	5.918 · ε _c

R²	0.9936
----------------------	--------

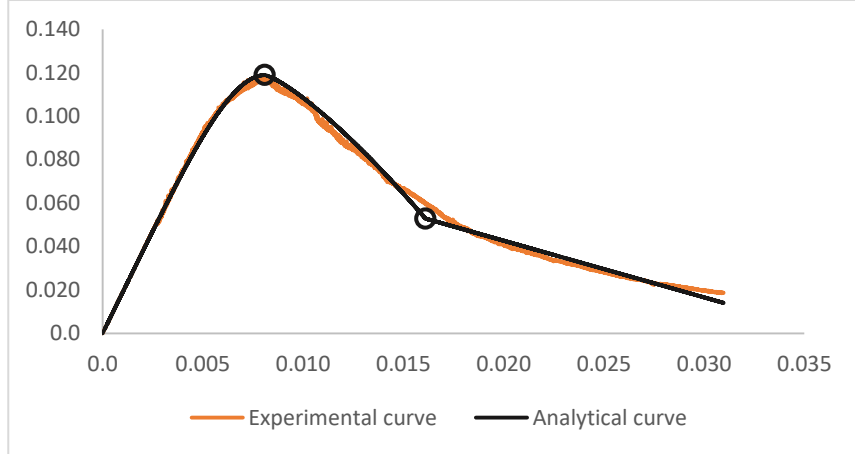


Parameters resulting from the experimental data

UHPC28D4SF000_1

f_c	118.9 Mpa
ϵ_c	0.0081
E_c	18.9 Gpa
σ_2	$0.444 \cdot f_c$
ϵ_2	$1.991 \cdot \epsilon_c$
σ_3	0 MPa
ϵ_3	$4.491 \cdot \epsilon_c$

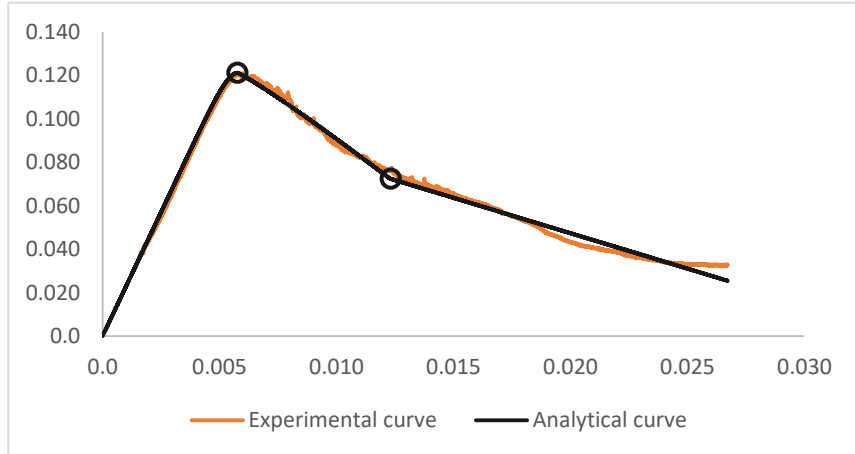
R^2	0.9950
-------	--------



UHPC28D4SF000_2

f_c	121.2 Mpa
ϵ_c	0.0058
E_c	22.8 Gpa
σ_2	$0.598 \cdot f_c$
ϵ_2	$2.126 \cdot \epsilon_c$
σ_3	0 MPa
ϵ_3	$5.978 \cdot \epsilon_c$

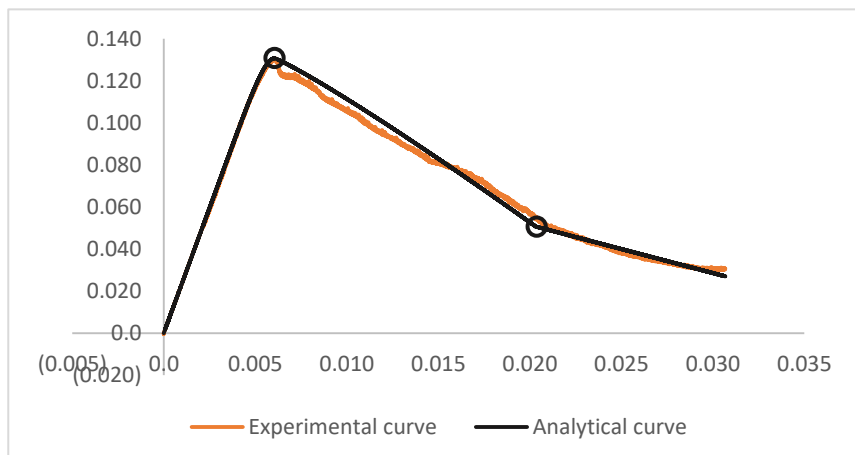
R^2	0.9941
-------	--------



UHPC28D4SF000_3

f_c	130.7 Mpa
ϵ_c	0.0061
E_c	23.8 Gpa
σ_2	$0.388 \cdot f_c$
ϵ_2	$3.356 \cdot \epsilon_c$
σ_3	0 MPa
ϵ_3	$7.019 \cdot \epsilon_c$

R^2	0.9955
-------	--------

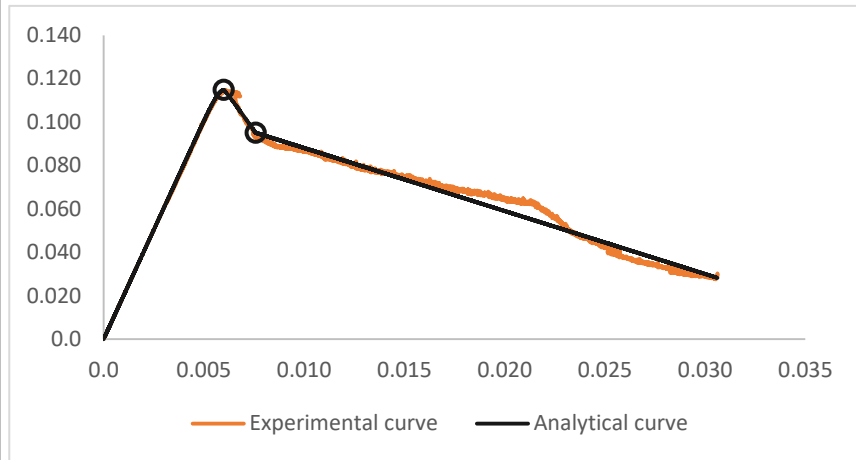


Parameters resulting from the experimental data

UHPC28D4SF008_1

f_c	114.8 Mpa
ε_c	0.0060
E_c	20.1 Gpa
σ₂	0.828 · f _c
ε₂	1.264 · ε _c
σ₃	0 MPa
ε₃	6.729 · ε _c

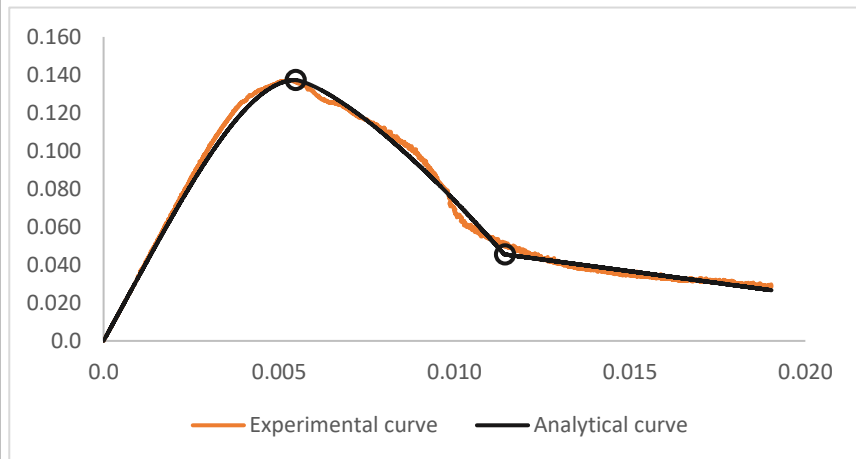
R²	0.9911
----------------------	--------



UHPC28D4SF008_2

f_c	137.3 Mpa
ε_c	0.0055
E_c	33.9 Gpa
σ₂	0.332 · f _c
ε₂	2.083 · ε _c
σ₃	0 MPa
ε₃	5.436 · ε _c

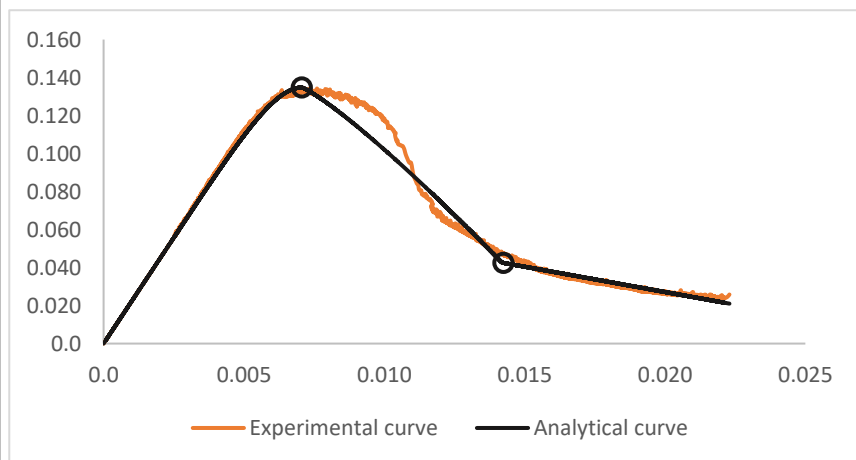
R²	0.9958
----------------------	--------



UHPC28D4SF008_3

f_c	134.8 Mpa
ε_c	0.0071
E_c	22.3 Gpa
σ₂	0.316 · f _c
ε₂	2.009 · ε _c
σ₃	0 MPa
ε₃	4.274 · ε _c

R²	0.9917
----------------------	--------

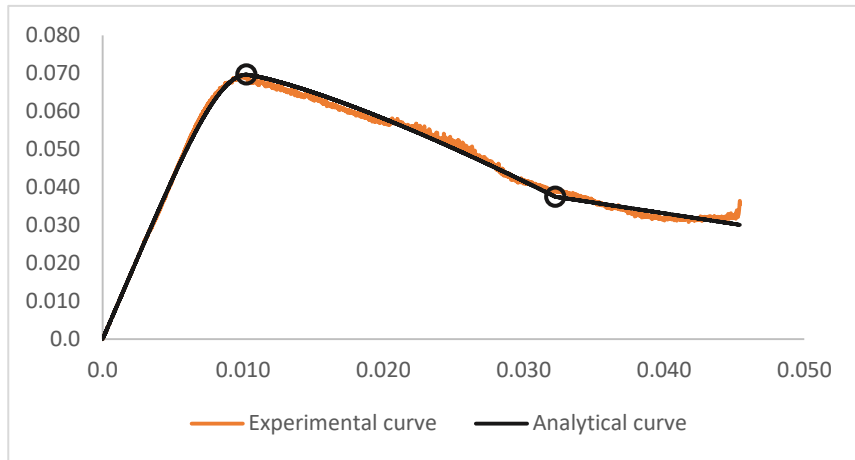


Parameters resulting from the experimental data

UHPC28D4SF050_1

f_c	69.6 Mpa
ε_c	0.0102
E_c	8.6 Gpa
σ₂	0.539 · f _c
ε₂	3.148 · ε _c
σ₃	0 MPa
ε₃	9.664 · ε _c

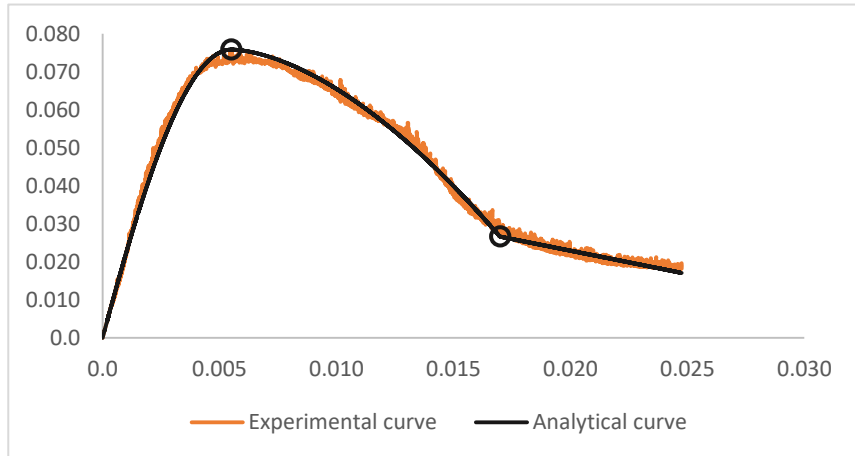
R²	0.9968
----------------------	--------



UHPC28D4SF050_2

f_c	75.9 Mpa
ε_c	0.0055
E_c	22.9 Gpa
σ₂	0.351 · f _c
ε₂	3.083 · ε _c
σ₃	0 MPa
ε₃	7.020 · ε _c

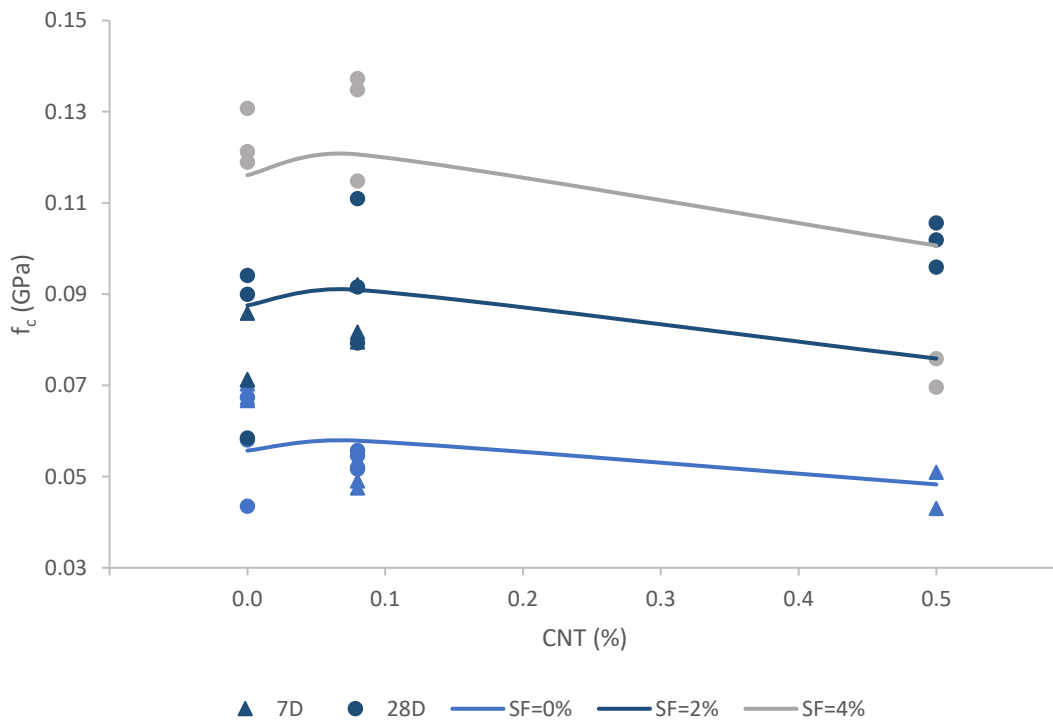
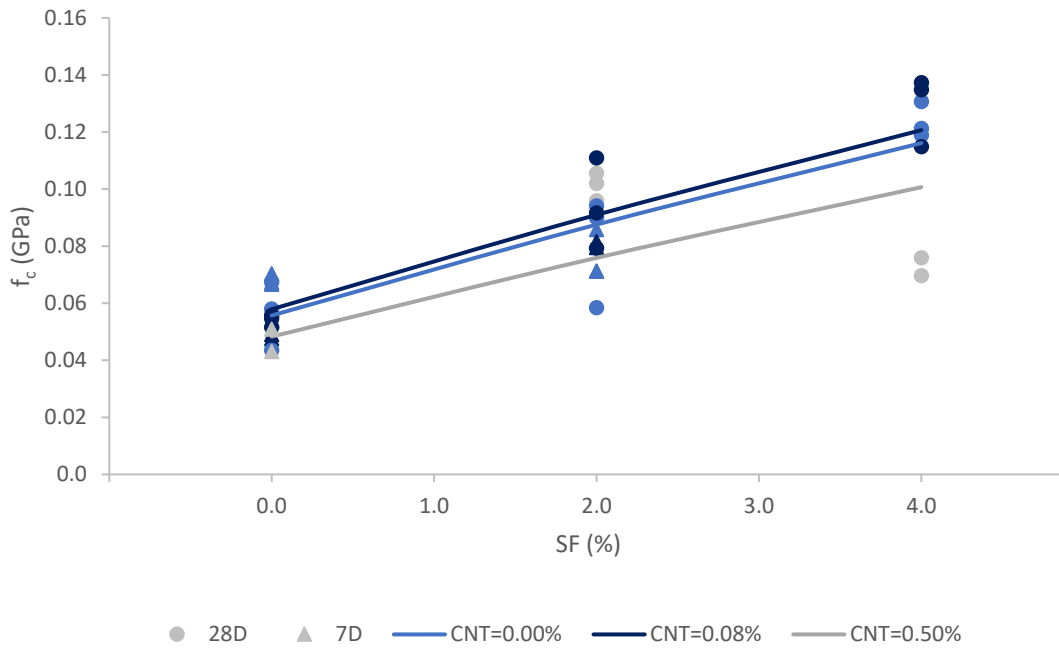
R²	0.9955
----------------------	--------



Annex 4 Parametric analysis of SF and CNT

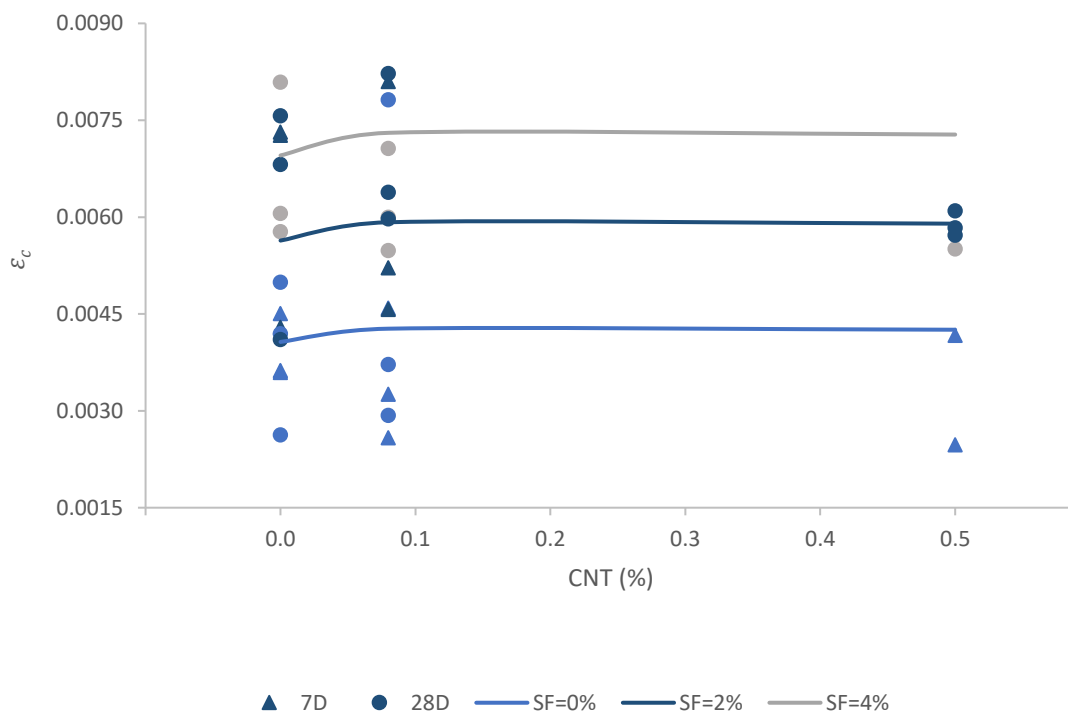
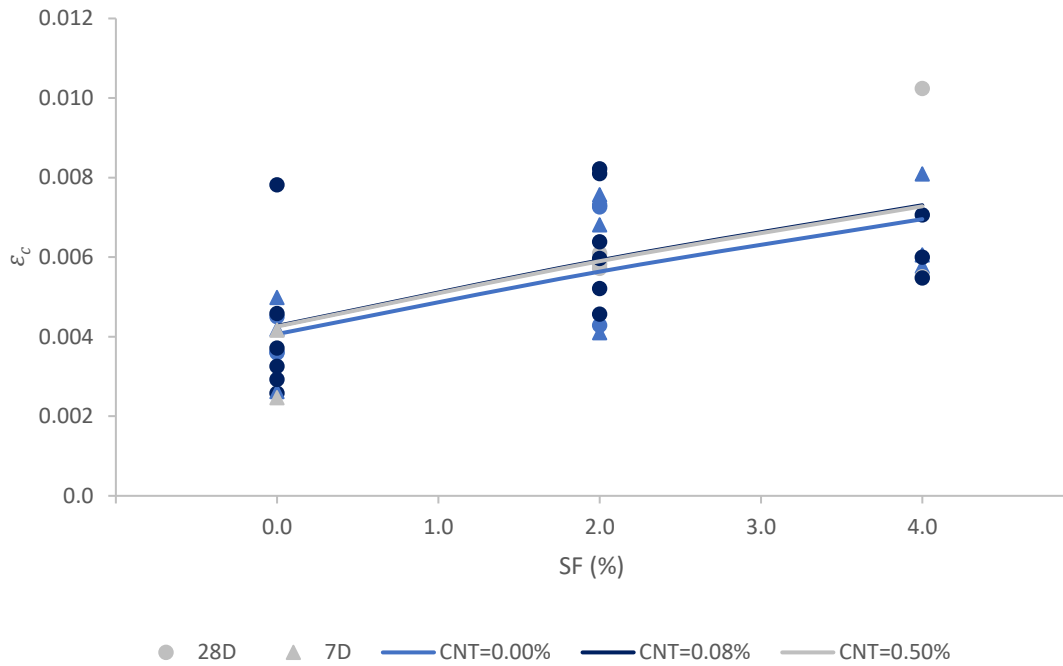
$$f_c(\text{UHPC}, \%SF, \%CNT) = f_c(\text{UHPC}, 0, 0) \cdot (-0.007 \cdot x^2 + 0.301 \cdot x + 1) \cdot (-1.796 \cdot y^2 + 0.632 \cdot y + 1)$$

where x: SF(%) the concentration of steel fibers, expressed on % by volume
y: CNT(%) the concentration of CNT, expressed on % weight material/weight cement



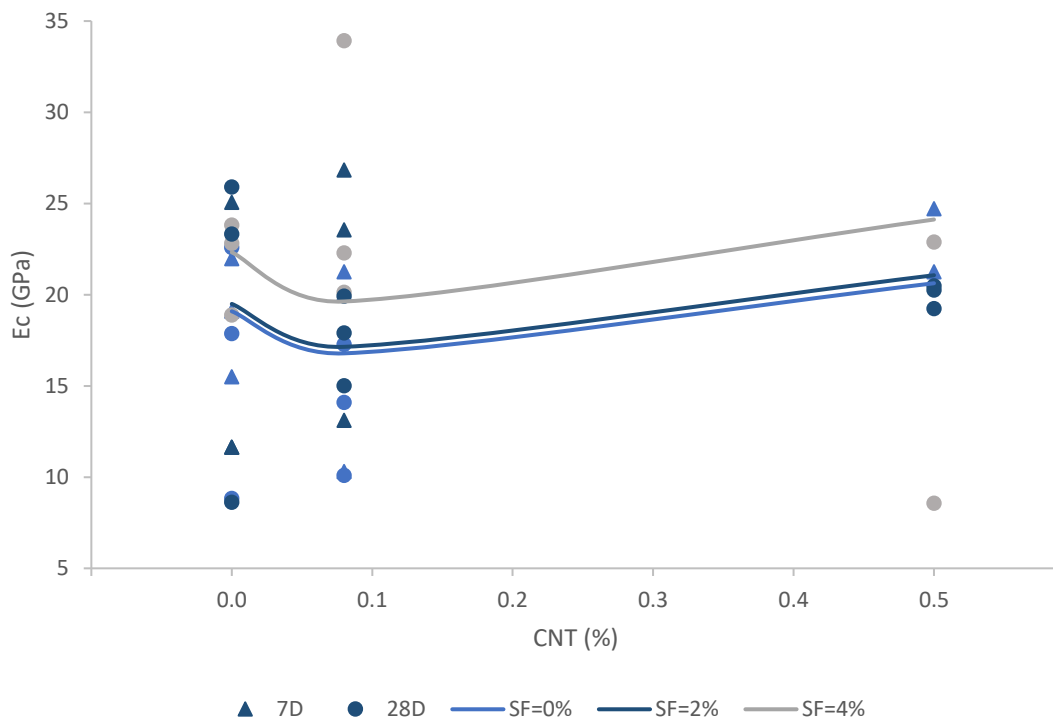
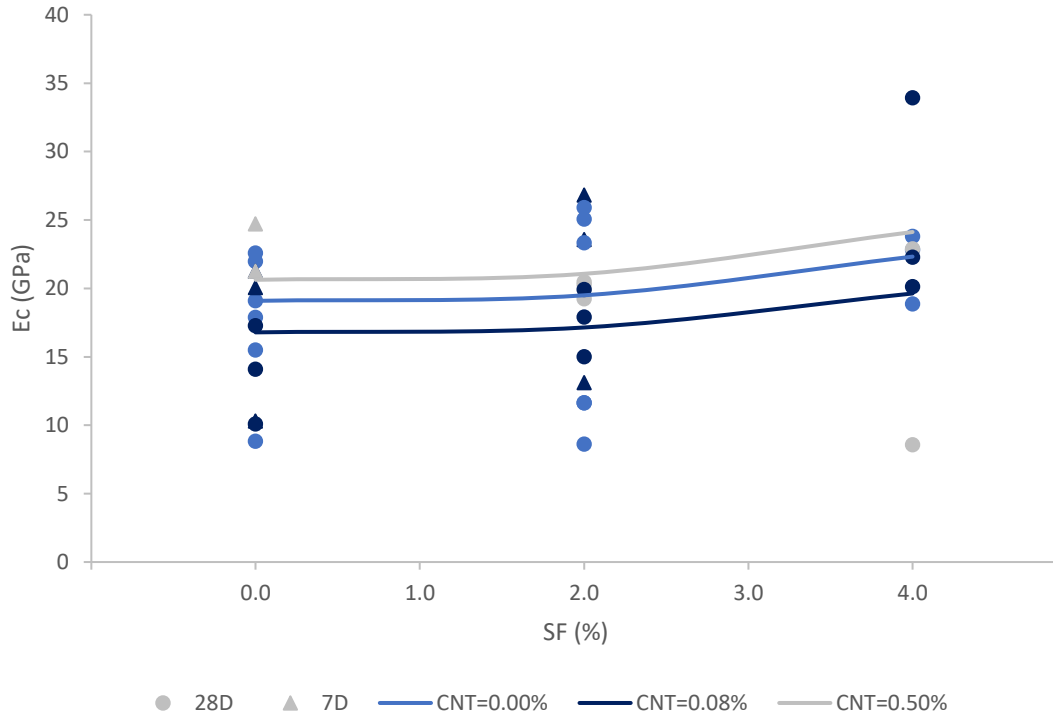
$$\varepsilon_c(\text{UHPC}, \%SF, \%CNT) = \varepsilon_c(\text{UHPC}, 0, 0) \cdot (-0.008 \cdot x^2 + 0.208 \cdot x + 1) \cdot (-1.276 \cdot y^2 + 0.731 \cdot y + 1)$$

where x: SF(%) the concentration of steel fibers, expressed on % by volume
y: CNT(%) the concentration of CNT, expressed on % weight material/weight cement



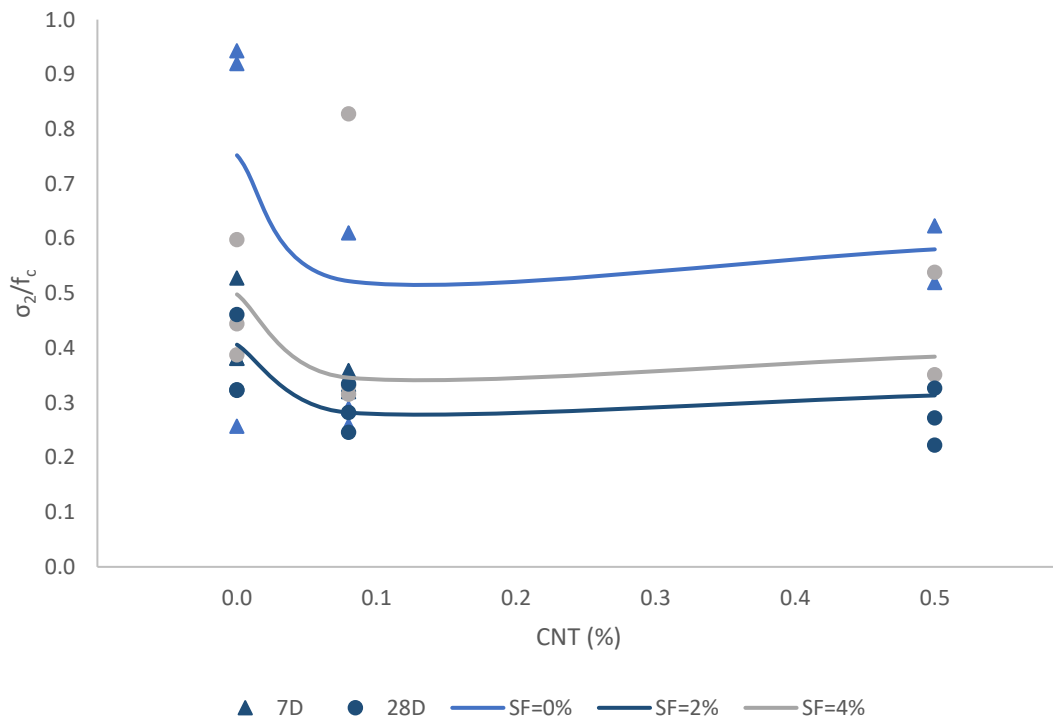
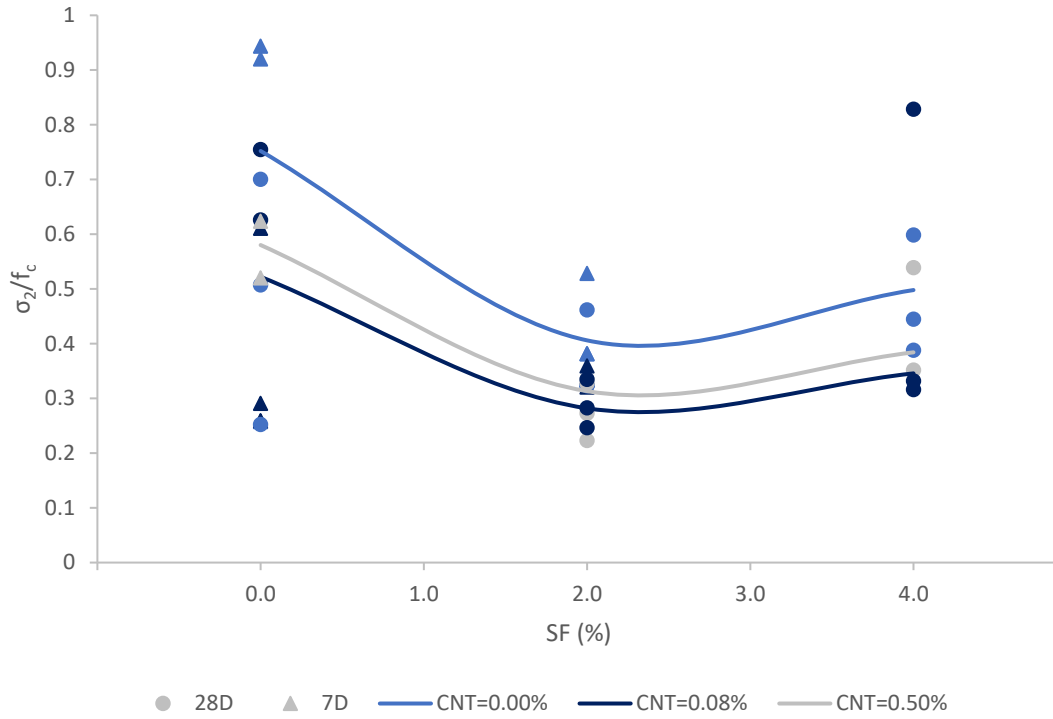
$$E_c(\text{UHPC}, \%SF, \%CNT) = E_c(\text{UHPC}, 0, 0) \cdot (0.016 \cdot x^2 - 0.021 \cdot x + 1) \cdot (3.977 \cdot y^2 - 1.827 \cdot y + 1)$$

where x: SF(%) the concentration of steel fibers, expressed on % by volume
y: CNT(%) the concentration of CNT, expressed on % weight material/weight cement



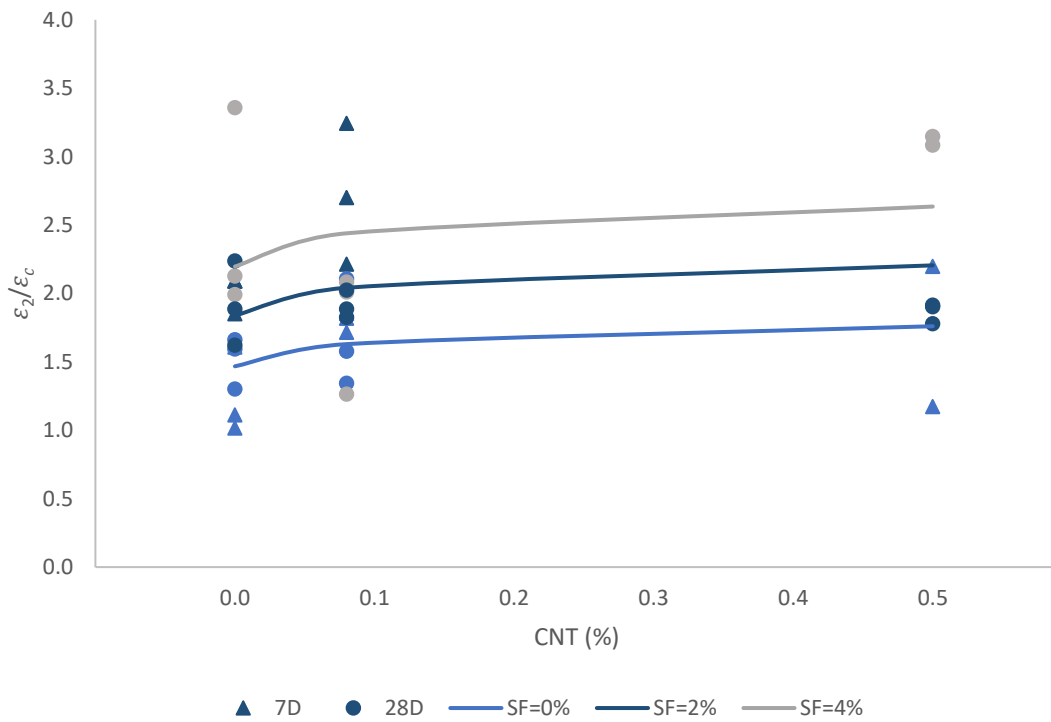
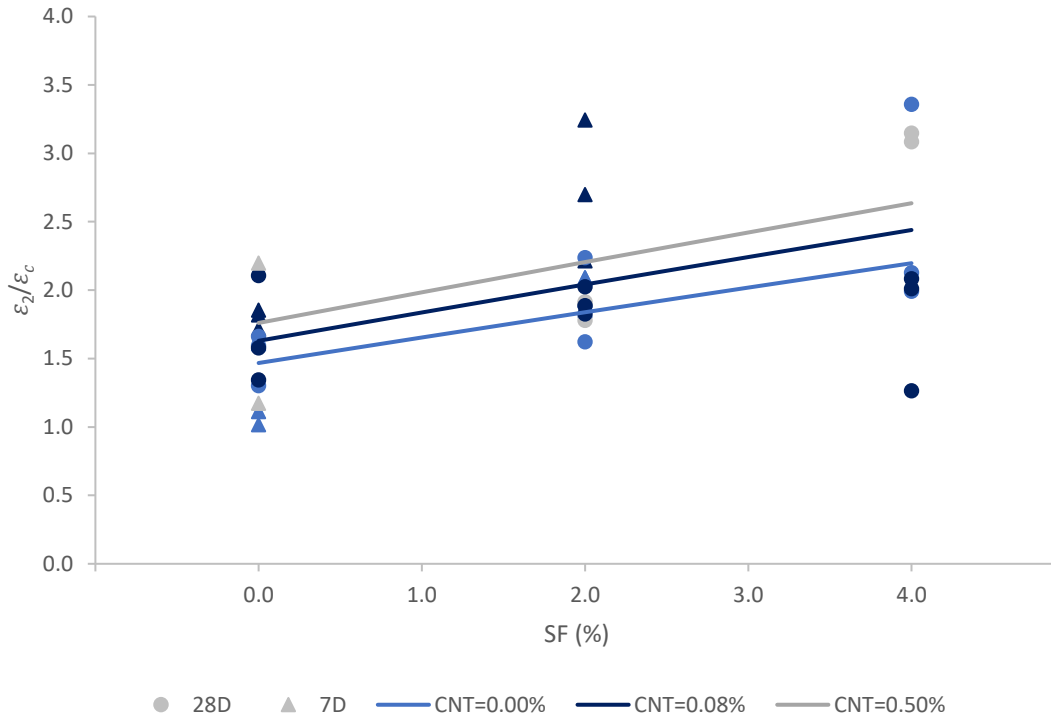
$$\frac{\sigma_2}{f_c}(\text{UHPC}, \%SF, \%CNT) = \frac{\sigma_2}{f_c}(\text{UHPC}, 0, 0) \cdot (0.073 \cdot x^2 - 0.376 \cdot x + 1) \cdot (8.011 \cdot y^2 - 4.462 \cdot y + 1)$$

where x: SF(%) the concentration of steel fibers, expressed on % by volume
y: CNT(%) the concentration of CNT, expressed on % weight material/weight cement



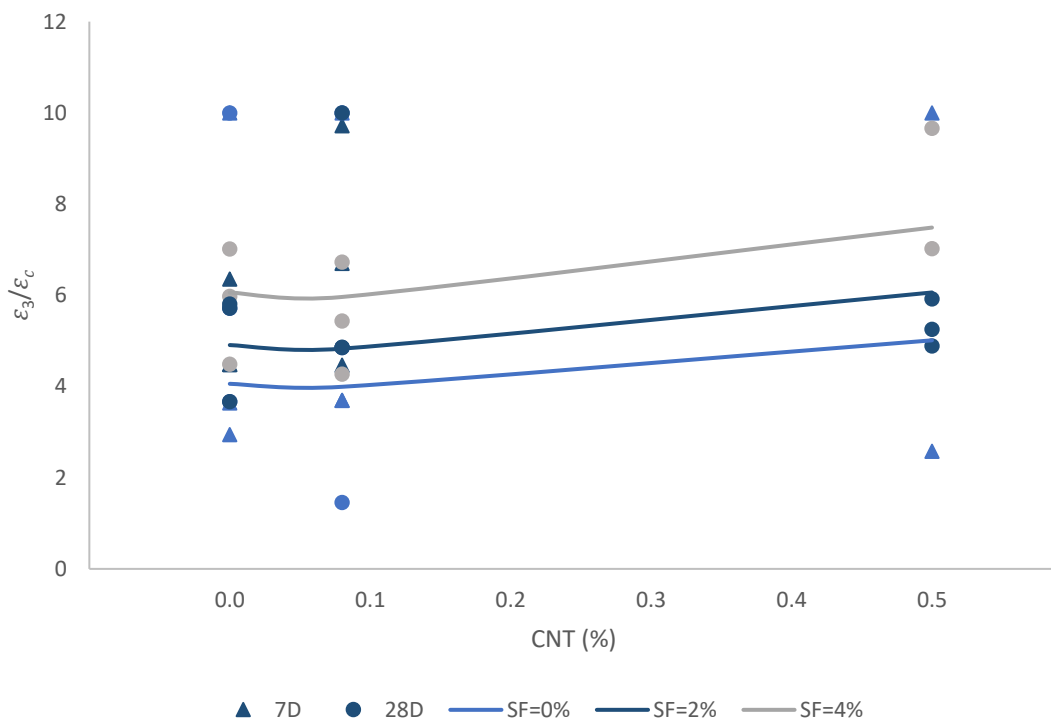
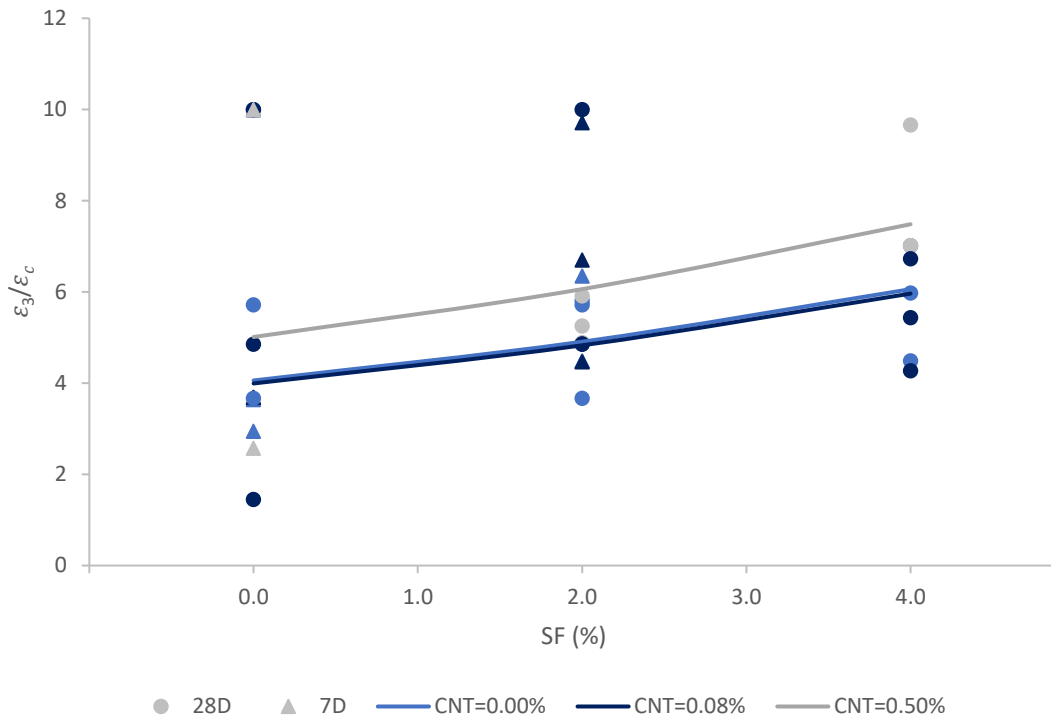
$$\frac{\varepsilon_2}{\varepsilon_c}(\text{UHPC}, \%SF, \%CNT) = \frac{\varepsilon_2}{\varepsilon_c}(\text{UHPC}, 0, 0) \cdot (0.129 \cdot x + 1) \cdot (-2.338 \cdot y^2 + 1.568 \cdot y + 1)$$

where x: SF(%) the concentration of steel fibers, expressed on % by volume
y: CNT(%) the concentration of CNT, expressed on % weight material/weight cement



$$\frac{\varepsilon_3}{\varepsilon_c}(\text{UHPC}, \%SF, \%CNT) = \frac{\varepsilon_3}{\varepsilon_c}(\text{UHPC}, 0, 0) \cdot (0.009 \cdot x^2 + 0.086 \cdot x + 1) \cdot (1.597 \cdot y^2 - 0.328 \cdot y + 1)$$

where x: SF(%) the concentration of steel fibers, expressed on % by volume
y: CNT(%) the concentration of CNT, expressed on % weight material/weight cement



Annex 5 FEM Results output – Monitor Data File

Monitor Data File

PROCESSING PART, INSTANCE, AND ASSEMBLY INFORMATION

END PROCESSING PART, INSTANCE, AND ASSEMBLY INFORMATION

OPTIONS BEING PROCESSED

*Heading
*Node
*Element, type=CAX4
*Nset, nset=ASSEMBLY_PART-1-1__PICKEDSET2
*Nset, nset=ASSEMBLY_PART-1-1__PICKEDSET8
*Elset, elset=ASSEMBLY_PART-1-1__PICKEDSET2
*Elset, elset=ASSEMBLY_PART-1-1__PICKEDSET8
*Node
*Element, type=CAX4
*Nset, nset=ASSEMBLY_PART-2-1__PICKEDSET2
*Elset, elset=ASSEMBLY_PART-2-1__PICKEDSET2
*Node
*Element, type=CAX4
*Nset, nset=ASSEMBLY_PART-2-COPY-1__PICKEDSET2
*Elset, elset=ASSEMBLY_PART-2-COPY-1__PICKEDSET2
*Nset, nset=ASSEMBLY_SET-1
*Nset, nset=ASSEMBLY_SET-2
*Nset, nset=ASSEMBLY_SET-3
*Elset, elset=ASSEMBLY_SET-1
*Elset, elset=ASSEMBLY_SET-2
*Elset, elset=ASSEMBLY_SET-3
*Elset, elset=ASSEMBLY__SURF-1_S3
*Elset, elset=ASSEMBLY__SURF-2_S1
*surface, type=ELEMENT, name=ASSEMBLY_SURF-1
*surface, type=ELEMENT, name=ASSEMBLY_SURF-2
*surface, type=ELEMENT, name=ASSEMBLY_SURF-1
*surface, type=ELEMENT, name=ASSEMBLY_SURF-2
*surfaceinteraction, name=INTPROP-1
*surfacebehavior, noseparation, pressure-overclosure=HARD
*contact

```

*contactinclusions, allexterior
*contactpropertyassignment
*solidsection, elset=ASSEMBLY_PART-1-1__PICKEDSET8, material=MATERIAL-1
*solidsection, elset=ASSEMBLY_PART-2-1__PICKEDSET2, material=STEEL
*solidsection, elset=ASSEMBLY_PART-2-COPY-1__PICKEDSET2, material=STEEL
*material, name=MATERIAL-1
*usermaterial, constants=9
*material, name=STEEL
*elastic
*surfaceinteraction, name=INTPROP-1
*friction, sliptolerance=0.005
*surfacebehavior, noseparation, pressure-overclosure=HARD
*surfaceinteraction, name=INTPROP-1
*solidsection, elset=ASSEMBLY_PART-1-1__PICKEDSET8, material=MATERIAL-1
*solidsection, elset=ASSEMBLY_PART-2-1__PICKEDSET2, material=STEEL
*solidsection, elset=ASSEMBLY_PART-2-COPY-1__PICKEDSET2, material=STEEL
*boundary
*boundary
*boundary
*solidsection, elset=ASSEMBLY_PART-1-1__PICKEDSET8, material=MATERIAL-1
*solidsection, elset=ASSEMBLY_PART-2-1__PICKEDSET2, material=STEEL
*solidsection, elset=ASSEMBLY_PART-2-COPY-1__PICKEDSET2, material=STEEL
*surfaceinteraction, name=INTPROP-1
*surface, type=ELEMENT, name=ASSEMBLY_SURF-1
*surface, type=ELEMENT, name=ASSEMBLY_SURF-2
*output, field, variable=PRESELECT
*output, history, variable=PRESELECT
*output, field, variable=PRESELECT
*output, history, variable=PRESELECT
*output, field, variable=PRESELECT
*output, history, variable=PRESELECT
*output, field, variable=PRESELECT
*output, history, variable=PRESELECT
*output, field, variable=PRESELECT
*output, history, variable=PRESELECT
*output, field, variable=PRESELECT
*output, history, variable=PRESELECT
*output, field, variable=PRESELECT
*output, history, variable=PRESELECT
*Step, name=Step-1, nlgeom=NO, extrapolation=PARABOLIC, amplitude=STEP,
inc=10000
*output, field, variable=PRESELECT
*output, history, variable=PRESELECT
*Step, name=Step-2, nlgeom=NO, extrapolation=NO, inc=10000, unsymm=NO
*output, field, variable=PRESELECT
*output, history, variable=PRESELECT
*Step, name=Step-1, nlgeom=NO, extrapolation=PARABOLIC, amplitude=STEP,
inc=10000
*Step, name=Step-2, nlgeom=NO, extrapolation=NO, inc=10000, unsymm=NO

```

```

*Step, name=Step-1, nlgeom=NO, extrapolation=PARABOLIC, amplitude=STEP,
inc=10000
*static, direct
*boundary
*output, field, variable=PRESELECT
*output, history, variable=PRESELECT
*endstep
*Step, name=Step-2, nlgeom=NO, extrapolation=NO, inc=10000, unsymm=NO
*static, direct
*boundary
*output, field, variable=PRESELECT
*output, history, variable=PRESELECT
*endstep
*boundary

```

***WARNING: DEGREE OF FREEDOM 6 IS NOT ACTIVE IN THIS MODEL AND CAN NOT BE RESTRAINED

```

*boundary
*Step, name=Step-1, nlgeom=NO, extrapolation=PARABOLIC, amplitude=STEP,
inc=10000
*static, direct
*boundary

```

***WARNING: DEGREE OF FREEDOM 6 IS NOT ACTIVE IN THIS MODEL AND CAN NOT BE RESTRAINED

```

*endstep
*Step, name=Step-2, nlgeom=NO, extrapolation=NO, inc=10000, unsymm=NO
*static, direct
*boundary
*endstep

```

***WARNING: USER SUBROUTINE UMAT WILL BE USED WITH THE STAVEV ARRAY DIMENSIONED TO ZERO SINCE THE *DEPVAR OPTION IS NOT USED WITH THIS MATERIAL. CONSEQUENTLY, DEFINING STATEV ENTRIES IN SUBROUTINE UMAT WILL CAUSE CODE EXECUTION ERRORS.

PROBLEM SIZE

NUMBER OF ELEMENTS IS	176	
NUMBER OF ELEMENTS DEFINED BY THE USER AND *TIE	60	
NUMBER OF INTERNAL ELEMENTS GENERATED FOR CONTACT	116	
NUMBER OF NODES IS	324	
NUMBER OF NODES DEFINED BY THE USER	92	

NUMBER OF INTERNAL NODES GENERATED BY THE PROGRAM 232
TOTAL NUMBER OF VARIABLES IN THE MODEL 416
(DEGREES OF FREEDOM PLUS MAX NO. OF ANY LAGRANGE MULTIPLIER VARIABLES.
INCLUDE *PRINT,SOLVE=YES TO GET THE ACTUAL NUMBER.)

END OF USER INPUT PROCESSING

JOB TIME SUMMARY

USER TIME (SEC) = 0.20000
SYSTEM TIME (SEC) = 0.10000
TOTAL CPU TIME (SEC) = 0.30000
WALLCLOCK TIME (SEC) = 1

1

Abaqus 6.13-1 Date 23-jul.-2018 Time 11:12:14
For use by under license from Dassault Systemes or its subsidiary.

STEP 1 INCREMENT 1
TIME COMPLETED IN THIS STEP 0.00

STEP 1 STATIC ANALYSIS

FIXED TIME INCREMENTS

TIME INCREMENT IS 1.00
TIME PERIOD IS 50.0

LINEAR EQUATION SOLVER TYPE DIRECT SPARSE

UNSYMMETRIC MATRIX STORAGE AND SOLUTION WILL BE USED

MEMORY ESTIMATE

PROCESS	FLOATING PT OPERATIONS PER ITERATION	MINIMUM MEMORY REQUIRED (MBYTES)	MEMORY TO MINIMIZE I/O (MBYTES)
1	5.15E+004	17	24

NOTE:

(1) SINCE ABAQUS DOES NOT PRE-ALLOCATE MEMORY AND ONLY ALLOCATES MEMORY AS NEEDED DURING THE ANALYSIS,

THE MEMORY REQUIREMENT PRINTED HERE CAN ONLY BE VIEWED AS A GENERAL GUIDELINE BASED ON THE BEST

KNOWLEDGE AVAILABLE AT THE BEGINNING OF A STEP BEFORE THE SOLUTION PROCESS HAS BEGUN.

(2) THE ESTIMATE IS NORMALLY UPDATED AT THE BEGINNING OF EVERY STEP. IT IS THE MAXIMUM VALUE OF THE

ESTIMATE FROM THE CURRENT STEP TO THE LAST STEP OF THE ANALYSIS, WITH UNSYMMETRIC SOLUTION TAKEN

INTO ACCOUNT IF APPLICABLE.

(3) SINCE THE ESTIMATE IS BASED ON THE ACTIVE DEGREES OF FREEDOM IN THE FIRST ITERATION OF THE

CURRENT STEP, THE MEMORY ESTIMATE MIGHT BE SIGNIFICANTLY DIFFERENT THAN ACTUAL USAGE FOR

PROBLEMS WITH SUBSTANTIAL CHANGES IN ACTIVE DEGREES OF FREEDOM BETWEEN STEPS (OR EVEN WITHIN

THE SAME STEP). EXAMPLES ARE: PROBLEMS WITH SIGNIFICANT CONTACT CHANGES, PROBLEMS WITH MODEL

CHANGE, PROBLEMS WITH BOTH STATIC STEP AND STEADY STATE DYNAMIC PROCEDURES WHERE ACOUSTIC

ELEMENTS WILL ONLY BE ACTIVATED IN THE STEADY STATE DYNAMIC STEPS.

(4) FOR MULTI-PROCESS EXECUTION, THE ESTIMATED VALUE OF FLOATING POINT OPERATIONS FOR EACH PROCESS

IS BASED ON AN INITIAL SCHEDULING OF OPERATIONS AND MIGHT NOT REFLECT THE ACTUAL FLOATING

POINT OPERATIONS COMPLETED ON EACH PROCESS. OPERATIONS ARE DYNAMICALLY BALANCED DURING EXECUTION,

SO THE ACTUAL BALANCE OF OPERATIONS BETWEEN PROCESSES IS EXPECTED TO BE BETTER THAN THE ESTIMATE

PRINTED HERE.

(5) THE UPPER LIMIT OF MEMORY THAT CAN BE ALLOCATED BY ABAQUS WILL IN GENERAL DEPEND ON THE VALUE OF

THE "MEMORY" PARAMETER AND THE AMOUNT OF PHYSICAL MEMORY AVAILABLE ON THE MACHINE. PLEASE SEE

THE "ABAQUS ANALYSIS USER'S MANUAL" FOR MORE DETAILS. THE ACTUAL USAGE OF MEMORY AND OF DISK

SPACE FOR SCRATCH DATA WILL DEPEND ON THIS UPPER LIMIT AS WELL AS THE MEMORY REQUIRED TO MINIMIZE

I/O. IF THE MEMORY UPPER LIMIT IS GREATER THAN THE MEMORY REQUIRED TO MINIMIZE I/O, THEN THE ACTUAL

MEMORY USAGE WILL BE CLOSE TO THE ESTIMATED "MEMORY TO MINIMIZE I/O" VALUE, AND THE SCRATCH DISK

USAGE WILL BE CLOSE-TO-ZERO; OTHERWISE, THE ACTUAL MEMORY USED WILL BE CLOSE TO THE PREVIOUSLY

MENTIONED MEMORY LIMIT, AND THE SCRATCH DISK USAGE WILL BE ROUGHLY PROPORTIONAL TO THE DIFFERENCE

BETWEEN THE ESTIMATED "MEMORY TO MINIMIZE I/O" AND THE MEMORY UPPER LIMIT. HOWEVER ACCURATE

ESTIMATE OF THE SCRATCH DISK SPACE IS NOT POSSIBLE.

(6) USING "**RESTART, WRITE" CAN GENERATE A LARGE AMOUNT OF DATA WRITTEN IN THE WORK DIRECTORY.

1

Abaqus 6.13-1

Date 23-jul.-2018 Time 11:12:17

For use by under license from Dassault Systemes or its subsidiary.

STEP 2 INCREMENT 1
TIME COMPLETED IN THIS STEP 0.00

STEP 2 STATIC ANALYSIS

FIXED TIME INCREMENTS
TIME INCREMENT IS 1.00
TIME PERIOD IS 100.

LINEAR EQUATION SOLVER TYPE DIRECT SPARSE

MEMORY ESTIMATE

PROCESS	FLOATING PT OPERATIONS PER ITERATION	MINIMUM MEMORY REQUIRED (MBYTES)	MEMORY TO MINIMIZE I/O (MBYTES)
1	5.43E+004	17	24

NOTE:

(1) SINCE ABAQUS DOES NOT PRE-ALLOCATE MEMORY AND ONLY ALLOCATES MEMORY AS NEEDED DURING THE ANALYSIS,

THE MEMORY REQUIREMENT PRINTED HERE CAN ONLY BE VIEWED AS A GENERAL GUIDELINE BASED ON THE BEST

KNOWLEDGE AVAILABLE AT THE BEGINNING OF A STEP BEFORE THE SOLUTION PROCESS HAS BEGUN.

(2) THE ESTIMATE IS NORMALLY UPDATED AT THE BEGINNING OF EVERY STEP. IT IS THE MAXIMUM VALUE OF THE

ESTIMATE FROM THE CURRENT STEP TO THE LAST STEP OF THE ANALYSIS, WITH UNSYMMETRIC SOLUTION TAKEN

INTO ACCOUNT IF APPLICABLE.

(3) SINCE THE ESTIMATE IS BASED ON THE ACTIVE DEGREES OF FREEDOM IN THE FIRST ITERATION OF THE

CURRENT STEP, THE MEMORY ESTIMATE MIGHT BE SIGNIFICANTLY DIFFERENT THAN ACTUAL USAGE FOR

PROBLEMS WITH SUBSTANTIAL CHANGES IN ACTIVE DEGREES OF FREEDOM BETWEEN STEPS (OR EVEN WITHIN

THE SAME STEP). EXAMPLES ARE: PROBLEMS WITH SIGNIFICANT CONTACT CHANGES, PROBLEMS WITH MODEL

CHANGE, PROBLEMS WITH BOTH STATIC STEP AND STEADY STATE DYNAMIC PROCEDURES WHERE ACOUSTIC

ELEMENTS WILL ONLY BE ACTIVATED IN THE STEADY STATE DYNAMIC STEPS.

(4) FOR MULTI-PROCESS EXECUTION, THE ESTIMATED VALUE OF FLOATING POINT OPERATIONS FOR EACH PROCESS

IS BASED ON AN INITIAL SCHEDULING OF OPERATIONS AND MIGHT NOT REFLECT THE ACTUAL FLOATING

POINT OPERATIONS COMPLETED ON EACH PROCESS. OPERATIONS ARE DYNAMICALLY BALANCED DURING EXECUTION,

SO THE ACTUAL BALANCE OF OPERATIONS BETWEEN PROCESSES IS EXPECTED TO BE BETTER THAN THE ESTIMATE

PRINTED HERE.

(5) THE UPPER LIMIT OF MEMORY THAT CAN BE ALLOCATED BY ABAQUS WILL IN GENERAL DEPEND ON THE VALUE OF

THE "MEMORY" PARAMETER AND THE AMOUNT OF PHYSICAL MEMORY AVAILABLE ON THE MACHINE. PLEASE SEE

THE "ABAQUS ANALYSIS USER'S MANUAL" FOR MORE DETAILS. THE ACTUAL USAGE OF MEMORY AND OF DISK

SPACE FOR SCRATCH DATA WILL DEPEND ON THIS UPPER LIMIT AS WELL AS THE MEMORY REQUIRED TO MINIMIZE

I/O. IF THE MEMORY UPPER LIMIT IS GREATER THAN THE MEMORY REQUIRED TO MINIMIZE I/O, THEN THE ACTUAL

MEMORY USAGE WILL BE CLOSE TO THE ESTIMATED "MEMORY TO MINIMIZE I/O" VALUE, AND THE SCRATCH DISK

USAGE WILL BE CLOSE-TO-ZERO; OTHERWISE, THE ACTUAL MEMORY USED WILL BE CLOSE TO THE PREVIOUSLY

MENTIONED MEMORY LIMIT, AND THE SCRATCH DISK USAGE WILL BE ROUGHLY PROPORTIONAL TO THE DIFFERENCE

BETWEEN THE ESTIMATED "MEMORY TO MINIMIZE I/O" AND THE MEMORY UPPER LIMIT. HOWEVER ACCURATE

ESTIMATE OF THE SCRATCH DISK SPACE IS NOT POSSIBLE.

(6) USING "**RESTART, WRITE" CAN GENERATE A LARGE AMOUNT OF DATA WRITTEN IN THE WORK DIRECTORY.

THE ANALYSIS HAS BEEN COMPLETED

ANALYSIS COMPLETE

WITH 3 WARNING MESSAGES ON THE DAT FILE

AND 236 WARNING MESSAGES ON THE MSG FILE

236 WARNINGS ARE FOR NEGATIVE EIGENVALUES

JOB TIME SUMMARY

USER TIME (SEC) = 5.7000

SYSTEM TIME (SEC) = 2.3000

TOTAL CPU TIME (SEC) = 8.0000

WALLCLOCK TIME (SEC) = 12

Annex 6 FEM Results output – Monitor Message File

Due to its length, we will show the beginning of the file and the first time increment, together with the last part of the file.

MESSAGE FILE

STEP 1 INCREMENT 1 STEP TIME 0.00

STEP 1 STATIC ANALYSIS

FIXED TIME INCREMENTS

TIME INCREMENT IS 1.00

TIME PERIOD IS 50.0

LINEAR EQUATION SOLVER TYPE DIRECT SPARSE

CONVERGENCE TOLERANCE PARAMETERS FOR FORCE

CRITERION FOR RESIDUAL FORCE FOR A NONLINEAR PROBLEM 5.000E-03

CRITERION FOR DISP. CORRECTION IN A NONLINEAR PROBLEM 1.000E-02

INITIAL VALUE OF TIME AVERAGE FORCE 1.000E-02

AVERAGE FORCE IS TIME AVERAGE FORCE

ALTERNATE CRIT. FOR RESIDUAL FORCE FOR A NONLINEAR PROBLEM 2.000E-02

CRITERION FOR ZERO FORCE RELATIVE TO TIME AVRG. FORCE 1.000E-05

CRITERION FOR RESIDUAL FORCE WHEN THERE IS ZERO FLUX 1.000E-05

CRITERION FOR DISP. CORRECTION WHEN THERE IS ZERO FLUX 1.000E-03

CRITERION FOR RESIDUAL FORCE FOR A LINEAR INCREMENT 1.000E-08

FIELD CONVERSION RATIO 1.00

CRITERION FOR ZERO FORCE REL. TO TIME AVRG. MAX. FORCE 1.000E-05

CRITERION FOR ZERO DISP. RELATIVE TO CHARACTERISTIC LENGTH 1.000E-08

VOLUMETRIC STRAIN COMPATIBILITY TOLERANCE FOR HYBRID SOLIDS 1.000E-05

AXIAL STRAIN COMPATIBILITY TOLERANCE FOR HYBRID BEAMS 1.000E-05

TRANS. SHEAR STRAIN COMPATIBILITY TOLERANCE FOR HYBRID BEAMS 1.000E-05

SOFT CONTACT CONSTRAINT COMPATIBILITY TOLERANCE FOR P>P0 5.000E-03

SOFT CONTACT CONSTRAINT COMPATIBILITY TOLERANCE FOR P=0.0 0.100

CONTACT FORCE ERROR TOLERANCE FOR CONVERT SDI=YES 1.00

DISPLACEMENT COMPATIBILITY TOLERANCE FOR DCOUP ELEMENTS 1.000E-05

ROTATION COMPATIBILITY TOLERANCE FOR DCOUP ELEMENTS 1.000E-05

EQUILIBRIUM WILL BE CHECKED FOR SEVERE DISCONTINUITY ITERATIONS

ITERATION CONTROL PARAMETERS:

FIRST EQUILIBRIUM ITERATION FOR CONSECUTIVE DIVERGENCE CHECK 4

EQUILIBRIUM ITERATION AFTER WHICH ALTERNATE RESIDUAL IS USED 9

MAXIMUM EQUILIBRIUM ITERATIONS ALLOWED 16

MAXIMUM ITERATIONS FOR SEVERE DISCONTINUITIES

12

CONTACT CONTROLS APPLIED TO ALL CONTACT PAIRS:

GLOBAL STABILIZATION CONTROL IS NOT USED

RELATIVE PENETRATION TOLERANCE FOR AUGMENTED LAGRANGE CONTACT:

FINITE-SLIDING SURFACE-TO-SURFACE 5.000E-02

OTHERWISE 1.000E-03

PRINT OF INCREMENT NUMBER, TIME, ETC., EVERY 1 INCREMENTS

THE MAXIMUM NUMBER OF INCREMENTS IN THIS STEP IS 10000

UNSYMMETRIC MATRIX STORAGE AND SOLUTION WILL BE USED

DISPLACEMENT-BASED PARABOLIC EXTRAPOLATION WILL BE USED

CHARACTERISTIC ELEMENT LENGTH 9.38

DETAILS REGARDING ACTUAL SOLUTION WAVEFRONT REQUESTED

DETAILED OUTPUT OF DIAGNOSTICS TO DATABASE REQUESTED

PRINT OF INCREMENT NUMBER, TIME, ETC., TO THE MESSAGE FILE EVERY 1
INCREMENTS

EQUATIONS ARE BEING REORDERED TO MINIMIZE WAVEFRONT

COLLECTING MODEL CONSTRAINT INFORMATION FOR OVERCONSTRAINT CHECKS

COLLECTING STEP CONSTRAINT INFORMATION FOR OVERCONSTRAINT CHECKS

INCREMENT 1 STARTS. ATTEMPT NUMBER 1, TIME INCREMENT 1.00

NUMBER OF EQUATIONS = 184 NUMBER OF FLOATING PT. OPERATIONS =
1.03E+05

CHECK POINT START OF SOLVER

CHECK POINT END OF SOLVER

ELAPSED USER TIME (SEC) = 0.10000

ELAPSED SYSTEM TIME (SEC) = 0.0000

ELAPSED TOTAL CPU TIME (SEC) = 0.10000

ELAPSED WALLCLOCK TIME (SEC) = 0

CONVERGENCE CHECKS FOR EQUILIBRIUM ITERATION 1

MAX. PENETRATION ERROR -252.453E-12 AT NODE PART-2-COPY-1.1 OF CONTACT
PAIR (GENERAL_CONTACT_FACES_2,GENERAL_CONTACT_FACES_1)
MAX. CONTACT FORCE ERROR -189.280E-06 AT NODE PART-2-COPY-1.1 OF
CONTACT
PAIR (GENERAL_CONTACT_FACES_2,GENERAL_CONTACT_FACES_1)
THE CONTACT CONSTRAINTS HAVE CONVERGED.

AVERAGE FORCE 345. TIME AVG. FORCE 345.
LARGEST RESIDUAL FORCE 188. AT NODE 1 DOF 1
 INSTANCE: PART-1-1
LARGEST INCREMENT OF DISP. -1.000E-02 AT NODE 1 DOF 2
 INSTANCE: PART-2-1
LARGEST CORRECTION TO DISP. -1.000E-02 AT NODE 1 DOF 2
 INSTANCE: PART-2-1
 FORCE EQUILIBRIUM NOT ACHIEVED WITHIN TOLERANCE.

NUMBER OF EQUATIONS = 184 NUMBER OF FLOATING PT. OPERATIONS =
1.03E+05

CHECK POINT START OF SOLVER

CHECK POINT END OF SOLVER

ELAPSED USER TIME (SEC) = 0.0000
ELAPSED SYSTEM TIME (SEC) = 0.0000
ELAPSED TOTAL CPU TIME (SEC) = 0.0000
ELAPSED WALLCLOCK TIME (SEC) = 0

CONVERGENCE CHECKS FOR EQUILIBRIUM ITERATION 2

MAX. PENETRATION ERROR 1.12162E-09 AT NODE PART-2-COPY-1.1 OF CONTACT
PAIR
(GENERAL_CONTACT_FACES_2,GENERAL_CONTACT_FACES_1)
MAX. CONTACT FORCE ERROR 840.954E-06 AT NODE PART-2-COPY-1.1 OF CONTACT
PAIR (GENERAL_CONTACT_FACES_2,GENERAL_CONTACT_FACES_1)
THE CONTACT CONSTRAINTS HAVE CONVERGED.

AVERAGE FORCE 339. TIME AVG. FORCE 339.
LARGEST RESIDUAL FORCE 2.43 AT NODE 41 DOF 1
 INSTANCE: PART-1-1
LARGEST INCREMENT OF DISP. -1.000E-02 AT NODE 1 DOF 2
 INSTANCE: PART-2-1
LARGEST CORRECTION TO DISP. 1.805E-04 AT NODE 1 DOF 1
 INSTANCE: PART-1-1
 FORCE EQUILIBRIUM NOT ACHIEVED WITHIN TOLERANCE.

NUMBER OF EQUATIONS = 184 NUMBER OF FLOATING PT. OPERATIONS = 1.03E+05

CHECK POINT START OF SOLVER

CHECK POINT END OF SOLVER

ELAPSED USER TIME (SEC) = 0.0000
ELAPSED SYSTEM TIME (SEC) = 0.0000
ELAPSED TOTAL CPU TIME (SEC) = 0.0000
ELAPSED WALLCLOCK TIME (SEC) = 1

CONVERGENCE CHECKS FOR EQUILIBRIUM ITERATION 3

MAX. PENETRATION ERROR 105.079E-15 AT NODE PART-2-1.21 OF CONTACT PAIR
(GENERAL_CONTACT_FACES_3,GENERAL_CONTACT_FACES_1)
MAX. CONTACT FORCE ERROR 78.7843E-09 AT NODE PART-2-1.21 OF CONTACT PAIR
(GENERAL_CONTACT_FACES_3,GENERAL_CONTACT_FACES_1)
THE CONTACT CONSTRAINTS HAVE CONVERGED.

AVERAGE FORCE	339.	TIME AVG. FORCE	339.
LARGEST RESIDUAL FORCE	2.008E-04	AT NODE	1 DOF 1
INSTANCE: PART-1-1			
LARGEST INCREMENT OF DISP.	-1.000E-02	AT NODE	1 DOF 2
INSTANCE: PART-2-1			
LARGEST CORRECTION TO DISP.	1.836E-06	AT NODE	41 DOF 1
INSTANCE: PART-1-1			

THE FORCE EQUILIBRIUM EQUATIONS HAVE CONVERGED

ITERATION SUMMARY FOR THE INCREMENT: 3 TOTAL ITERATIONS, OF WHICH
0 ARE SEVERE DISCONTINUITY ITERATIONS AND 3 ARE EQUILIBRIUM ITERATIONS.

TIME INCREMENT COMPLETED 1.00 , FRACTION OF STEP COMPLETED 2.000E-02
STEP TIME COMPLETED 1.00 , TOTAL TIME COMPLETED 1.00

Last part of the File

THE ANALYSIS HAS BEEN COMPLETED

ANALYSIS SUMMARY:

TOTAL OF 150 INCREMENTS
0 CUTBACKS IN AUTOMATIC INCREMENTATION
299 ITERATIONS INCLUDING CONTACT ITERATIONS IF PRESENT
299 PASSES THROUGH THE EQUATION SOLVER OF WHICH
299 INVOLVE MATRIX DECOMPOSITION, INCLUDING
0 DECOMPOSITION(S) OF THE MASS MATRIX
1 REORDERING OF EQUATIONS TO MINIMIZE WAVEFRONT
0 ADDITIONAL RESIDUAL EVALUATIONS FOR LINE SEARCHES
0 ADDITIONAL OPERATOR EVALUATIONS FOR LINE SEARCHES
3 WARNING MESSAGES DURING USER INPUT PROCESSING
236 WARNING MESSAGES DURING ANALYSIS
0 ANALYSIS WARNINGS ARE NUMERICAL PROBLEM MESSAGES
236 ANALYSIS WARNINGS ARE NEGATIVE EIGENVALUE MESSAGES
0 ERROR MESSAGES

JOB TIME SUMMARY

USER TIME (SEC) = 5.7000
SYSTEM TIME (SEC) = 2.3000
TOTAL CPU TIME (SEC) = 8.0000
WALLCLOCK TIME (SEC) = 12